

PANTSat Technical Report

30310 Space Systems Engineering



**PULSAR AUTONOMOUS NAVIGATION
AND TIMING CUBESAT**

Abstract

PANTSat is a mission proposal to test an innovative instrument for better navigation in space named "Spacecraft Bolt-On Pulsar X-ray Receiver Concept for Autonomous Navigation and Timing". The instrument is based on a miniature bolt-on prototype X-ray receiver combined with a poly-capillary X-ray focusing optic. Specifically, it was derived from the MARS 2020 PIXL instrument design with the addition of a high-precision timing source, sufficient for pulsar-based navigation. This technical report describes the design of a low cost in-orbit demonstrator based on a wide 6U CubeSat platform containing the aforementioned payload, in order to validate the potential applicability of autonomous pulsar-based navigation. The result is compact in size, mass, power consumption (9-12 kg, 25-30W) and the expected mission cost is estimated 1M \$US. The current approach aims to the successful deployment of the instrument from the ISS into a LEO orbit. The objective of the project is the proof of concept of a potentially flight-proven system that will provide mission-enabling navigation autonomy, with possible future applications including GNSS and ground-independent backup navigation, reducing staffing during long cruise phases, and offloading over-prescribed Deep-Space Network resources. This technology will be especially useful for small and medium-sized spacecraft that cannot afford traditional ground-based navigation options and may have significant defence applications as well.

Name	Student N.	Nationality	Field of Study	Responsibility
Francesco Nardo	s212978	IT	Systems Engineering	Project Leader
Evangelos Istantiadis	s212888	GR	Systems Engineering	Management / Systems Eng.
Thomas Taxis	s212408	GR	Systems Engineering	Management / Systems Eng.
Cecilie Koertz Wedderkopp	s174026	DK	Space Research	Management / Sys. Eng. and Thermal
Sarah Franze	s222444	US	Earth Observations	Thermal
Anuj Nigam	s226722	IN	Aerospace Engineering	Thermal
Eva S. Jensen	s190964	DK	Systems engineering	Mechanical
Cato Nørrung Poulsen	s194127	DK	Systems engineering	Mechanical
Joachim Harding	s194116	DK	Systems engineering	Mechanical
Bruno Menezes	s212595	BR, IT	Systems Engineering	Payload
Cæcilie Lundahl Andersen	s194118	DK	Space Research	Payload
Andrew Blumensen	s194139	DK	Space Research	Payload
Søren Staal	s194125	DK	Space Research	Payload
Sandra Martos Sánchez	s213238	ES	Systems Engineering	EPS
Pau Fabregat Carrascal	s212739	ES	Earth Observation	EPS
Hannah van Gemert	s222684	NL	Systems Engineering	ACDS/OBC
Bjarke Nilsson	s180866	DK	Earth Observations	ACDS/OBC
David van Scheppingen	s222902	NL	Autonomous Systems	ACDS/OBC
Santa Rappoccio	s223691	IT	Space Research	ADCS
François Goor	s222722	IT	Earth Observation	Communications
Alessandro Morello	s222688	IT	Systems engineering	Communications
Artemis Vrettou	s222726	GR	Earth Observation	Communications
Athanasis Athanasiadis	s222651	GR	Earth Observation	Communications
Tor Woodhams Lund	s194128	DK	Mapping and Navigation	Orbit
Hugo Aranha	s226807	PT	Aerospace Engineering	Orbit

Table 0.1: The students involved in the project and their responsibilities.

Contents

Abstract	i
List of Figures	iv
List of Tables	ix
Glossary	xi
1 Mission Description	1
1.1 Mission Motivation	1
1.2 Mission Statement and Objectives	2
1.3 Mission Constraints	3
1.4 Mission Timeline Overview	5
1.5 PANTSat Operational Modes	7
2 Design Definition	9
2.1 System Description	9
2.2 System Budgets, Relevant Margins and Accuracy	12
2.3 Analysis	21
2.4 Radiation Tolerance Provisions	23
3 Sub-System Design Definition	29
3.1 Payload	29
3.2 Attitude Determination and Control Subsystem (ADCS)	49
3.3 Onboard Computer (OBC)	66
3.4 Orbit, Launch and Deployment	70
3.5 Electrical Power Subsystem (EPS)	80
3.6 Telemetry, Tracking and Communications (TT&C)	93
3.7 Structures and Mechanism	111
3.8 Thermal Control	125
4 Assembly and Verification	143
4.1 Systems Engineering Management Plan (SEMP)	143
4.2 AIT Activities and Schedule	150
4.3 Technical Challenges	153
4.4 Validation Model Philosophy	156
4.5 Verification Philosophy	157
5 Conclusion	160
Bibliography	161
A Appendix A: Thermal Properties Tables	II
B Appendix B: Requirements	III

List of Figures

1.1	Visualization of mission phases and timeline.	6
2.1	Interface diagram showing the connections between the subsystems, and the communication lines.	10
2.2	Block diagram of the satellite - ground station link	11
2.3	The Solidworks PANTSat assembly seen in two configurations. A stowed configuration for launch and release of the satellite (left) and a deployed configuration after deployment of the solar panels and the optical extension mechanism (right).	12
2.4	Mission power budget	14
2.5	Schematic of the thermal ranges for spacecraft operation.	18
2.6	Work Breakdown Structure for a project of level 2 and showing level 3 for Payload and Spacecraft systems.	19
2.7	Cost budget in USD showing estimations based on different methodologies ([14] [16]).	21
2.8	Steps involved in setting up Thermal Model	22
2.9	Flux map of charged protons above 0.1 MeV for Pulsar Autonomous Navigation and Timing Satellite (PANTSat)'s orbit ($\text{cm}^{-2}\text{s}^{-1}$).	24
2.10	Dose-depth curve for PANTSat's orbit over the period of three months.	25
2.11	Sector Shielding Analysis Tool (SSAT)'s direction window for calculation of shielding distribution [25].	26
2.12	Dose results from the anisotropic shielding simulation (dosage values are for a period of one year in orbit).	27
2.13	Linear Energy Transfer (LET) spectra along PANTSat's orbit.	28
3.1	X-ray polycapillary optic used for PIXL. (a) The end of the optic. (b) A blowup of a small section of the optic. (c) High magnification image of individual capillary tubes. Credit: [29]	30
3.2	Simulation results of pulsar navigation solutions for three different optic apertures with and without an angular filter package installed. The light blue curve shows the performance of a NICER element for comparison, which converges to a solution of 21.4 km. Credit: Robert Sharro et al. [30]	31
3.3	Left: 3.5 cm diameter x 6.5 cm long polycapillary optic package with alignment features to mount an angular filter. Right: angular filter element of ≈ 70 mm length. Credit: [30].	32
3.4	The sketch is modified from Robert Sharro et al. It shows the optics with its dimensions outlined. The dimensions are estimated using information from [31] and [30]. The length of the angular filter is estimated from Figure 3.3. The reduced focal length is calculated from geometry considerations. Note: The dimensions are not correctly scaled with respect to each other, the figure is only for illustration purposes.	33

3.5	X-ray light curve of the Crab Pulsar at 5-8 keV. Image credit: European Southern Observatory.	35
3.6	a) Conceptual illustration of a Silicon Drift Detector. b) Ketek H50 SDD. Image credit: Ketek	35
3.7	Microsemi SA.45s Space CSAC integrated with the payload. Coin for scale reference.	36
3.8	Left) Visualization of headers included in FITS-file. Right) Visualization of event-list format for FITS-files according to HEARSAC convention	37
3.9	Concept for a pulsar observing instrument for navigation and timing with scan platform. Credit: Robert Sharrow et al [31].	40
3.10	Visualization of possible disc and hinge system for the movable pointing of the payload.	41
3.11	Considerations about the consequences of misalignment of the boom within the pointing accuracy requirement. Note: The dimension and angles are not correctly scaled, the figures are only for conceptual illustration purposes.	43
3.12	a) An artist's visualization of an MSP. b) Visualization of how X-ray pulsar navigation and timing (XNAV) works	44
3.13	a) Table showing the pulsar catalog for the PANTSat-mission. b) J2000 map of the location of our pulsar catalog with the Crab source highlighted in red.	45
3.14	Pulsar visibility throughout the year for the PANTSat catalog [36]	46
3.15	Block diagram for an attitude-control system. Figure from [41].	50
3.16	XACT-50 from Blue Canyon Technologies, figure from [42].	51
3.17	Reaction wheels of the RWP050 type from Blue Canyon Technology [12].	51
3.18	Star Tracker of the Standard NST type from Blue Canyon Technology [12].	52
3.19	Pointing stability over 20 minutes [42]	53
3.20	Rotation DOF	55
3.21	Equations describing an elliptical orbit. Here a is the semi-major axis, b is the semi-minor axis, c is the distance to the foci, \mathbf{f} is the vector to the Earth focus, \mathbf{r} is the position vector to a point j at time t_j and corresponding true anomaly θ_j . R_y is the rotation matrix around the y-axis, i is the inclination and P the period.	58
3.22	Blockage overview	59
3.23	Intervals in which each of the targets is not blocked by either Earth, Moon or Sun. Note that seemingly continuous lines contain small scale gaps.	59
3.24	Comms window	60
3.25	Power charge schedule	60
3.26	Intervals in which targets, power and communications are all available at the same time while pointing at the target. Note that seemingly continuous lines contain small scale gaps.	61
3.27	Detumbling simulation results. The reference system in red and green refers to the CubeSat's body frame, while the reference system in white is the ECI frame.	65
3.28	Endurosat OBC Type I	67
3.29	State diagram showing different modes of operation in software.	69
3.30	Nano-satellites approximate orbits after launch. [55]	72
3.31	Orbit visualization, orbit trajectory in red and downlink cycles in blue.	73
3.32	Eclipse cycles over the course of 2 days of simulation.	74
3.33	Downlink cycles simulation.	74

3.34	Crude simulation of the drag area for a fixed orbit position while pointing at the chosen pulsars as a function of the angle of the solar array rotation around the z-axis.	75
3.35	Orbit lifetime study for different drag areas over a period of one year.	77
3.36	Orbit altitude decay considering a launch on August 1 st 2025, assuming a mean drag area of 0.06 m ²	77
3.37	Nanosatellite launches per year by deployer company.[55]	78
3.38	EPS block scheme	80
3.39	Solar Array configurations studied.	82
3.40	Battery capacity simulated under multiple target, eclipse and battery conditions.	84
3.41	Experimental test results of batteries performance. Left: Available capacity, when charging it under standard conditions, for multiple cycle depths. Right: Distribution of the battery state based on cycle depth and an average of 5500 cycles x year (close to the cycles per year of the mission). Figure from [64].	85
3.42	ACU and PDU internal flowchart	85
3.43	The interface schematic of the P60 dock or motherboard. It acts as the hub for proper functioning of the EPS and used for its protective features. Figure from [59].	86
3.44	Power interfaces schematic	87
3.45	(a) Switching on the Payload is optional and won't burden the EPS. (b) If the transmission takes place during eclipse switching on the heater is possible. (d) If only thermal system is used during eclipse	88
3.46	Battery capacity behaviours when risk situation "2 out of 3 working solar panels" is met. The left plot shows the pre-defined modes under a continue scientific mode operation. The right plot shows how the scientific mode operation under the risk changes proposal would look.	90
3.47	Modified power modes under risk conditions.	90
3.48	Battery capacity behaviours when risk situation "1 out of 3 working solar panels" is met. The first row shows the original operation modes power definition, while the second row shows the modified under risk situation power modes. The first column show a continuous scientific mode operation, while the second row shows a "forced" period observation.	91
3.49	A typical, but simplified ground station setup operating in C-Band [70].	96
3.50	ESA ground station network. [72]	97
3.51	Nasa ground station network. [73]	97
3.52	Ksat ^{lite} Ground Stations Network	98
3.53	DTU ground station antennas on top of building 348. Credits: Flemming Hansen	99
3.54	60 cm parabolic dish antenna. Credits: Flemming Hansen	100
3.55	60 cm antenna dish controller and interfaces. Credits: Flemming Hansen	100
3.56	RTL-STR dongle configuration [75]	101
3.57	Trade-off between possible High Gain Antenna configurations for CubeSats [76]	102
3.58	Possible mounting configurations for the ISIS 6U UHF Antenna [77]	102
3.59	Design of the antenna and its possible mounting positions in a 6U CubeSat.	103
3.60	ANT2190 Radiation Pattern [79]	104
3.61	104
3.62	CubeSat Space Protocol [81]	105

3.63	Atmospheric losses from horizon to zenith. Red line is the Cosmic microwave background, the blue line represents the receiver quantum noise and the purple one represents the galactic synchrotron radiation in the direction of the galactic plane (left) and away from it (right). [Credit: Flemming Hansen]	108
3.64	Gain attenuation as a function of the pointing accuracy [79]	109
3.65	BER vs EBN0 for different modulations	110
3.66	NanoRacks DoubleWide Deployer [82]	111
3.67	NRDD with Rails Payload Envelop and +/-Z Load Points [82]	112
3.68	Random Vibration Test Profiles [82]	113
3.69	The frame made of GomSpace[84]	114
3.70	The different ways the mounting rings can be placed[84]	115
3.71	Example of extendable boom mechanism[41]	116
3.72	Optical extension mechanism using a spur-rack system with a dual axis 15 mm long electric motor	117
3.73	Nanotec electrical motor with worm drive, rack system	117
3.74	Complete Optical System	119
3.75	The simple Solidworks assembly seen in two configurations. A stowed configuration for launch and release of the satellite (left) and a deployed configuration after deployment of the solar panels and the optical extension mechanism (right).	121
3.76	The COM of the satellite showed in the stowed (left) and deployed (right) configurations. The deployed configuration shown here does not show the entire solar array.	122
3.77	The detailed assembly of the spacecraft	123
3.78	Illustration of the attitude control system being too large to fit within the satellite in two different orientations.	124
3.79	Schematic of the thermal environment for a satellite in LEO [41].	126
3.80	(a) Visibility factor F as a function of altitude and β angle. (b) Beta angle, β is defined as the angle between local vertical and the Sun's rays [41].	127
3.81	Trade analysis of passive cooling systems.	133
3.82	Trade analysis of active heating systems.	134
3.83	Schematic of the thermal design consisting of MLI (the outer silver layer) the kapton patch heaters (the inner orange layer) and the TEC. Images of MLI and kapton heaters from [97] and [98].	136
3.84	Diagram of thermal operations.	136
3.85	The standard heating mode as a percentage of orbit.	138
3.86	Details of Mesh	139
3.87	Meshed Geometry of PANTSat	139
3.88	Configurations used to setup model	140
3.89	Side#1 showing Temperature distribution over the CubeSat	141
3.90	Side#2 showing Temperature distribution over the CubeSat	141
3.91	Side#1 showing Directional Heat Flux distribution over the CubeSat	142
3.92	Side#2 showing Directional Heat Flux distribution over the CubeSat	142
4.1	Dependencies and communication flow between all the subsystems.	144
4.2	NASA Space Flight Project Life Cycle from NPR 7120.5E. Source [99].	145
4.3	PANTSat Project Planning	147
4.4	Different design approaches. Source ESA.	148
4.5	S-curve, current position in red. Source ESA.	149

A.1	Various surfaces and finishes and their respective emissivity and absorptivity [41].	II
-----	--	----

List of Tables

0.1	The students involved in the project and their responsibilities.	ii
1.1	Requirements for subsystems imposed by the payload.	4
1.2	Designed orbit parameters.	4
2.1	Main components in the PANTSat model.	12
2.2	Mass Budget and relative margin.	13
2.3	Telemetry, Global Navigation Satellite System (GNSS) and payload data in bits per second	16
2.4	Pointing and angular velocity design drivers for each of the four states of mode during satellite operations.	17
2.5	Pointing performance for drift, accuracy and slew.	17
2.6	Thermal requirements of components across all subsystems. ¹ Optimal performance assumed at 20°C. ² Assumed structure made from Al 6061-T6 (Compass-1). ³ Standard range for solar panels [13].	17
2.7	Summary of sources of radiation, their energy and Flux at 422 km altitude, 51.6° inclination.	24
3.1	Parameters for the optics package. The information is retrieved from [31] and [30], and the reduced focal length is calculated from geometry considerations. In case the information was ambiguous, the most restrictive limit was chosen.	34
3.2	This table shows three cases of expected data transfer rates for the payload and the resulting data redundancy	38
3.3	RWP050 characteristics [12].	51
3.4	Pointing table with the performance at several situations.	54
3.5	Intertia Mass Properties	54
3.6	Pointint Requirements	56
3.7	ORbital parameters of observed bodies	57
3.8	Time schedule of observations	61
3.9	Connector overview for the Endurasat OBC	69
3.10	Orbit Design Range for XNAV Tracking. Adapted from [54]	71
3.11	Chosen EPS commercial options, including model and corresponding provider.	81
3.12	Ground Station choices though out the whole process.	99
3.13	GomSpace Antenna ANT2150: Parameters	103
3.14	List of components with dimensions used for the optical extension (* <i>Diameter of cylinder first</i>)	120
3.15	Components and their sizes in the simple model	120
3.16	COM stowed and deployed	121
3.17	Calculated radiation intensity values from equations 3.31 - 3.35.	127
3.18	Steady State analysis applied to various surfaces and finishes.	129

3.19	Mass and specific heat for the aluminum structure (Al) and the internal spacecraft components (SC).	130
3.20	Transient analysis applied to various surfaces and finishes with $c_{w,sc} = 800$ Nm/kgK.	130
3.21	Thermal component list for active and passive systems. SA = Surface Area of the satellite. TCB = Thermal Control Box.	134
3.22	Transient analysis for various average spacecraft internal specific heats for one full orbit after the warm up period.	137
3.23	Transient analysis for $c_{w,sc} = 800$ Nm/kgK over 10 orbits periods after warm up.	138
3.24	Power demands of the active thermal system for the warm-up and standard modes. Power efficiency is assumed to be 70%.	138
3.25	Thermal properties of materials used	139
3.26	Constant Parameters used in the Model	140
4.1	Models of validation and Model Philosophy application (DM & VM)	156
4.2	Requirements Matrix	159

Glossary

- ACS** Attitude and Computer System. 7, 20, 39, 41, 42, 76, 118, 143
- ACU** Array Conditioning Unit. 84, 85, 88, 151
- ADCS** Attitude Determination and Control System. 9, 13–15, 39, 49–51, 53, 55, 64, 68, 80, 82, 83, 87, 119, 153, 161
- AG** Aerogel. 150, 153
- AGI** Ansys Government Initiatives. 22, 73
- AIT** Assembly, Integration and Testing. 143, 150
- BER** Bit Error Rate. 109
- COM** Center of Mass. 22, 112, 113, 121
- ConOps** Concept of Operation. 9, 55
- COTS** Commercial off the shelf. 5, 19, 156
- CSAC** Chip-Scale Atomic Clock. 36, 48
- DAEP** Deep Space Network Aperture Enhancement Project. 1
- DC** Duty Cycle. 13, 14
- DEC** Declination. 37, 62
- DSN** Deep Space Network. 1, 2, 48, 78, 97, 160
- EHF** Extremely High Frequency. 95
- EKF** Extended Kalman Filter. 71
- EPS** Electrical Power System. 7, 13–15, 70, 76, 80–82, 84, 86, 89, 95, 115, 143, 151, 153, 157, 160
- FDIR** Fault Detection, Isolation and Recovery. 28
- FEC** Forward Error Correction. 105
- FoV** Field of view. 30, 31, 38
- FYS** ESA's Fly Your Satellite. 2, 3, 63, 77
- GEO** Geosynchronous Equatorial Orbit. 71
- GNSS** Global Navigation Satellite System. ix, 1, 15, 16, 36, 44, 67, 68
- GSaaS** Ground Station as a Service. 98
- IDD** Interface Definition Document. 111

- IMU** Inertial Measurement Unit. 50, 52
- IOD** In-Orbit Demonstration. 12, 157
- ISS** International Space Station. 2, 3, 6, 38, 70, 73, 78, 79, 111
- ITU** International Telecommunicaton Union. 95
- KSAT** Kongsberg Satellite Service. 98
- LEO** Low Earth Orbit. 2–4, 14, 20, 73, 93, 98, 127
- LEOP** Launch and Early Operation Phase. 6, 7, 14, 91
- LET** Linear Energy Transfer. iv, 27, 28
- LNA** Low Noise Amplifier. 96, 99, 106
- LOS** Line of Sight. 44
- MCU** Master Control Unit. 84
- MDR** Mission Definition Review. 146
- MJD** Modified Julian Date. 37
- MLI** Multi-layer Insulation. 9, 125, 152, 153, 160
- MPPT** Maximum Power Point Tracking. 83, 85, 151
- MSP** Milisecond Pulsars. 2, 44
- NICER** The Neutron Star Interior Composition Explorer.
- NRDD** Nanoracks Doublewide Deployer. 79, 111, 112, 157
- NST** Nano Star Tracker. 52
- OBC** On-Board Computer. 9, 10, 13, 15, 49, 52, 66–69, 87, 115, 143, 152, 157, 161
- OC** Over Current. 86
- ODAR** Orbital Debris Assessment Report. 70
- OS** Operation System. 68
- OV** Over Voltage. 86
- PANTSat** Pulsar Autonomous Navigation and Timing Satellite. iv, v, 1, 3, 4, 7, 9–13, 17, 18, 23–29, 35, 36, 39, 41, 44–47, 53, 64, 70, 95, 109, 111, 114, 119, 122, 125, 143, 160, 161
- PDR** Preliminary Design Review. 5, 12, 47, 76, 80, 145, 146, 154, 161
- PDU** Power Distribution Unit. 84, 88, 151
- PIXL** Planetary Instrument for X-ray Lithochemistry. 29, 30, 32, 36, 39, 40
- PP** Peak Power. 13, 14
- PV** Photovoltaic. 80, 83

- QPSK** Quadrature Phase-Shift Keying. 96, 105
- RA** Right Ascension. 37, 62
- RF** Radio Frequency. 96
- RSS** root sum square. 30–32, 45, 48
- S/C** spacecraft. 23, 25, 47, 63, 64
- SA** Solar Array. 4, 11, 14, 16, 80, 81
- SAA** South Atlantic Anomaly. 23, 39
- SCL** Serial Closk Line. 10
- SDA** Serial Data Line. 10
- SDD** Silicon Drift Detector. 35, 36, 39
- SEB** Single Event Burnouts. 27
- SEE** Single Event Effects. 23, 27, 28
- SEGR** Single Event Gate Ruptures. 27
- SEL** Single Event Latch-ups. 27, 28
- SEMP** Systems Engineering Management Plan. 146
- SEU** Single Event Update. 27
- SEXTANT** The Station Explorer for X-ray Timing and Navigation Technology.
- SHF** Super High Frequency. 95
- SIR** System Integration Review.
- SNR** Signal-to-Noise Ratio. 30, 45, 96, 105, 107
- SPENVIS** ESA's SPace ENVironment Information System. 23, 25, 27
- SSAT** Sector Shielding Analysis Tool. iv, 25, 26
- STK** Systems Tool Kit. 23, 73, 74
- TCB** Thermal Control Box.
- TEC** tailorable emissivity coating. 9
- TECs** Thermal Electric Cooler. 17, 36
- TID** Total Ionising Dose. 23, 25, 26, 47
- ToA** Time of Arrival. 38, 44
- TT** Terrestrial Time. 37
- TTC** Telemetry, Tracking and Communication.
- UHF** Ultra High Frequency. 98, 102, 104
- UV** Under Voltage. 86

VHF Very High Frequency. 98

WBS Work Breakdown Structure. 19, 20

XNAV X-ray pulsar navigation and timing. v, 1–3, 18, 20, 32, 36, 38–40, 44, 47, 48, 71, 73, 160

1 Mission Description

Pulsar Autonomous Navigation and Timing Satellite (PANTSat) is a mission proposal to test an innovative instrument for better navigation in space named "Spacecraft Bolt-On Pulsar X-ray Receiver Concept for Autonomous Navigation and Timing". In this chapter a description of the mission in terms of mission statement and objectives, main mission phases and satellite operational activities is presented.

1.1 Mission Motivation

X-ray pulsar navigation and timing (XNAV) is a method of navigation where the periodic X-ray signals emitted from pulsars are used to determine the position of a spacecraft. The concept of XNAV has been in development since the discovery of pulsars in the 1960s [1]. Pulsars are highly magnetized and rapidly rotating neutron stars that emit beams of high-energy radiation from their magnetic poles. The baseline of XNAV is to use highly stable millisecond pulsars like celestial beacons. The time-of-arrival of the pulse can be accurately determined through the use of onboard atomic clocks. The X-ray signal is then compared to a known catalog of pulsar frequencies and positions. The position of the spacecraft can then be determined anywhere in the Solar System in a similar manner to Global Navigation Satellite System (GNSS) by using at least 4 pulsars.

Today, the increasing number of maturing technologies for XNAV hold great potential for realizing fully autonomous navigation both in planetary orbit or deep-space. The technological feasibility was demonstrated on the NICER/SEXTANT on ISS in 2018 where a position accuracy of 7 km in 2 days was reported [2]. However, for the technology to be practical, the current dimensions (100 cm on the long axis) of the instrument must be significantly reduced.

Precise and reliable data on position and velocity is vital for the navigation systems and therefore the success of any mission in space. This holds especially true for deep space missions, where real-time navigation is not feasible simply owing to the immense distances reached. In the past, navigation for deep space missions has relied on NASA's Deep Space Network (DSN), which provides accurate three-dimensional position and velocity information thanks to three huge antenna stations located across the globe [3]. However, the continued over-reliance on the DSN for positioning is starting to pose difficulties for deep-space communications, where the missions are restricted by limited telemetry budgets [4]. Due to new missions with increased observation resolution and cadence, demanding greater data volumes, this problem is expected to further aggravate in the near future. In fact, the demand for short duration peaks for positioning is predicted to reach 10-15 antennas in 2025-2030. This excessive demand will mean that science down-link requests cannot be accommodated.

Autonomous XNAV could therefore be an attractive alternative for future deep-space missions to help alleviate some of the predicted load from the DSN. XNAV could be used for missions with relaxed positional requirements. Also, it could serve as a backup on manned and un-manned missions, providing redundancy in case of DSN over-loading.

Besides just alleviating the current demand, XNAV could also provide future economic benefits. There are already plans to expand and improve the DSN, such as the Deep Space Network Aperture Enhancement Project (DAEP), however these expansions are a costly affair, requiring the construction of several 34-meter telescopes [5]. Moreover, DSN

operations have an hourly cost of \$1057 for a single 34-meter station [6]. Therefore, deep-space missions such as the Voyager missions can have total DSN costs in the millions [7]. Incidentally, XNAV could not only alleviate demand but also potentially provide huge savings from both DSN upgrades and mission costs, meaning more funds can be used on actual science.

1.2 Mission Statement and Objectives

Space exploration and the increasing number of deep-space missions demand more efficient and reliable navigation systems. Conventional navigation techniques, supported ground stations are not always feasible for deep-space missions due to various constraints such as range and signal strength, while dedicated ones, such as the DSN, are reaching their schedule limit. XNAV pulsar based navigation has emerged as a promising solution to address those challenges. The precise and periodic nature of Millisecond Pulsars (MSP), makes them ideal candidates to be utilized as beacons for autonomous navigation.

The PANTSat mission concept aims to bring XNAV one step closer to realization by designing an in-orbit demonstrator for the XNAV technology thanks to a miniature X-ray receiver.

Three potential proposals that intend to design a mission to validate the concept of pulsars used as navigation mechanisms and test the relevant technology were studied:

- A Satellite in Sun-Jupiter elliptical orbiter (Proposal 1)
- A ride-share or piggy-back approach where the payload is attached to an existing mission (Proposal 2)
- A CubeSat demonstrator using ESA's Fly Your Satellite (FYS) programme¹ (Proposal 3)

Each proposal has its own distinct advantages and disadvantages. The first proposal indicates an elliptical Sun-Jupiter orbit with the objective to test pulsar-based navigation in proper deep-space conditions. The DSN can be utilized as a mean of validation. While this approach properly tests the payload in the environment it is supposed to be utilized, presents a higher factor of risk and cost. Moreover, this mission proposal has the longest life-cycle.

The second proposal consists of attaching the payload to an existing deep-space mission, possibly as a back-up instrument. The advantages are the simplified demonstrator design and testing of the payload in proper deep-space conditions. This approach yields simpler subsystems that require integration but is bounded to the main mission's platform and objectives which have to be suitable.

The final proposal is essentially a technology demonstration and validation of pulsar based navigation in space using the FYS programme. The CubeSat platform provides a cost effective and feasible solution to our mission, that also has shorter life span and can provide results quicker. It also serves as a mid-step validation of the payload functionality in Low Earth Orbit (LEO) before testing it to deep-space. Deployment from the International Space Station (ISS) provides an ideal playground to test the relevant technology in a cost efficient and low risk implementation. The obvious drawback is that the payload will not be utilized in the actual Deep Space environment. Furthermore, the CubeSat platform introduces constraints associated with the mass and dimensions of our system. Moreover, testing the payload in LEO means that we will have to account for the payload's sensitivity

¹Fly Your Satellite! programme

to the Earth's magnetic field.

After careful consideration and analysis, we decided to pursue the CubeSat option for our project. While, this approach does not expose the payload to the conditions it was intended to be used, it serves as a valuable technology demonstration and validation platform, allowing us to test the payload in LEO before committing it to a deep-space mission. The CubeSat option, offers several key advantages that make it an attractive choice for our project. First and foremost, the mission design is significantly simpler, both as a whole and for each subsystem specifically. This enables a more streamlined development process, allowing us to focus more on the pulsar navigation system performance. Furthermore, the CubeSat platform does not require a dedicated propulsion system, further simplifying the design and reducing the associated costs and complexities. This is a critical factor, since developing a propulsion based system suitable for Deep Space missions could turn out to be a significant challenge in the scope of this project. Another benefit of the CubeSat option is its shorter life-cycle, allowing us to obtain results more rapidly and reducing the risk associated with long term space missions. In addition to this, the standardized nature of the CubeSat platform leads to lower costs, making it a more feasible alternative for an academic project. **In summary, while the CubeSat proposal may not provide the required testing environment for a pulsar-based autonomous navigation system, it serves as a cost-effective ideal testing bed for our system, functioning as a technology validation.** The results from this mission can be applied to refine the system and prepare it for future deep-space missions, which is the bigger goal of this exciting new technology.

1.3 Mission Constraints

Based on the mission statement, the main requirements were derived from the FYS programme specification document [8]. However, as the mass and volume constraints were too tight for the payload and the sub-systems a deviation from the original specification was necessary and documented in Appendix A. Within these new requirements the current mission proposal does not fit the ESA framework anymore and a new launch solution with deployment from the ISS has been investigated, Section 3.4.4. Therefore, more requirements, based on the launcher platform [9], are added. A complete list of them is presented with the Requirement Matrix in Section 4.5.

As an overview, the main constraints and characteristics for the PANTSat missions are:

- Demonstrate the capability of XNAV and validate the on-board payload
- CubeSat Platform
- Low Earth Orbit
- Low cost and short schedule (typically 1M \$ US and <2 years to flight readiness)
- Short operational lifetime (typically <1 year in low altitude LEO)
- Acceptance of single point failures
- Limited redundancy (where possible within the constraints)
- Extensive use of commercial off-the-shelf elements (modules that have previous flight heritage and are supplied by small industrial suppliers at a fixed price)

Additionally, more specific requirements, Table 1.1, are imposed on other subsystems by the XNAV instrument (payload) as it will be presented in Section 3.1.

Subsystem	Parameter	Requirement
Attitude	Pointing + stability accuracy	< 0.03 deg
Communication	Minimum Data rate	> 145kB/orbit
Electrical	Minimum Power	> 5 W
Mechanical	Optics dimensions	2 cylinders of 6 cm diameter x 14 cm length + 42 cm focal distance
Mechanical	Minimum Optics Mass	> 3.3 kg
Mechanical	Minimum Radiation Shielding	> 2.5 mm aluminium paneling
Thermal	Max detector housing temperature	< 80° C

Table 1.1: Requirements for subsystems imposed by the payload.

The spacecraft design presented in this report will satisfy these constraints. In particular, PANTsat is a CubeSat, size of 6U with a mass of 8.9 kg and a total cost of approximately 1M \$ US. The payload has a 60 cm linear dimension (including optics and focal length) and will require an external extension mechanism. No propulsion system is present and the total power required is approximately 25W generated via Solar Array (SA). The final orbit is a near-circular LEO and the chosen orbit parameters are compiled in Table 1.2, where further explanation of the reasoning behind this choice was documented in section 3.4.3. The orbit of choice provided a series of constraints that each subsystem had to be aware of in their design, namely solar exposure, down-link availability and mission lifetime (11.5 months).

Orbit parameter	Value
a	6794.64 km
e	$5.15 \cdot 10^{-4}$
i	51.6°
ω	-
Ω	-

Table 1.2: Designed orbit parameters.

1.4 Mission Timeline Overview

In this section a brief description of the mission main phases is given, explaining the major tasks and importance of each stage from inception, all the way to the mission closeout. It is by no means an extensive records of all and every small detail of the project timeline, but a more general overview that provides a clarification of past, present, and future milestones and important tasks duration.

Prior to the initial project development phase, known as Phase A, there is a preliminary stage called Pre-Formulation, which of course includes the Concept Studies. During this stage, 3 main mission ideas and options were generated to create a pool of potential proposals or approaches, which were described in detail in subsection 1.2. After several iterations of discussions, and a preliminary feasibility study, the team converged on the desired mission idea, and the mission concept was formulated. The aim of this phase is to assess the feasibility of the desired system, define high-level requirements, evaluate performance, cost, and schedule viability, while establishing the project's scope. This is followed by the Concept and Technology Development, known as phase A, where all the aforementioned procedures converge into a cohesive final mission concept along with system-level requirements, needed system technology developments and a technical management plan. Every sub-system was defined, people were accordingly assigned to it and started iterating upon it, while a communication strategy in between each team was established, namely the concurrent engineering method.

The successful completion of those two phases is defended and characterized by the Preliminary Design Review (PDR). The purpose of the preparation prior to this review is to establish a baseline that can meet the requirements of the mission, meaning that the project needs to be defined with sufficient detail. This involves creating product requirements for both the system structure and any supporting elements and creating a preliminary design for each of the system structures. This process belongs to Phase B, where a board consisting of DTU professors, specialists, and the publisher of the original mission and project science case, namely Prof. Robert Sharrow, test and challenge the validity of the mission analysis up to that date, pointing out to essential insights, potential problems, misconceptions and relevant discrepancies to the team. The entirety of those distinct three phases lasted for 2 months.

The continuation of those processes leads to Phase C, where the final design and fabrication of each subsystem takes place. This means that, in order to produce the necessary hardware and software, the process of fabrication and programming development needs to be carried out at that time. Additionally, it is necessary to create ultimate designs for every system structure end product. This will also include outsourcing and ordering Commercial off the shelf (COTS) products and solutions for the sub-systems that provided a detailed final design which is handed out to the respective provider. This is further explained in 2.2.6. It should be noted that, such a process includes lead time, which can and most likely will take up quite a lot of effort, depending on many details. This upcoming phase is determined to last 6 months, with a margin for up to 1 year depending on the availability and lead time of individual parts as well as prototyping.

Then, we enter Phase D which is the integration phase. During this stage the system's various components, including hardware, software, and human elements, are assembled and combined while ensuring that it can fulfill the system requirements with a high degree of certainty. This is a quintessential and lengthy phase as every sub-system needs to be integrated into a whole, while following very strict conditions, timelines and certifica-

tions. It also includes a variety of different tests, carried out by various independent and national sectors and organizations as well as the shipment to the main testing facilities and the launch facility in the USA. The two most important carriers of those operations, namely assembly, integration and testing, are DTU labs, and the ESA Belgium facility, who will handle the bulk of critical verification stages. It is planned to last for 12 months, with a margin of 2 extra months to account for any obstacles that may be encountered along this long phase.

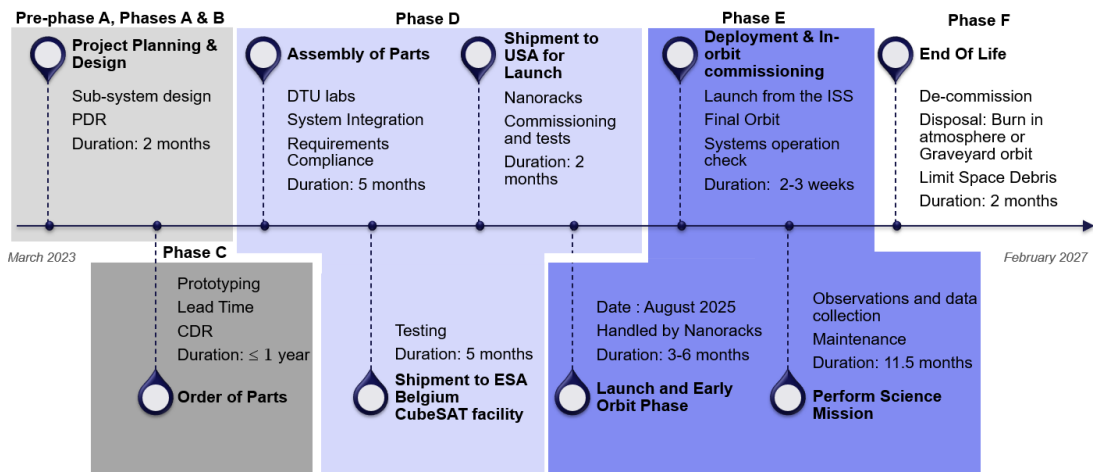


Figure 1.1: Visualization of mission phases and timeline.

Next up, the main phase of operations takes place, namely Phase E, which can be organized into four distinct sub-phases. The first of them is the Launch Preparation Phase lasting 3 months. This phase involves preparing the CubeSat for launch, including design, testing, and integration of the spacecraft and the payload with the launch vehicle. The objectives of this phase are to ensure that the CubeSat is ready for launch and that it meets all the safety and regulatory requirements, handled in our case from Nanoracks USA. After that, the Launch and Early Operation Phase (LEOP), lasting another 3 months, begins with the launch of the CubeSat and includes the initial operations and commissioning of the spacecraft to rendezvous with the ISS. The objectives of this phase are to verify that the CubeSat has been deployed correctly and that all the integrity of the system remains at its full potential.

The In-Orbit Commissioning Phase will take place from the ISS and is planned to last from 2 to 3 weeks. During this phase, the CubeSat's systems and payloads are commissioned and calibrated to ensure that they are operating correctly in the space environment. The optical extension subsystem, described at 3.7.1.2, will be initialized during that time. The objectives of this phase are to verify that the CubeSat is performing its intended mission and to identify any anomalies or issues that need to be addressed. Finally, we enter the Operational Phase which is planned to last for 11.5 months. The operational phase is the main mission phase, during which the CubeSat performs its scientific or technological objectives. The objectives of this phase are defined in detail in various sections of this document (1.2, 4.1.1). It should be noted that performing any necessary maintenance,

and operations to ensure the CubeSat's continued functionality, is an essential part of this phase.

Lastly, we have Phase F, the Post-Mission Phase, which is determined to last for a few months. At the end of the operational phase, the CubeSat's mission is complete, and it is decommissioned. The objectives of this phase are to dispose of the CubeSat as safely as possible and to analyze the data collected during the mission. During this closeout, adhering to very strict and cohesive rules governing the end-of-life disposal, CubeSats are typically designed to re-enter the Earth's atmosphere and burn up upon re-entry, minimizing the risk of debris impact on Earth or other space objects. The specific end-of-life disposal plan for your CubeSat will be determined during Phase E based on the regulations and guidelines of the launch provider and space agency for the scope of our mission considering scale limitations.

1.5 PANTSat Operational Modes

The need for a reliable method to change between states of operation for any kind of satellite cannot be overstated. Each mission entails a variety of different states in which the satellite has to adapt to wildly different conditions, while always maintaining a rudimentary way to communicate with the ground station. To accommodate all these different states, all satellites are designed to operate in different operational modes. The PANTSat satellite is designed to operate in 4 distinct modes in order to tackle every possible situation that may occur during its lifetime, including unexpected errors or changes in its general plan.

- **Commissioning:** booting up and stabilizing the satellite from the moment of ejection while also deploying the optical module and the solar array.
- **Safe Operations (safe-ops):** a mode designed to deal with power issues, resetting/rebooting software (sub)-systems, and attitude control for an optimal solar panel configuration or gradually powering down non essential sub-systems.
- **Observe Operations (observe-ops):** responsible for attitude control, making observations, and automatic system tests.
- **Communication Operations (comm-ops):** a mode activated by an up-link command requesting measurement data to be transferred, which will automatically go back into observe operations once finished.

These modes of operation are also described in figure 3.29, in the section on software, in the operational modes diagram, indicating the transitions between the modes, which may occur automatically or by command. Each mode has its own set of operational constraints, which must be followed to ensure the safety and success of the mission.

During the LEOP, as well as the In-Orbit Commissioning Phase, the CubeSat operates in the Commissioning mode. This mode involves verifying that the spacecraft has been deployed correctly and that all subsystems are functioning as expected. Specifically, instruments and parts belonging to Electrical Power System (EPS), Thermal, as well as the Attitude and Computer System (ACS)(de-tumbling) will be enabled for this mode to de-tumble the satellite. After, it will also test and calibrate the spacecraft's systems and payloads to ensure they are operating correctly in the space environment. In addition, elements from the Mechanical system will be initialized, for instance, the optical extension subsystem will be deployed during this phase and via this operational mode.

Then, during the Operational phase, the CubeSat operates in Observe Operations mode,

Communication Operations mode, and Safe Operations mode. Observe-ops involves the realization of its central science case by ultimately collecting data, where the comms-mode transmits it back to Earth. The satellite is in observe-ops by default, where the comms-mode is triggered by an uplink command from ground station (or when the satellite hasn't had an uplink command for a long time). For both observe-ops and comms-ops a specific attitude is required.

The safe-ops mode is triggered when the satellite struggles with issues related to power, software, or other subsystems. It will go into power-conserving mode, and try to restart/re-boot specific systems accordingly. It has to be noted that there is not a specific battery-charging mode. Since the solar-array is orient-able, it has been estimated, Section 3.5.7.2, that enough energy is always provided either by the array or by batteries.

Lastly, during the Post-Mission Phase, the CubeSat operates in the Decommissioning mode. This mode involves safely disposing of the spacecraft by de-orbiting it or sending it to a graveyard orbit.

2 Design Definition

This chapter gives a description of PANTSat as a whole system, space and ground segment. It contains an overview of PANTSat main features in terms of architecture, design, technical specifications and performance including also the system budgets.

2.1 System Description

2.1.1 Functional Description

The Concept of Operation (ConOps) during mission phase E and the different satellite modes have been explained in Sections 1.4 and 1.5. In this paragraph, we want to describe the main functions that the system (space and ground segment) shall execute after in-orbit commissioning is concluded and while fully operational.

By design, the satellite must be as autonomous as possible, i.e. the On-Board Computer (OBC) shall be able to independently switch between mission modes without any external command. In particular, the cubesat antenna is directional, therefore to initiate the link, pointing from the Attitude Determination and Control System (ADCS) is required. The choice of a directional rather than an omni-directional antenna is justified by the deployment of the optical module and solar array that will interfere with external wire antennas. Conversely, a patch antenna has greater bandwidth capabilities thus permitting large transfers of data during rare and short communication windows.

The communications with the ground base are limited to transmitting the science and housekeeping data. Thanks to the large memory storage capacity, it is not critical to transmit in each orbit or ground pass, conversely priority is given to battery charging, if enough power is not available then communication mode is not executed.

The satellite antenna operates mainly as a passive listener (receiver) while the ground antenna is active and sends out commands (transmitter) when in range. After the hand-shaking procedure a link is established between the two and the ground station can send a command to start the down-link of stored data or an up-link in case of software patches or anomalies.

The thermal control system consists of passive and active systems. The satellite is covered in Multi-layer Insulation (MLI) over all but one face of the satellite and exposed edges are coated in tailorabile emissivity coating (TEC). Below the MLI and aluminum plates of the cubesat structure, patch heaters are lined on the internal side of the aluminum. The thermal control will operate in two different modes: warm-up and standard. The warm-up mode will occur at the beginning of the mission, during which the active heaters will warm the cubesat to 20°C. For standard operations, the thermal control system will operate in a control loop that activates the patch heaters when temperatures onboard the satellite drop below a threshold value (+11.6°C). It is estimated that the heaters will activate once per orbit during eclipse and the heaters will be activated for 9% of every orbit.

2.1.2 System Architecture

The interfaces and the data communications between the subsystems are an important part of the spacecraft and the OBC. The OBC needs to handle the operational mode, subsystems communication/control, and data handling. Most of this can be achieved with the communication bus, Figure 2.1. The subsystems are responsible for the internal integration between the components (illustrated by the blue box). The inter-system combination

is then controlled by the I2C bus, where the Serial Data Line (SDA) is responsible for the data transfer, and the Serial Clock Line (SCL) controls the system-wide clock. The OBC is then central and can communicate with the different subsystems in serial. Serial means that through the I2C bus, the subsystems are not able to communicate at the same time, however, given the high frequency of the system (480 MHz), this is not critical for real-time control.

In Figure 2.1, the link between the spacecraft and the ground-segment is also represented. The data communication path starts from the storage on the onboard memory, which is an integrated part of the OBC. Then, the data are transferred to the communications module, using the UART bus. The communication mode is scheduled so that it fits in between the pulsar observations according to Table 3.26.

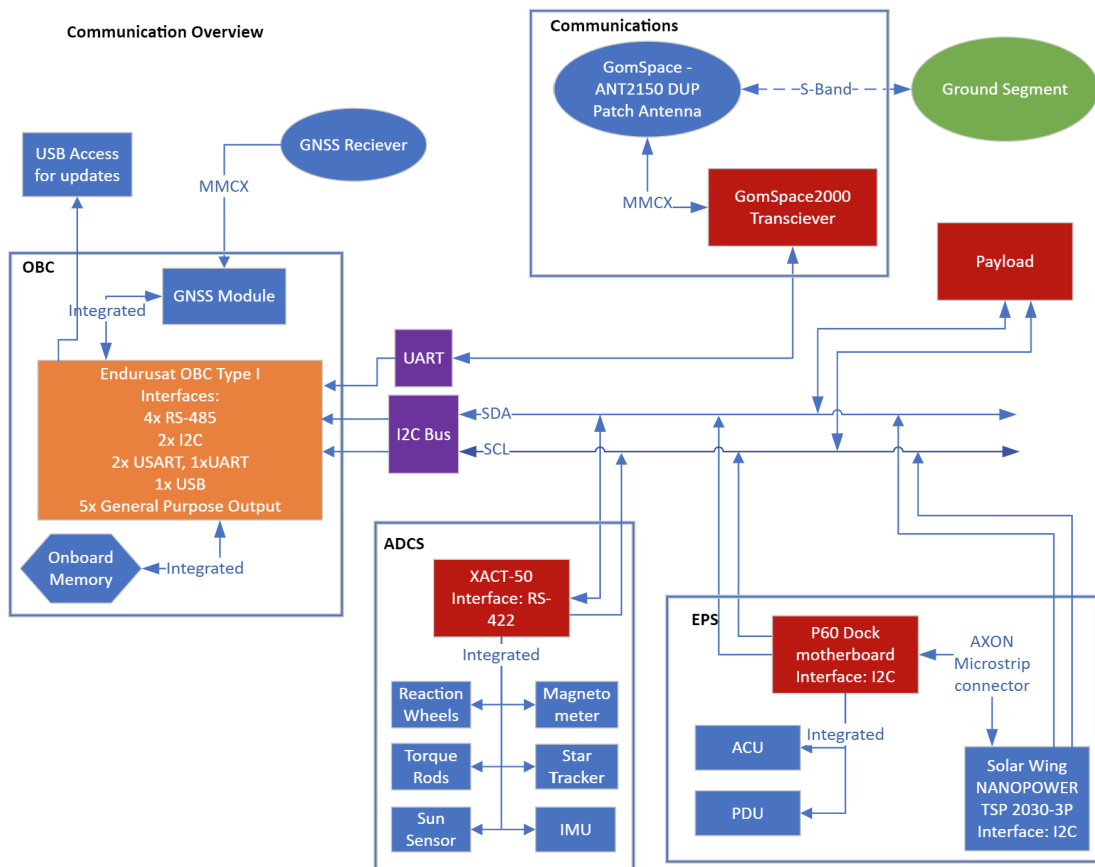


Figure 2.1: Interface diagram showing the connections between the subsystems, and the communication lines.

In Figure 2.2 the link between the spacecraft and the ground station is specifically shown in detail. The signal is transmitted from the PANTSat as scheduled and it is received at the DTU ground station at Building 348. The ground sub-system consists of a parabolic dish that feeds a horn antenna, then the signal is filtered and down-converted immediately. Afterwards the signal is transferred to the actual receiver and finally the computer where it is demodulated, decoded and the data can start getting processed.

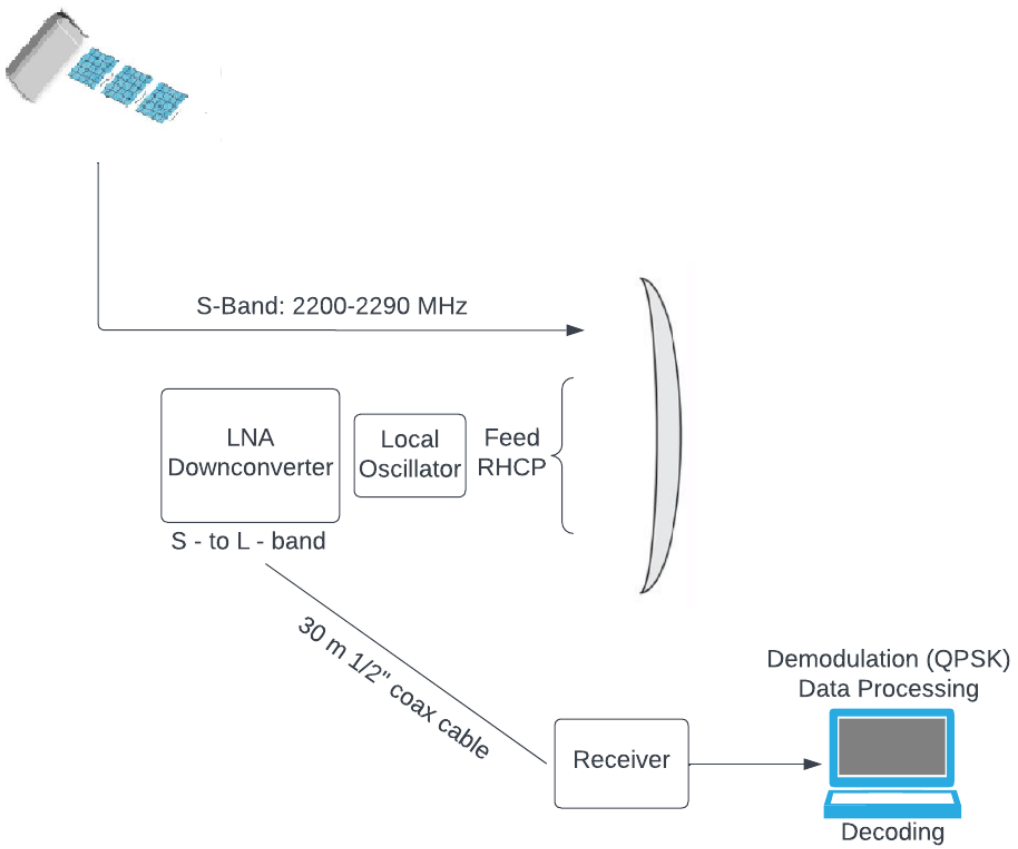


Figure 2.2: Block diagram of the satellite - ground station link

2.1.3 Spacecraft System Configuration

The SolidWorks¹ software has been used to model the configuration of PANTSat in its two different configurations. There are two deployable devices on board the satellite: the solar array and the optical extension mechanism.

During launch, the satellite will be in the stowed configuration where no devices are deployed. This configuration is illustrated in the simplified design in Figure 2.3a. In the early orbit phase before observations commence, the SA will be deployed. Once power and all other subsystems are operational, the optics will be deployed as seen in Figure 2.3b. This is the final configuration of the satellite which it will retain until the mission ends.

A detail record of all the components included in the PANTSat design is given in Table 2.2 together with the mass budget. In Table 2.1 a limited list of the main components is provided to show the overall system configuration. The components are color-coded with the drawings in Figure 2.3 and showing both the stowed and deployed models. In the table references to the report are available to simplify the readings.

¹SolidWorks is a solid modeling computer-aided design and computer-aided engineering application published by Dassault Systèmes. SolidWorks

Component	Number of components	Colour	Section
6U structure	1	Grey	3.7.2
Optical system	1	Blue	3.7.3
X-ray Detectors	1	Turquoise	3.1.2
Atomic clock	1	White	3.1.3
Aluminium side panels	1	See through	2.4
Thermal control box	2	Dark red	3.8.5.2
OBC	1	Purple	3.3
Attitude	1	Pink	3.2.3
Transceiver	2	Yellow	3.6.4
GNSS	1	Dark green	3.3.3.2
Antenna	1	Green	3.6.3
Battery pack	1	Red	3.5.4
Power Delivery Unit	1	Orange	3.5.5
Solar Panels	1	Light grey	3.5.3

Table 2.1: Main components in the PANTSat model.

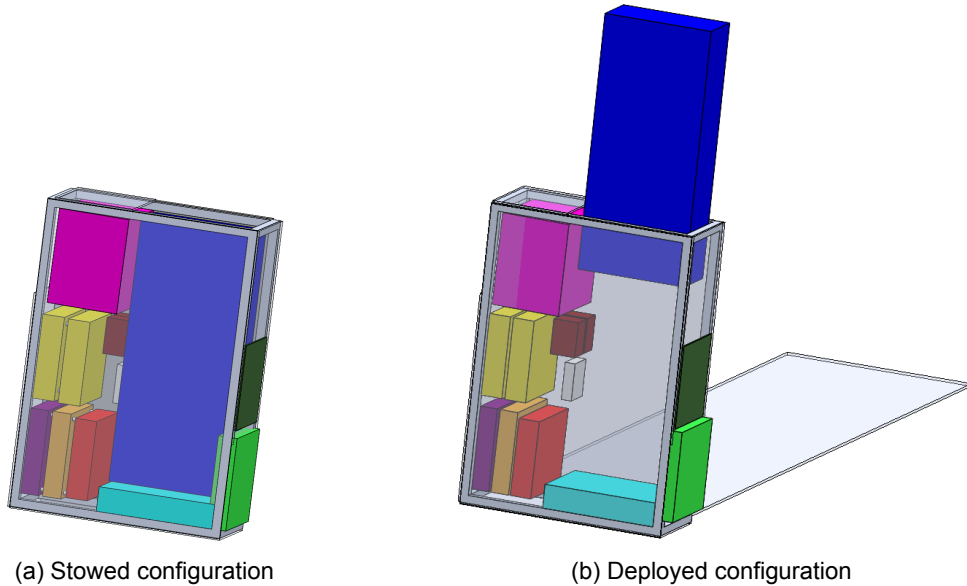


Figure 2.3: The Solidworks PANTSat assembly seen in two configurations. A stowed configuration for launch and release of the satellite (left) and a deployed configuration after deployment of the solar panels and the optical extension mechanism (right).

2.2 System Budgets, Relevant Margins and Accuracy

The PANTSat mission shares different attributes with the ESA In-Orbit Demonstration (IOD) project, as shown in Section 1.3. At such the *System Margin Policy for ESA IOD CubeSat Projects* [10] applies to the current mission design. In general the following margin philosophy shall be used at PDR level:

- **System level margin:** 20% applies to mass and power budgets
- **Data processing margin:** 50% and for on-board memory and processor peak usage
- **Communication margin:** 3dB on the link budget
- **Thermal margin:** 15% on Radiator Surfaces (passive cooling), 10% shall be applied on the effect of the aging.

- **General margin for all the components/subsystems:** 10% for existing units requiring minor modifications or 20% for new developments

2.2.1 Mass Budget

Providing the mass budget is a task linked with the a deep knowledge of all the components and structure present in PANTSat. It is presented in Table 2.2.

Subsystem:	Product Name	N.	Unit Mass [Kg]	Dimensions [cm]			Volume [cm3] / Note
				X	Y	Z	
Attitude & Computer	XACT-50 (Attitude Control System)	1	1.23	10	10	7.54	754.00
	Endurasat OBC Type I	1	0.13	9	9	1.9	153.90
	GNSS Receiver	1	0.019	Internal to XACT-50			
	Data Cables	10	0	N.a.			
Electrical Power	Battery pack	1	0.27	9.4	8.4	2.3	181.61
	EPS: motherboard +2 daughters (ACU + PDU)	1	0.191	9	9.6	1.98	171.07
	Solar array (1 wing)	1	0.75	33	20.8	9	Deployed length: 93cm Stowed: 33 x 20.8 x 9
Comm.	Transceiver: NanoCom SR2000	2	0.27	8.89	9.2	2.34	191.38
	Antenna: NanoCom SR2000	1	0.11	9.8	9.8	2.01	193.04
	RTL-SDR dongle for GS	1	0	N.a.			
Mechanical & Thermal	W6U Structure (GOM Space)	1	0.73	34.1	26.6	10	34.05 x 26.6 x 10
	Aluminium Side panels	1	0.81	Custom made			Thickness: 2mm
	Optical extension subsystem	1		Custom made			Depl. Length: 50cm
	Thermal Control Box (Model CT325)	2	0.028	2.77	1.54	3.81	16.25
	MLI blankets	10	0.01226	25.8	0.5		Thickness: 5mm
	DC Motor	2	0.07	N.a.			
Orbit	Thermal Sensors	14	0.002	0.76	0.76	0.2	0.12
	Active thermal elements (patch heaters) .04 g/cm^2	14	0.01	Custom made			Thickness: 2.3mm
	Nanorack launch for W6U	1	0	N.a.			
Payload	Optic (2 lenses)	1	3.3	6.5	13.5		447.74
	Detector	1	0.3	1.4	2.1	2.2	6.47
	SA.45s Space Chip-Scale Atomic Clock	1	0.035	4.06	3.53	1.14	16.34
				Mass tot. [Kg]			
				8.9016			
					Vol. tot. [cm3]		
					2131.92		
				Requirements:	12		
				Margin:	35%		
					6000		
					181%		

Table 2.2: Mass Budget and relative margin.

Due to the structure (CubeSat) and launcher (Nanoracks) platforms constraints, the total available mass is 12 kg while the volume is 6000 cm³. The 20% margin policy is not applied a priori, instead, after summing up all the components, the residual margin is calculated. In particular, regarding the mass budget the PANTSat mission has a 35% mass margin which provides room for missing or not available specifications such the cabling system and the extension mechanism.

2.2.2 Power and Energy Budget

EPS is an essential component of any spacecraft that is designed to operate in space. It provides electrical power to all the spacecraft subsystems that require it including the scientific instrument, communication, ADCS, OBC and thermal control. The primary objective of this section is to determine the power budget of the EPS and set the requirements the EPS parts must provide with.

The power budget defines how much power is assigned to each subsystem for different modes. Each subsystem uses a different power magnitude for a different amount of time per orbit (duty cycle) for each operational mode. In order to ensure that the power budget can be matched by the proposed EPS, the Peak Power (PP) of each subsystem with a 100% Duty Cycle (DC) is taken into account during the most demanding modes. Such considerations are more strict than the real power behaviour of the satellite. For the selected low Earth trajectory, a significant portion of the orbit will be in shadow for around

30 out of every 90 minutes. As a result, to provide sufficient power, the solar array needs to be oversized relative to the amount of sunlight available by a factor of approximately 1.5 according to [11] recommendations for LEO missions. This means that the power output of the array in LEO must exceed the bus load by 50%. The eclipse duration can vary based on the orbit's inclination, but it's generally predictable, leading to an estimated 5000 to 6000 battery charge/discharge cycles per year. On top of that, a 25% margin is added to all power modes aiming to never reach a shortage of power because of a down-dimension of the subsystem.

SUBSYSTEM	Instrument	SCIENCE MODE			TELECOM MODE		DEPLOY MODE		SAFE MODE	
		MODULE PP (W)	PP (W)	DC (%)	PP (W)	DC (%)	PP (W)	DC (%)	PP (W)	DC (%)
PAYOUTLOAD	Pulsar X-ray Receiver	5	5	100	0	0	0	0	0	0
COMMS	TX	1,5	0	0	1,5	80	0	0	1	5
	RX	1	0	100	1	20	0	0	1	100
ADCS	ADCS	7,6	7,6	100	7,6	100	7,6	100	3	100
	OBC	1	1	100	1	100	1	100	1	100
THERMAL CONTROL		3	3	100	3	100	3	100	3	
POWER	PDU + ACD + DOCK	1,1	1,1	100	1,1	100	1,1	100	1,1	100
TOTAL		20,2	17,7		13,00		11,60		5,05	
+ Margin (25%)		25,25	22,13		19,00		15,88		12,63	

Figure 2.4: Mission power budget

The mission defines 4 different operational modes, each of them having its own power budget assigned, as explained in section 1.5. The power budget for this mission is shown in Figure 2.4. This table contains the PP and DC of each subsystem for every satellite mode. It should be noted that as the mission is designed, the solar array would be able to generate power for the majority of the time, only limited by the part of the orbit when the satellite is in eclipse.

Some subsystems are considered essential to stay alive. These subsystems are the ADCS, since keeping control of the attitude is essential for either observing a source with the instrument in science mode, down-linking or up-linking data to or from Earth, commissioning the satellite or pointing to the Sun to charge the batteries. Some on board data processing is necessary always on, as well as thermal control to keep with the restriction of every subsystem's temperature and the EPS itself to be able to distribute the power required by others systems.

The main and most power-demanding mode is the science mode at 22.13 Watts. Such mode sets up the characteristics that the EPS subsystem must have such as:

- The Solar Array (SA) must be able to **at least** deliver an input power higher than the most demanding mode plus a typical battery charge power value of 5.6 Watts, in order to charge the batteries while operating the satellite. Therefore, the SA must deliver at least 27.23 Watts of input power.
- The batteries and their charging - discharging cycles must ensure that the scientific mode can be executed during a sun-eclipse for the 2 year duration of the mission, meaning it must perform under a 2-year degraded batteries condition.

When the satellite enters the *telecom* mode, the payload will be turned off and the communication subsystem will demand its peak power to perform its operations, as well as the ADCS subsystem, in order to achieve the appropriate antenna pointing.

The deployment mode is only executed after the lunch of the satellite in LEOP, just before

finishing the commissioning phase of the satellite, in order to deploy the antennas, solar panels and the telescope's focal length. Once the deployment mode is over, the satellite can be considered commissioned and start making observations.

The safe mode, which is only accessed in case of system failure event or if the batteries level goes below a minimum threshold, risking their depletion during a demanding operational mode, therefore risking the success and continuity of the mission. The Safe Mode contemplates a situation where most of the subsystems are disabled, only providing power to the subsystems that contribute to the batteries charging process, such as the ADCS, thermal control, OBC and the EPS itself. Thus, the payload is not supplied and the other subsystems are minimally powered.

2.2.3 Link Budget and Data Rates

The amount of data that has to be transmitted comprehends first of all the data acquired from the payload during the observations, then the telemetry with all the housekeeping data necessary to control the conditions of the spacecraft and eventually the data from the GNSS network to validate the data acquired by the payload. An estimate of the amount of data per second is provided in Table 2.3

	H/W	I'face	Bits	Hex
Time stamp				
year	RTC	I2C	12	3
month	RTC	I2C	4	1
date	RTC	I2C	8	2
hour	RTC	I2C	8	2
minute	RTC	I2C	8	2
seconds	RTC	I2C	8	2
Solar Array				
voltage 1	EPS	I2C	10	3
voltage 2	EPS	I2C	10	3
voltage 3	EPS	I2C	10	3
current 1	EPS	I2C	10	3
current 2	EPS	I2C	10	3
current 3	EPS	I2C	10	3
Batteries				
voltage	EPS	I2C	10	3
current	EPS	I2C	10	3
current direction	EPS	I2C	10	3
temperature	EPS	I2C	10	3
overcurrent event	EPS	I2C	1	1
Temperature				
2 x side 1	STCS	I2C	2 x 10	2 x 3
2 x side 2	STCS	I2C	2 x 10	2 x 3
2 x side 3	STCS	I2C	2 x 10	2 x 3
2 x side 4	STCS	I2C	2 x 10	2 x 3
3 x side 5	STCS	I2C	3 x 10	3 x 3
3 x side 6	STCS	I2C	3 x 10	3 x 3
Antenna	Telecom	CAN	10	3
Solar Array	EPS	I2C	10	3
OBC	OBC	I2C	10	3
IMU	OBC	SPI	12	3
IMU				
X	OBC	SPI	14	4
Y	OBC	SPI	14	4
Z	OBC	SPI	14	4
Sun Sensors				
XACT-50	ACS	I2C	12	3
MPPT	EPS	I2C	12	3
Star Tracker				
quaternion 1	ACS	I2C	64	16
quaternion 2	ACS	I2C	64	16
quaternion 3	ACS	I2C	64	16
quaternion 4	ACS	I2C	64	16
GNSS				
Navigation Data	OBS	I2C	50	13
Payload				
Scientific Data (WCS)	Payload	-	215	54

Table 2.3: Telemetry, GNSS and payload data in bits per second

The total amount of data in the worst case scenario in which the payload produces 140 KByte per orbit is therefore $V_{tot} = 0.59 \text{ Mbyte/orbit}$ or $V_{tot} = 9.5 \text{ MByte/day}$. The link budget is further analysed in section 3.6.5.1.

2.2.4 Pointing Budget

To determine the pointing accuracy, we have determined the design drivers for the pointing for each of the operational modes. The design driver for the different mission states can be seen in table 2.4. Here we can then see that in the detumbling phase, the angular velocity required by the ESA standard is the design driver whereas during safe mode the solar array (SA) is the pointing design driver. During observation phase, we have the payload, and transmission we have the antenna. This determines the most strict pointing requirement to be 0.03° , with a 10% margin, as well as the angular velocity required to handle of $90^\circ/\text{s}$. The angular velocity of $10^\circ/\text{s}$ for payload is the maximum achievable rotation speed for target switching, not the angular velocity during observations [12].

Modes	Detumbling	Safe	Observation	Transmission
Design Driver	ESA Req.	Solar Array	Payload	Antenna
Pointing	NA	50°	0.03°	30°
Ang. Vel.	90°/s	90°/s	10°/s	NA

Table 2.4: Pointing and angular velocity design drivers for each of the four states of mode during satellite operations.

In table 2.5, we see the pointing achieved for PANTSat at different stages. The stability states the drift over 20 minutes, the accuracy determines the pointing accuracy at a perfect target. The sum of these two determine the expected accuracy for the system over time. Slew and slew sum state how the accuracy is expected during a movement of 1 degree per second, giving a larger error. The range is given by the low and high margin of expectation, and all values are 1-sigma values. The expected performance is then 0.008 degrees pointing accuracy.

	Stability	Accuracy	Sum	Slew@(1°/s)	Slew Sum
arcsec	2.33-3.28	10.9-25.2	13.13-28.48	15-200	28.13-228.48
deg	0.00065-0.00091	0.0030-0.0070	0.0036-0.0079	0.0042-0.056	0.0078-0.064

Table 2.5: Pointing performance for drift, accuracy and slew.

2.2.5 Thermal Budget

Table 2.6 shows the required thermal operating range as provided by the engineers for each subsystem. The payload control box houses within itself Thermal Electric Cooler (TECs) that ensure the payload is within its operating range, as long as it is kept within (0, +80)°C by the thermal control system. However, the optimal temperature for taking measurements is 20°C, and this is considered in the thermal design. Based on these ranges, the required thermal range for the satellite must be within (0, +50)°C. Taking a 10 degree margin on either side, the desired thermal range for the overall satellite becomes (+10, +40)°C, and when considering the optimal temperature for the payload, the upper limit of the design range is reduced to +30°C, such that the satellite is kept close to the optimal temperature throughout the mission.

Component	Required Thermal Range [°C]
Payload ¹	(0, +80)
XACT-50 (ACS)	(-20, +60)
Battery Pack	(-20, +75)
Structure ²	(-40, +65)
EPS computer	(-35, +85)
NanoCom SR2000 Transceiver and Antenna	(-40, +85)
Solar Arrays ³	(-100, +100)
Other Electronic Equipment	(-20, +50)
<i>Overall Required Range</i>	(0, +50)
Ideal Operations (incl. margins)	(+10, +30)

Table 2.6: Thermal requirements of components across all subsystems.

¹Optimal performance assumed at 20°C.

²Assumed structure made from Al 6061-T6 (Compass-1).

³Standard range for solar panels [13].

Figure 2.5 demonstrates the various thermal ranges for the mission. Outside of $(0, +50)^\circ\text{C}$, the payload and electrical components within PANTsat will experience critical failure. The ideal operating temperatures $(+10, +30)^\circ\text{C}$, for which the thermal system is designed, incorporate at least a 10 degree margin on either side of the true operating temperatures. Within the ideal operations range, the actual thermal system is designed to maintain a minimum cold-side temperature of $(+11.60, +11.76)^\circ\text{C}$ and a maximum hot-side temperature of $(+16.92, +17.12)^\circ\text{C}$. This is maintained by a heating cycle on the eclipse side of each orbit and is explained further in section 3.8. The operational limit $(0, +50)^\circ\text{C}$ provides room for error in the case that the heating system does not perform as efficiently as expected.

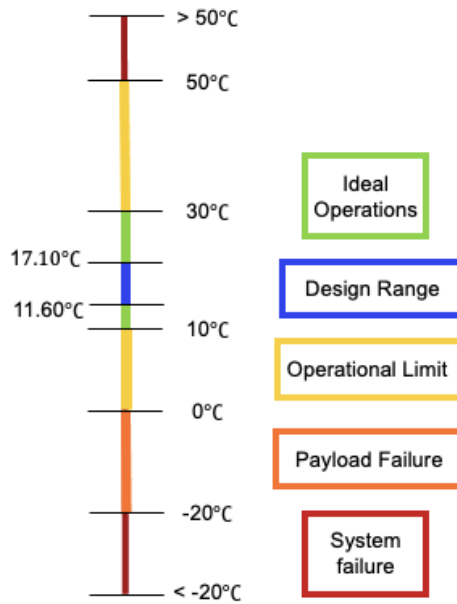


Figure 2.5: Schematic of the thermal ranges for spacecraft operation.

2.2.6 Cost Budget

The Cost Budget for this project is of relatively high importance. Since this mission is a proof-of-concept only and is not tested in a deep-space environment, we are highly focused on keeping risk, cost and time consumption to a minimum where it is possible.

As seen from the requirements, there is one main driver both in setting physical limitations but also for the cost. Since the entire mission is a technology demonstration of the XNAV system, this sets a baseline for our cost budget and risk, as the reduction of cost should not be compromising the test and validation of the system.

2.2.6.1 Budget Estimation

The budget estimation has been carried out by a mix of research on similar missions, consulting NASAs Space Mission Budgets and the AMES Cost Model ([14]) and by following the guidelines setup by NASA in their Cost Estimating Handbook ([15]) and a technical report published by the United States Air Force on Guidelines and Metrics for Assessing Space System Cost Estimates ([16]).

To carry out a proper budget estimate we need to set up a baseline budget for the project. This will change throughout the different project phases, which should be taken into account for the final budget.

For this a Work Breakdown Structure (WBS) is build, which covers all areas of the project included in the cost estimate. An example hereof can be seen in Figure 2.6 showing a WBS down to level 2 and to level 3 for the most important elements.

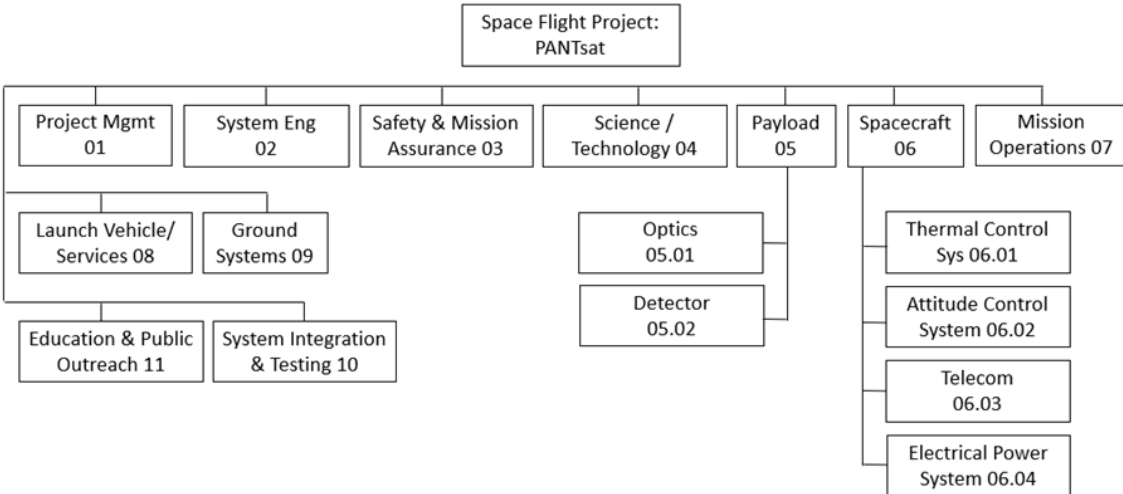


Figure 2.6: Work Breakdown Structure for a project of level 2 and showing level 3 for Payload and Spacecraft systems.

2.2.6.1.1 COTS A great part of the mission is affected by the requirement of low risk and cost. For example a high percentage of components used in this mission will be Commercial-of-the-shelf parts (COTS). To reduce risk most of the chosen components will be components build for space, which shortens the development time and simplifies the mission. This also ensures that only few parts will have to be re-designed and tested, and in general minimizes design-related cost and risk ([16]).

COTS seems to generally lower costs as they have low prices due to a competitive markets, which also results in high quality components. Furthermore, since the time necessary for development is shortened, the mission can be carried out faster, fewer costs will go to storage facilities and fewer tests has to be carried out.

Although COTS are not problem free and often they are not build to survive radiation-hardness levels and many products do not meet requirements. Which makes COTS a common issue when estimating space program cost ([16]). Another common issue for cost estimation is using small spacecrafts.

2.2.6.1.2 Small Spacecrafts Using small spacecraft results in potential for both reduced and increased cost of different areas. The reason for this is that the cost does not necessarily scale directly with size, as smaller spacecraft in general tends to be of higher complexity. Furthermore, they typically have higher launch-related cost, when considering cost per kg, but lower absolute cost. Smaller teams reduces labor cost and also ensure a more efficient communication which help reduce failures and therefore cost.

2.2.6.2 Methodology

To carry out cost estimation of a general space system or mission knowledge about similar mission and historical costs are necessary. All cost-estimation-methodologies comes with there own uncertainties, which affect the final budget and therefore needs to be quantified for a final cost budget.

Different cost estimating methodologies can be used, and we need to choose the most appropriate for the data we have available. All methodologies have different advantages and disadvantages and can also be used in combination.

The cost estimate for this space mission is very general due to lack of information on cost of components and equipment as well as cost of analogues missions, whereas the cost estimation has been done by combining the Analogy Method and Engineering Build-up Method.

Analogy Method, is based of comparisons, by considering cost of analogous systems and adjusting for differences to get an estimate ([15]). It is useful in the early design phase and to get rough estimates. This method is readily understood, quick and based on historical data, although it can be very difficult to identify an appropriate analogy.

Engineering Build-up Method, also called the Bottom-up, the project cost estimate is created by estimating the cost of every activity in a WBS, summing the estimates, and adding everything with an appropriate error-margin([15]). It provides great insight and high credibility but can be quite costly and with no information on cost drivers.

For the spacecraft and its subsystem the Engineering build-up method is mainly applied, but supported by typical cost, found by using a crosscheck method for navigation and experimental spacecraft cost compositions[16]. Using the Engineering build-up method is fairly simple as most parts for the subsystem is already-developed and tested components. The main change in this part of the budget is due to larger cost necessary for the ACS, as well as large uncertainties for the price. Taking the worst case, the cost of the ACS is doubled the amount of the first estimate, the price of this is what mainly drives the price of the spacecraft. The increase in cost is accepted as our budget already where on the cheaper part of the spectrum and since this system is necessary to ensure that the test of the XNAV system can be carried out correctly.

When the satellite has been assembled it needs testing, both environmental and mechanical test needs to be done. For this we are planning on using the testing facilities available at DTU, again to lower cost, and to use ESA's test facilities, ESTEC, in the Netherlands. We will need transportation to and from the testing facility, but these tests need to be carried out to reduce risk of our system not surviving launch or the environment in LEO. The costs hereof has been difficult to find whereas these are also estimated based on the analogy method for now.

Other parts of the mission, such as the development and operation, labor, safety and mission assurance etc. is estimated by using the Analog method and considering comparable systems and cost distributions found from NASAs Space Mission Budgets and the AMES Cost Model ([14]).

2.2.6.3 Cost Budget

The cost budget is created by combining results for the different methodologies. The total cost budget is illustrated in Figure 2.7 Based on this we get an upper limit for the cost budget om 4.8 Mio US dollars. This includes a margin of 10 % for all parts of the mission. The relatively high cost is just an upper limit as construction and salaries and development and operations mainly are carried out by ourselves, which limits the cost hereof. For the Ground data system, we planned on using DTU for the main part, whereas this cost also will be minimized greatly. Removing these areas from the budget we get a total cost estimate of $\sim 1 \text{ M \$ US}$.

The total cost estimate is well within what could be expected to be obtained by funding, which seems to be somewhere around 180 – 800 K US Dollars from a single Funding

Organisation, considering Grants from the UK Space Agency [17], Federal grants [18], National Space Grant Foundation[19], National Science Foundation [20], etc.

METHOD	Generic Cubesat cost	WBS project level cost	Engineering Build-up	Analogy	Combination
AOCS	2.6		100		100
EPS	2.6				2.6
TELECOM	14.95				14.95
MTS	11.18				11.18
ORBIT					
SPC		1193		246	128.73
PAYOUT		750	127		127
Project Management		874			
Systems Engineer		911			
Safety and miss. Assur		935			
Construction, salaries, etc		2720		166	1443
Development and assesment		1861			
Mission operation		777			
System integration and test		874			
Development and operation		3512		87	1799.5
Launch	500	935	300	300	300
Ground data system		874			874
				TOTAL	4800.96

Figure 2.7: Cost budget in USD showing estimations based on different methodologies ([14] [16]).

2.3 Analysis

In this section any performed analysis/ simulation model of the satellite is reported in the dedicated subsections.

2.3.1 Thermal Modelling

Thermal modelling is the process of creating a mathematical model to simulate the temperature distribution and heat transfer within a physical system. It is a valuable tool used in various industries to predict and optimize the thermal performance of a system. In this part of the report, we will focus on thermal modelling in the context of developing a CubeSat.

Matlab is utilized for the calculation of the steady state and transient thermal balance equations. These calculations were used during the design process as first estimate of the thermal design. The model assumes the satellite is a box with W6U cubesat dimensions made of an aluminum shell with specific heat 980 Nm/kg-K and internal components modeled as a solid block within the shell with a combined specific heat of 800 Nm/kg-K. This simplified model assumes that heat will be distributed equally throughout the satellite and is utilized only for pre-phase A design considerations. A more detailed model is not yet utilized due to time constraints, unknown orientation of the satellite throughout the orbit and unknown specific heats of all internal components.

The transient thermal model shows that the satellite will be kept within the desired thermal range throughout the entire orbit when passive and active thermal control systems are implemented.

The simplified model used here is limited in that it does not properly capture the conduction of heat between components or the heat distribution due to the orientation of the satellite with respect to radiating bodies.

Detailed Thermal modelling and Analysis in this project is done using ANSYS software [21]. The software uses mathematical equations to represent the physical properties of

the system, including material properties, boundary conditions, and heat sources/sinks. These equations are solved using numerical methods to determine the temperature distribution and heat flow within the system.

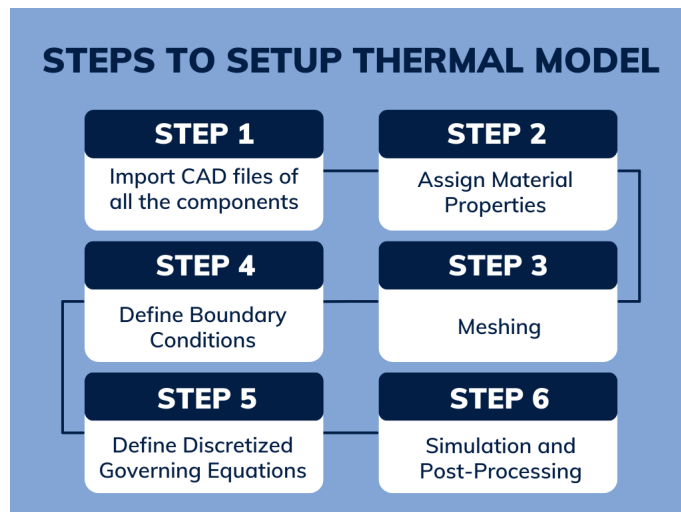


Figure 2.8: Steps involved in setting up Thermal Model

The thermal analysis software can then perform both steady-state and transient simulations to determine the temperature distribution and heat flow within the CubeSat. The steady-state simulation is used to determine the temperature distribution under normal operating conditions, while the transient simulation is used to determine the temperature response to sudden changes in the operating conditions.

The results of the thermal modelling are then analyzed to identify any hotspots or areas where the temperature is higher than the maximum allowable temperature for the components. Modifications to the design can be made to reduce the temperature in these hotspots and improve the overall thermal performance of the CubeSat.

Future iterations of the design process will utilize Ansys thermal modeling to create complex real-world like simulation which can be combined with data from orbit modelling to generate more accurate transient thermal distribution over the CubeSat.

2.3.2 Structure Modelling

For the structural modelling, SolidWorks has been used. In SolidWorks, it is easy to move the different subsystems in compared to each other and try some different placements. This program also makes it easy for the other subsystems to see where we think their components can sit and if it fits with their requirements.

In SolidWorks, each part can get a material and a mass. From this, it can provide the Center of Mass (COM) for the structure. This is been used to see if it keeps the requirements and as information to the other subsystems. If we had more time a vibration test would be made. To do this all components should be connected correctly and a lot of small parts were needed.

2.3.3 Orbital Modelling

For initial guesses and estimates of orbit parameters using simple Keplerian orbits, Matlab and Python have been used. To perform educated estimates of orbit parameters, Ansys

Government Initiatives (AGI)'s Systems Tool Kit (STK) software has been utilized. From the modeling and simulation results parameters such as orbit lifetime, number of orbits, time spent in the Earth's shadow and others have been found in order to provide a set of constraints for the remaining teams. A more detailed specification of the models used within the software is described in sections 3.4.3.1 and 3.4.3.2.

A simplified drag area estimation model was created using Matlab to calculate the projected area of the spacecraft, given a part of the set of pulsars to be observed within the mission lifetime.

2.3.4 Attitude Modelling

Python script with data from astronomical tables was used to determine the pointing direction with reference to the Earth reference frame. Matlab simulations has been carried out for de-tumbling requirement testing, with Runge-Kutta-1 iterative methods.

2.3.5 Radiation Modelling

During the mission's lifetime, the spacecraft will be subjected to hazardous ionizing radiation from different sources. The section 2.4 aims to analyse such sources, their severity and impacts upon the final design. The software used for the simulations presented here is ESA's SPace ENVironment Information System (SPENVIS). The sources and the standards followed for them are listed below:

- Trapped protons and electrons (AP-8 & AE-8)
- Solar particle fluences (95% confidence interval)
- Solar particle peak fluxes
- Galactic cosmic ray fluxes

2.4 Radiation Tolerance Provisions

The reasoning behind the analysis of the space environment is to assess the survivability of the spacecraft and estimate performance impacts on its instruments in harsh environments. To judge these factors, two scenarios are considered:

- Total Ionising Dose (TID), is a term used to describe the long-term degradation of the electronics present in the spacecraft (S/C). The electronics degrade due to the accumulation of ionizing defects in the material. This may cause current leakage and functional failures, among others. The main causes include the trapped protons and electrons, and solar protons [22].
- Single Event Effects (SEE) result from ionization by a single charged particle as it passes through a sensitive and critical junction of an electronic device. SEE are caused by heavier ions, but for some devices, protons can also contribute [22].

2.4.1 In-orbit radiation environment

The selected orbital trajectory selected for PANTSat's deployed operations phase presents an attenuating factor with regards to the harshness of the radiation environment. The relatively low altitude and circular orbit ensures limited exposure to the Van Allen belts of trapped particles. Additionally, Earth's magnetosphere provides significant protection against solar particles. On the other hand, the inclination of the orbit periodically exposes the spacecraft to the South Atlantic Anomaly (SAA), a region over the South Atlantic Ocean where the Earth's inner Van Allen radiation belt comes closest to the planet's surface, resulting in a higher-than-normal concentration of energetic particles. This exposure

produces a significantly higher flux of charged protons, as can be seen from Figure 2.9 below.

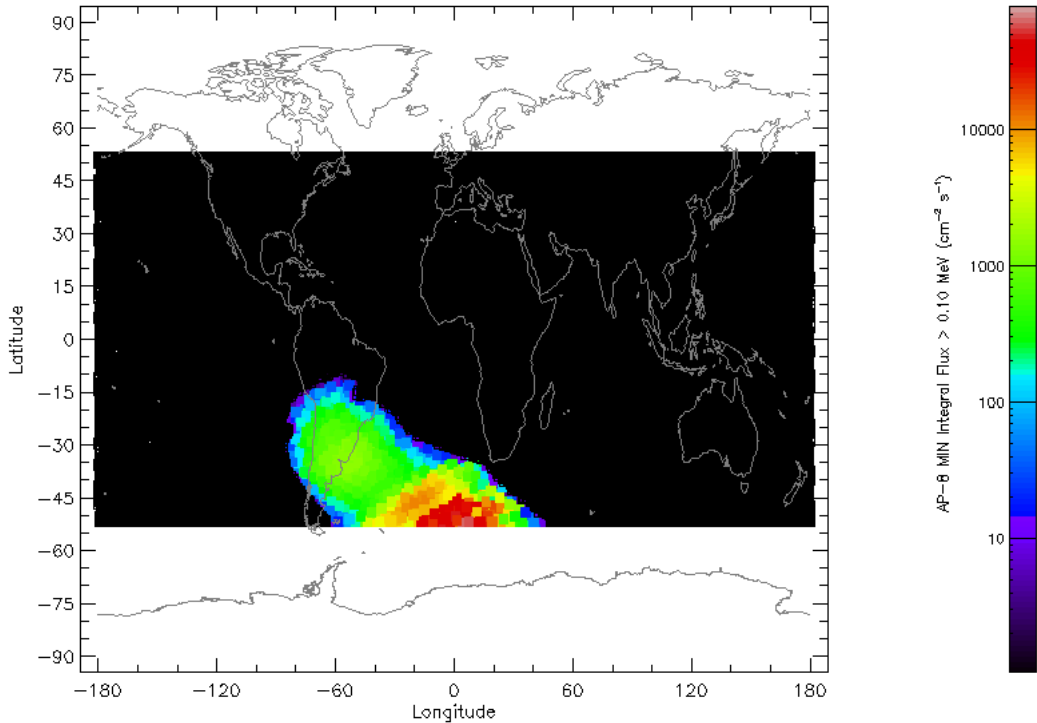


Figure 2.9: Flux map of charged protons above 0.1 MeV for PANTSat's orbit ($\text{cm}^{-2}\text{s}^{-1}$).

Table 2.7 below summarizes the contribution from each of the sources in terms of energy and particle flux for PANTSat's orbit.

Radiation Source	Energy (MeV)	Flux (particles/ cm^2/s)
Trapped particles		
- Protons	0.1 - 100000	5.93 - 0.15
- Electrons	0.04 - 3.75	54.94 - 0.03
Solar energetic particles	0	0
Galactic cosmic rays (from H to U ions)	$(1 - 100,000)*N^a$	0.13 - 0.004

N^a : Number of nucleons.

Table 2.7: Summary of sources of radiation, their energy and Flux at 422 km altitude, 51.6° inclination.

2.4.2 Total Ionizing Radiation (TID)

Based on the radiation environment specific to PANTSat employing the models associated to the different radiation sources, we can estimate the received ionizing dose over a period of time. There is an interest in including as many off-the-shelf components in PANTSat's design. Commercial components are notably less rad-tolerant than dedicated space-rated hardware, and can withstand anywhere from 2-10 krad [23]. The assumed radiation hardness level for such components was 2 krad. Envisioning a mission duration of possibly two years in the early development stage, a requirement was put forth,

specifying that the TID per year inside the S/C should not surpass 1 krad.

The TID was calculated through SPENVIS's SHIELDOSE-2, which determines the absorbed dose as a function of depth in aluminum shielding material of a spacecraft, expressed in a graph called the *dose-depth* curve. This curve specifies the expected TID only for isotropic shielding of a simple geometry such as an aluminum solid sphere. Figure 2.10 below shows the dose depth curve of PANTSat's orbit over a period of three months.

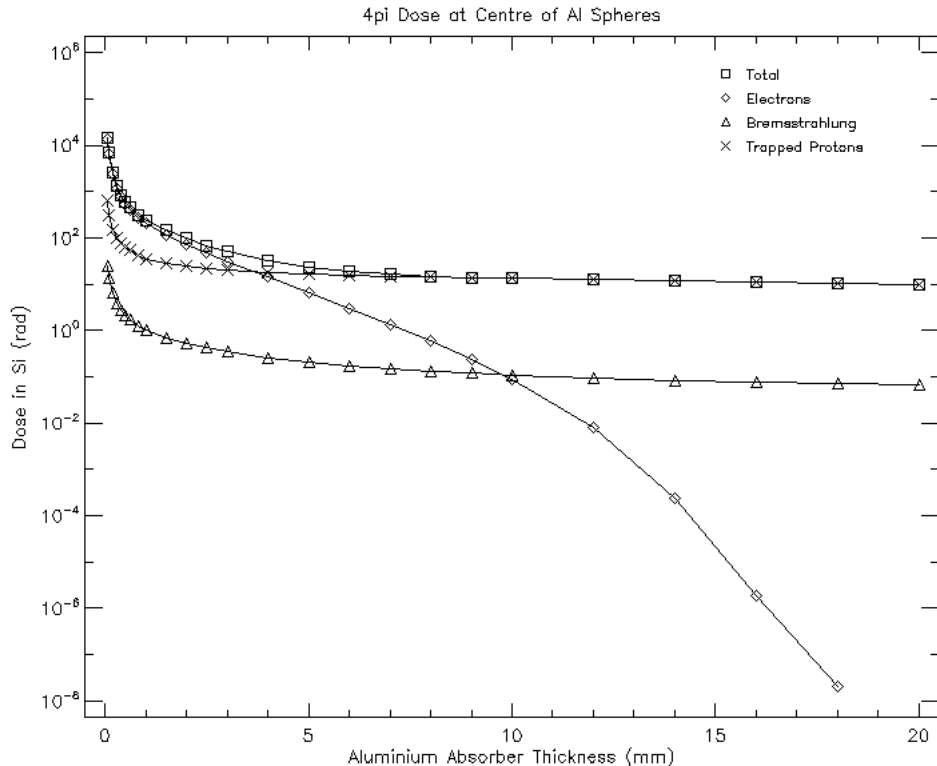


Figure 2.10: Dose-depth curve for PANTSat's orbit over the period of three months.

It can be seen from Figure 2.10 above that trapped protons contribute to most of the total dose, and that the maximum TID over one year would be 14 krad with zero shielding. Far surpassing the assumed radiation hardness of 2 krad. However, a shielding equivalent to 2.5 mm of aluminum can reduce the total dose by orders of magnitude to ≈ 1 krad, with sharply diminishing returns in protection with thicker shielding.

In order to calculate TID in an anisotropic shielding like most spacecraft, the Sector Shielding Analysis Tool (SSAT) was employed. SSAT is able to determine the shielding distribution of a spacecraft using the ray-tracing method at a user-defined point within the spacecraft. Specifically, SSAT divides the shielding structure into small angular sectors, called the direction windows, in terms of polar angle θ and azimuthal angle ϕ , with respect to all 4π solid angles. Figure 2.11 shows the concept of direction window as implemented in SSAT. At the origin of the polar/azimuthal angles is a fictitious *geantino* particle, which undergoes no physical interactions, but flags boundary crossings along its straight trajectory. Knowledge of the positions of these boundary crossings, together with the density of the material through which the particle has passed can be used to profile the shielding for a given point within the spacecraft.

The TID at the location of the *geantino* particle can be calculated by summing the ionizing does values that penetrated through every shielding sector, i.e the *direction window*. This can be written in an equation as follows [24]:

$$TID = \sum_i \frac{F_i(t)d\Omega_i}{4\pi} \quad (2.1)$$

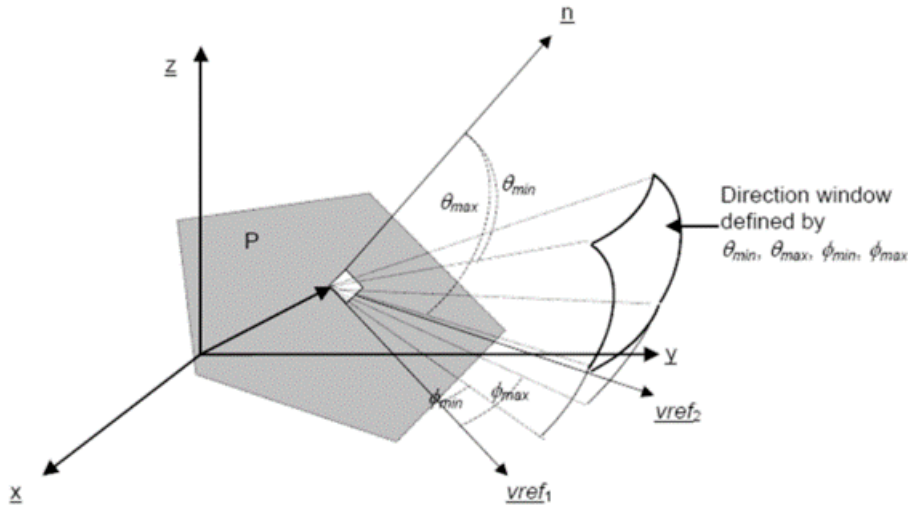


Figure 2.11: SSAT's direction window for calculation of shielding distribution [25].

Where $F_i(t)$ is the absorbed dose for a given thickness t (taken from the dose-depth curve), $d\Omega_i$ is the differential solid angle of the shielding sector, and i is the index associated with each sector. For our simulation, we divide the spacecraft into 1800 shielding sectors (40 polar sectors and 45 azimuthal sectors).

The anisotropic TID was calculated for each of the subsystems in PANTSat at the center of their enclosures, assuming a spacecraft at its deployed configuration and with a shielding of 2.5 mm of aluminum. The mass and dimension figures for each component were taken from the project's component list to provide an approximation of the densities of each subsystem. Figure 2.12 shows the anisotropic shielding simulation results in PANTSat for the period of one year.

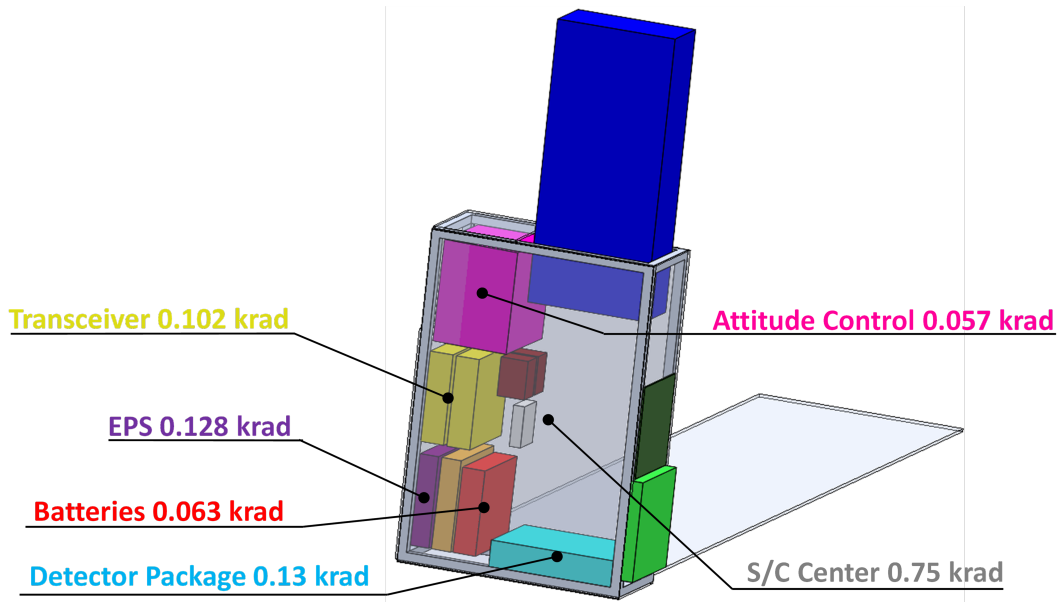


Figure 2.12: Dose results from the anisotropic shielding simulation (dosage values are for a period of one year in orbit).

From the results, we can see that the subsystems that are sandwiched by others receive the lowest dose. Naturally, the center points of each subsystem are expected to receive less cumulative radiation as compared to locations near the edges, and these figures should be taken as a baseline to guide more specific design considerations for radiation mitigation. Additionally, it can be noted that the center of the spacecraft itself receives the highest dose. This is because all other calculation points enjoy the additional protection of their own enclosures, while the center is a "free floating" point within the spacecraft that is protected only by the outer aluminum, and by the other components at certain direction windows.

2.4.3 Single Event Effects (SEE)

SEE happen randomly by nature and hence are more difficult to predict. There are mainly three categories of SEE, which can be transient or permanent [22]:

- Single Event Update (SEU): changes in the state of memory elements.
- Single Event Latch-ups (SEL): short circuits caused by a single energetic particle; may cause permanent damage if not mitigated.
- Single Event Burnouts (SEB) and Single Event Gate Ruptures (SEGR): destructive events most common in power MOSFETs.

The incidence of SEE correlates with a quantity called the Linear Energy Transfer (LET), which describes how much energy an ionizing particle deposits into a matter per unit distance. A simulation run on SPENVIS's CRÈME software [25] (Figure 2.13), shows the flux spectra as a function of LET values on Silicon material for PANTSat's orbit. According to tests conducted by [26], the sensitivity of a component to an SEL can range from LET values from $1,000 \text{ MeVcm}^2\text{g}^{-1}$ to above $50,000 \text{ MeVcm}^2\text{g}^{-1}$. This means that PANTSat is subjected to SEL and possibly other kinds of SEE.

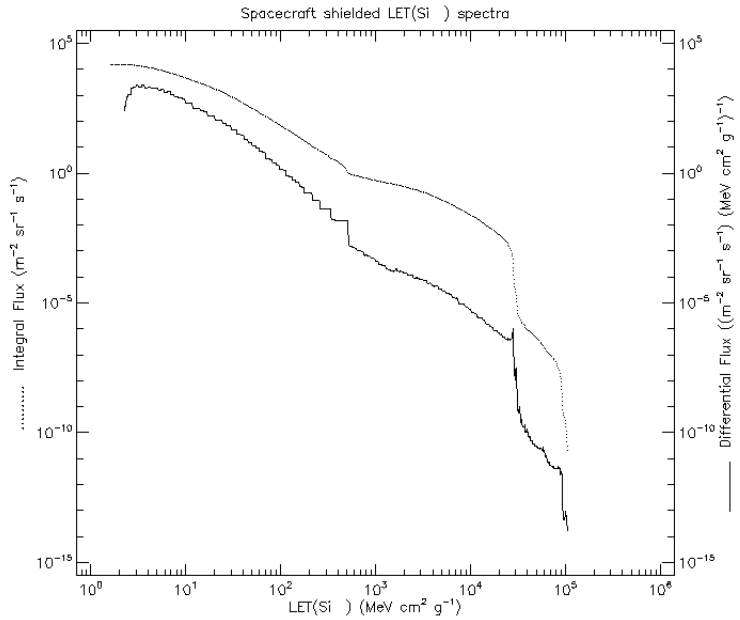


Figure 2.13: LET spectra along PANTSat's orbit.

Due to the damaging nature, SEE have to be taken into consideration. Mitigation techniques called Fault Detection, Isolation and Recovery (FDIR) have to be implemented on board every satellite during the design phase. For PANTSat, some low-level FDIR should be implemented. These are primarily tasked with protecting system from SEL and to restart parts that fail in an unrecoverable way due to other SEE:

- Autonomous de-latch circuit
- Hardware watchdog circuit
- Software watchdog timers

3 Sub-System Design Definition

This chapter includes detailed specifications of each sub-systems including the payload and trajectory analysis of PANTsat. Each subsystem description includes its capabilities and a short justification for the chosen design. Block diagrams and schematic descriptions of key features and interfaces are also presented.

3.1 Payload

The following subsections focus on selecting an optimal payload for the purpose of technology demonstration within the requirements of the project and the limitations of other subsystems. First, the working methods and the selection of the optics, detectors, and the clock are described. Then the data files, data transfer, and data processing are described. A trade-off analysis of mounting options is performed, and a characterization of pulsars is given. Finally, the requirements for other subsystems from the payload are presented.

3.1.1 Polycapillary Optics

Polycapillary optics are arrays of small hollow glass tubes. X-rays are guided down these curved tubes by multiple reflections, analogous to how optical fibers guide light. Beams coming from thousands of channels will overlap and converge to a small spot at some distance from the exit of the optic where a detector is placed. The benefit in general of using focusing X-ray optics rather than just a detector is the signal-to-noise advantage. The X-ray flux is focused onto a small detection area which greatly reduces the background and dramatically improves the signal-to-noise[27]. Polycapillary X-ray optics generally result in an efficient collection of X-rays, however, they do not produce submicron beam spot sizes like the big imaging X-ray telescopes. This is however not an issue for this application, since only the counting of photons is important.

Polycapillary optics serve for multiple applications where the manipulation of a beam of X-rays is needed. Planetary Instrument for X-ray Lithochemistry (PIXL) features a polycapillary optics package to perform X-ray fluorescence for spectroscopy studies of Martian soil. The idea of the pulsar X-ray receiver for this application is to use PIXL high-heritage polycapillary optics to focus a parallel beam coming from an X-ray pulsar in space down to a small spot where the photons are detected. To make the design as compact as possible, the spot size shall ideally match the active area of the detector.

The X-rays can be transmitted down the tubes as long as the angles of incidence are smaller than the critical angle for total external reflection. A typical material for the tubes is borosilicate glass which has very high durability due to its low coefficient of thermal expansion. This means that it does crack during extreme temperature changes, and is a good material to shape thermally. It makes very precise optical surfaces that change very little with temperature. The critical angle for borosilicate glass is energy dependent and is approximately

$$\theta_c \approx \frac{30\text{keV}}{E} \text{mrad.} \quad (3.1)$$

For example, for a telescope like NICER, designed to reflect X-rays up to 12 keV, the critical angle at the maximum energy is $\theta_c \approx 0.14^\circ$.

The tubes must be designed such that the maximum angle of incidence is below the critical angle of the maximum energy to be transmitted. The maximum angle of incidence is controlled by the diameter and the radius of curvature of the tube

$$\theta_{max} \approx \sqrt{\frac{2c}{R}} \quad (3.2)$$

where c is the tube diameter in m , and R is the radius of curvature in m [28]. The tubes must be extremely narrow at the order of μm and only slightly bent to comply with the small grazing incidence angles required for X-ray optics. The PIXL poly-capillary optic is shown in Figure 3.1 to illustrate the extremely narrow tubes required.

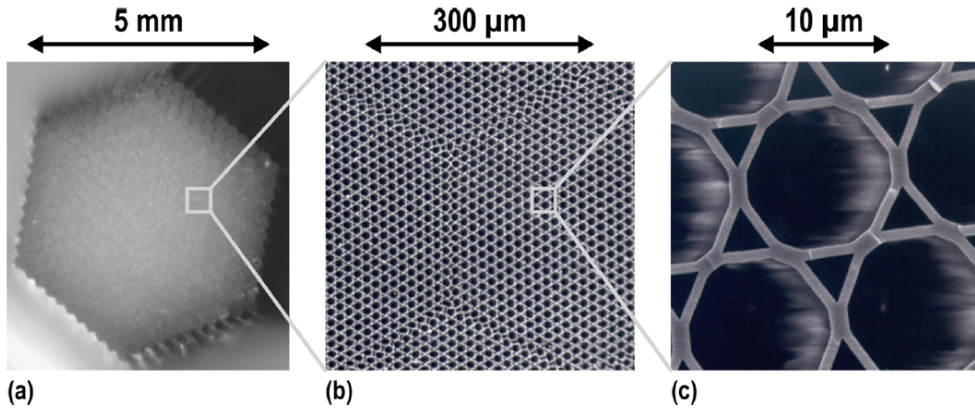


Figure 3.1: X-ray polycapillary optic used for PIXL. (a) The end of the optic. (b) A blowup of a small section of the optic. (c) High magnification image of individual capillary tubes. Credit: [29]

3.1.1.1 Design Drivers

Dr. Robert Sharrow and his team recognized two design parameters that most significantly affect navigation accuracy: the aperture size and the field of view. The aperture size should be large to collect many photons. The collecting area can further be increased by using an array of optics and detectors. For instance, NICER used an array of 56 optics. The Field of view (FoV) should be small to reduce noise entering the system. The beam coming from the X-ray pulsar will be collimated while the unwanted background radiation will be omni-directional and uniform. Background radiation entering at an angle higher than the angle-of-acceptance (half the FoV) will be absorbed. The FoV can be decreased by installing an angular filter optics package in front of the focusing optics which reduces the angle at which X-ray noise can enter the system.

3.1.1.2 Optics Selection

Dr. Sharrow and his team analyzed and modeled 3 different pulsar navigation instruments of 3 different aperture sizes (2 cm, 4 cm, and 10 cm in diameter), with and without an angular filter package installed. The 3 optics without the filter have an angle-of-acceptance of 0.5 deg (FoV = 1 deg). However, the optics supplier XOS successfully built a compact angular filter element that reduces the angle-of-acceptance by a factor of almost 10, to 0.06 degrees (FoV round up to ≈ 0.2 deg in the graph). This dramatically increases the Signal-to-Noise Ratio (SNR) by ≈ 100 . The simulation of the performances of the optics is shown in Figure 3.2. It shows the convergence of a pulsar navigation solution as the root sum square (RSS) position error in [km] as a function of observation days for each optic in pairs of two. The light blue curve shows the performance of a NICER element for comparison. The analysis by Sharrow et al. indicates that a 10 cm diameter optic of 20 cm length is the most optimal size to support pulsar navigation. The length of the angular

filter of ≈ 70 mm should be added to this as well. Figure 3.2 shows that the "2 x 10 [cm] FoV 0.2 [deg]" optics performs better than a NICER element, cutting the RSS position uncertainty to only 18.4 km.

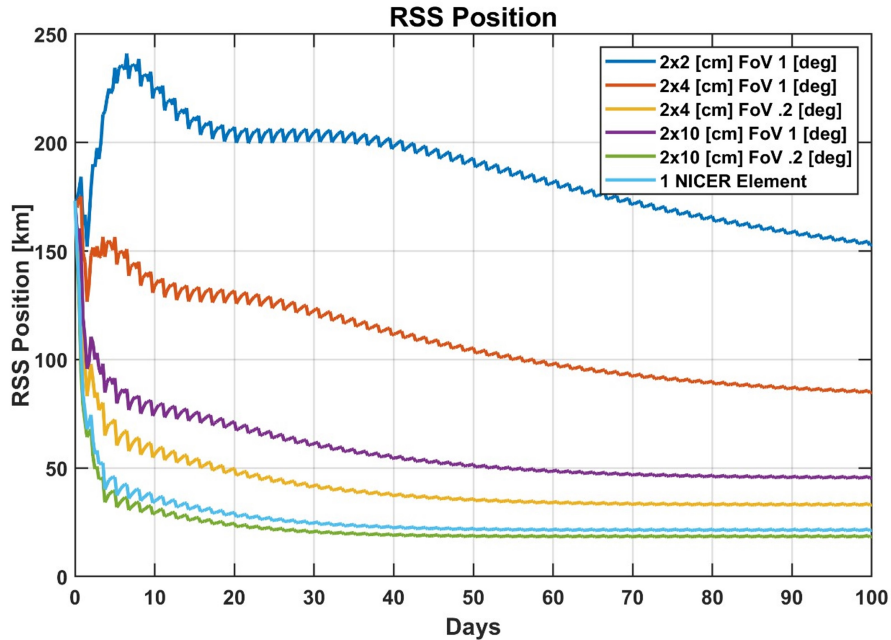


Figure 3.2: Simulation results of pulsar navigation solutions for three different optic apertures with and without an angular filter package installed. The light blue curve shows the performance of a NICER element for comparison, which converges to a solution of 21.4 km. Credit: Robert Sharrow et al. [30]

However, the size of the optics put a strong constraint on their practicality. The focal length of all 3 optics is 500 mm for the best focus of 3 mm [31]. The best focal spot is thus independent of the diameter of the optics [32]. This brings the challenge that the focal length for the best focus in all cases exceeds the dimensions of the W6U. How to mitigate this is later discussed in subsection 3.1.5 when different mounting options are described. Nevertheless, the optics modules themselves must fit within the spacecraft during launch. The selection of the optics was therefore made in close dialogue with especially the mechanical sub-team. The dimensions of the biggest optics are simply not possible to fit in the W6U cubesat. Therefore, the more practical optics package of 2 x 4 cm arrays with a FoV of 0.12 deg is chosen, which performs second best in the simulation (yellow curve) compared to a NICER element. It converges to a position uncertainty of 33 km. Moreover, this optics has successfully been developed and prototyped by Sharrow et al, which increases its flight-readiness. The prototype was manufactured by XOS and has an aperture diameter of 3.5 cm and a length of 6.5 cm. Note, that the 4 cm diameter optics in the simulation is interpreted as a round-off of the in fact 3.5 cm diameter optics, and the FoV of 0.2 deg in the graph is a round-up from 0.12 deg. Pictures of the optic package are shown in Figure 3.3.



Figure 3.3: Left: 3.5 cm diameter x 6.5 cm long polycapillary optic package with alignment features to mount an angular filter. Right: angular filter element of ≈ 70 mm length. Credit: [30].

The optic is sketched and its dimensions are outlined in Figure 3.4. The design can be made more compact by decreasing the focal length to $f = 422$ mm to achieve a focal spot corresponding to the active area of the detector, assuming that the exit aperture equals the entrance aperture. The optics package of two units has a mass of 3.3 kg and draws 3-5 W. The instrument will require pointing, and since the optic accepts X-rays within the angle-of-acceptance of 0.06° , the pointing should be controlled to half of that [31]. The pointing requirements if thus $< 0.03^\circ$. Slewing times should be minimized to maximize the observation time on targets. The parameters are summarized in Table 3.1. Since this optics is significantly bigger than the one used for PIXL, it has a TRL of 4. The next step is thus to test the component in a relevant environment. An environmental flight-unit could be flown as-is.

3.1.1.3 Minimum observation time

The small cycles on each graph in the simulation in Figure 3.2 show a drop in uncertainty during the gap of measurements when maneuvering between pulsar targets and acquiring the signal. The new geometric information then allows the solution to converge to lower uncertainty. Each pulsar is observed for ≈ 1 day. A minimum of 4 pulsars are required for the best performance. The level 1 requirement of the mission is to demonstrate one XNAV solution. Based on the simulation, it is estimated that 20 days of accumulated observation of a minimum of 4 pulsars is adequate for demonstrating one XNAV solution, which would have ≈ 50 km RSS position uncertainty according to the yellow curve. Constant integration of measurements is not required, and the measurements may be disrupted by eclipses as long as the accumulated integration time is greater than the minimum required observation time.

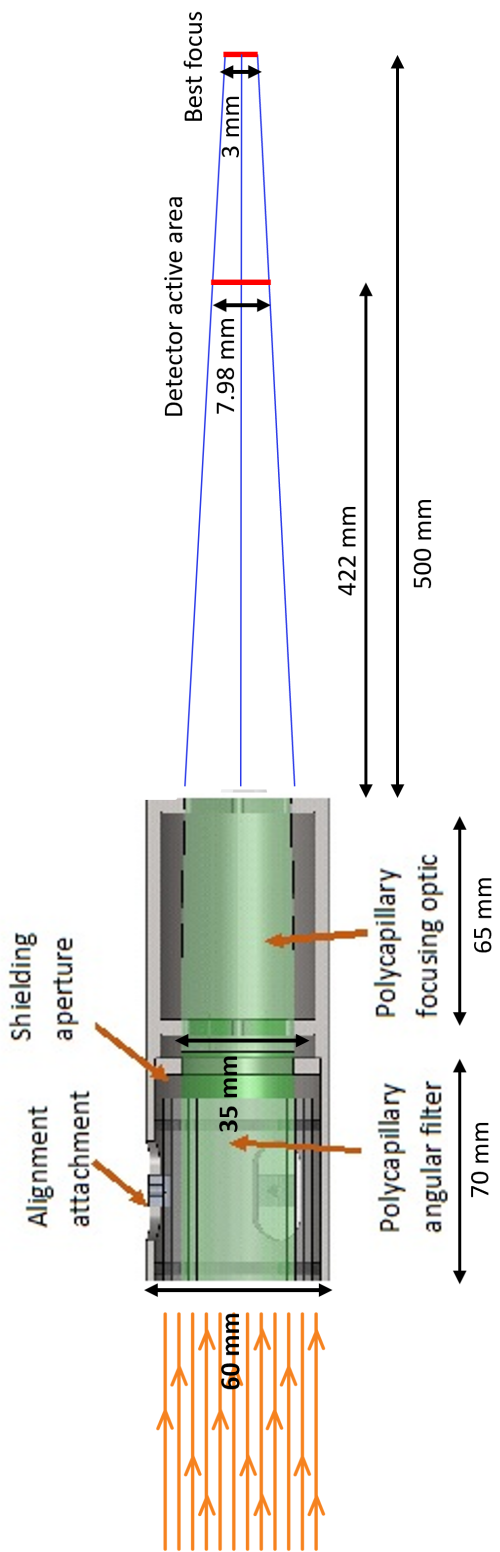


Figure 3.4: The sketch is modified from Robert Sharow et al. It shows the optics with its dimensions outlined. The dimensions are estimated using information from [31] and [30]. The length of the angular filter is estimated from Figure 3.3. The reduced focal length is calculated from geometry considerations. Note: The dimensions are not correctly scaled with respect to each other, the figure is only for illustration purposes.

Parameter	Value
Length of focusing optics + angular filter	135 mm
Optics aperture diameter	35 mm
Optics enclosure diameter	60 mm
Focal length (best focus)	500 mm
Focal spot (best focus)	3 mm
Focal length (matching detector)	422 mm
Focal spot (matching detector)	7.98 mm
Angle of acceptance	0.06 deg
FoV	0.12 deg
Mass (2 units)	3.3 kg
Power (2 units)	3-5 W

Table 3.1: Parameters for the optics package. The information is retrieved from [31] and [30], and the reduced focal length is calculated from geometry considerations. In case the information was ambiguous, the most restrictive limit was chosen.

3.1.2 X-ray Detectors

At the X-ray wavelengths of the Pulsars' emission, the measured components of the emitted signal are the individual photons released in the source's energy discharge. The observed profile is created via the detection of these photons from the source as they arrive. The typical energy range associated with the X-ray emission from the Pulsars targeted by this mission is approximately 1 to 12 keV. Figure 3.5 below shows the light curve at 5-8 keV from the Crab Pulsar, an extensively studied X-ray Pulsar.

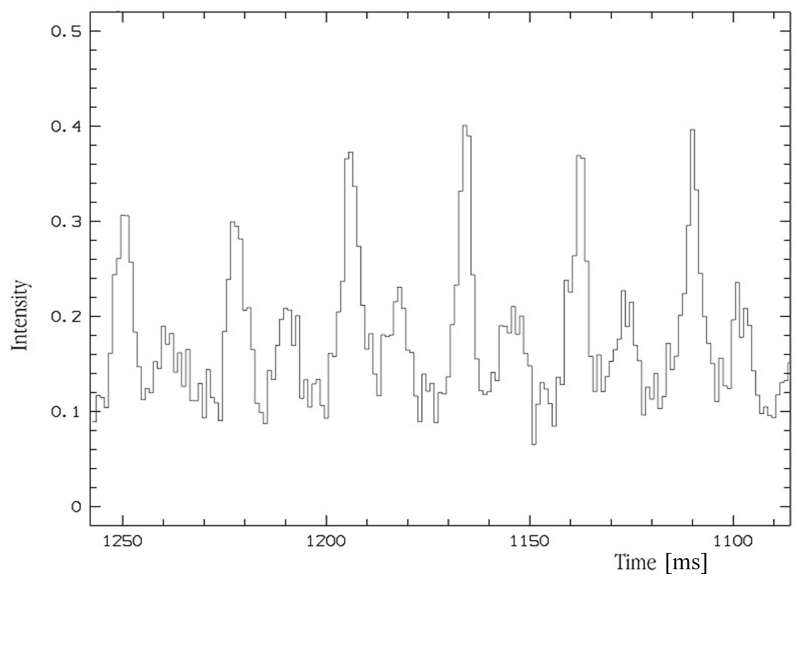


Figure 3.5: X-ray light curve of the Crab Pulsar at 5-8 keV. Image credit: European Southern Observatory.

The first step in generating the pulse profile is to detect the onset of photons from the source above the nominal X-ray background signal. For this application, no imaging capabilities are required. Instead, Solid-State Semiconductor detectors sensitive to the emission's energy range and sufficiently fine timing resolution are adequate. It has been demonstrated that, in order to produce an accurate position determination system, a timing resolution in the order of a microsecond is required. For the case of PANTSat's technology demonstration of X-ray pulsar navigation, a pair of Silicon Drift Detector (SDD) is adopted, each aligned with the Polycapillary optic elements.

A SDD consists of a thin silicon wafer with multiple concentric ring electrodes on one side and a common electrode on the other side, where an applied voltage creates an electric field that sweeps charge carriers (electrons and holes) to the center of each ring, where the charge is collected and converted into an electrical signal that is proportional to the energy of the X-ray photons that were absorbed in the detector material.

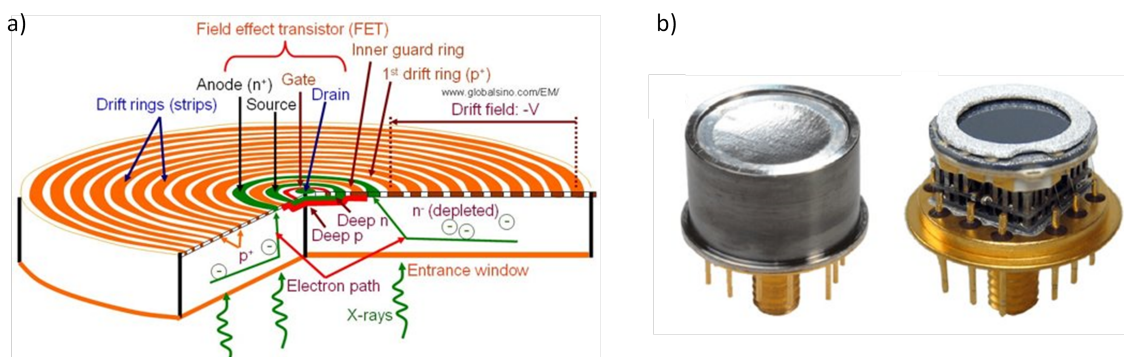


Figure 3.6: a) Conceptual illustration of a Silicon Drift Detector. b) Ketek H50 SDD. Image credit: Ketek

The detector package leverages a direct heritage from the Planetary Instrument for X-ray Lithochemistry (PIXL) [29] aboard the Perseverance rover, consisting of two Ketek H50 VITUS SDDs, shown in Figure 3.6 above.

As is the case for all SDDs, the sensitive silicon chips need to be operated at significantly low temperatures of -60 to -20°C. The H50 detectors achieve this operating range through built-in Peltier elements for active cooling, also called Thermoelectric Coolers (TECs).

Following the SDDs, PANTSat also inherits a similar design of the instrumentation electronics from PIXL.

3.1.3 On-board reference clock

Accurately measuring the photon time of arrival is essential to pulsar-based navigation. Much like for GNSS satellites, a highly precise internal reference clock with atomic clock precision is therefore required. The payload will therefore include a SA.45s Space Chip-Scale Atomic Clock (CSAC) from the manufacturer Microsemi [33]. This choice of clock is especially suited for this mission due to its low footprint ($< 17 \text{ cm}^3$), low mass (35 g), low power consumption ($< 120 \text{ mW}$) and a high radiation tolerance of 20 krad, which should make it last well beyond the expected lifetime of the mission. Most importantly, it has an accuracy of $\pm 5 \times 10^{-11} \text{ s}$, which as previously mentioned is crucial for XNAV. Having a dedicated reference clock integrated directly in the payload rather than e.g. simply using the one in the on-board computer has two major advantages: first, it ensures that the clock is suitably accurate. Second, it helps further integrate the payload subsystem into a complete package. The more "plug and play" the payload, the more useful it will be as a proof of concept while also providing more heritage for future missions utilizing the concept. The SA.45s Space CSAC used can be seen in Figure 3.7, showing its small footprint.



Figure 3.7: Microsemi SA.45s Space CSAC integrated with the payload. Coin for scale reference.

3.1.4 Data Files and Data Transfer

As mentioned earlier, the measurements made by the PANTSat payload will be single detections of X-ray's and other events which gets telemetered to ground when the orbit allows for it. Since each event only contains a single measurement they can be characterized by a time stamp, a pulse height amplitude, and the detector in which the event was detected. An event may be an X-ray photon from the sky, energy deposition from a particle, or a signal originating in the detector electronics. In the end these results would end up in HEARSAC which is a NASA archive that serves as a repository for astrophysics data in the high-energy range, such as X-rays and gamma rays. [34]. They are a resource for the astrophysics community to access and share data, and to support research and discovery

in the field. They have ideal conventions for data-formats as described by "The Proposed Timing FITS File Format for High Energy Astrophysics Data" [35]. Therefore when describing the properties of each detected event, we want to record them as binary tables in a FITS-format. There are 4-different default conventions described by HEARSAC which are: Event, Equally Spaced, Unequally Spaced, and Packet. Since our payload will measure single photons we will follow the guidelines specified for an events-list where each row in the FITS binary table extension corresponds to a single event. In our case we have opted for a TIME, ENERGY and ERROR column as can be visualized in figure 3.8.

When it comes to Timing it is standard procedure for X-ray telescopes to reference elapsed Terrestrial Time (TT) in days since the launch of the mission[34]. The ENERGY-column will present the energy of the photon which instigated each event, measured in keV, while lastly the ERROR column will include the error on these measurements also measured in keV. Included in the FITS file there will be a header which has some minimum set of keywords that should be supplied as described by HEARSAC. These includes both descriptive keywords and time definition keywords. The descriptive keywords provide general information about the FITS file, including the type of file (RATE or EVENTS), the mission or telescope name (TELESCOP), the instrument name (INSTRUME), the object observed (OBJECT), the Right Ascension (RA) and Declination (DEC) of the source and lastly proposed scheme for time definition. In our case we will go with the standard use of the Modified Julian Date (MJD) for the reference time. So much more information can be included into the FITS-header but for this technology demonstration of X-ray pulsar navigation a appropriate choice would be to include around 50 headers. A visualization of this can also be seen on Figure 3.8.

TIME	ENERGY	ERROR
Select All	1D d	1E keV
1	1.136733217595E+03	1.107495E+02
2	1.136734375003E+03	1.144522E+02
3	1.136735532410E+03	1.145109E+02
4	1.136736689817E+03	1.095571E+02
5	1.136737847225E+03	1.147926E+02
6	1.136739004632E+03	1.089948E+02
7	1.136740162040E+03	1.087064E+02
8	1.136741319447E+03	1.101730E+02
9	1.136742476854E+03	1.151152E+02
10	1.136743634262E+03	1.163567E+02
11	1.136744791669E+03	1.035959E+02
12	1.136745949077E+03	1.117107E+02
13	1.136747106484E+03	1.112031E+02
14	1.136748263891E+03	1.100757E+02
15	1.136749421299E+03	1.126435E+02
16	1.136750578706E+03	1.127710E+02
17	1.136751736114E+03	1.095074E+02
18	1.136752893521E+03	1.091928E+02
19	1.136754050928E+03	1.120376E+02
20	1.136755208336E+03	1.109635E+02

Figure 3.8: Left) Visualization of headers included in FITS-file. Right) Visualization of event-list format for FITS-files according to HEARSAC convention

The telecommunications subsystem allowed 11 MB/orbit of data transfer for our payload which is a lot. By the nature of our optics and the fact that we only have two detectors, we actually do not expect a particularly high count rate from our sources. Rob Sharow and his team estimated the count rate to be around 100 counts/min depending on the source which is a lot lower in comparison to the full energy range count rate in the order of 10^3 with the NICER telescope which has also been used to test XNAV [36].

Even though this makes the convergence time for position determination slower it does have an upside when dealing with data transfer. If we estimate 4 bytes for each value of TIME, ENERGY, and ERROR we end up with 12 bytes per event. At 100 events per min and a ISS-like orbit period of 90 min that gives us around 110kB/orbit of data transfer, also included the 50 headers of each 4 bytes also. A table of these results and a best-case and worst-case scenario for the data transfer is shown in the following table:

	C_{rate} [c/min]	Orbit [min]	Data rate [kB/orbit]	Data-redundancy
Best-Case	75	≈ 90	≈ 80	$\approx 99.3\%$
Average-Case	100	≈ 92.5	≈ 110	$\approx 99\%$
Worst-Case	125	≈ 95	≈ 145	$\approx 98.5\%$

Table 3.2: This table shows three cases of expected data transfer rates for the payload and the resulting data redundancy

The main takeaway from the table and calculation of both the best-case and worst-case scenarios is that in every case, we are far under the limit set by the telecommunications subsystem. These data rates are also present in the link budget, Table 2.3. Even in the case of calibration, communication with instruments, and updates we still have around 80%-70% of our data transfer limit in redundancy which is a very comfortable stance to be in.

3.1.4.1 Data processing and Background Count Rate

The described events will afterward be cleaned and calibrated by a processing pipeline similar to "nupipeline" or "nicerl2" each for the NuSTAR or NICER telescopes [37]. In the case of the PANTSat-mission we have identified 4 physical phenomenons we should address when cleaning and processing our data and they are:

- **Background Count Rate**
- **South Atlantic Anomaly (SSA)**
- **Dark currents**
- **Low energy noise**

When measuring Time of Arrival (ToA), a Poisson noise is introduced due to various causes, including background X-ray sources. These background sources are defined by the FoV of the instrument and the system's imaging or concentrating performance and include flux from diffuse X-ray background and nearby sources. By reducing the Field of View, such contributions can be lessened, albeit requiring a more precise pointing system. Additionally, any unpulsed flux from the pulsar source creates an infinite background.

High-energy photons or particles that arrive at the detector via a path other than the optical path can interact, resulting in spurious events that add to the background. The rate varies

with the spacecraft's movement through its orbit and solar activity but is expected to be 0.05 counts/s. The occurrence of interfering background events and flares due to charged particles was investigated, and is presented in section 2.4. Taking these background-induced events into account in the data pipeline is therefore essential.

The SAA is a region above the South Atlantic Ocean where the Earth's magnetic field is weaker than usual, allowing more charged particles from space to penetrate the atmosphere and reach the Earth's surface. These high-energy particles can interfere with sensitive electronics and produce non-cosmic background noise, which can corrupt our data and lead to misinterpretations [34]. Therefore, it is important to take the SAA into account when processing data. By filtering times based on the knowledge of our instrument's position relative to the SSA, we can ensure that there is high-quality data while also avoiding interference from the charged particles. Proper care and attention should specifically be given to data taken near the SAA region to prevent the miscommunication of non-valid scientific data.

When the instrument has been in orbit for a longer amount of time radiation damage will slowly increase the number of dark current in the SDDs[34]. Dark currents are defined as electrical current that flows through a detector when no light is present and these currents can become a problem for us because they can produce false signals that can be misinterpreted as actual scientific data. To combat this we will introduce a regular routine of dark frames, where we focus our instrument on different patches of the sky with no X-ray source. Here we will be able to identify if any dark-currents are present and make sure to calibrate for these when extracting our scientific data.

Lastly, we have low energy noise. This will not necessarily be the biggest obstacle for the PANTSat-payload as its effective energy-band is close to 1-12 keV but for data taken during orbit day, the low energy noise peak may intrude into the low energy band. We should therefore be careful about interpreting events in the ranges of $0.5 \text{ keV} \leq E \leq 1.5 \text{ keV}$.

3.1.5 Mounting

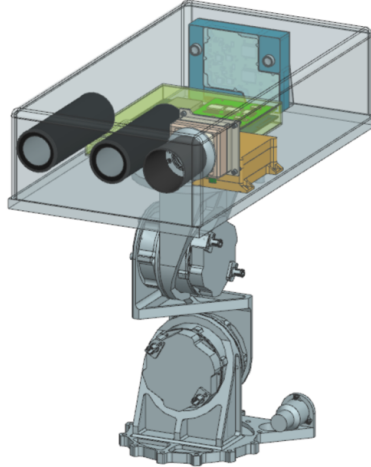
Proper mounting of the payload is essential to its performance, and the optimal solution must be balanced between the mechanical and ADCS teams in particular. The mounting platform should comply with the dimensions of the optics and its optimal focal length $f = 422 \text{ mm}$ while offering high stability and pointing accuracy better than 0.03° . Four different concepts were discussed: a gimbal platform, a rotating disk and hinge, direct mounting on the spacecraft body, and an extendable boom.

3.1.5.1 Gimbal platform

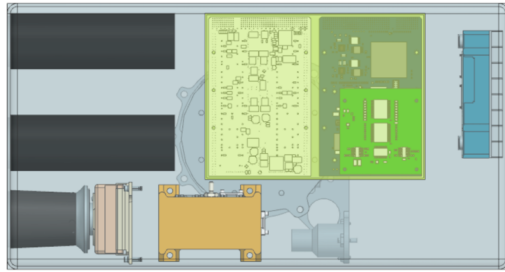
A deployable gimbal platform could be developed leveraging PIXL flight electronics and chassis designs. The concept design by Robert Sharrow et al is shown in Figure 3.9. The concept enables autonomous pointing of the payload using a star tracker and delivers a full instrument package ready to bolt-on an existing spacecraft. It is thus a good option for a commercialized XNAV instrument with well-defined interfaces that would not need to be significantly adapted for different spacecraft. Moreover, the payload itself would be able to fine-tune its pointing and be less restricted by the spacecraft ACS.

For our case, the chassis mounted on the scan platform would need to be longer than the longest dimension of the CubeSat to accommodate the needed focal length, and therefore this option is discarded. Moreover, gimbals are generally heavy and of high mechanical

complexity with parts moving around three axes, and a simpler option is preferred for the technology demonstration of XNAV as a concept.



(a) Deployed gimbal configuration leveraging on the PIXL flight electronics and chassis design.



(b) Top view of the chassis leveraging on PIXL. It features two 3.5 cm polycapillary optics, a camera star tracker (left), digital and power electronics (green box), sensor box (blue).

Figure 3.9: Concept for a pulsar observing instrument for navigation and timing with scan platform.
Credit: Robert Sharrow et al [31].

3.1.5.2 Rotating disk and hinge

A rotating disk and hinge would be a solution similar to the deployable gimbal platform which could help decrease mechanical complexity. The idea is to attach a rotating disc with a hinge onto the spacecraft with the payload on top of it. With this replacement for the gimbal, only two axes with moving parts are needed and a full 180-degree observation field is still accessible (the spacecraft will obstruct the rest). Even though the mechanical complexity is lower for this solution compared to the PIXL-heritage chassis design, it still suffers from several downsides. This solution would require a new special design and would not reuse many assets from PIXL which would be a risk. At the same time the focal length requirement of $f = 422$ mm would challenge the design of the hinge. Lastly, the size constraints of our W6U cubesat would not make this solution possible unless extra moving parts were added to extend the design out from a compact version inside the spacecraft. This can be visualized with a sketch shown in figure 3.10

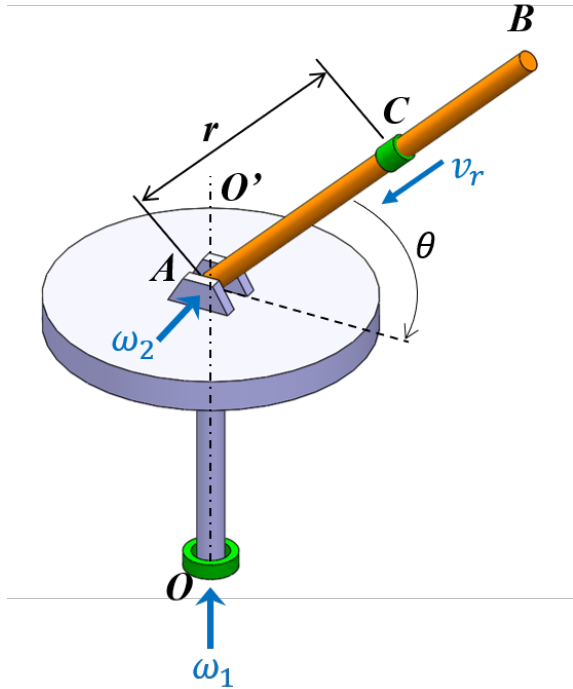


Figure 3.10: Visualization of possible disc and hinge system for the movable pointing of the payload.

3.1.5.3 Direct mounting on spacecraft body

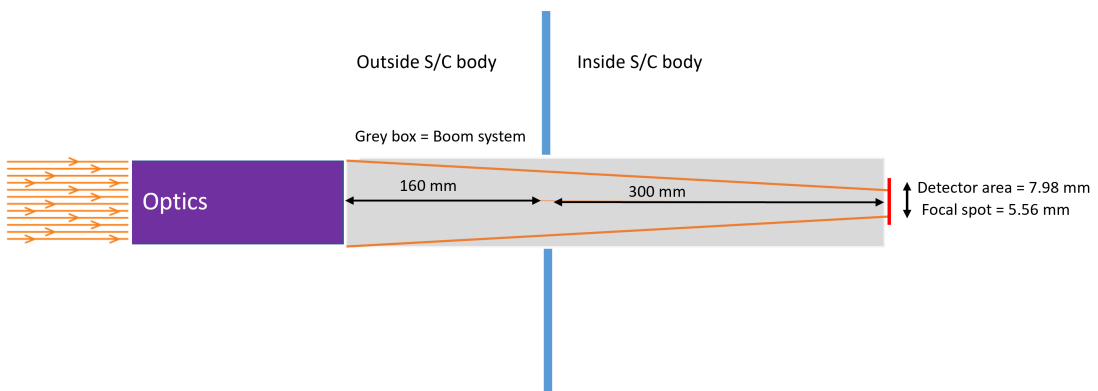
Mounting the payload in a static position inside the spacecraft body would be the option with the least mechanical complexity. The payload would be pointed solely using the spacecraft ACS, which could be limiting to certain mission profiles where separate pointing of the payload from solar cells and antennas is needed. Reduction of observation time which could be due to directional communication systems and requirements to pointing of solar cells must therefore be taken into consideration for this option. In any case, the size constraints of our W6U cubesat would decrease the performance, since the optimal focal length is not achievable and the X-ray beam would overshoot the detector. To what extent the performance would be compromised would have to be evaluated by simulation.

3.1.5.4 Extendable boom

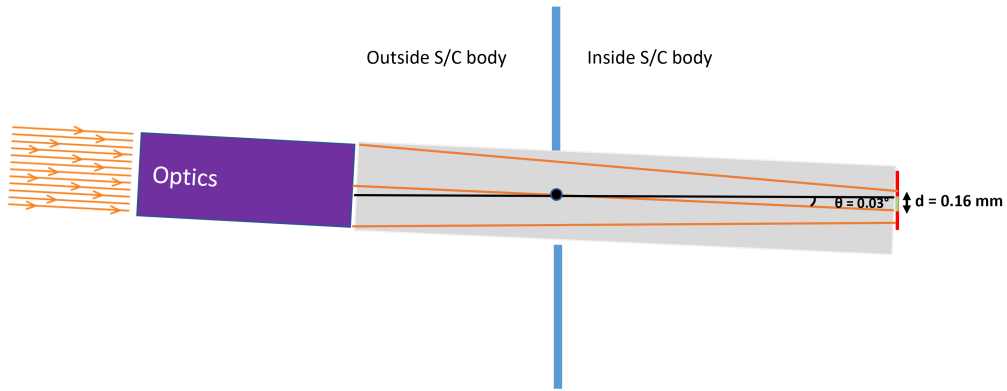
An extendable mechanism with the optics attached would make it possible to achieve the optimal focal length and mitigate the size constraints of the W6U cubesat. The payload and its extendable boom have to fit inside the spacecraft body during launch and deploy afterward. The payload will be pointed using the spacecraft ACS. The boom must be rigid and of high stability to stay on target. Moreover, its redundancy must be considered, since it would potentially kill the mission if the boom does not deploy. The concept of an extendable boom is chosen for mounting the payload for PANTSat since it is the only of the four investigated options that accommodates the optimal focal length of the optics.

A suitable boom was successfully developed by the mechanical team which is described further in Section 3.7.1.2 and particularly in Figure 3.74. Potential jitter from the boom should be added to the sum of the ACS pointing and stability accuracy which should be $< 0.03^\circ$. Moreover, jitter from the boom could potentially lead to misalignment of the focal spot and the detector resulting in fewer photons collected. Some margin is therefore added to the focal length, and when fully extended, the boom reaches a focal length of $f = 460$ mm. The focal spot will in this case be 5.56 mm. From the extension mechanism

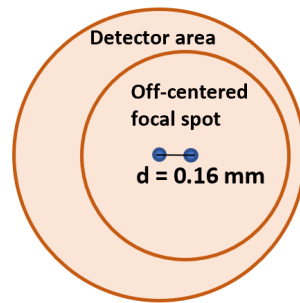
designed by the mechanical team, see Section 3.7.1.2, we get that 300 mm of the focal length is inside the spacecraft, while the last 160 mm is delivered by the extension outside the spacecraft. We can calculate how much the center of the focal spot (assumed circular) would move from the center of the circular detector area in the limit of perfect ACS pointing and stability and where the optic is misaligned by 0.03° . From Figure 3.11 it is calculated that the center of the focal spot would be misaligned by $d \approx 0.16$ mm from the center of the detector area. The full beam would thus still be within the detector area meaning we would not lose any photons in this case.



(a) Concept of optics on the extendable boom. 300 mm of the focal length will be inside the spacecraft while 160 mm will be outside. The focal spot on the detector will be 5.56 mm.



(b) The boom is rotated 0.03° with respect to the black point.



(c) The rotation results in a misalignment of $d = 0.16 \text{ mm}$ of the focal spot from the center of the detector area. The X-ray beam, assumed circular, will stay within the detector area.

Figure 3.11: Considerations about the consequences of misalignment of the boom within the pointing accuracy requirement. Note: The dimension and angles are not correctly scaled, the figures are only for conceptual illustration purposes.

3.1.6 Pulsar Characteristics and Catalog

Pulsars are some of the most extreme physical objects known in our universe. MSP, which is what we are interested in, are rapidly rotating neutron stars with rotational periods less than 10 milliseconds [38]. They have been recycled and spun up through the accretion of matter from a companion star in a close binary system and given their immense magnetic-field they emit radiation in various parts of the electromagnetic spectrum, including radio, X-ray, and gamma-ray regions. Due to the extreme rotation and conservation of angular momentum they are stable and reliable in their pulses which makes them such good objects for navigational purposes. They are known as celestial lighthouses due to this highly stable oscillating signal, which we will use to determine time and position in a manner similar to GNSS. This physical description can be visualized on figure 3.12. Position determination based on these pulsar measurements is made possible by the pulsar's well-defined pulse-timing model, providing pulse period and higher-order derivatives, and additional characteristics like pulsar Line of Sight (LOS) direction, distance and proper-motion. To achieve a continuous, accurate navigation solution, there are two methods of position and velocity determination: Absolute Mode and Delta Mode.

- **Absolute Mode:** The absolute mode is used to determine the absolute three-dimensional position and/or velocity in an inertial reference frame BY monitoring several pulsars simultaneously and merging their pulse ToA information into a single solution. This requires multiple X-ray detectors pointed towards all these individual sources, or a single X-ray detector system that has all-sky monitoring capabilities[36].
- **Delta Mode:** The Delta mode is a single detector technique that provides corrections to estimated range, and hence position, solutions. It only needs to point at one source at a time and can converge its positional accuracy with interrupted data. Blending this information with the estimated position from an orbit propagator produces corrections to the position and velocity solution, which maintains accurate solutions over time. In the PANTSat mission, we want to demonstrate the technology for a single-pointed X-ray detector and therefore it is the Delta Mode we will utilize[36]. A visualization of this technique is shown in figure 3.12.

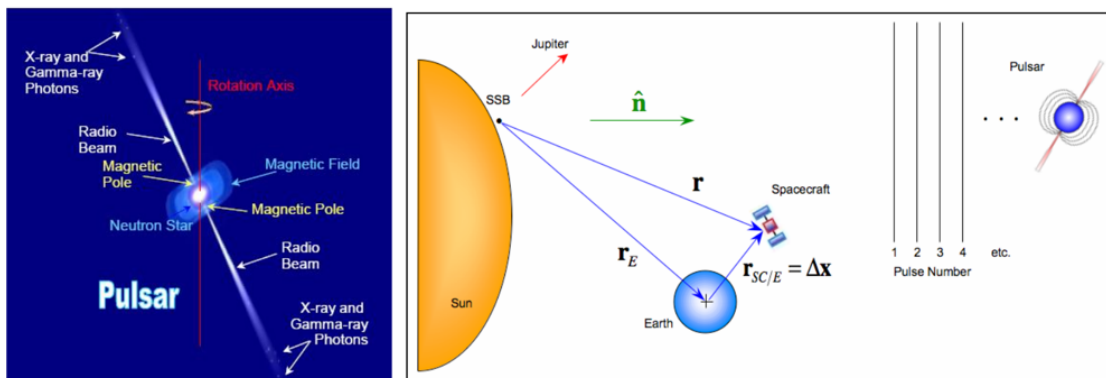


Figure 3.12: a) An artist's visualization of an MSP. b) Visualization of how XNAV works

With the knowledge of the physical nature of MSP and how this affects the overall XNAV-technique used we can define the criteria for the sources included in our pulsar catalog for the PANTSat-mission [36]. There are three keywords when it comes to the PANTSat-catalog chosen: Stability, Predictability, Availability. This comes on the background of the following criteria.

1) A stable pulse period: The pulsar should have a stable pulse period, meaning that the time between pulses should remain relatively constant over time. Any variation in the pulse period can cause errors in timing solutions, which in turn can affect accuracy. Since we want to test PANTSat accuracy against the NICER-element RSS uncertainty of 21.4 km, we actually constrained ourselves to sources with model timing accuracies of at least 100 μ s.

2) A high Signal-to-Noise Ratio (SNR): The pulsar included in our catalog should ideally have a high SNR. This goes back to the earlier mentioned background count rates, meaning that the signal from the pulsar should be much stronger than the background noise. This ensures more accurate and predictable timing measurements.

3) No visibility constraints and ideally an isotropic population in the catalog: The pulsars used in the PANTSat mission should be distributed evenly across the sky, as this helps ensure good geometry for measurements throughout the year.

Visibility constraints due to the Sun, Earth, or other blockages should be taken into account when selecting our pulsars. Pulsars that are concentrated in a particular region or direction may also lead to biases or errors. Now combining these criteria with the possible list of known pulsar candidates from the literature of the NICER-SEXTANT mission and for example "*The use of variable celestial X-ray sources for spacecraft navigation*"[39], we end up with the following list seen on figure 3.13. On this figure the pulsar catalog is given together with pulse periods and position of the object. Also on the figure is given a J2000 map of all our sources which are clearly isotropically spread out to give us the best viewing geometry throughout the year.

PSR	P(ms)	RA	DEC
Crab Pulsar	0.33	05 34 31.95	+22 00
B1937+21	1.56	19 39 39.62	+21 37 21.7
J0218+4232	2.32	02 18 06.36	+42 32 17.4
J0030+0451	4.87	00 30 27.43	+04 51 39.7
J1012+5307	5.26	10 12 33.43	+53 07 02.5
J1024-0719	5.20	10 24 38.70	-07 19 19.1
J0751+1807	3.48	07 51 09.15	+18 07 38.3
J0437-4715	5.75	04 37 15.80	-47 15 08.5
J2124-3358	4.93	21 24 43.85	-33 58 45.0

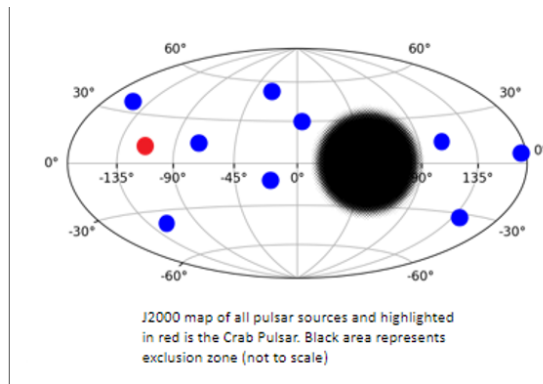


Figure 3.13: a) Table showing the pulsar catalog for the PANTSat-mission. b) J2000 map of the location of our pulsar catalog with the Crab source highlighted in red.

3.1.7 Observation Windows and Calibration on sources

The instrument used in the PANTSat mission will need calibration or else its performance can drift or change over time due to various environmental factors such as temperature, radiation, and vibrations. It is a necessary practice to start with a calibration and check-period before using the instrument for scientific means [36]. Therefore the first 2 months after operational status has been achieved, will be dedicated to calibration and test procedures to ensure that the telescope was functioning properly and to establish a baseline performance for future observations. Regular calibration checks will also be planned to ensure that the data collected remains accurate later on. When it comes to our mission we will have four major calibration needs for our telescope which are: Energy calibration, Timing calibration, Pointing calibration, and lastly Background calibration.

Specifically, the timing and pointing calibration will be of importance, as it is the timing of our instrument which dictates the errors on positional estimates of our spacecraft, and the pointing accuracy is also required to be very precise for our instrument due to the optics. To get the best possible calibration we have chosen B0531+21, also known as the Crab pulsar, as our calibration source. The Crab pulsar has been observed since 1054 and is the most well-studied pulsar source in X-ray astrophysics. It is conveniently also one of the most stable sources which makes it ideal to test and calibrate the timing accuracy of our instruments on [40].

As mentioned earlier availability was one of the key focuses for our pulsar catalog. There will be obstructions from the Sun, Moon, and Earth throughout the mission life cycle but we have chosen a pulsar catalog that should reflect at least 3-4 available sources all year around. This can also be visualized in figure 3.14 showing pulsar visibility throughout the year for the PANTSat catalog:

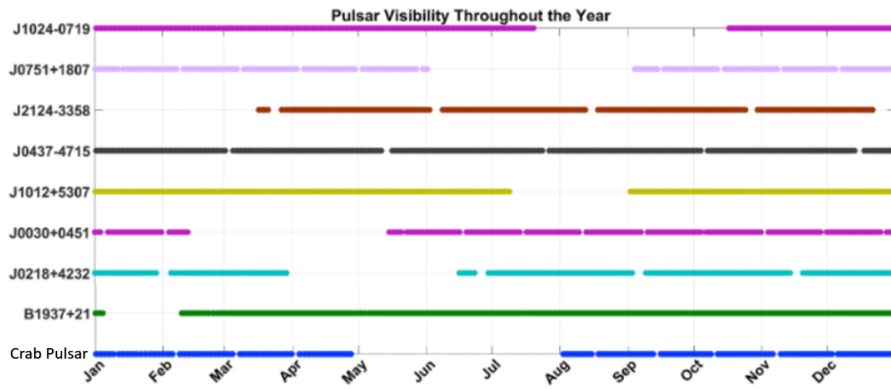


Figure 3.14: Pulsar visibility throughout the year for the PANTSat catalog [36]

Notice that the Crab pulsar is not available in the time interval between May and Aug, due to the sun's position relative to the earth [40]. This of course constraints the mission plan of using the Crab pulsar for the initial checkout and calibration phase. In the worst-case scenario, launch date is chosen such that the operational status of the spacecraft is achieved around late April or early May which will limit the total observation time in the mission life cycle as around three months will go by before the Crab is visible again. Though this should not be overstated as the total lifetime of the mission is far beyond the 2 months potentially lost and the leftover time is more than enough to reach the goal of technology demonstration. Also, other potential sources could serve as calibration candidates such as B1937+21 which is available in the time period where the Crab is obscured and is also known to be a very stable pulsar source.

The three different observation windows based on pulsar visibility throughout the year for the PANTSat catalog can be seen in figure:

- **1 Sources for Jan-May window:**
 - PSR B0531+21 (Crab): RA 053431.95 , Dec +22 0052.2
 - PSR J1024-0719: RA 102438.70 , Dec -071919.1
 - PSR J0751+1807 : RA 075109.15 , Dec +180738.3
 - PSR. J0437-4715: RA 0437 15.80, Dec -471508.5
 - PSR. J1012+5307: RA 1012 33.43, Dec +53 0702.5

- PSR J0218+4232: RA 021806.36 , Dec +423217.4

- **2 Sources for May-August window:**

- PSR J1024-0719: (repeat from Jan-may window)
- PSR J2124-3358: RA 2124 43.85, Dec -33 5845.0
- PSR J0437-4715 (repeat from Jan-may window)
- PSR. B1937+21: RA 193939.62 , Dec +21 3721.7

- **3 Sources for August-December window:**

- PSR. B0531+21 (Crab nebula again)
- PSR. J0751+1807: RA 0751 09.15, Dec +18 0738.3
- PSR. J2124-3358: (repeat from May-August window)
 - PSR J0437-4715 (repeat from Jan-may window)
 - PSR. J1012+5307 (repeat from Jan-may window)
- PSR J0030+0451: RA 0030 27.43, Dec +04 5139.7
 - PSR. J0218+4232 (repeat from Jan-may window)
- PSR. B1937+21: (repeat from May-August window)

Note: all listed (full) RA, Dec coordinates are in the J2000 coordinate system. Sources whose names begin with B have slight deviations w.r.t. the coordinates in their names, since these are in the B1950 system.

3.1.8 Action Items From Preliminary Design Review

Our reaction to the action items and questions received at the Preliminary Design Review (PDR) is given below.

- **What are the key technologies for enabling the final mission?**

The key technologies enabling this mission are the PIXL-heritage polycapillary optics for focusing the X-ray beam, the XOS-built angular filter element, and the extendable boom. While polycapillary optics have been used to great success on the Perseverance rover, it's still vital to test their performance in the context of XNAV. Likewise, the angular filter element is vital in its role of reducing the angle-of-acceptance, which enables the small footprint of the payload compared to NICER-/SEXTANT. Lastly, the extendable boom also greatly reduces the footprint. As the extendable boom is specially designed for PANTSat, prototyping, testing and verification of this part is especially vital.

- **Is it true that the center of the spacecraft is the most radiated?**

Each component subsystem is modeled as a solid enclosure with a specific density to reflect the parts weight. Additionally, the calculation points for TID were the center of the enclosures, meaning that these points are protected by their own enclosure in every viewing angle, as well as by other subsystems and the S/C's protective shielding. In contrast, the free floating point at the center of the S/C only "sees" the other enclosures and the aluminum shielding. Therefore, it is actually expected that the center would receive the highest dose. This calculation point at the center was used to provide an estimate of the dosage at any given point inside the S/C, in order to show compliance the requirement of < 1krad per year in orbit.

- **Is the listed pointing accuracy just for moving the optics or also for staying on target?**

The angle of acceptance of the optics is 0.06° . The spacecraft shall be able to move and stay on the target with a maximum angular separation by half of that, so $< 0.03^\circ$ for the target to stay in sight. The listed pointing accuracy is thus the sum of the stability and pointing accuracy.

- **What's the minimum observation time to adequately demonstrate the concept and technology?**

The minimum observation time to adequately demonstrate one pulsar navigation solution is estimated to be 20 days as described in Section 3.1.1.3.

- **How flexible is the requirement of the summer launch window?**

The current plan for launch is set around August 2025. As mentioned in the section about calibration sources, it would be ideal to have a summer launch of the spacecraft as this would give us a high probability to begin the initial checkout and calibration phase well inside the Crab pulsar visibility window of August to May. However the summer launch is not strictly necessary as the calibration window extends all the way to May and the time needed for technology demonstration is estimated to be only 20-days after the calibration phase. Therefore we have a large amount of flexibility when it comes to the choice of launch window. The worst case would be a late spring launch where the initial checkout and calibration phase begins in the period of May-August where the Crab pulsar is obstructed. But as discussed earlier other potential sources could serve as calibration candidates such as B1937+21 which is available in the time period and is also known to be a very stable pulsar source.

- **How does the accuracy of the DSN compare to the required accuracy of this mission?**

The DSN has an accuracy of approx. 0.3 km pr. AU away from Earth[1], which our minimum required accuracy of 50 km RSS obviously cannot compete with if navigation accuracy is essential for a prospect mission. However as outlined in Section 1.1, there are still cases where XNAV could be highly useful such as a cost saver for small satellites with looser positional requirements or an emergency backup for manned flights. Moreover, the analysis from P. Graven et. al (2008) [1] finds that XNAV improves performance over DSN at about 15 AU. At 100 AU, XNAV offers 3 times better position uncertainty than DSN.

- **What lead times can we expect for the components in the payload?**

Estimating lead times for all components in the payload can be difficult. However, two of the components where lead times could be a potential cause of concern are the optics and the reference clock. The optics could be a cause of concern not only due to their importance to the mission, but also because the current tests have only been done with designs from XOS, which could cause problems if the lead times from XOS are too long. From Robert Sharrows presentation, the expected lead time for our chosen optics design from XOS is approx. 20 weeks. Although alternatives exist for the integrated reference clock, the global nature of the current chip shortage means that other manufacturers are affected as well, which could potentially mean long lead times. The current estimate from the Microsemi CSAC FAQ is 4-6 weeks, though this could be subject to change depending on the status of the on-going chip shortage.

3.2 Attitude Determination and Control Subsystem (ADCS)

3.2.1 Introduction

The ADCS is a major part of most spacecraft, as a basis for the payload to perform its mission successfully. Therefore there also exists an abundance of methods and concepts to achieve this. Some missions do not require a highly accurate pointing, but might just need a consistent directionality. Others might be highly dependent on the directions it is pointing.

With the increase of nanosatellites, the commercial interest in developing off-the-shelf solutions for this increased. Today, multiple companies have produced attitude control and determination systems, as a cornerstone in their business. Just as with conventional large satellites, nanosatellites carry many different kinds of payloads. The ADCS should of course mirror these different requirements, as the attitude control and determination can be achieved by a number of different systems. What kinds of systems are best in turn relates to the orientation, accuracy and torque requirements as well as the momentum stored for operations. In this case, [41]. tells it as this: "...it is worth considering it also (the attitude control system) as a momentum management system. Angular momentum is a commodity that can be acquired and disposed of, or stored" [41]. Good control of this commodity is therefore necessary for a successful operation and control of the spacecraft.

The attitude determination and control system is by nature dual purpose; determination of the attitude of the satellite platform, as well as controlling the pointing of the system to the desired target. This is by nature very integrated, and controlled in a loop as illustrated in figure 3.15. We need to be able to determine which direction the spacecraft is pointing (attitude sensors), to determine a direction change command by the OBC, before we send the command to the control system to apply a torque to the spacecraft, to turn it in the desired direction. This is controlled in the loop shown in figure 3.15. This makes it clear that control theory holds a corner part of the ADCS. Not only do we need to account for the movement of the spacecraft, in relation to the torques we can apply, we have also other disturbances from external and internal sources. These could come from atmospheric drag, solar pressure, or other instruments turning, such as solar panels. Some ADCS's use these external influences as a way to turn the spacecraft, however they need to be accounted for either way.

As there was stated before, many methods and systems exists for the control of the space-craft, and many methods exists for the determination as well. We will here show a short overview of the most used systems, to get a sense for the application for our current mission. The primary classification of these systems can be divided into internal and external systems.

There are multiple mission phases during a spacecrafts lifetime, and the ADCS needs to be properly suited for each of these to allow for optimal performance.

3.2.2 Requirements

The requirements for this sub-system are summarized here¹. We then state what the response for each requirement is.

- The attitude control and determination system of the CubeSat shall be sized to meet the pointing and attitude rate requirements of all the other subsystems onboard the CubeSat, including power and telemetry.

¹Further details are in paragraph 4.5.

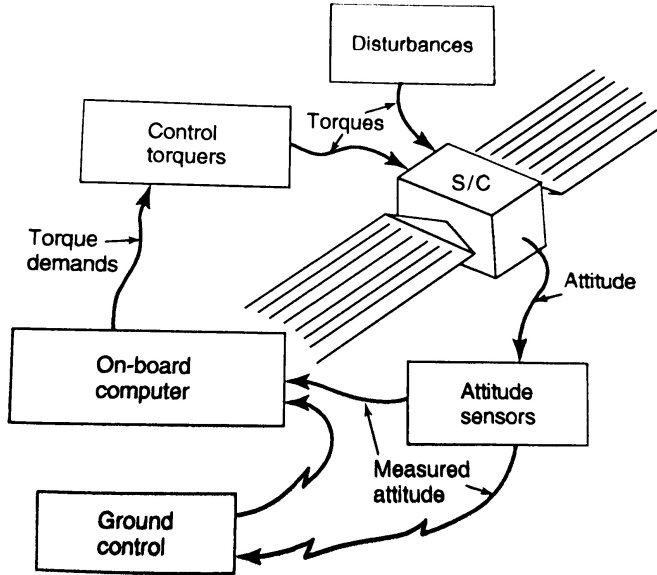


Figure 3.15: Block diagram for an attitude-control system. Figure from [41].

- The CubeSat shall be tolerant to an initial tumbling rate of 90 deg/s per axis at deployment.
- The CubeSat attitude control and determination systems shall be sized to account for additional spin-up of the CubeSat by its own magnetic characteristics, including unintentional dipoles.
- If a passive magnetic attitude control system is foreseen, the position and the alignment, with respect to the body axes, and the strength of the permanent magnet shall be declared.
- The magnetic field outside the CubeSat static envelope shall be limited to 0.5 Gauss above Earth's magnetic field.

3.2.3 System Overview

All the following sub-components are integrated into the XACT-50 system [12]. We therefore list the individual components, their purpose and other information, but the specific integration is not discussed. The benefit of providing an integrated ADCS system is the validation. This specific system has in flight heritage, and the loop as described in figure 3.15 has been rigorously tested. Thereby the link between the star-camera and the needed response for the reaction wheels have a larger technology readiness level, than if we were to introduce them at different locations ourselves, even though it would be possible to get them separately.

In figure 3.16, we can see a photograph of the XACT-50 unit fully assembled. In the following sections we will introduce the subcomponents included, which are; reaction wheels, torque rods, star tracker, sun sensor, magnetometer, Inertial Measurement Unit (IMU) and a processing unit.

	RWP050
Momentum [Nms]	0.050
Max torque [Nm]	0.007
Mass [kg]	0.24
Voltage [VDC]	10-14
Power at full momentum [W]	<1.0
Volume [mm]	58 x 58 x 25

Table 3.3: RWP050 characteristics [12].

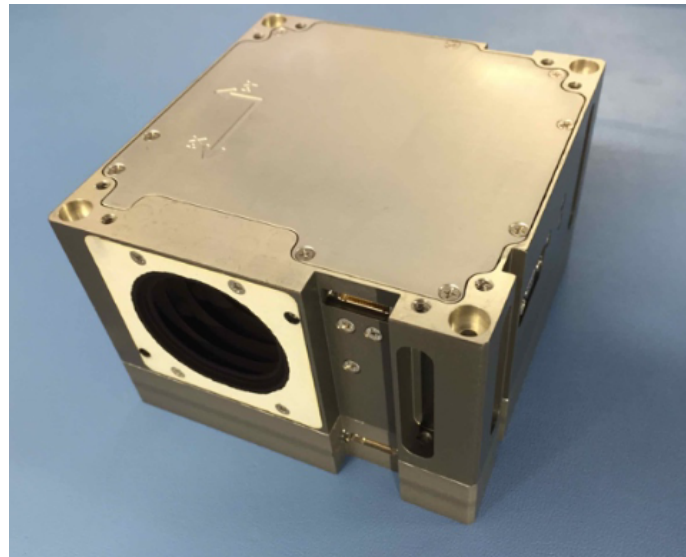


Figure 3.16: XACT-50 from Blue Canyon Technologies, figure from [42].

3.2.3.1 Reaction Wheels

We are using reaction wheels of the type RWP050. The XACT enables either three or four reaction wheels, where in this case, we opt for four, due to redundancy, and the importance of high-precision pointing for the mission success. The ADCS relies on the reaction wheels for the precision pointing, with the torque rods acting as a supporting element. The operation of the wheels needs to be taken into consideration with speed reversals increasing the pointing error substantially, and momentum dumping needed occasionally to allow for fine operations. The used reaction wheel can be seen in figure 3.17.



Figure 3.17: Reaction wheels of the RWP050 type from Blue Canyon Technology [12].

3.2.3.2 Torque Rods

The three-axis torque rods work by applying a voltage to each of the three rods, which then apply a magnetic field, and moves the spacecraft in relation to the Earth's magnetic field. This is not for finer movement, as the spacecraft can't be controlled as good as with reaction wheels, and a high precision map of the magnetic field is needed. However, it is good for detumbling and enabling momentum dumping of the reaction wheels. The torque rods produce a dipole moment of 0.125 Am^2 [42], where finer magnetic modelling and measurements of the fully assembled spacecraft is needed to determine how reliant on the torque rods we can be, as well as the distributed power between each of the axis. Our simulation shows a peak magnetic field just outside the torque rods of $5 \times 10^{-5} \text{ T}$, which corresponds to 0.5 Gauss. This is in relation to a zero-field, and with a Earth magnetic field of 0.25 Gauss we are well within the requirement for 0.5 Gauss above the Earth reference field.

3.2.3.3 Star Tracker

Star cameras are not standard issue equipment for cubesats. This is also one of the reasons why the solution from Blue Canyon Technology was chosen, as they provided an integrated solution with the attitude control system and the high precision determination system applied. We use the integrated Standard Nano Star Tracker (NST), as seen on figure 3.18. The processing unit on the XACT contains a star catalogue, which enables the classification of stars required for the attitude determination. The accuracy cross-boresight and about-boresight for the camera is not identical, with the system being more accurate cross-boresight. This is influential in our choice of having the camera point the same direction as the payload, as also ensuring star coverage when observations are made. The cross-boresight one-sigma accuracy is 1 arcseconds, while the about-boresight is 10 arcseconds.



Figure 3.18: Star Tracker of the Standard NST type from Blue Canyon Technology [12].

3.2.3.4 Additional Attitude Determination Systems

The XACT unit also encompasses a sun-sensor, magnetometer and IMU. These are all important systems that support the high precision star-camera, and provides somewhat of a redundancy for each other. The sun-sensor is especially important for large manoeuvres, such as detumbling, lost-in-space manoeuvres as well as when put into safe-mode, to allow for maximum solar exposure for the solar panels.

3.2.3.5 Processing Unit

The integrated processing unit takes care of the attitude side, such that the OBC only needs to pass commands for pointing targets and states to this system. The software includes star-tracking (with star-map), attitude estimation, attitude control, momentum control and orbit propagation [42].

3.2.4 Pointing

One of the primary functions of the ADCS system, and in the following sections describes the expected performance of the system.

3.2.4.1 Pointing Accuracy

The attitude system needs to be dimensioned to match the mass and size of the spacecraft. This is due to the limited momentum storage in the reaction wheels, and a limited slew rate for too heavy systems. This is why the XACT-50 was chosen, as it is designed for up to a 14 kg 6U CubeSat, and has flown with 10 kg 6U CubeSats with good performance [42]. At this rate, the pointing accuracy at a steady state is at ± 10.8 arcsec for 2 axes, and ± 25.2 for the third. During turning, this increases allot, with the numbers being 15 arcsec at cross-boresight and 200 arcsec around-boresight at a turning rate of 1 degree per second. This is also summarized in table 3.4.

3.2.4.2 Pointing Stability

While the attitude system itself might be accurate for an initial correction, it might not fare as well when observing over longer stretches of time. We deem this measure the pointing stability, and is of importance when aggregating observations from a payload such as the one on this spacecraft. The ASTERIA mission from 2017 was launched with the same attitude control system as for the PANTSAT system, the XACT-50, with the same location and shape (W6U) [42]. They tested in-flight the accuracy and stability of the pointing for the XACT unit, which we can use to determine the expected performance and worst case scenarios for our system. As we see in figure 3.19, we see the pointing error in X and Y axis, for an observation of a target, over a time frame of 20 minutes. During this time frame, they experienced a small bias, and a variance of 2.33 to 3.28 arcseconds for each axis. We have here unique data for the pointing accuracy, that allows us for determining the expected over-time performance of the system. One of the major influences to the noise of the system, they found out was the thermal influence to the disagreement between the attitude control system and the star-camera. Correct thermal control should mitigate this problem.

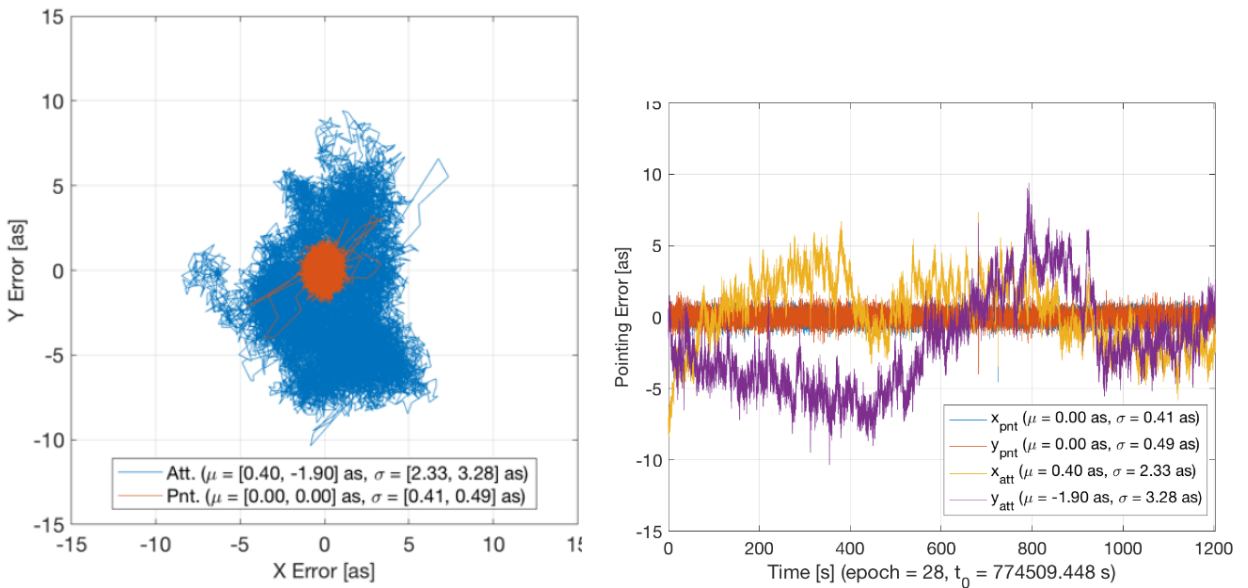


Figure 3.19: Pointing stability over 20 minutes [42]

3.2.4.3 Pointing Performance

As a summary for the pointing performance, we see in table 3.4 how the expected performance is during operations. The numbers are all 1-sigma ranges, and would therefore fulfil the pointing requirements put up by the payload, and enables pulsar observations.

	Stability (20 min)	Accuracy	Sum	Slew@(1°/s)	Slew Sum
arcsec	2.33-3.28	10.9-25.2	13.13-28.48	15-200	28.13-228.48
deg	0.00065-0.00091	0.0030-0.0070	0.0036-0.0079	0.0042-0.056	0.0078-0.064

Table 3.4: Pointing table with the performance at several situations.

Resulting in a worst-case pointing accuracy of 0.008 degrees, we are below the required 0.03 degrees for the payload, even considering the 10% margin for this requirement.

3.2.5 Moment of Inertia

For specific modelling of the attitude system, the moment of inertia of the spacecraft is needed. As we have a deployable system, the moment of inertia changes quite drastically for these two systems. In the mechanical section, in figure 3.76, we see how the center of mass is located with reference to the attitude control system. This mirrors the location of a similar setup from the ASTERIA mission [42]. As we wanted the best pointing accuracy and control to be during the observation phase, we opted to be as close to the center of mass in the deployed configuration. As an overview of the inertia from the solidworks files, we have the tables as seen in 3.5.

Stowed: Principal axis of inertia [gmm²]			
Ix	-0.16	0.99	0.0
Iy	-0.99	-0.16	0.03
Iz	0.03	0.01	1.00
Deployed: Principal axis of inertia [gmm²]			
Ix	0.05	0.65	0.76
Iy	-0.17	-0.74	0.65
Iz	0.98	-0.17	0.07

Table 3.5: Intertia Mass Properties

3.2.6 Inflight Vibrations

Several outside influences can hurt the pointing performance during operations. Some of them are small size vibrations during operation, some can be larger and caused by the movement of systems. As we do not have many moving systems in the satellite, we do not have as many sources for error as could be feared. One of the things we do have however, is the solar panel motor, that is able to turn the solar wings to face the sun. To get an idea of the size of the effect, we calculate the corresponding turning of the spacecraft body, when moving the solar wings. The moment of inertia can be approximated as a flat rectangle and a box respectively, with different angles of rotation. The moments of inertia are determined by:

$$I_{wings} = M \frac{b^2}{12}, \quad I_{S/C} = \frac{M}{12}(4h^2 + w^2). \quad (3.3)$$

We can then, by conservation of angular momentum, determine the angular velocity of the spacecraft, when turning the solar wings by up to 10 degrees per second. The equation

for angular momentum states:

$$\tau = I\alpha, \quad (3.4)$$

and we can then input the numbers for the masses and sizes of the elements. We get that the spacecraft turns with 0.09 degrees per second, in response to the solar panels turning 10 degrees per second. If we assume linear slew-induced-error, we get a cross-boresight error of 1.35 arcsec, well within the requirements specified, and can be handled by the ADCS. However, when determining the mission planning, we see that we would not have to turn the solar wings that often, at least after the spacecraft has positioned itself on a target. So this might not affect the performance in this order at all.

Another source for potential error, might be the micro jitter by the reaction wheels. In flight tests by the ASTERIA CubeSat determined that the effect from these reaction wheels we have used, is minimal, and can be neglected [42].

3.2.7 Integration with the Operational Modes

3.2.7.1 Timing requirements

According to the ConOps introduced in Section 1.5, there are three principal sub-systems that the ADCS must take into when re-pointing. These are the payload, the power system and the communications ones. Each of these systems have their own requirements in terms of pointing time, pointing accuracy and angular acceptance. The requirements for each system are summarized in Table 3.6 and explained below. For the following orientation discussion the reference system as shown in figure 3.20 is used, where "forward" is the pointing direction of the optics. This axis is considered parallel to the focal length of the missions instrument and will from here on be referred to as the main axis or pointing direction.

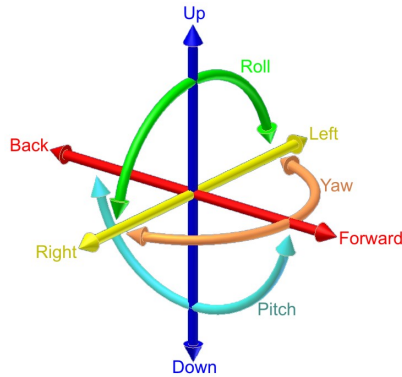


Figure 3.20: Possible rotational degrees of freedom and their corresponding rotational axes. Here the red axis is considered the main axis, parallel to the focal length of the instrument. [43]

	Payload				Comms	Power
	Target	Earth	Moon	Sun	DTU	Sun
Blockage (\circ)	N/A	± 30	± 15	± 45	N/A	N/A
Acceptance (\circ)	± 0.03	N/A	N/A	N/A	90 ± 30	180 ± 25
Minimum time	20 days	N/A	N/A	N/A	160s/day	+120, -112min
Axis	pitch/yaw	pitch/yaw	pitch/yaw	pitch/yaw	pitch/yaw/roll	pitch/yaw/roll

Table 3.6: Pointing requirements inherent to the different subsystems. Here "Blockage" indicates the angular separation from the center of an object within which targets cannot be observed [34]. "Acceptance" is the angular separation from an object's center within which the corresponding subsystem can function. "Minimum time" is the minimum amount of time that the spacecraft needs to be pointing at the related object. For the power system the +indicates the time needed to fully charge the batteries from zero. The minus indicates the discharge time of the batteries, in which thus the power system needs no specific pointing. Finally, the "Axis" indicates the DOF's involved in meeting the requirements.

- **Payload:** The payload needs to be pointing at the target with a maximum angular separation of 0.03° . While pointing at the target the line of sight gets interrupted by three bodies: Earth, Moon and Sun. The minimum angular separation required from these bodies to still be able to observe the target is 30° , 15° , and 45° respectively, which are based on the restraints listed for NICER [34], which has a similar optics system as this mission. The pointing to target requires adjustments in the pitch and yaw axes of the spacecraft and does not depend on the roll of the spacecraft, as defined in 3.20. The minimum time requirement for the science goals set by chapter 3.1 is 20 days of accumulated observation, with a minimum of 4 targets.
- **Communications:** The telecommunication uses a fixed directional antenna on the bottom of the spacecraft. This antenna sits on the side of the spacecraft (see figure 3.75) and can handle a separation from the Earth receiver up to a maximum of 30° . Assuming no restriction in roll, this means communications can take place when the angular separation from the forward direction is $90 \pm 30^\circ$. The time requirement for communication and data transmission as set in chapter 3.6.3 is a minimum of 160s/day. If this number can be met within the angular range during the science observations, then no additional pointing adjustments are needed for communications and data transfer. If this minimum is not met, then the pitch and yaw DOF's must be adjusted to account to fulfill the requirement. But this might take away time from the science targets.
- **Power:** In order for the spacecraft to receive sufficient power, the solar panels need to be turned towards the Sun under an angle of maximal 25° . The solar panel has its surface parallel to the detector surface when first deployed (see figure 3.75). The panel can rotate itself independently from the rest of the spacecraft in the yaw direction. The panel does require the spacecraft roll to orientate, which manoeuvres thus might overlap with those of the comms. Because the payload targets have been picked in such a way as to avoid Sun blockage, the Sun has the most change of hitting the solar panel when it is orientated parallel but opposite the detectors incident face. This prompt the acceptance angle in table 3.6 of $180 \pm 25^\circ$. The power systems batteries can last up to 112 minutes outside of the Sun. From empty they then need 120 minutes on average of charging in the Sun (chapter 3.40). Since $112 \cdot 60 > 160$ seconds, it is possible to perform communications during battery time, and thus prioritize communications over power when these two need conflicting orientations in the shared roll axis.

3.2.7.2 Time schedule simulation

From the above discussion it is clear that the main conflicting orientations are the pitch and the yaw. It is therefore relevant to make a schedule of the pointing direction to ensure minimum requirements are met. The most strict requirements are set by the science goals. The targets need the longest period of time and the most accurate direction. They will therefore be the main drive in the following pointing simulation. For simplicity the acceptance of the targets is assumed to be $\pm 0^\circ$ instead of $\pm 0.03^\circ$) since this angle is much smaller than the other acceptance angles.

For spacecraft's orbit is taken as a first order ellipse, and any perturbations and deviations from this are neglected since these will be much smaller than the orbit as a whole, and here we are only interested in the angular movement of the spacecraft. For the actual and precise positions, refer to Chapter 3.4. The primary targets for this mission can be found in Section 3.1.7, based on an estimation of visibility. The targets are split into two periods: Jan-May and Aug-Dec. Blockages in observing time are caused by the Earth, Moon and Sun. The orbital parameters for these bodies and the spacecraft are listed in Table 3.7

	i ($^\circ$)	r_a (km)	r_p (km)	P (days)	RA_0 ($^\circ$)
Sat	51.6	6798	6791	0.0645139	0
Earth	0	0	0	0	0
Moon	5	405400	363228.9	27.32	30.65
Sun	23.4+7.155	152.1e6	147.1e6	365.256	282.2

Table 3.7: Orbital parameters of the observation block related bodies. Here i is the inclination, r_a is the radius at apoapsis, r_p is the radius at periapsis and RA_0 is the initial right ascension of an orbit at 01-01-2025 00:00:00, 55h45m48s 12h29m41s (year of launch above Kongens Lyngby,DK). All values are with the Earth's equatorial plane a reference and with the Earth as focal point. This is why the Earth has only zero values and the inclination of the Sun is the Earth's axis tilt + its orbital plane inclination respectively. The right ascension of the satellite is dependent on the launch and is defined as zero, specification pending. Ref: tab. 3.10, [44], [45],[46],[47], [48]

The reference frame for the simulation is Cartesian with the Earth's equatorial plane coinciding with the xy-plane. The positive z-axis aligns with the Earth's rotational North pole. The Earth itself is in the focal point on the negative x-axis and the positive x-axis goes through $RA = 0^\circ$. The orbits are constructed with an ellipse in the xy-plane, which is then rotated by i around the y-axis. Finally the focus point is subtracted to center the orbit around the Earth.

$$a = \frac{r_a + r_p}{2} \quad (3.5a)$$

$$e = \frac{r_a - r_p}{r_a + r_p} \quad (3.5b)$$

$$c = e\dot{a} \quad (3.5c)$$

$$b = \sqrt{a^2 - c^2} \quad (3.5d)$$

$$\mathbf{f} = [-c, 0, 0]^T R_y \quad (3.5e)$$

$$\mathbf{r} = [x, y, z]^T R_y - \mathbf{f} = [a \cos(\theta), b \sin(\theta), 0]^T R_y - \mathbf{f} \quad (3.5f)$$

$$\text{where : } R_y = \begin{bmatrix} \cos(i) & 0 & \sin(i) \\ 0 & 1 & 0 \\ -\sin(i) & 0 & \cos(i) \end{bmatrix} \quad (3.5g)$$

$$\text{and : } \theta_j = \frac{2\pi t_j}{P} \% 2\pi \quad (3.5h)$$

Figure 3.21: Equations describing an elliptical orbit. Here a is the semi-major axis, b is the semi-minor axis, c is the distance to the foci, \mathbf{f} is the vector to the Earth focus, \mathbf{r} is the position vector to a point j at time t_j and corresponding true anomaly θ_j . R_y is the rotation matrix around the y-axis, i is the inclination and P the period.

To determine the blockage by a body, the pointing direction is compared to the vector from the spacecraft to the body. The later is calculated by centering the spacecraft: $\mathbf{r}_k = \mathbf{r}_k - \mathbf{r}_{sat}$. Where $k = \{\text{Earth, Moon, Sun}\}$. The resulting position vector can be used to calculate the declination ϕ_j at each time j . Which in turn can be related to the angular separation $\Delta\alpha_{j,k,l}$ of the objects k and the targets l according to Pythagoras' law. The results are shown for the individual bodies in Figure 3.22. The total of these can be inverted to visualize the available observing time (Figure 3.23).

$$\phi_j = \arcsin\left(\frac{z_k}{\|\mathbf{r}_k\|}\right) \quad (3.6)$$

$$\Delta\alpha_{j,k,l} = \sqrt{(\theta_{j,k} - \theta_l)^2 + (\phi_{j,k} - \phi_l)^2} \quad (3.7)$$

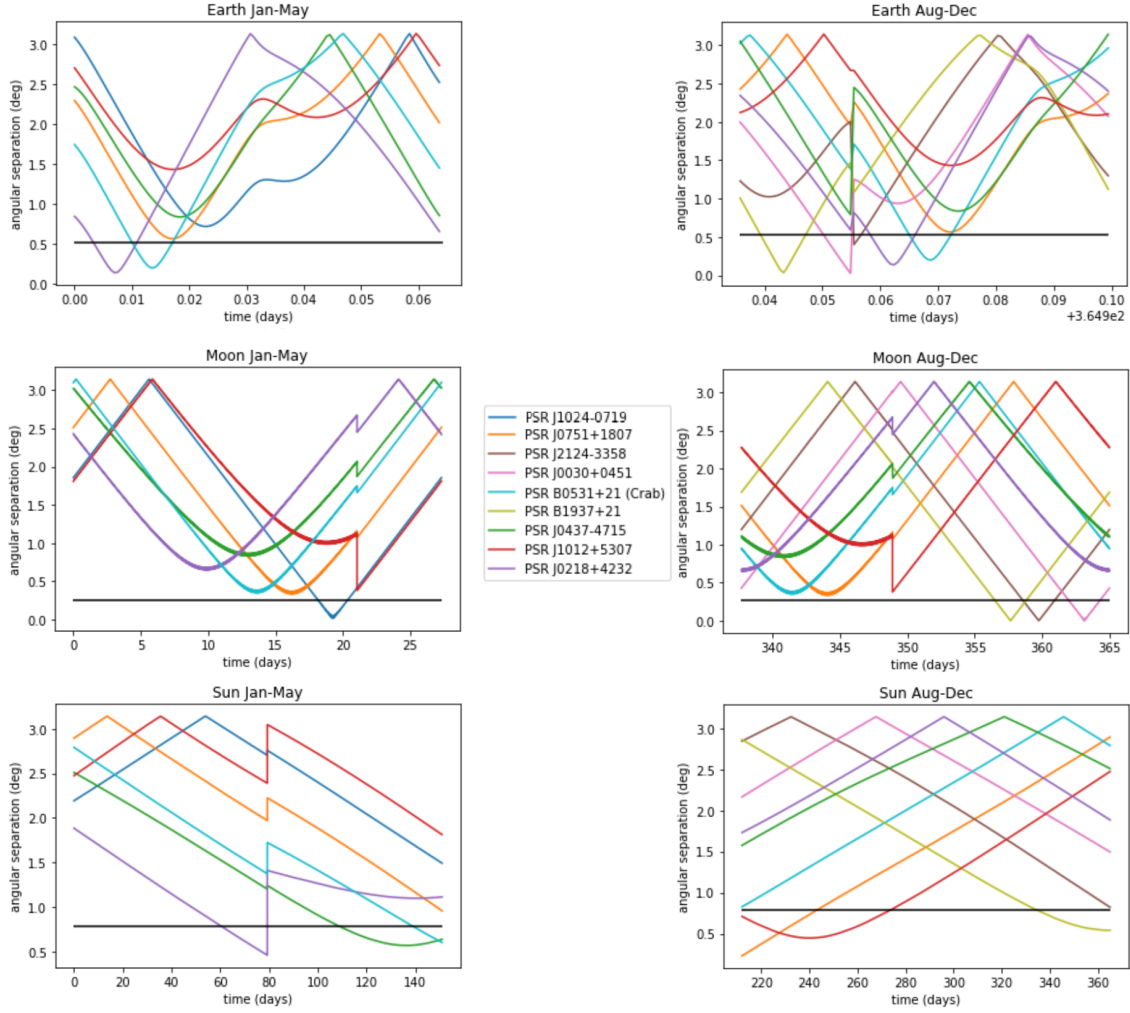


Figure 3.22: Angular separation $\Delta\alpha_{k,l}$ between the target blocking bodies $k = \{\text{Earth, Moon, Sun}\}$ and the pointing directions l . The left column displays the Jan-May period and the right column the Aug-Dec period. The x-axes correspond with this in terms of days from the start of the year 2025. The black line in each of the figures indicates that object's blockage angle. Anything below this line will not be visible.

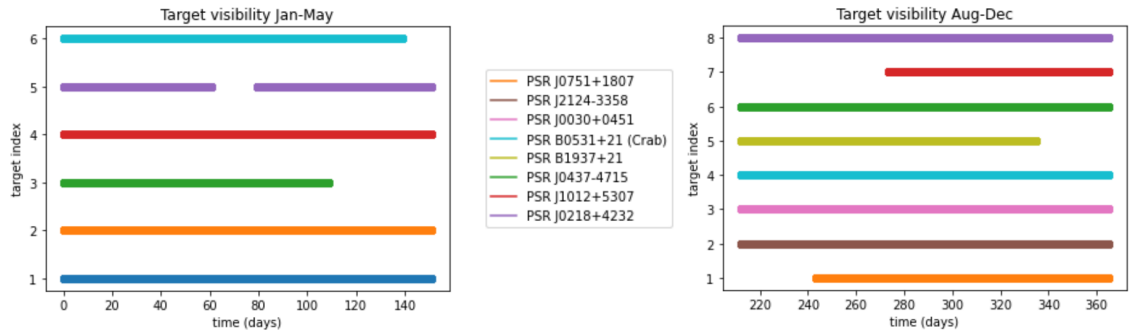


Figure 3.23: Intervals in which each of the targets is not blocked by either Earth, Moon or Sun. Note that seemingly continuous lines contain small scale gaps.

Similar calculations are preformed for the communications and power systems. For communications the position vector from the center of the Earth to the ground station was

calculated (Kongens Lyngby, DK; lat:55.763516°, long:12.494943°), and rotated with the Earth's rotation according to $\mathbf{r}_{GS,j} = \mathbf{r}_{GS,0}R_z$, with:

$$R_z = \begin{bmatrix} \cos(j) & -\sin(j) & 0 \\ \sin(j) & \cos(j) & 0 \\ 0 & 0 & 1 \end{bmatrix} \quad (3.8)$$

The direction from the spacecraft to the ground station is the above ground station vector minus the spacecraft position vector. Assuming the roll of the spacecraft is free, the angular separation between target and ground station is calculated similar to the blockage for the limiting angles listed in table 3.6.

For the power system the same strategy is applied, now comparing the earlier calculated separation between Sun and target to the power requirement angle.

Figures 3.24 and 3.25 show the time at which the spacecraft is pointing to a target and using comms or solar panels at the same time, respectively.

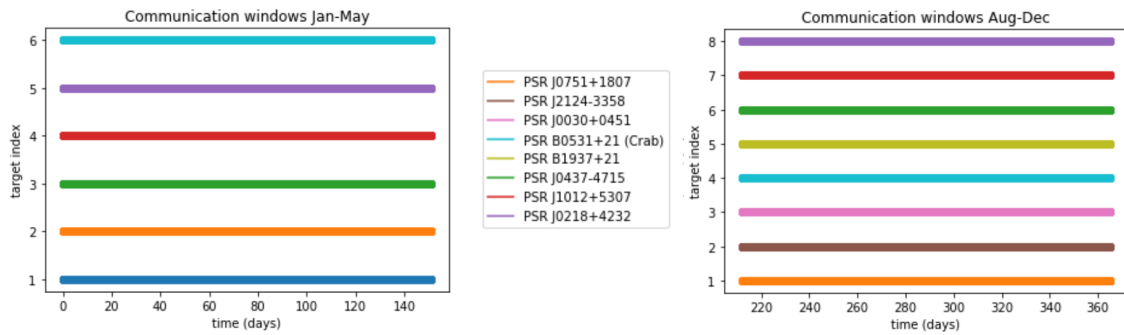


Figure 3.24: Intervals at which the spacecraft can point at a target and use communication with Earth at the same time. Note that seemingly continuous lines contain small scale gaps.

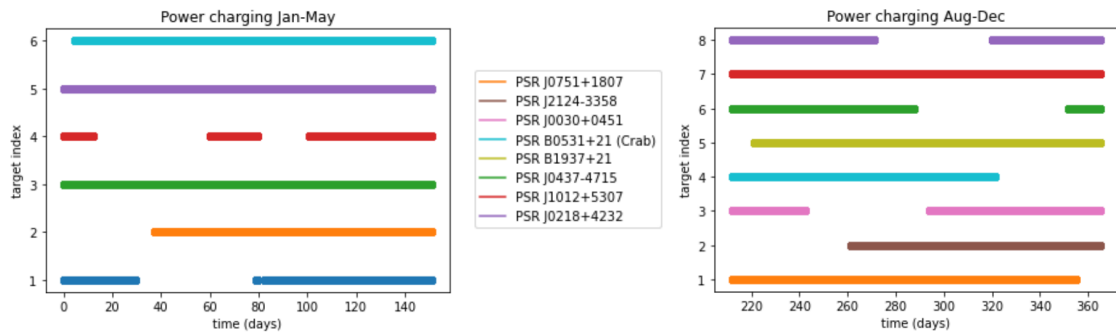


Figure 3.25: Intervals in which the spacecraft can point at a target and charge its solar panels at the same time. Note that seemingly continuous lines contain small scale gaps.

Ideally, the spacecraft will have to turn as little as possible. A time schedule can thus be proposed in which re-pointing is only done to switch targets after the observing time requirement of 20 days has been met. For such a schedule one would include only intervals in which:

1. solar panels are in the Sun,
2. communication with Earth is possible,

3. and the target in question is observable.

To achieve this, figures 3.25, 3.24, and 3.23 can be combined. The resulting available intervals are shown in figure 3.26 and listed quantitatively in table 3.8.

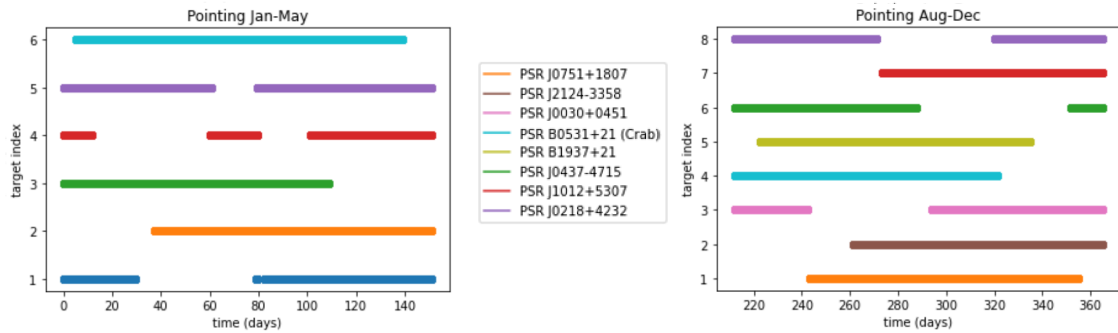


Figure 3.26: Intervals in which targets, power and communications are all available at the same time while pointing at the target. Note that seemingly continuous lines contain small scale gaps.

	Jan-May				Aug-Dec			
	Visibility (days)	Comms (hours)	Power (days)	Total (days)	Visibility (days)	Comms (h/day)	Power (days)	Total (days)
PSR J1024 -0719	139.7	9.4	98.1	36.3	-	-	-	-
PSR J0751 +1807	151.0	10.9	113.6	50.9	121.9	10.9	142.7	49.8
PSR J2124 -3358	-	-	-	-	135.8	9.3	103.8	35.9
PSR J0030 +0451	-	-	-	-	128.9	9.1	101.5	31.5
PSR B0531 +21(Crab)	123.6	11.5	146.4	58.8	136.0	11.3	109.1	47.6
PSR B1937 +21	-	-	-	-	97.9	11.7	143.8	44.9
PSR J0437 -4715	108.9	10.4	151.0	47.5	153.0	10.4	88.8	38.9
PSR J1012 +5307	151.0	8.2	81.4	27.1	91.4	8.1	153.0	30.2
PSR J0218 +4232	116.3	10.4	151.0	49.8	134.8	10.5	103.6	39.8

Table 3.8: These numbers express the total time that a subsystem can fulfill its pointing requirements while the spacecraft as a whole is pointed to one of the sources. All times are over the full periods Jan-May or Aug-Dec, except for the telecommunication, which is expressed in hours per day to compare to its requirement. The columns with the total time contain the times for which all three systems could be active at the same time.

From a attitude point of view, science mode, safe mode (charging) and telecommunication mode can be active at the same time during the intervals in figure 3.26. Targets could therefore be picked and chosen at will during these intervals without the need to switch modes. However, there might be constraints from the point of view of other subsystems, such as the power system not being able to supply all systems at the same time or the ground station not being active at all times. A more realistic time schedule would thus be

made by switching between communication mode and science mode. This switch does not necessarily require re-pointing, just the on-off switching of the relevant systems. For the numbers in table 3.8 it is clear that the requirements of the different subsystems listed earlier in table 3.6 are easily fulfilled within the plotted intervals. The total available time is > 20 days for all targets, even with 160 s of telemetry mode per day subtracted from the total. As for the power, during the intervals the solar panel is always receiving sunlight so no discharge time is used. Although the requirements are thus nicely met, the future work should include a few improvements to the simulation, which are listed below.

- Antenna/panel conflict: The roll angle might be conflicting for the comms and power system, so there might not exist a way for which both can be pointed in their desired direction at the same time. This is a point that should be considered in more detail in future research.
- Solar panel independence: Not included here is that the solar panels can rotate independently. The solar panel has its own pitch/yaw (depending on the roll of the whole spacecraft) rotation axis and might therefore not always require full spacecraft turning to be in the Sun. This characteristic could also partially compensate for the roll conflict with the antenna.
- White spaces between the total pointing intervals: In the total pointing intervals, only those times are considered for which all three systems are available at once. But from figures 3.24, 3.25, and 3.23, it is clear that these white spaces include times in which individual systems are available. Utilizing these and optimizing the order in which to observe the different targets will thus eventually add extra observing time.
- Rotation time: Missing from the total available time is the time it takes to rotate. An estimation can be made from the maximum turning speed of 10deg/s (sec. 2.2.4). The maximum amount of turning that's possible in general is 180deg in both RA and DEC. This is a worse case scenario which would result in $2180/10 = 36\text{s}$ per turn. Since in the currently proposed schedule the spacecraft only turns for the targets, that would at most result in $(8 + 6) * 36 = 504\text{s}$ for the whole year. Since this is so little it is for now neglected. However, if a schedule is proposed with more turns, it is relevant to calculate the individual turning times. In these calculations it should also be considered the maximum speed might not always be available and that a turn might take longer than the above estimate due to the attitude control system needing to balance out the induced angular momentum for a turn.
- Drag constraints: In section 3.4.3.2 the drag coefficient during the orbit and its effect on the spacecraft is discussed. The curve in figure 3.34 shows this progression. In order to avoid extreme drag effects, the solar panels should ideally be constant with respect to the orbit's velocity vector. However, this can be in direct conflict with the sunlight acquisition at times. Study is thus needed on accepted angular separation between panel and velocity, on the time at which this angle is exceeded, and on how that might be compensated by the spacecraft's pointing and the battery time. Drag is an important disturbance factor for the spacecraft. It is therefore crucial to add its constraints as requirements to the time schedule simulation.

3.2.7.3 Detumbling

When a spacecraft is launched into space, external disturbances such as gravitational gradients, atmospheric drag, solar radiation pressure and Earth's magnetic field can cause the spacecraft to lose its stability and begin tumbling. Tumbling refers to an uncontrolled spin of the satellite, and it can cause undesired effects and actual damage. Therefore, it is critical to detect and correct tumbling as quickly as possible through a process called

detumbling. The detumbling process typically involves using the S/C's actuators and control mechanisms to reduce the rotation rate and bring the spacecraft back to its desired attitude. This can be a complex and challenging process that requires careful planning and execution, as well as a sufficiently accurate control system that fulfills the satellite's features and mission requirements. CubeSats experience a high angular velocity when deployed into orbit due to the uneven force of deployment. This initial spinning motion is not suitable for accurate attitude control, and therefore, it is necessary to reduce the angular velocity of the CubeSat to an acceptable level before transitioning to an attitude control approach. From FYS program's requirements, it is stated that the CubeSat's system has to prove being able to detumble an initial spin of $\omega = 90$ [deg/s] on each of the three axes x, y, z .

Different techniques can be implemented in order to achieve the detumbling of the satellite. The choice of technique depends on the specific characteristics of the spacecraft's rotation and the available resources. For spacecraft rotating around a single axis, spin-stabilization is a common detumbling technique. The fundamental concept involves utilizing the spacecraft's thrusters to apply a counter-rotational force, slowing down and ultimately stopping its rotation. The thrusters are fired intermittently in short bursts timed to coincide with the spacecraft's rotation. This technique can be quite successful, particularly when the spacecraft is rotating at a relatively low speed. However, it may not be effective for spacecraft that are tumbling on multiple axes or rotating at high speeds. Moreover, this method can consume a significant amount of fuel, leading to a reduced operational lifetime of the spacecraft.

When dealing with satellites that are rotating rapidly or tumbling on multiple axes, momentum unloading is a more suitable approach. The fundamental concept involves utilizing the spacecraft's reaction wheels to transfer the excess momentum of the rotation to the spacecraft's body. This is achieved by controlling the reaction wheels to spin in the opposite direction of the spacecraft's rotation, enabling them to absorb the excess momentum and reduce the rotation rate. Once the tumbling has been halted, the reaction wheels can be employed to stabilize the spacecraft in the desired orientation. While this technique can be challenging to implement and requires precise control of the reaction wheels, it doesn't consume fuel and does not necessitate additional thrusters. PANTSat has to be stabilized for rotation along the three axes, and isn't equipped with a propulsion system. Therefore, momentum unloading seems the most suitable technique to detumble it.

Among all the different actuators that can be used for this purpose, magnetorquers present various advantages. A magnetorquer works by interacting with Earth's magnetic field to generate a magnetic moment, which produces a control torque that can be used to detumble or control the attitude of the spacecraft. The strength of the torque depends on factors such as the dipole moment generated by the magnetorquer, the intensity of Earth's magnetic field at the spacecraft's location in orbit, and the relative orientation of these two fields. The highest magnetic torque is achieved when the moment produced by the magnetorquer and Earth's field are perpendicular to each other. In a LEO orbit, the primary disturbance encountered is from the Earth's magnetic field, indicating that utilizing actuators like magnetorquers is a valuable choice in these kinds of orbits.

Here, the detumbling control law is developed following the B-Dot controller. Equation 3.9 shows the torque generated by the magnetorquers:

$$\mathbf{L} = \mathbf{m} \times \mathbf{B} \quad (3.9)$$

$$\mathbf{m} = \frac{k}{\|\mathbf{B}\|} (\omega \times \mathbf{b}) \quad (3.10)$$

where \mathbf{m} is the commanded magnetic dipole moment generated by the torquers, ω is the angular velocity, \mathbf{B} is the magnetic field sensed by the onboard magnetometer and \mathbf{b} is equal to $\frac{\mathbf{B}}{\|\mathbf{B}\|}$ and k is a positive scalar gain that can be computed as:

$$k = \frac{4\pi}{T} (1 + \sin\xi_m) J_{min} \quad (3.11)$$

where T is the orbital period in seconds, ξ_m is inclination of the spacecraft orbit relative to the geomagnetic equatorial plane and J_{min} is the minimum principal moment of inertia. k is always >0 .

This generates a control torque perpendicular to \mathbf{b} :

$$\mathbf{L} = \frac{k}{\|\mathbf{B}\|} (\omega \times \mathbf{b}) \times \mathbf{B} = k(\omega \times \mathbf{b}) \times \mathbf{b} \quad (3.12)$$

The detumbling control command for each of the torque rods can be written as:

$$m_i = -m_i^{max} \text{sign}(\mathbf{u}_i \cdot \mathbf{B}) \quad (3.13)$$

for $i=1,\dots,4$, where m_i^{max} is the maximum dipole that the i -th rod can produce and the unit vector \mathbf{u}_i indicates the direction.

To demonstrate the stability of this control law, the following Lyapunov function for kinetic energy is examined:

$$V = \frac{1}{2} \omega^T J \omega \quad (3.14)$$

$$\dot{V} = -k \omega^T (I_3 - \mathbf{b} \mathbf{b}^T) \omega \quad (3.15)$$

which results in $\dot{V} = 0$ when ω is parallel to \mathbf{b} . n

This technique has been successfully simulated in a MATLAB environment. The simulation was conducted to investigate the effectiveness of the B-Dot technique in stabilizing PANTSat with the chosen ADCS. The Runge-Kutta-1 iterative methods were implemented in the algorithm, as well as filtering methods due to the fact that attitude sensors usually accumulate some measurement noise (here implemented as white Gaussian noise). The algorithm takes into account a set of 3-axis magnetorquers, a gyroscope and a magnetometer [49]. The results of this simulation will be presented and discussed in further detail, allowing for an evaluation of the control law's response. Figure 3.27 shows the result of the simulation, where the angular speed of the satellite has been successfully decreased after 10 orbits. It is possible to note that both the current dedicated to the magnetorquers and the angular spin of the satellite converge to zero after roughly 4×10^4 seconds. Heritage from previous similar missions suggest that a S/C presenting similar characteristics to PANTSat with regards to mass, volume and orbit, and implementing the same ADCS, XACT-50, are considered effectively de-tumbled when $\omega < 0.13$ [deg/s] [42]. Such value is achieved by the examined control law in approximately 2×10^4 seconds.

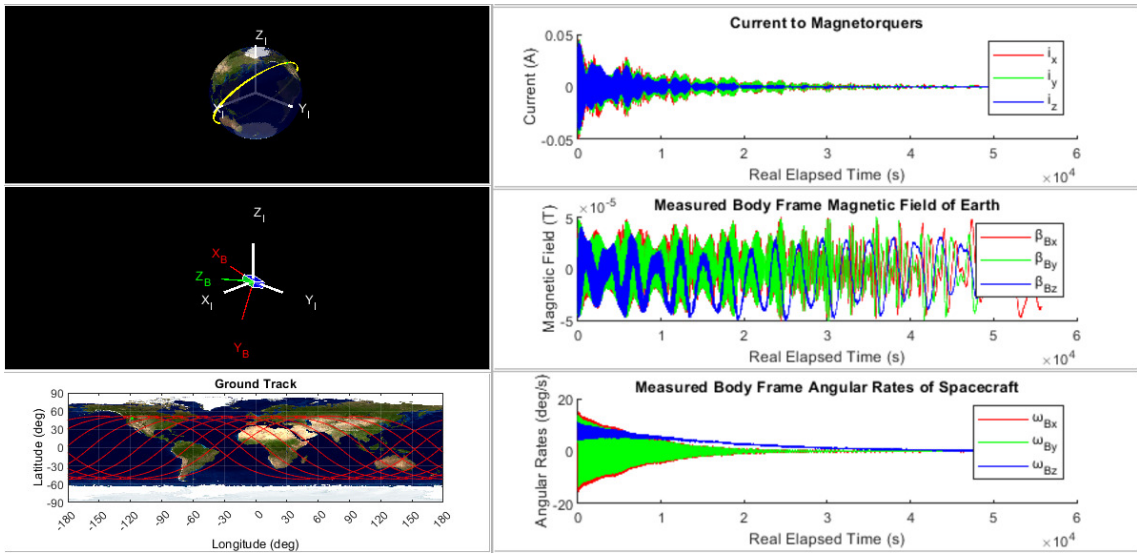


Figure 3.27: Detumbling simulation results. The reference system in red and green refers to the CubeSat's body frame, while the reference system in white is the ECI frame.

3.3 Onboard Computer (OBC)

3.3.1 Introduction

The Onboard Computer (OBC) is responsible for connecting and controlling various critical systems of the satellite, as it handles data processing, control, and communication functions. The OBC and its software should be robust, reliable, and autonomous, as actions are often required without a stable connection with a ground station.

Selecting an OBC compatible with the other sub-systems in the CubeSat is crucial, there are requirements such as power and form factor, but also mission-specific requirements such as reliability and radiation hardening. As to decrease the workload, a focus has been on existing CubeSat OBCs and operating systems.

Next to hardware, software design and verification is also critical in a well functioning OBC. This starts with selecting the right operating systems and tools to work with, but also requires careful consideration of what the software requirements are. As software development is a dynamic process different suggestions for these steps are given, but it is ultimately up to the (software) engineers to decide on these tools.

The mission modes given in Section 1.5 provide the CubeSat software with enough autonomy to perform its tasks, and are designed to cover any situation the satellite might find itself in. Together with the rest of the satellite systems the OBC and its software should be modelled and simulated.

3.3.2 Requirements

ESA lists essential requirements for CubeSat missions as the following:

- The CubeSat should allow modifications to the on-board software after the satellite assembly is complete and while on ground.
- The on-board software should allow in-orbit changes to its configuration.
- The on-board software shall implement a command-loss timer that triggers a recovery routine if a telecommand from the Ground Station is not received after a certain period.
- It shall be possible to switch the satellite ON and OFF via an umbilical connection.
- The CubeSat shall have the capability to send telemetry and receive telecommands through an umbilical connection.
- It shall be possible to recharge the CubeSat batteries once the satellite is fully integrated, for example via the umbilical connection.

These OBC requirements have been extended to the following list, and are driven by various sub-systems of the CubeSat (power, mechanic, etc.), but also has its own requirements (reliability, radiation hardening):

- **High reliability:** the system should be fault tolerant, have redundancies built in, and minimized risk of (sub) system failures.
- **Low power consumption:** the OBC should be power efficient, and have a low power mode built into its software.
- **Flight-proven system:** the OBC should be a flight-proven system, as the focus is on testing other components in the CubeSat.

- **Sufficient memory and processing power:** the system should have enough memory to store data and software between downlinks, and the power to process all this data and simultaneously control various systems.
- **Radiation resistant:** the computer should be able to withstand radiation in a space environment, as a small radiation fault could cause the satellite to malfunction.
- **Small form factor (mechanical compatibility):** the system should be lightweight, compact, and naturally fit in a CubeSat system.
- **Built-in Global Navigation Satellite System (GNSS):** as support and verification of other systems.
- **Sufficient data-transfer rates:** data transfer rates are handled by the telemetry and communications sub-system, though it is important that the OBC is compatible with this.
- **Fault tolerance:** the system should have both hardware (such as an I2C bus), and software fault tolerance (autonomous testing and error handling).
- **Modern software support:** the OBC should be able to support modern CubeSat operating systems and software.

3.3.3 System Overview

3.3.3.1 OBC

According to requirements the Endurosat OBC Type I has been selected, which stood out as it was a flight-proven system developed specifically for CubeSat missions [50]. Its main strengths are advertised as being power efficient, radiation resistant, and robustly tested on previous CubeSat missions.

It measures roughly 94x89x20mm in its casing, and has various interfaces such as UART, I2C, SPI, and Ethernet (described in detail in figure 2.1).

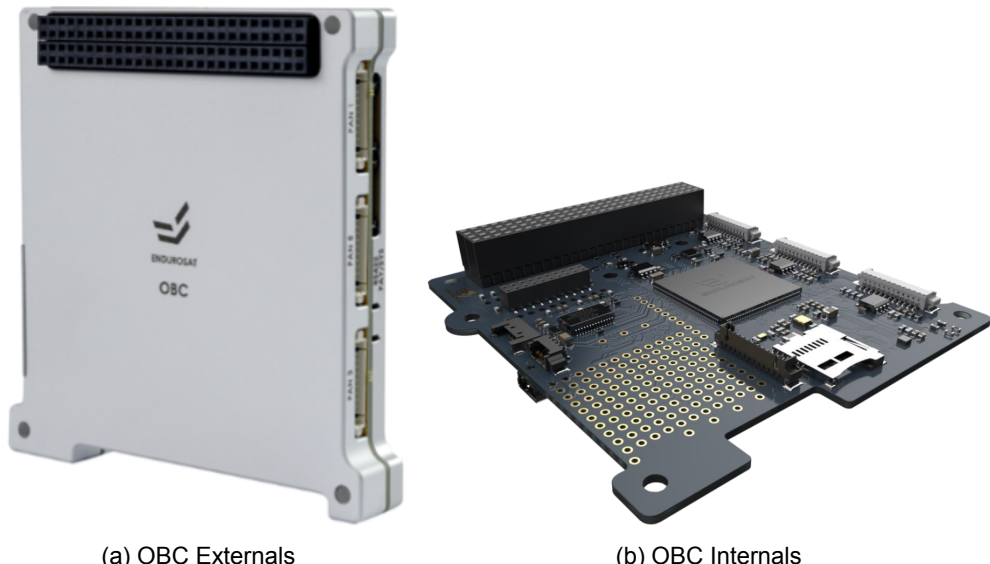


Figure 3.28: Endurosat OBC Type I

3.3.3.1.1 Processor and Onboard Memory The Endurosat OBC has an ARM Cortex-M7 processor with 2MB Flash, 1MB SRAM, DPFPUs, and 8-Mbit External FRAM. The OBC

also has a Micro SD card slot that allows for an 8GB-32GB card. This is by far plenty of processing power and memory for the simple tasks and data processing the satellite will be doing (depending on OS choice this will take up around 100MB-1GB, and leave plenty of space for observation data). The expected worst-case memory accumulation between transmissions is 9.5 MB, which means we have a margin of up to 96% with an onboard memory of 32 GB.

3.3.3.1.2 Power The Endurosat spec sheet communicates average power usage of 0.9W, though further testing with the hardware will have to show what power usage in different modes of operation is.

3.3.3.2 GNSS

The Global Navigation Satellite System (GNSS) is an important part of the satellite validation system. With this we are able to accurately determine the location of the spacecraft. The GNSS module is an integrated part of the Endurusat OBC (it's an opt-in). This allows for seamless communication between the onboard-software, and the GNSS module. The GNSS antenna needs to be connected and mounted outside the frame of the spacecraft, to support the satellite-observations. The location of the patch-antenna can be seen in the mechanical section.

The Endurusat GNSS module expects an absolute positional error of 1.5 m, with a velocity error of 0.03 m/s [51]. This is an important additional source of data for the ADCS system, and the validation for the mission success and orbital determination.

3.3.4 Software

Four main modes of operation have been considered based on power requirements and reliability measures, namely Commissioning, Safe Operations, Observe Operations, and Communication Operations. These modes have been introduced in section 1.5. Each of these modes have their own sub-states and sub-modes, partially described in the state diagram, and partially up to implementation by the software team.

Existing software solutions for CubeSat satellites have been considered, as this reduces the amount of work required to develop the software functionality. One of these is FreeRTOS, which has been used and flight-proven on the Endurosat OBC missions before [52]. This Operation System (OS) is fairly basic and would most likely need quite some implementation, but is lightweight. Another OS considered is the Linux-based open-source KubOS, which provides detailed mission tools and an extensive platform, but has not been used for Endurosat OBC missions prior (it has flown on other missions).

Endurosat also has its own proprietary operating system called EnduroOS, together with an SDK, designed to be modular, scalable, and customizable, though this is not publicly accessible. Ultimately the decision on what software platform to use is up to the developers and engineers implementing the systems.

The safe mode has several instances where it would be necessary to go into this mode. Some of these are detected errors that could not be resolved, when pointing or stability can not be achieved, when not enough power is delivered or communication issues. Many of these would already be handled by the commercial software, however some design decisions need to be made. Here we would need a command-loss timer, such that we automatically enter safe mode when no communication link can be achieved. We expect to be able to observe the satellite for 15 minutes while it passes over the ground station. During this fly-over pass, if (during the 15 minutes) we receive no communication link, or heartbeat from the satellite, we initialize safe mode, until communication can be established.

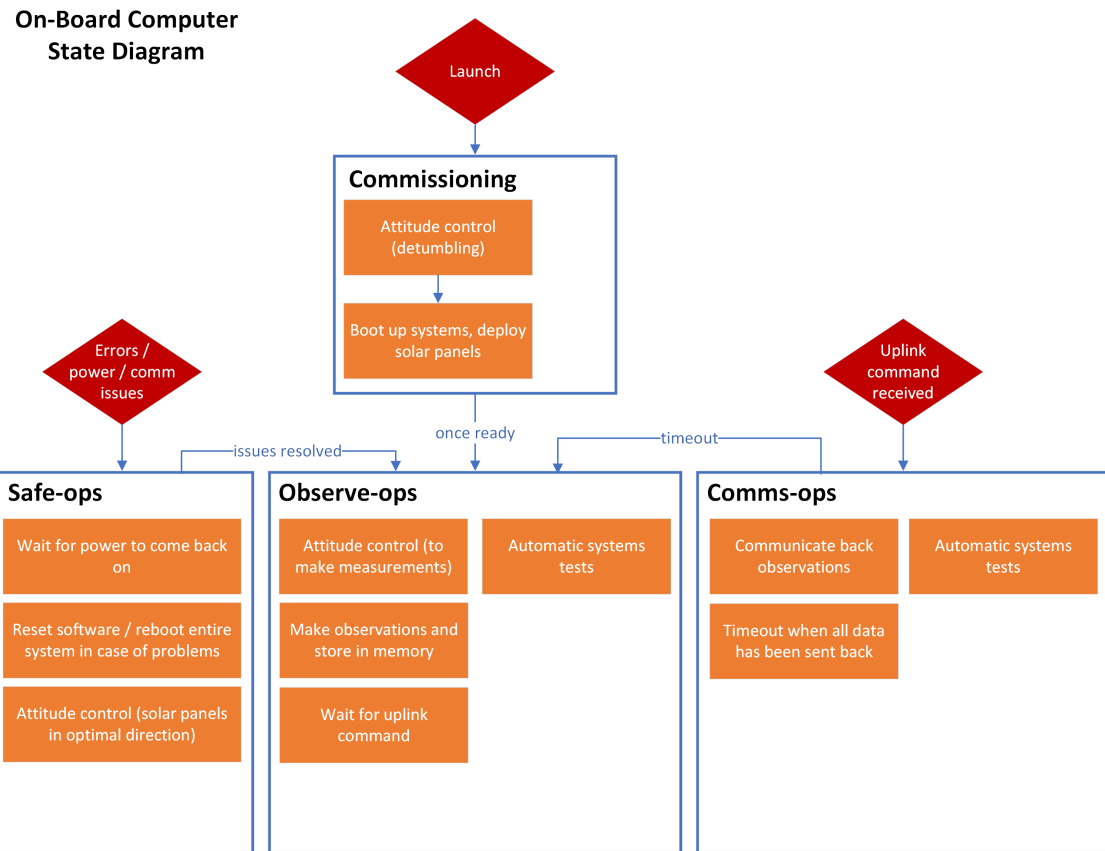


Figure 3.29: State diagram showing different modes of operation in software.

3.3.4.0.1 Connectors The connectors provided by the OBC can be seen summarized in table 3.9, along with the dedicated system for the interface. We can then see that we have a large variety of ports, when the majority are able to be accommodated by the I²C bus. An important part of the OBC connectors, to support the requirements for the OBC, is the USB connector. Or, at least, the possibility to test and update during the commissioning phase, and testing phase of the spacecraft.

Ports	Interface	Used by
4	RS-485	
2	RS-422	
3	UART	Communication Subsystem
2	I ² C	Data Bus
1	SPI	
1	CAN	
1	USB-C	On-site test and updates

Table 3.9: Connector overview for the Endurasat OBC

The interface diagram is shown in 2.1, in the design chapter. This shows an overview of the interfaces, however the table below shows which ports of the OBC are used.

3.4 Orbit, Launch and Deployment

3.4.1 Introduction

Orbit design and, consequently the orbit deployment choices, are quite significant for any space mission, as they bring to the table a diversity of requirements that flow down to the remaining teams and subsystems, ultimately influencing their design choices. Furthermore, given the shortage of time to come up with a feasible solution, these choices gain even more importance, since presenting a solution solely focused on ensuring the best environment for payload performance can overwhelm the remaining teams involved with work that might have not been necessary considering the context of the mission.

This being said the choice of the orbit is pivotal to the mission design, development and science phases, in which a mischoice of it could bring the whole process to start over, which was something we could not afford within the 10-week period allocated to the project.

3.4.2 Requirements

The orbit, launch and deployer are constrained by the various subsystems of the CubeSat. The principal and most critical effects and requirements are listed below. They are requirements that are either imposed upon us or requirements that we set upon other subsystems.

1. Orbit lifetime, imposed by the mission's scientific objectives. If the orbit lifetime is not long enough, PANTSat won't have enough time to fulfill the mission objectives
2. Communication up-link, or minimum necessary communication windows, defined by the telecom. subsystem. The orbit must fulfill this requirement, or we won't be able to download the data in time
3. The orbit lifetime must be between 6 months and 25 years, requirements set by ESA. We fulfill this requirement by having an orbital lifetime of 11.5 months
4. No on-board propulsion system. The CubeSat deployer demands that there is no onboard propulsion system, and as the mission design does not include a propulsion system, this requirement is fulfilled.
5. Orbital Debris Assessment Report (ODAR). This report is mandatory for all satellites with a mass larger than 5 kg. This requirement is set by NASA, and has, as of the date of writing, not been made. However, this would definitely be on the priority list in the future.

These are requirements that we set upon other subsystems:

1. Mechanical structure, defined by the CubeSat deployer onboard the International Space Station (ISS). The mechanical team must comply with the deployer's constraints or else the CubeSat will not be able to be deployed. They comply with this requirement, as seen in Section 3.7.1.1.
2. Time spent in the Earth's shadow (eclipse), constraining the EPS subsystem and Thermal subsystem. The time spent in Earth's shadow affects the battery lifetime needed, the amount of solar radiation the CubeSat receives, and the amount of time the solar panels get to recharge.

We end up meeting all requirements, or at the very least have plans to meet requirements. The other subsystems also end up meeting the requirements that we set upon them.

3.4.3 Orbit determination

The first thing we looked into for the first iteration of the orbit was ensuring that the environment in which the science phase of the mission was being conducted was as close as possible to the optimal environment. According to [53], where it is studied how the different Keplerian elements that characterize an orbit affect the performance of position and velocity estimation using an Extended Kalman Filter (EKF), within a wide trade space of bounded Earth orbits, the effects of the orbit choice on pulsar XNAV performance, in a sense of lower tracking error within the same amount of estimation time, are summarized in Table 3.10.

Orbit parameter	Influence (increasing parameter value)	Ideal orbit range for XNAV tracking
Semi major axis, a	+ Major driver of pulsar visibility and orbit average speed - Can place orbit in an area of high background radiation	High values (maximum value within the trade space of the study, $a = 42158$ km)
Eccentricity, e	+ Increases visibility at apogee - Decreases photon timing information around perigee	0-0.2 (depending on the semi-major axis)
Inclination, i	- Pulsar occultation due to magnetic poles causing visibility breakups	Dependent of pulsar choices
Argument of perigee, ω	Shifts pulsar visibility cycles in time	Dependent of pulsar choices
Right ascension of the ascending node, Ω	Used for initialization of XNAV measurements in EKF	ω unnecessary if $e = 0$ Ω unnecessary if $i = 0$

Table 3.10: Orbit Design Range for XNAV Tracking. Adapted from [54]

The results presented in Table 3.10 come down to maximizing the time in which a pulsar can be continuously observed by the instrument. For example, by choosing an orbit with a bigger radius a pulsar would have way less observation downtime due to Earth's occlusion. The same line of thought can be applied to eccentricity because if the orbit is very eccentric the perigee might be too close to Earth generating a very likely occlusion window to a variety of pulsars.

The choice of inclination angle is more related to the pulsar catalog chosen to perform measurements on, taking as an example the study, for the chosen pulsars (PSR_B 1937+21, PSR_B 1821-24, PSR_J 0218+4232 and PSR_J 0437-4715), an orbit with an inclination too close to 90° would lead to an increase of occlusion time.

The last two Keplerian elements, ω and Ω , are not only very dependent on the pulsar catalog chosen but also on the other orbit parameters, as the optimal value for performance varies from orbit to orbit. In addition, depending on the orbit chosen, these parameters may change over time due to J_2 perturbation which is something that, ideally, we would want to avoid as this implies a heavier re-scheduling of the observations.

Based on this information, the first orbit of choice was relatively straightforward: we would go for a Geosynchronous Equatorial Orbit (GEO) as it provides what appears to be the best performance environment, with a big radius, low eccentricity, plenty of room for long observation windows giving us more freedom to choose which pulsars to go for and we would not have to deal with the problems caused by J_2 perturbation.

The problem with such a choice was that, despite giving the best environment for the payload team to work with, we were not really looking into possible problems that we may

be causing to other teams, so, in the orbit design, we could not simply forget the fact that we proposed to design a CubeSat. This fact coupled with the inexperience of the team, the shortage of time and, especially, the data presented in Figure 3.30 made us reconsider the initial choice.

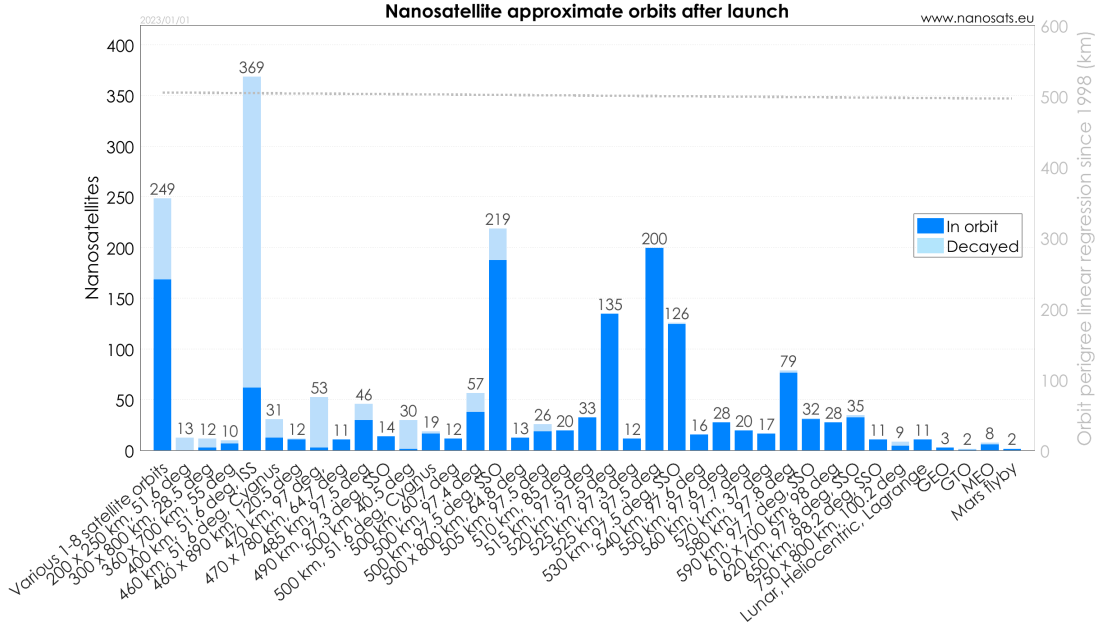


Figure 3.30: Nano-satellites approximate orbits after launch. [55]

The step back for us was quite obvious to be made as, looking at the data from Figure 3.30, the reduced number of Nano-satellites deployed into medium/high Earth orbits was too little to make us believe that, as a team, we would not run into data problems, possibly resulting in a task too big to be achieved within the design period. Furthermore, once looking at data within the same database, out of these launches 50% were 12U CubeSats and none were 6U, amplifying this belief that we were going for a treat if we were to choose a medium Earth orbit.

Merging these two major design drivers, we opted to go for a low Earth orbit. This obviously has consequences in what regards the payload performance, namely an increase in the convergence time of the position solution, a tighter schedule of pulsar availability, in other words, lower time available for continuous observations, and, as a consequence of the orbital period being relatively small, the number of daily occultations of pulsars would be higher than in the optimal case. Nevertheless, we strongly believe that paying this price in performance is worthwhile considering that we wanted to get an actually feasible solution out of the project and, in a technology demonstration mission, we want to show whether the instrument works or not, which is effectively possible in this environment.

The last step was to choose where within the low Earth orbit space we were going to put our satellite on. Here there were two paths: we could have gone for something completely customized with a very specific design based on a pulsar catalog we would choose or we could go for the data side of things by using an orbit similar to the one in which NICER is on. We opted to go for the second option simply because the data availability would be bigger than in the first case, which, in our opinion, was way too powerful considering the timeline. In addition, designing a pulsar catalog from the get-go was no easy task, the teams were

still investigating how XNAV actually works, so coming up with a random catalog of pulsars could have netted us some problems in the long run and therefore we chose a safer approach. Lastly, having an orbit closer to NICER's allowed us to use all the data available from performance reports and a variety of studies, namely in pulsar catalog choosing and observation schedules, and also we would operate in an environment relatively close to a 1:1 comparison between the two instruments, which can be seen as an objective of the mission.

3.4.3.1 Orbit characterization

As described previously, through the iteration process, we arrived at a LEO similar to NICER's, which is on board the ISS, whose parameters are compiled in Table 1.2. The parameters were also chosen taking into account data from the latest deployment of CubeSats made by the chosen deployment provider, which was made available by NASA. [56]

The orbit itself is not that revolutionary. It uses the orbit of the ISS, which is very well known, so the only thing we would like to point out, is that the ω and Ω are not specified in the table because they are heavily dependent on the ISS position in which the satellite will be launched and is something we cannot control that easily, thus we just set them to 0° for the simulations. Further visualization of the orbit can be seen in Figure 3.31, where, in red, it is shown the orbit trajectory and, in blue, it is shown the downlink region in which communications can be made with the chosen ground station. The simulation results were used to further characterize the orbit designed in order to provide information to the other teams and were obtained through simulation using the AGI's (Ansys Government Initiatives) STK . [43]

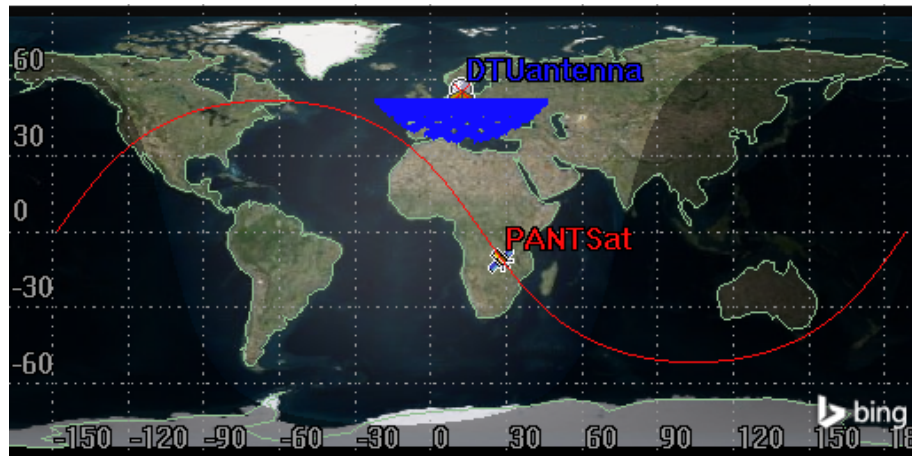


Figure 3.31: Orbit visualization, orbit trajectory in red and downlink cycles in blue.

Looking into the eclipse cycles, it is possible to see in the following figure that they occur relatively often due to the low orbital period, lasting from 2083 seconds (≈ 34.7 minutes), during Summer and Winter, up to 2161 seconds (≈ 36 minutes) during Spring and Autumn. Due to orbit decay, the minimum value tends to decrease with time, whereas the maximum tends to increase.

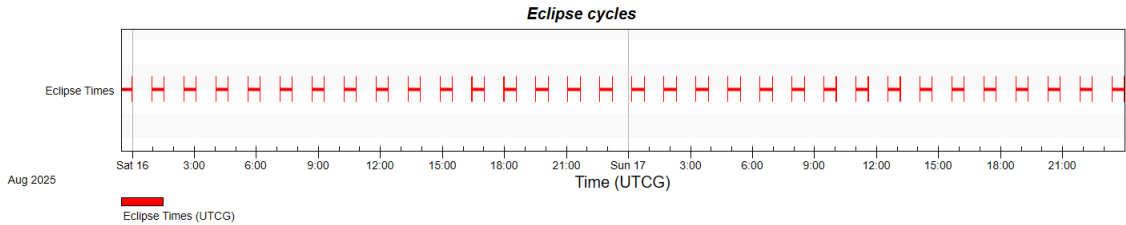
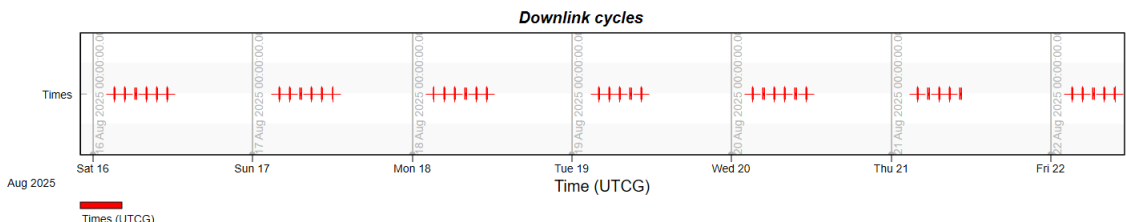


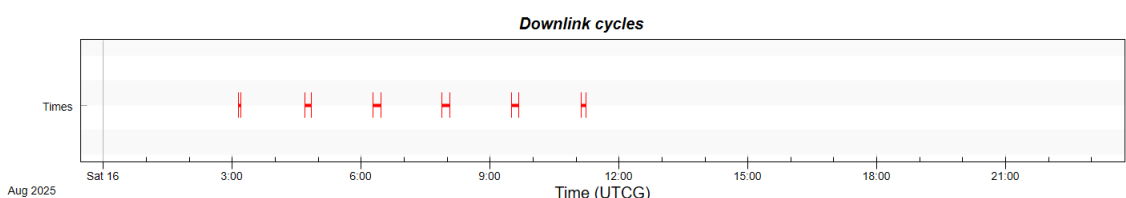
Figure 3.32: Eclipse cycles over the course of 2 days of simulation.

One important aspect to also take into account for the design of the communication system is how much time we have available to send data or receive data from the ground, so we looked into it. Based on the chosen ground stations, the simulation results for the downlink cycles obtained are presented in Figure 3.33. Over a daily basis, there are usually 6-7 cycles in which communication with the ground is possible from 4 are always long cycles of about 9-10 minutes and 2-3 shorter cycles lasting from 3 up to 7.5 minutes, making them a little more unreliable to consider as cycles to include in the scheduling of downlinking data. These daily cycles repeat themselves throughout time as illustrated in Figure 3.33a.

In addition, these time lengths tend to decrease with the orbit decay as the orbit average speed increases, so it is important to have a good margin in the time available to downlink when compared to the time we actually need. Considering the fact that, per day of operation, the whole data can be downlinked within a 3 minutes period (worst-case scenario), we have a considerable margin on the duration of these periods to deal with the orbital decay and a possible no downlink for a few days.



(a) Simulation over one week.



(b) Simulation over one day.

Figure 3.33: Downlink cycles simulation.

3.4.3.2 Orbit lifetime

For the given orbit design, another major constraint to the mission that comes out of it is the expected lifespan of the mission, which is related to the orbit lifetime. The estimation of the orbit lifetime was performed through STK, using the Jacchia 1970 atmospheric density model.

Through simulations, we realized that the major driver of the orbit lifetime was the drag area, so it was a parameter that could not be estimated roughly, we had to get a decently

accurate number to provide. This was a relevant problem because the solar array size is rather big compared to the most common design, which could hurt the mission's lifetime. We started by simulating the drag area of the spacecraft for a fixed position in the orbit while pointing at a few different pulsars, namely the calibration pulsar and some others included in our catalog of observations. We did this in Matlab, by approximating the Cubesat to a simple box and calculating the projected area. This was done by calculating the perspective transformation matrix that projects the CubeSat onto a 2D plane. Then the boundary of this projection was found, and finally the area of this boundary. In the simulation, we varied the one degree of freedom of the solar array, a rotation around the z-axis of the CubeSat, and the results can be found in Figure 3.34.

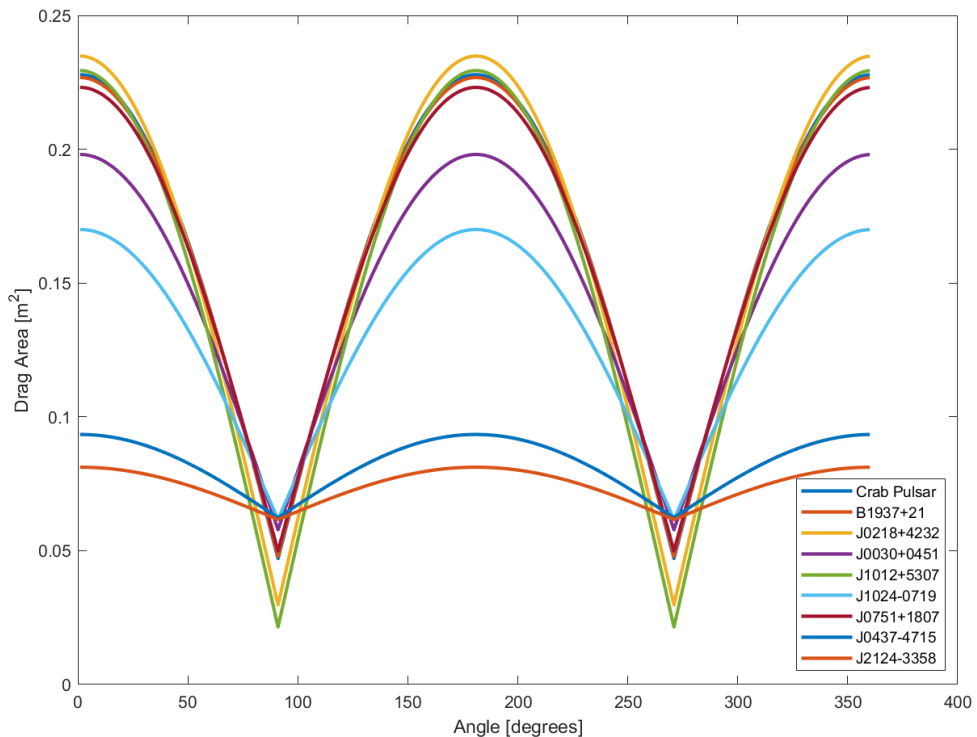


Figure 3.34: Crude simulation of the drag area for a fixed orbit position while pointing at the chosen pulsars as a function of the angle of the solar array rotation around the z-axis.

These are only crude simulations to expose the problem being analyzed, as these calculations could be made for the whole orbit, so a more rigorous model would have to be developed moving further in the project phases. The plot was obtained by assuming the position of the satellite in the orbit to be fixed, followed by a rotation of the whole satellite according to the pulsar to be observed location in the sky, coupled with a rotation along the nadir axis of the CubeSat was applied to the solar panel and, lastly, we take the projected area along the velocity axis. The maximum value observed corresponds to a situation in which the solar panel rotation is such that it is aligned perpendicularly to the velocity of the CubeSat, working like a sheet of paper perpendicular to the airflow, while the minimum corresponds to a situation in the solar panel is aligned with the velocity of the Cubesat, therefore, minimizing the drag produced by the solar panel.

The simulation results clearly illustrate the problem we are trying to bring up in this section,

if there isn't good enough tracking in this angle the drag area would start getting too big, Drag Area>0.1 m², the orbit lifetime would start being lower than 4 months. Based on the design of the CubeSat, the ACS team guarantees that it is possible to design a control loop for reference tracking of this angle, to minimize the drag area, based on rotating the spacecraft along the focal length axis.

If there is no control over the drag area, this is definitely a major mission-killer problem, because the mission lifetime decays too fast as we increase the drag area. This was something that was never brought up during any of the discussions, so this problem was never addressed in the sense that continuously rotating the spacecraft to track this optimal range that provides low drag areas will surely introduce vibrations in the pointing and will pose a major challenge to the EPS team because, in the simulations, it was assumed that the power production could be maximized by changing this angle. But there was never any constraint on the angle that could be tracked, introducing a sub-optimal power production scenario, which would not be as devastating as the situations presented in section 3.5.7.2, but we could end in a similar position where we can not produce enough power. This is definitely something that needs to be addressed moving forward in the mission design because there has to be made a trade-off between power production and orbit lifetime, otherwise the lifespan of the science could be too small to have the required data to show that the instrument works as intended.

This study would have to be performed by merging simulations together, in which we would simulate situations where we prioritize power production over minimizing the drag area or prioritize mission lifetime over power production and find a good balance between these two. In addition, there would have to be an analysis of the degradation of the pointing accuracy that results from the constant tracking of this angle. Based on this discussion, despite not being brought up at any point of the design or the PDR, we decided to include it as an action point that has to be addressed with major priority. The action item is identified as part of the Orbit team, but this is a complex problem that involves a variety of teams.

An example of the described analysis is illustrated in Figure 3.35, where it is studied the effect of increasing the drag area of the spacecraft on the orbit lifetime, in the number of orbits before reentry. It is possible to see that by loosening the importance we put into prioritizing mission lifetime, allowing a bigger drag area, we end up with a mission that may very well come down to just a few months.

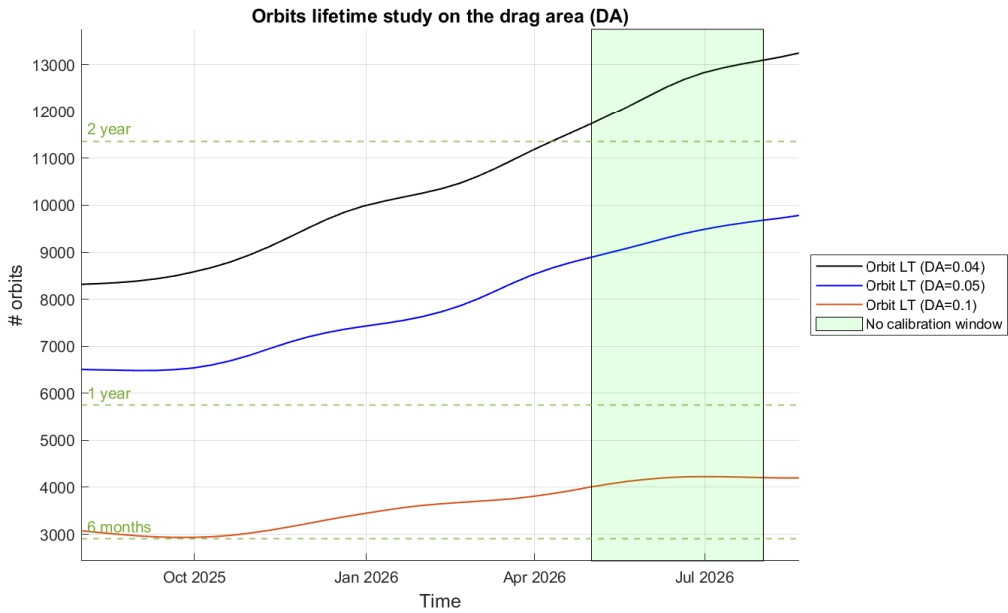


Figure 3.35: Orbit lifetime study for different drag areas over a period of one year.

Based on these results, assuming the worst-case scenario was not a good idea as the mission lifetime would come down to values lower than 3 months, but we still had to provide a placeholder number for the mission lifetime. Based on the discussion, we felt that assuming a maximum drag area acceptance of 0.06 would be reasonable because it does not put much pressure on the controller still allowing some loosen-ability of changes in the solar panel's angle. This yielded an orbit lifetime of 350 days (11.5 months). The orbit evolution through time is shown in Figure 3.36 assuming the planned launch in August 2025.

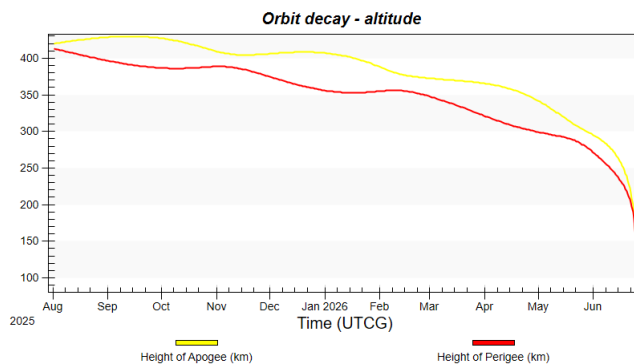


Figure 3.36: Orbit altitude decay considering a launch on August 1st 2025, assuming a mean drag area of 0.06 m^2 .

Once again, it is key to remark that this is very susceptible to changes moving forward as this was not addressed as a problem by the whole group, due to being too close to the deadline.

3.4.4 Launch

There are several different ways to get a CubeSat into orbit. We started this project with the goal of using FYS program, which offers an opportunity for universities to launch their

own CubeSat. This was abandoned from the get-go because it was rapidly concluded that meeting ESA's size requirements was impossible due to the payload's size. Unfortunately, we could not expect to be under ESA's guidance anymore in what concerns ensuring a launch to get us to orbit, so we looked into what the market currently offers. Figure 3.37 contains data on the number of nanosatellite launches per year performed by active companies in the market, according to the database already used in section 3.4.3.

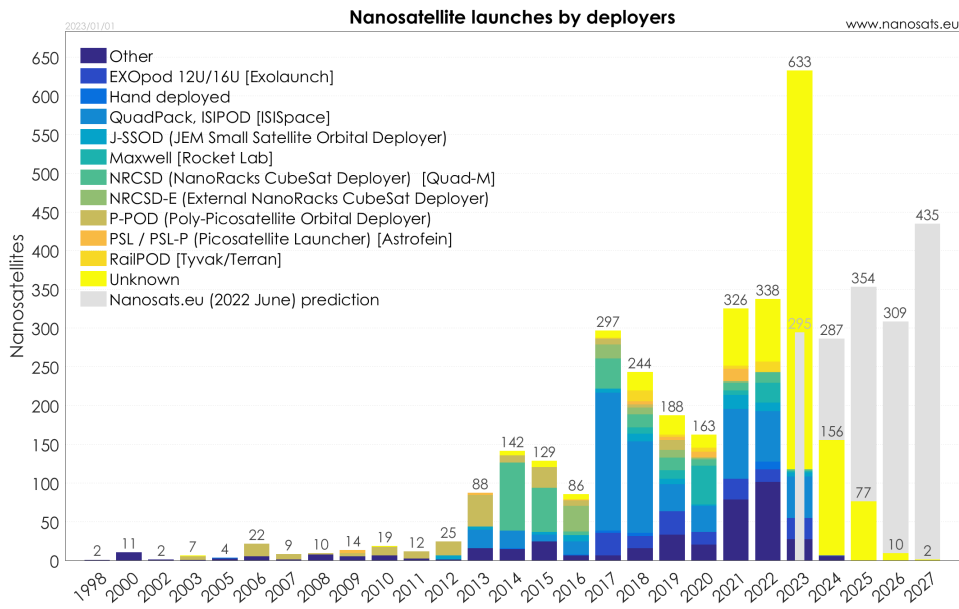


Figure 3.37: Nanosatellite launches per year by deployer company.[55]

There is obviously a wide variety of companies providing this type of service as a consequence of the growth of space exploration, nevertheless, a few companies caught our attention due to the high volume of launches, namely ISISpace, NanoRacks and Rocket Lab. All these companies offer a very similar type of service: they arrange the launch and take care of the logistics behind it. Here it may have been interesting to consider other types of options, such as smaller companies that would practice lower prices as it was brought up during the discussions, but the matter of fact is that, according to forecasts, the pressure on DSN would reach oversubscription values by 2030, making it a quite urgent matter to solve, leaving little room to afford a failed launch considering that preparing a mission, even this small, takes a good amount of time, so we did not consider such options.

ISISpace and Rocket Lab offer more orbit possibilities as they provide launches to any orbit within the demand range, whereas NanoRacks offers launches only to the ISS. In addition, NanoRacks and ISISpace make use of ridesharing in order to get the customer's satellites to orbit, in opposition to Rocket Lab, which uses its own rocket, making, as of this moment, their price per launch far above SpaceX's, resulting in a price less competitive.

Further investigating the number of launches done by each company, according to information published on ISISpace's website, out of the 618 launches mentioned more than 40% were made with a rocket specifically designed to get satellites to sun-synchronous orbits. On the other hand, NanoRacks, despite claiming a lower number of launches, was responsible for the deployment of more than 200 satellites from the ISS, as of 2020.

Combining this information, for this project, we believed that choosing NanoRacks was the better option, as their vast experience in launches from the ISS is far superior compared to the others, which, in our case, if the project were to move forward, would be optimal to make us of. In addition, their deployer isolates the CubeSat mechanically and electronically from the ISS, ensuring that as little as possible can go wrong. One of the other reason for this choice was their access to all resupply missions to the ISS, which happen usually three to four times a year. While this may not be that often, having this type of availability for the launch could be important, especially in a situation where we run into problems with the testing phase of the CubeSat, which are very likely to happen rather than not happen.

Finally, in what concerns the launch vehicle, NanoRacks operates mostly with SpaceX's launch vehicles, namely Falcon 9 for the ISS resupply missions. This result obviously brought to the table a number of requirements that either had to be taken into account in the design or will have to be addressed in testing, for example, vibration and temperature environments during launch.

3.4.5 Cubesat Deployment

NanoRacks offers the possibility of a deployment above the ISS's altitude, using the Cygnus, an American expendable cargo spacecraft, or a deployment to an orbit around ISS's altitude using their own CubeSat deployer onboard the ISS. Based on the orbit specifications chosen the obvious choice was to use NanoRacks' deployer.

Based on our CubeSat design, the deployer to be used is the Nanoracks Doublewide Deployer (NRDD), which can hold up to a maximum of 48U per deployment with a maximum volume per CubeSat of $2 \times 6\text{U}$. According to NanoRacks, upon arrival to the ISS, the CubeSat will have to wait a mandatory period of at least 3 months, which can go up to 6 months.

This pre-deployment mandatory wait is actually a piece of very important information to take into account because, based on the necessity of having to calibrate the instrument with a specific pulsar ($\text{PSR}_B0531+21$), whose observability is not possible from the start of May to the start of August, according to Figure 3.14, it may appear that the launch and deployment sequences would have to be scheduled carefully to ensure that we would not deploy during this phase of the year. This is actually not the case because this difference of 3 months between the minimum and maximum mandatory wait times, gives us enough margin to delay the deployment in the case of being too close to the start of May due to a mis-schedule or a launch delay. The mission timeline launch date in Section 1.4 is based on these considerations.

3.5 Electrical Power Subsystem (EPS)

3.5.1 Definition

This section presents a detailed description of the power requirements and power generation capabilities of the proposed system for the PDR stage. The EPS is an essential component of any spacecraft that is designed to operate in space. It provides electrical power to all the spacecraft systems that require power including the scientific instrument, communication, ADCS, On-board data handling, thermal and power.

The primary objective of this section is to propose the EPS subsystem design and evaluate whether it meets the power requirements of the spacecraft. For that purpose, a detailed analysis of the available power generation capabilities of the EPS is described below. Moreover, this section provides an assessment of the margins, the expected performance of the EPS and outlines the key design parameters, constraints, and assumptions that were used in the analysis.

Overall, this section demonstrates the feasibility and effectiveness of the proposed EPS design. It provides a solid foundation for further design and development of the EPS system as the spacecraft progresses. The Electrical Power Subsystem (EPS) is in charge of generating, storing, and managing the power for all the other subsystems in the satellite. Its design aims to satisfy the power budget defined for the mission, ensuring its correct performance throughout its duration, and accommodate the specific power requirements of each subsystem's hardware.

The EPS is mainly formed by 4 parts, as shown in Figure 3.38: the Solar Array (SA), the batteries, managing unit and interface connectors.

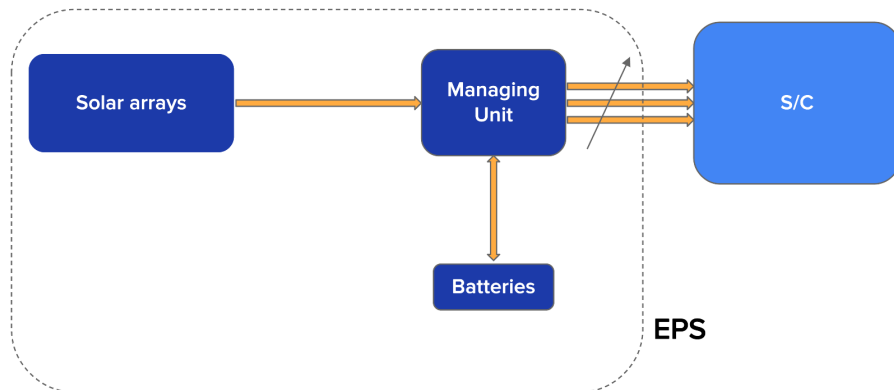


Figure 3.38: EPS block scheme

The SA acts as the power input source, using Photovoltaic (PV) energy, and it is connected to the managing unit. The managing unit is in charge of receiving the input power from the SA and both use it to deliver power to the other subsystems and to charge the batteries.

The batteries are in charge of storing the surplus power delivered by the SA that is not used by the other subsystems, and deliver such power to the subsystems when the satellite goes into the eclipse stage. During the eclipse stage, no power is generated by the SA since solar radiation is blocked by the Earth body, demanding a source of input power in order not to stop the satellite operations. The interface connectors are used to connect all the EPS blocks between them, and the managing unit to the rest of subsystems of the satellite. It is crucial to ensure that the power interface matches every subsystem's input requirements.

Each of the mentioned parts is selected from available commercial off-the-shelf products with flight heritage in CubeSat missions. The specific selected models for each part are listed in Figure 3.11, and the justification behind their choice is added below.

EPS part	Model	Provider
Solar Array [57]	NanoPower TSP 2030-3P	GOMspace
Batteries [58]	NanoPower BP4	GOMspace
Management Unit [59]	NanoPower P60 System	GOMspace

Table 3.11: Chosen EPS commercial options, including model and corresponding provider.

3.5.2 Requirements

The design and development of the EPS aims to comply with the requirements defined in 4.2. Next, we briefly define the state under which the requirements have been studied and achieved.

Requirements E-1 and E-4 have not been researched further, as they belong to phase D, for which physical interaction is needed, being far away in the development process.

Requirement E-3 is achieved by design, as batteries are wrapped up in the battery pack, shielded and kept inside the CubeSat platform.

Requirements E-2 and E-5 are perhaps the most discussed and researched requirements in the EPS section. Although being part of phase D, E-2 has been an important requirement when finding commercial options derived from the power budget needs. Initially, requirement E-2 was set to a 2 year duration, reason for which the battery degraded conditions explained further below in this section refer to such duration. The actual survival time for the satellite was changed recently. Fortunately, such change does not affect the performance of the chosen EPS hardware, as the previously set duration was more strict than the current one. E-2 is verified in a "theoretical" framework, not yet verified in a practical framework.

E-5 is verified after simulating how the chosen commercial options behave under the mission operational conditions. The EPS power budget margin is set 25%, a larger margin than the 20% initially required.

3.5.3 Solar Array

As mentioned in the power budget section, the SA has been selected taking two main considerations into account: it must provide enough power to operate the satellite under any circumstance (operation modes and eclipse periods) and charge the batteries following a suitable period, and reducing the pointing requirements assigned to the EPS.

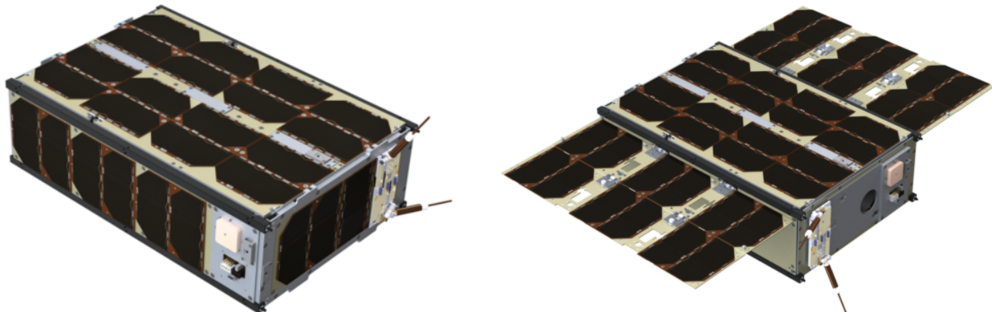
3.5.3.1 Studied configurations and trade-offs

Several solar array configurations were studied before arriving to the final design. Figure 3.39 shows the different solar array options analyzed before the final design was decided.

- Configuration 1: The initial attempt was to install solar panels on every face of the 3x2x1 satellite, but they could only provide up to approximately 20 W of power, which is insufficient based on the power budget estimated.
- Configuration 2: Then, it was considered adding deployable wings to increase the power output. By installing solar panels on one of the 3x2 faces and adding wings of varying sizes, up to 45 W of power generation can be achieved. However, this configuration would require a charging mode that would limit the time available for

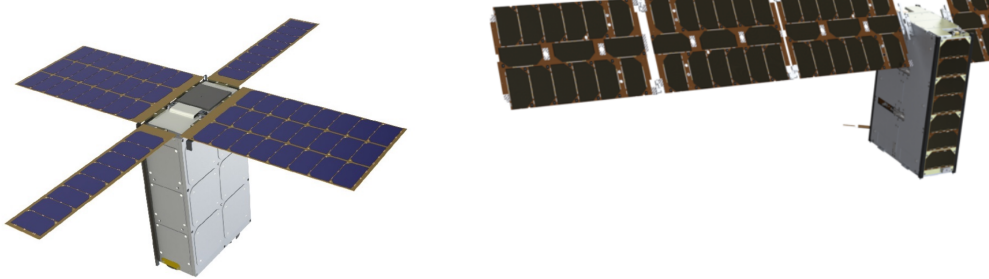
scientific operations, or it would have to include a large battery, which would exceed our mass restriction which initially was of 10 kg.

- Configuration 3: Another possibility that was examined was to place a solar panel on the face 3x1 along with deployable wings, which would generate approximately 48 W of power, depending on the number of panels in each wing. However, this option was also discarded due to the same constraints as configuration 2.
- Configuration 4: Similar to configuration 3 but with sun tracking along one axis. By adjusting the sun tracking to align with the axis perpendicular to the instrument's focal length and coordinating with the ADCS team to set the proper inclination in the axis of the instrument focal length, the solar array would be able to generate power continuously, regardless of the position of the target in the sky that the instrument is observing. However, during an eclipse, the solar array would not receive any sunlight, rendering it temporarily inactive. In such instances, the EPS would rely on the secondary power system that utilizes batteries to ensure uninterrupted operation of the spacecraft. Such configuration was chosen as the one to proceed with the EPS design.



(a) Configuration 1. Figure from [60].

(b) Configuration 2. Figure from [61].



(c) Configuration 3. Figure from [62].

(d) Configuration 4. Figure from [63].

Figure 3.39: Solar Array configurations studied.

3.5.3.2 Final configuration

As just mentioned, it was determined that the most suitable option would be a deployed SA with an independent rotation axis, similar to the one shown in the bottom-right plot from Figure 3.39. It satisfies the first requirement of having at least 27.73W of input power

to operate under scientific mode while charging the batteries. Furthermore, it complies with the second consideration mentioned in the power budget section: it must require the least pointing accuracy from the ADCS subsystem, as the payload measurements require a precise pointing while operating under the scientific mode.

Configurations with larger PV areas did not end up to be a suitable option since pointing can be required for its optimum tracking. The only options with a suitable average power were to use a rotation axis, as the one proposed. Having the rotation axis in the one proposed also allows to ask for pointing in the nadir direction of the satellites, since it does not affect the measurements greatly and it improves the amount of SA area facing the sun. The rotation axis is able to turn around $\pm 45^\circ$ and includes an Maximum Power Point Tracking (MPPT) to maximize its performance.

The *NanoPower TSP 2030-3P* SA from GOMspace is formed by a 3 piece deployable panel that unfolds providing a 3x3x2 Units PV area. Each fold is formed by 15 PV cells, and provides 15W of average power. In total, it is able to provide 45W of power, already taking into account the providers' margins.

3.5.4 Batteries

The chosen batteries are the NanoPower BP4 from GOMspace, which comply with the two main requirements for the batteries: ensuring enough power delivery capability during eclipse periods and maintaining a high enough performance for at least the 2-year mission duration.

The model is a battery pack formed by 4 individual batteries in a 2-in-parallel and 2-in-series configuration, having a voltage of 7.2V and a minimal battery capacity of 2100mAh.

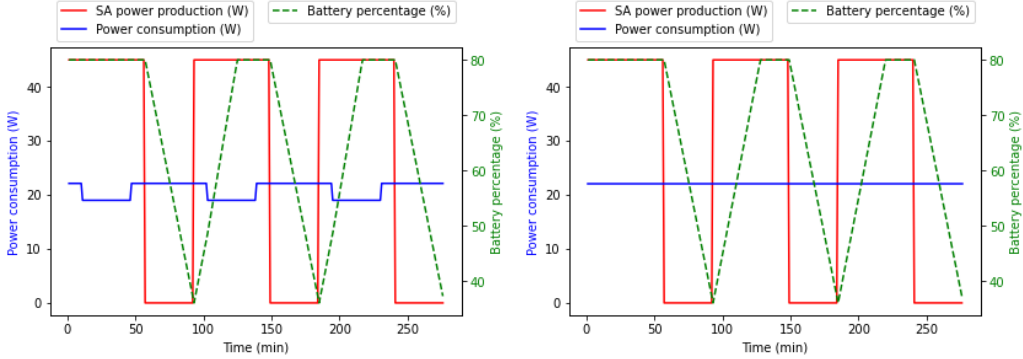
The worst-case scenario for the batteries is to power up the system during an sun-eclipse period while using the most demanding operational mode, and staying within a defined battery capacity margin.

In order to check if the chosen battery model complied with the worst-case scenario, a script was made to observe the battery capacity oscillations over time. Figure 3.40 shows 4 different plots. The first row simulates a contrary sun and payload eclipse combination and the second row shows a 100% scientific operation case, which is found when the target is perpendicular to the orbit: no target eclipse for the payload. The first column simulates a new-battery properties, while the second column adds the 2-year degraded battery properties. After 2-year use, the batteries have shown to decrease its minimum capacity. A reduced value of 1500mAh is chosen according to the degradation plot found in its datasheet, shown in Figure 3.5.4. The chosen value is based on a 20000 cycles degradation, instead of the 12000 cycles performed during 2 years, and a depth-of-discharge (DOD) larger than the ones on the plot curves. The left plot of Figure 3.5.4 shows the average distribution of the battery lifetime depending on the cycle depth and the temperature. For our case scenario, the cycle depth would be around 800 mAh, which points out that the battery capacity will not be as degraded as for larger cycle depths as long as the temperature is properly monitored and controlled.

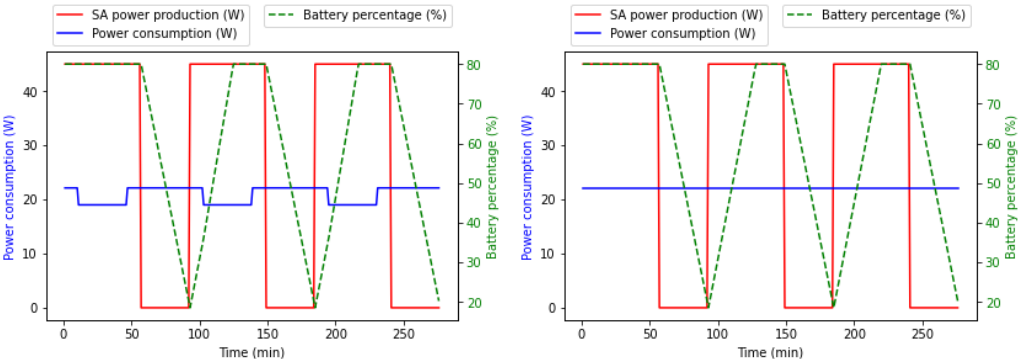
For all cases shown in Figure 3.40, the battery capacity oscillates between the proposed margins of 80% and 20% capacity, which are optimal to minimize the initial battery capacity degradation. Thus, it is confirmed that the chosen battery model would work for the specified mission requirements.

3.5.4.1 Battery depletion and Safe Mode

The batteries should never empty completely, since a full battery depletion risks the success of the mission, being a crucial aspect to take into account. To avoid such situation,



(a) Contrary eclipse period. New battery properties.
(b) Contrary eclipse period. 2-year degraded battery properties.



(c) Continuous target observation. New battery properties.
(d) Continuous target observation. 2-year degraded battery properties.

Figure 3.40: Battery capacity simulated under multiple target, eclipse and battery conditions.

a battery capacity threshold to trigger the safe mode operation must be set by the EPS. A 36 minutes solar eclipse under a safe mode regime with a 2-year degraded battery would deplete 60% of the total battery capacity. A strict threshold for the battery capacity would be 40%, aiming to stay in the 80-20 margin.

It is also worth mentioning that the batteries' model also count with flight heritage, ensuring that it has been successfully tested in similar environments.

3.5.5 Managing Unit

The managing unit is formed by an Array Conditioning Unit (ACU), a Power Distribution Unit (PDU) and a P60DOCK accommodating both as daughter boards and acting as co-ordinator for efficient functioning. The ACU in the P60DOCK acts as an input and the PDU acts as the output for the managing unit.

Having a DOCK allows for managing the input from the ACU and the output from the PDU effectively and implementing circuit breakers at important interfaces. It even allows for accurate power measurements at each terminal, as each terminal can report its individual current, voltage and temperature. The Master Control Unit (MCU) on the P60 Dock controls the system, monitors current, voltage and temperature. Having chosen the components from one provider not only makes the supply chain easy but also decreases interfacing challenges between different providers. All components for the EPS being

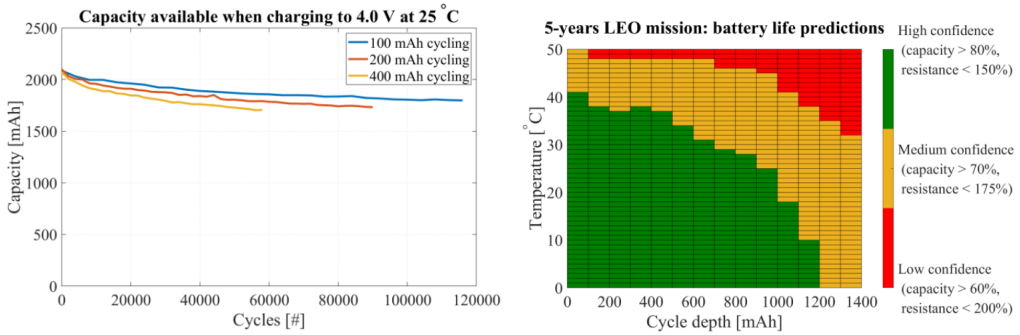


Figure 3.41: Experimental test results of batteries performance. Left: Available capacity, when charging it under standard conditions, for multiple cycle depths. Right: Distribution of the battery state based on cycle depth and an average of 5500 cycles x year (close to the cycles per year of the mission). Figure from [64].

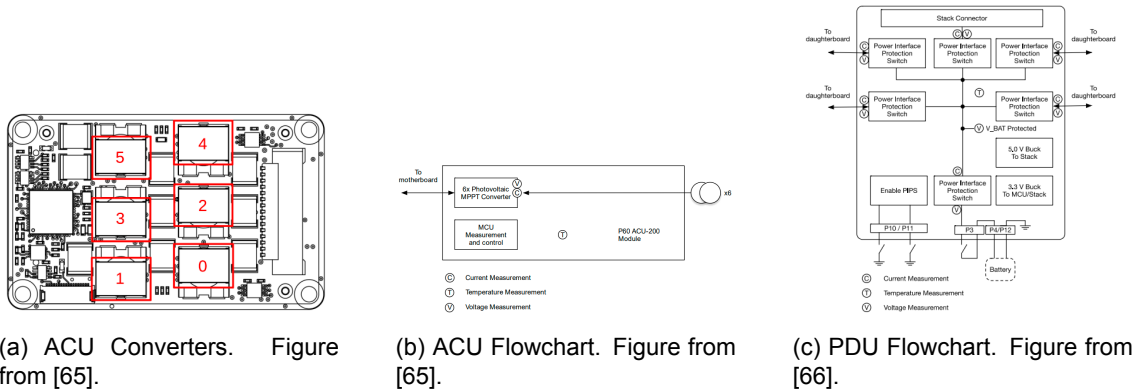


Figure 3.42: ACU and PDU internal flowchart

from GOMSpace ensure a reliable and robust AIO solution.

The operation of the managing unit can be explained starting from the ACU. The ACU offers 6 individual MPPT boost converters to interface with the SA, each offering a power measurement setup. Dual TFM pins in input mode are used to increase the current carrying capacity. Which is more than what is required for the proposed number of solar panels i.e., 3. To decrease the thermal giveaway from the boost converters a pair or 1,2 and 5 is used as they are placed the farthest. This way the ACU can achieve a high solar input from the SA up to 16V and 32V. This wide range of voltage can be later regulated at non-standard values to power the antenna sub-systems rated between 8-18V and the thermal sub-systems.

The PDU provides 9 output channels (0-8). As we have 5 separate subsystems 2 outputs are not used. Each PDU comes with 3 BUCK converters which are essential for dividing the operational voltage for all the subsystems. The converters can be connected to any of the 9 output channels using the stack connector, but as the configuration is not a stack only 6 channels can be used over the TFM connector. Furthermore, the system does not require more than 9 channels to operate, as we have 5 different subsystems to provide power to, requiring 7 power channels in total. Since the subsystems' PCBs are not in a PC104 stack but scattered throughout the chassis, the way to interface different subsystems is elaborated in the Power interface connections section.

Nonetheless, failures can occur during operation, leading to a fatal risks, sometimes the end of the mission. The protection circuits included are listed below.

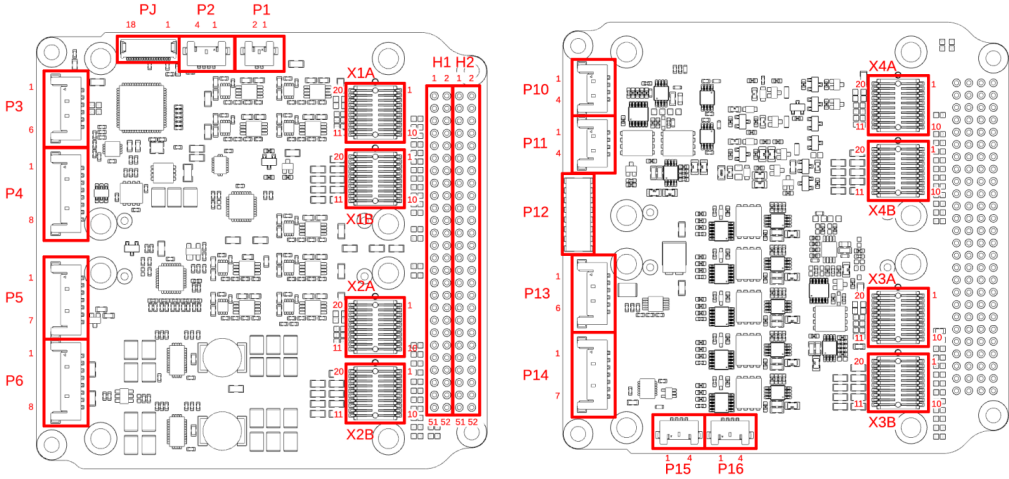


Figure 3.43: The interface schematic of the P60 dock or motherboard. It acts as the hub for proper functioning of the EPS and used for its protective features. Figure from [59].

The battery charging interface is located in connector P13 where the pins one through four is used for charging. Pin one and two is ground connection to the battery; pin three is a battery voltage sense output which should be used with the battery charger and pin four is the charge input for the battery. The battery protection built into the P60 power supply consists of three parts; over voltage protection, under voltage protection and over current protection. Each of the three serves to protect the batteries from strain that might damage or shorten the lifetime of the batteries.

- The Over Current (OC) ensure that the spacecraft subsystems are not allowed to draw more current from the batteries than the batteries are rated to. The OC protection is located in the PIPS directly connected to the batteries and the protection is triggered by the total current draw from the five PIPS outputs in the P60 Dock.
- The Over Voltage (OV) protection feature of the P60 protects the batteries from an over charge condition. If the voltage across the batteries reaches the maximum safe, then the OV protection stops the charging. When the batteries are discharged to the OV threshold minus a hysteresis band then the charging is allowed again.
- The Under Voltage (UV) protection feature protects the batteries from an under charge condition. When the discharge level of the batteries reaches the minimum safe level the UV protection turn off the power supply until the batteries are charged to a safe level plus a hysteresis band.
 - The OV protection thresholds levels 16 V: 16.8 V and 32 V: 33.6 V.
 - The UV protection threshold levels 16 V: 12 V and 32 V: 24 V.

3.5.6 Power Interface Connections

The power interface cables for the EPS parts match perfectly since they are from the same manufacturer (GOMSpace). The ACU and the PDU are connected to the DOCK using 1.0mm FSI connection that has an interface for i2c, CAN, cell voltages (VBAT) and even powers these boards. This is the only interface that is required for the EPS to work and hence makes the system very reliable.

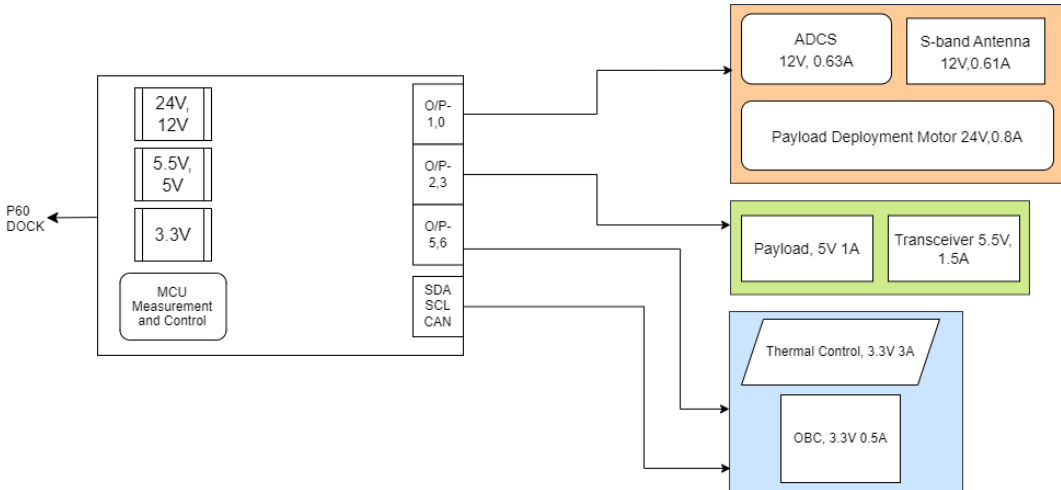


Figure 3.44: Power interfaces schematic

The rest of the sub-systems have different interfaces to receive power. The communication subsystem uses a J16 Molex Picohead 1.5mm for both the transceiver and the antenna. The thermal subsystem uses a 3m terminal block to draw power. The payload is assumed to be using standard ATX or Molex connectors. For the ADCS module Molex connector are used. The OBC uses the standard STACK Connectors present on the P60Dock. Motor used to deploy the payload use a 26AWG wire for the power connector.

As explained above the PDU uses 3 BUCK converters to power the 8 output channels. Only one BUCK converter has the capability to deliver voltages above 8V or VBAT. Hence, the sub systems using voltages above 8V are powered using one particular BUCK Converter using output channels 0 and 1 on the PDU. The first BUCK converter outputs 24V during deployment phase of the payload to power the motor that extends the payload out of the cubesat. During the same time the other 2 converters are used to power the Payload, Thermal control and the OBC. As the OBC only uses even less than 1A, the major current supply is consumed by the Thermal controller for the warm up phase. Having such a configuration allows to power the critical components needed at that state of the mission.

As the transmission phase arrives the antenna is operated a little below its maximum voltage at about 12V as there are no dedicated converters to provide 18V output. Pointing is much needed during the communication phase and hence the ADCS cannot be powered off and this power rail at output 2 and 3 is used to operate the antenna and the ADCS at 12V only.

During the eclipse phase only the heater is active drawing 3.3V at 3A from the output 5 or 6 depending on the configuration of that BUCK converter output used for it as shown in figure 3.44. Performing the transmission and running the thermal control is also possible as the maximum current from one converter is up to 4.5A. The OBC connected to the same BUCK as thermal control can draw maximum up to 1.5A only, which is much more than sufficient.

For the science mode only the ADCS, OBC and the Payload is powered. As all of them run on a different operational voltage all 3 converters are in operation. Running at 12V, 5V and 3V respectively. Running all the sub-system at once is not possible and hence the configuration for each mode of the mission is carefully selected.

The converters can be programmed according to the mission phase and selected channels can be powered at the particularly assigned voltages. The Converter with non-standard output covers for the ADCS, Antenna and the Motor for payload deployment, the other converter operates at 5 and 5.5V during the science and communication mode. The last converter is to be used at a constant 3.3V for the OBC and the Thermal control.

Power distribution configuration according to the converters in use.

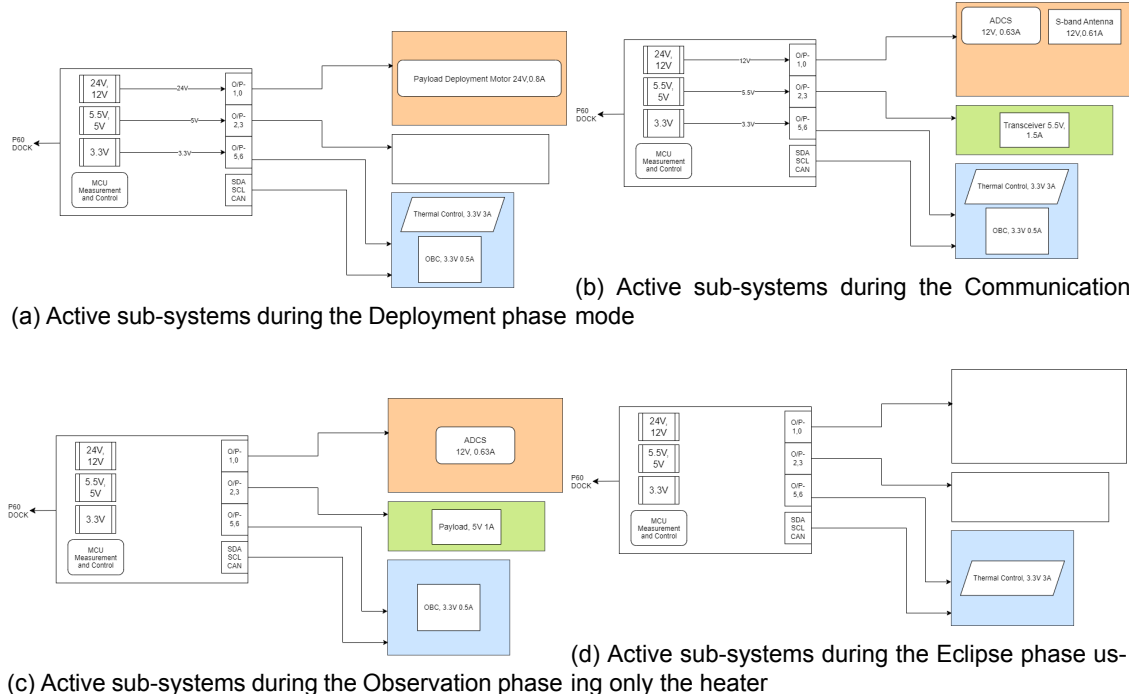


Figure 3.45: (a) Switching on the Payload is optional and won't burden the EPS. (b) If the transmission takes place during eclipse switching on the heater is possible. (d) If only thermal system is used during eclipse

The only remaining channel from the PDU can be covered up to reduce the open connections present in the EPS, minimizing the risk of failure events. The other connections - I2C and the CAN bus can be used for interfacing the OBC and the Dock to exchange the power consumption data by various subsystems using CSP packets. The DOCK can be used as well to gather info from the ACU and PDU together, in this configuration its easier to analyse the power generated by the SA i.e. the input and consumed by the sub-systems i.e. the output.

The EPS also enables debugging using PJ terminal present on the DOCK. This feature can only be used on ground to program the P60DOCK and in-flight use is not recommended. This J-TAG interface provides DMA and other useful features making debugging easier. The P6-GSSB interface is also used to connect the sun sensors present on the SA and to deploy the antenna if one connected. Kill switches are configured to be released before powering up the satellite, the default configuration of parallel switches is recommended and used. By connecting the two kill switches in parallel; only one of the switches has to be released for the satellite to power up. This works as redundancy system therefore the P10 connector is highly recommended for connecting the kill switches. There are two power converters located on the P60 Dock, a 3.3 V and a 5 V converter.

These two converters are used to supply the daughterboards, internal logic, 5 V and 3.3 V in the stack and for antenna release.

3.5.7 Risk assessment

This subsection includes a series of case-scenarios that would risk the success of the mission, and how it would affect the EPS.

3.5.7.1 No deployed Solar Array

The deployment of the Solar Array is crucial for the success and continuous operation of the mission, as it ensures that the EPS is able to deliver enough power following the initially defined power and pointing requirements.

In the case of an unsuccessful deployment, mechanism not working letting the panels on the satellite side, the pointing functionality delivered by the rotation axis for the MPPT is lost. Therefore the satellite would not be able to operate under scientific mode, since the requested power would much higher than the available.

3.5.7.2 Partially working Solar Array

A partially operating Solar Array situation could be met in different ways. The SA unfolding mechanism could fail, and only unfold 1 or 2 out of the 3 parts of the array. Electrical problems could also arise in 1 or 2 of the solar array modules, disabling their power capabilities.

Such conditions have been simulated by decreasing the SA power from 45W to 30W and 15W, depending on the case, and measures to work around it have been proposed.

In the case scenario where 1 out of 3 solar panels is disabled, the systems input power would be 30W. Figure 3.5.7.2 shows how the battery capacity for a 2-year degraded battery would behave on the left plot. As it can be observed, the battery could not operate between the 80-20 capacity margin, as it will not be charged up enough during charging periods.

Meeting such situation would be risky, as it would compromise the success of the mission. Since the system would not be able to operate under such conditions, a solution to work around such difficulty, if ever happened, would be to define a modified version of the power constraints for each of the operation modes. Such modifications can be observed in Figure 3.47.

The proposed modifications do not affect the operation modes themselves, as they are defined by the whole system, but their translation in terms of power would be simplified. The main actions from each operation mode would be isolated from the rest, focusing all the power in the relevant subsystem of each mode. For example, during acquisition mode, peak power should only be granted to the payload, while other high demanding subsystems should try not to ask for peak power, and maintain more typical power levels (checked on their datasheet) or be disabled if they are not crucial for the modes' operation.

As mentioned, this is just a proposal to work around a possible problematic, it should not be taken as an agreed definition of the operation of the satellite, but as a solution proposal from the EPS point of view.

The right plot on Figure 3.5.7.2 shows how the battery capacity would behave when applying the modified power of the operational modes under risk situations. The battery properties are the ones from a 2-year degraded battery. With such modifications, the battery capacity oscillations would be maintained within the 80-20 capacity margins for optimum operation level. It would also allow a continuous observation of the payload measures.

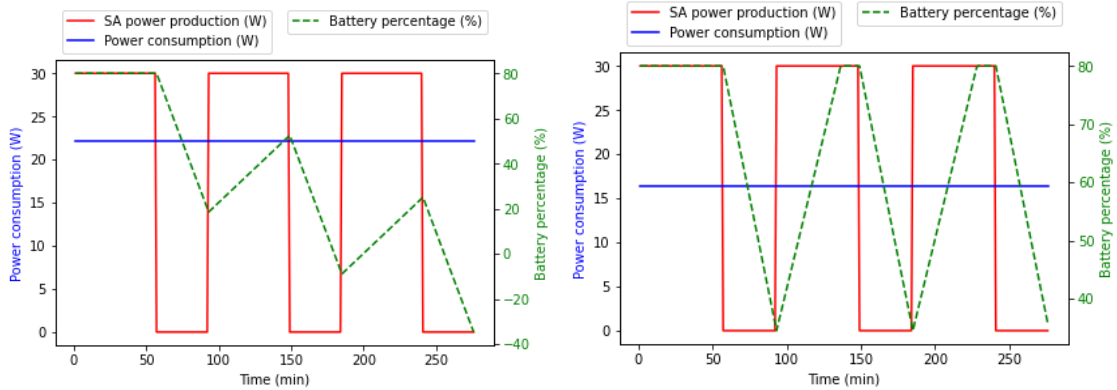


Figure 3.46: Battery capacity behaviours when risk situation "2 out of 3 working solar panels" is met. The left plot shows the pre-defined modes under a continue scientific mode operation. The right plot shows how the scientific mode operation under the risk changes proposal would look.

SUBSYSTEM	Instrument	SCIENCE MODE		TELECOM MODE		ADCS MODE		SAFE MODE		CHARGING MODE		
		MODULE PP (W)	PP (W)	DC (%)	PP (W)	DC (%)	PP (W)	DC (%)	PP (W)	DC (%)	PP (W)	DC (%)
PAYOUTLOAD	Pulsar X-ray Receiver	5	5	100	0	0	0	0	0	0	0	0
COMMS	TX	1,5	0	0	1,5	80	0	0	1	5	0	5
	RX	1	0	100	1	20	0	0	1	100	0	100
ADCS	ADCS	7,6	3	100	3	100	7,6	100	3	100	3	100
On-board data handling	OBC	1	1	100	1	100	1	100	1	100	1	100
THERMAL CONTROL		3	3	100	3	100	3	100				
POWER	PDU + ACD + DOCK	1,1	1,1	100	1,1	100	1,1	100	1,1	100	1,1	100
TOTAL		20,2	13,1		9,5		12,7		6,15		5,1	
+ Margin (25%)		25,25	16,38		11,88		15,88		7,69		6,38	

Figure 3.47: Modified power modes under risk conditions.

In the case scenario where 2 out of 3 solar panels are disabled, the systems input power would be 15W. Figure 3.5.7.2 shows how the battery capacity for a 2-year degraded battery would behave under various conditions. The first row of plots show how the battery capacity behaves if the power modes are left unmodified for both continuous and periodic observations. It can be observed how because the required power is much higher than the input power, the battery gets depleted in just 1 eclipse period.

The second row of plots show how the capacity behaviour changes if the proposed "under-risk" power modes from Figure 3.47 are applied. For a continuous observation (bottom-left plot) the battery gets depleted after 2 observation periods, which is not optimal at all, as it will cause the system to shut down for charging up every 2 sun-periods. Instead, the best option under this risk circumstance is to "force" a target eclipse period which matches the sun eclipse periods, as shown in the bottom-right plot.

Forcing and matching a target eclipse for the payload operational mode forces that the most demanding modified mode occurs when the input power is maximum, and the forced less demanding modified mode (modified Safe Mode) occurs during the sun eclipses,

reducing the battery depth of discharge. Such configuration is not enough to maintain the battery capacity between the 80-20 optimal margins for the battery, but it would allow to operate under the "forced" eclipse regime for at least 3 orbits, which measures could be integrated, being followed by a recharge period to charge up the battery to an 80% capacity.

It is worth repeating than the just-mentioned solutions are just a proposal from a power feasibility point of view.

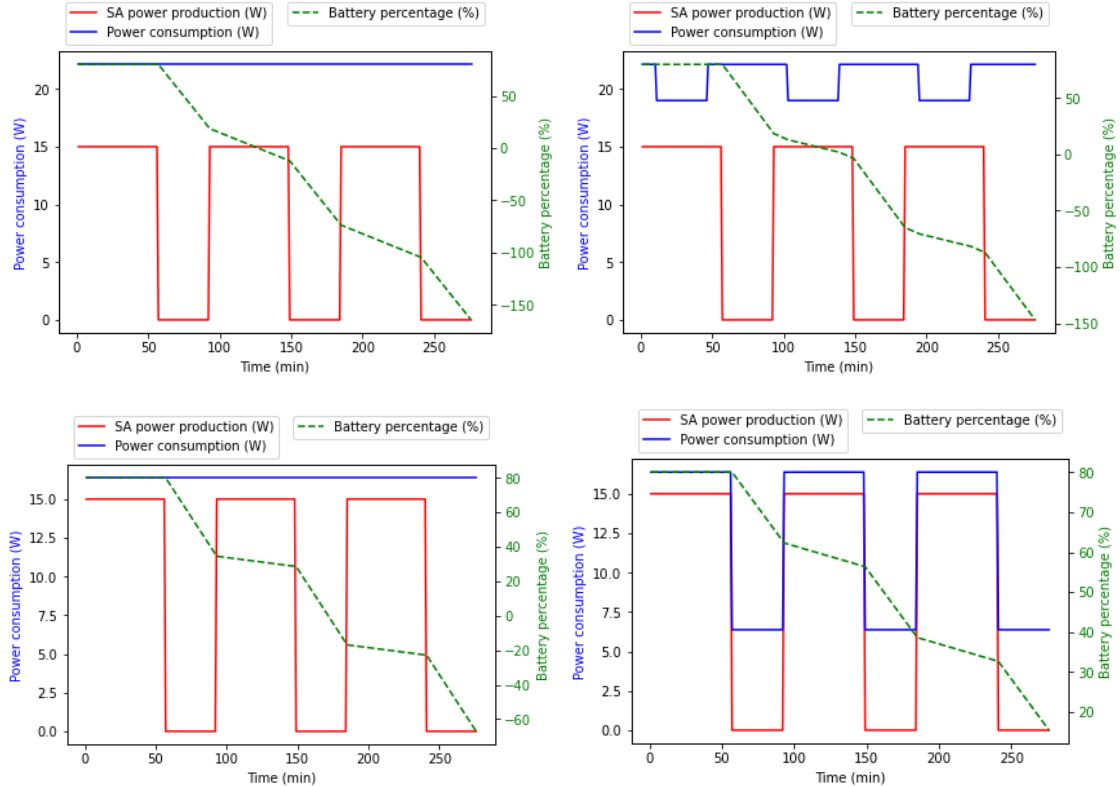


Figure 3.48: Battery capacity behaviours when risk situation "1 out of 3 working solar panels" is met. The first row shows the original operation modes power definition, while the second row shows the modified under risk situation power modes. The first column show a continuous scientific mode operation, while the second row shows a "forced" period observation.

The risk situations aim to highlight how critical the deployment of the SA is to maximize the success of the mission.

3.5.8 Future actions and considerations

This section includes the next steps for the EPS development, and considerations that have not been taken because of the project's scope and time constraints, and would have been necessary in a real case scenario.

3.5.8.1 Further research

Further research is needed to optimize the Electrical Power System for our space mission.

One area to investigate is the duration for which the batteries should be used before the deployment of the Solar Array during the Launch and Early Operations Phase (LEOP). The battery is initially charged up to 50%, having a limited lifetime before deploying the Solar Array.

The constraints for the EPS during the detumbling mode should also be further investigated. With an initial 50% battery capacity stopping tumbling after launch using the ADCS should be prioritize and timed, as the solar panel must be deployed as soon as possible to ahve enough power to operate. The exact time and required power for the detumbling period can only be properly tested under testing of the ADCS and the EPS together, to observe the rates and torque the ADCS can provide, as it is complex to exactly simulate in this stage of the mission.

Another aspect to consider is the effectiveness of different charging strategies for the batteries. For that matter, it could be studied to develop and to test different charging and discharge strategies for the batteries to optimize their performance and extend their lifespan.

Finally, conducting a thorough analysis of the EPS will be crucial to assess its capacity and effectiveness in different mission scenarios, particularly during emergencies and instances of unexpected power surges. This will involve developing contingency plans and procedures to guarantee the safe and successful recovery of the spacecraft, and to ensure that the EPS is capable of supporting such contingencies.

3.5.8.2 Hardware procurement

The next step after researching, simulating and making sure we can count with suitable commercial parts for the EPS is to make a procurement and testing plan.

Procurement of at least one unit of each EPS should be manufactured/purchased for in-house testing. Spare parts for connectors and auxiliary electronics should also be purchased, as their cost is more reduced in comparison with the primary parts, and a replacement of a secondary part during testing/assembling the EPS should not delay the schedule of the project.

It is also crucial to store and preserve all parts and electronics under recommended conditions by the manufacturer and out of reach from second-party people. For example, the batteries should be store under the specified temperature conditions and in a room with capabilities to allocate them in case The handling of the EPS parts should only be carried by trained staff, as some of them could require specific handling knowledge (static electrical handling, etc..).

In section 4.2 further details on hardware procurement and testing are provided.

3.6 Telemetry, Tracking and Communications (TT&C)

Telemetry, tracking and communication subsystem is one of the most important components of any Low Earth Orbit CubeSat mission. This subsystem actually enables the communication between the CubeSat and the ground stations that are used for this purpose. It is also the mean of transmission and reception of data that control and constantly monitor the health of the CubeSat. Without this subsystem, it would be impossible to control the CubeSat and retrieve the data that is observing and it is meant to collect. Additionally, TT&C ensures the safety and security of the CubeSat. Constantly monitoring the health of the CubeSat can provide the ground segment with information about alerts and some potential issues. Investing and developing a reliable TT&C subsystem increases the overall safety of the mission and contributes to the overall mission success.

3.6.1 Requirements

3.6.1.1 Introduction

In this section, the requirements of the PANTSat mission will be presented. These requirements were defined taking into account the ones that are set from the European Space Agency "Fly Your Satellite!" programme. Being lined up with the requirements is crucial for several reasons. First of all, ESA's programme is a prestigious opportunity for students and educational institutions to gain hands-on experience by applying their knowledge about designing, building and launching their own satellite. Aligning with the program's requirements ensures that the satellite mission meets the necessary operational and safety standards. Additionally, being in compliance with ESA's requirements guarantees that the CubeSat will be eligible for integration into ESA's launch vehicles and also compatible with the ground station infrastructure. Also, the collaboration with other participant in the program is being promoted in this way, so there are chances for knowledge-sharing and networking.

3.6.1.2 Requirement evolution

The first thought was about testing the mission in the deep space. This was considered as a correct idea due to the fact that the instrument that we want to test is supposed to be working in the same conditions as in the real situation (in this case, in deep space). Telecommunication requirements for a deep space mission are way different from those for a Low Earth Orbit (LEO) mission. This is due to the vast distances and the challenges that have to be faced in order to preserve the signal through these vast distances. Some key requirements that are worth mentioning when it comes to a deep space mission are:

- High-Gain antennas: Deep space missions require antennas that can transmit and receive signals over long distances. This kind of antennas need to be large enough so they can capture weak signals
- High Data Rates: Deep space missions generate a big amount of data which needs to be transmitted back to Earth. So, high data rates are required in order to provide an effective communication through advanced signal processing techniques and powerful transmitters
- Robust Communication Protocols: The used communication protocols need to be robust so they handle the long distances and delays. This also requires the use of error correction techniques and advanced protocols which can handle signal interruptions.
- Power Management: Especially for the telecommunications systems, deep space missions require detailed power management. Careful design of solar panels or

other power sources will provide sufficient power for the communication systems and at the same time will make sure that the operations will flow seamlessly on for extended periods

- Redundancy: Another important parameter for deep space missions is the redundancy. Multiple communication links, antennas and transmitters should be used in order to provide reliability and backup support in the case of various failures.

In overall, deep space missions require specialized and advanced communication systems with a lot of redundancy due to the vast distances between the satellite and the ground stations.

After meeting with the subgroups of the present mission, it was decided to modify the concept of going to deep space. The new idea - that was implemented - was to launch a CubeSat in a Low Earth Orbit (LEO). The reason behind this, is the fact that launching and handling a LEO satellite mission is less costly than a deep space one. Building or buying the parts of a LEO mission (as it will be analyzed in the following chapters) is feasible and cost effective. Also, another factor but also very important, was the validation of the data. Having a CubeSat in a LEO would provide easier validation process of the observed data, so there can be a continuous assessment of the data that the satellite measures. Finally, taking into account the opportunity that ESA offers, it was decided to design a CubeSat that is aligned with ESA's *Fly Your Satellite!* program with which the mission will have a lot of benefits regarding the launch and the ground systems infrastructure.

Having decided that the mission is gonna be executed by a CubeSat orbiting in LEO, it is important to consider about the general requirements that a LEO mission has. The requirements for a LEO mission depend on the mission objectives. In general, they can be summed up to the following ones:

- Antenna: A suitable antenna is required in order to transmit and receive signals from the ground station. The frequency bands should also be considered because there are some allocated frequency bands for CubeSat missions
- Transceiver: The conversion of the signals which are received by the antenna should be converted to data that can be processed by the onboard computer, and also to transmit the data back to the Earth
- Data rate: The objectives of the mission will define the required data rate because data rate controls the ability of the data transmission
- Communication protocol: As mentioned previously, the protocol ensures a reliable communication between CubeSat and ground station(s)
- Ground station(s): Suitable ground station network should be established in order to communicate with the CubeSat. The ground station(s) will have an antenna and a transceiver to handle the downlink and the uplink. Tracking antenna is also a requirement to utilize the full capacity, since the CubeSat flies too fast over the ground station(s) meaning short communication time (usually less than 15 minutes)

As for the ground network, it is generally preferred to employ more than one ground station in order to increase the redundancy and the download data capacity. Considering the type of data that this mission is going to handle, which is not a very demanding amount of data and also the requirements of the ESA's *Fly Your Satellite!* programme which will be analyzed in the following paragraphs.

The specific requirements (from Section 4.5) for the telecommunication subsystem that had to be met are listed and analyzed here:

- The radiofrequency power output should be less than 1.5 Watts at the transmitter's antenna (on-board). This requirement was defined in order to comply with some standards from the Electrical Power Subsystem (EPS) and ESA's *Fly Your Satellite!* programme requirement 4.2.11.
 - Even if both the antenna and the transciever choosen for the final design can handle up to 4 W, it was agreed in accordance with the Electrical and Power Subsystem, that the power during transmition will be limited to 1.5 W, as further described in Chapter 3.6.3. All the calculations that follows are computed with this value.
- At least one ground station shall be available for bidirectional communication with the CubeSat and preferably the ground station to be controlled and operated by the university (ESA's operational requirement)
 - With the equipment proposed in Chapter 3.6.2, DTU Ground Station will be able to perform bidirectional communication.
- The CubeSat and the ground station should comply with the International Telecommunicaton Union (ITU) regulations. The devices that are fitted into the CubeSat shall ensure immediate cessation of their radio emissions by telecommand whenever this is required under the provisions stated in ITU Radio Regulations Article 22.1
- PANTSat shall use passive or active on-orbit tracking aids for facilitating satellite identification, increasing satellite trackability and facilitating the precise determination of its position in orbit.
 - Active On-board tracking performed by GNSS module, further description in Chapter 3.3.3.2

3.6.2 Ground Station

3.6.2.1 Introduction

The Ground Station is the link between the satellite and its operators back on Earth. It is the ground segment part of the mission and it is designed to transmit and receive information and communicate with the spacecraft. The frequencies used for telecommunications are usually Super High Frequency (SHF) or Extremely High Frequency (EHF), like microwaves. A telecommunications link between the ground station and the satellite is established when the ground station successfully transmits information to the satellite. When the ground station receives telemetry data and follows the satellite is then referred to as a ground *tracking* station.

A ground station typically consists of the following (main) components:

- a reception antenna,
- a feed horn,
- a wave guide, and a
- receiver

A typical ground section setup is shown in Figure 3.49. The reception antenna is typically a parabolic dish antenna that amplifies the incoming signal, without adding significant noise to it and to accurately direct incoming waves onto the feed horn. The feed horn gathers the signal and usually a Low Noise Amplifier (LNA) is directly mounted on to it. Otherwise, a cable is mounted onto it transferring the signal from the feed horn to the Low Noise Amplifier that can be in the ground station's computer room. The second option presents the danger of the signal losing power during the transportation making it more difficult to detect valuable information.

The signal is gathered at the feed horn and starts its journey to be made into usable data, firstly by passing through a band pass filter. The band pass filter is used in order to obtain the specific frequency band used for the telecommunication with the satellite, blocking higher and lower frequencies that could be causing interference [67]. Afterwards the signal passes through the low noise amplifier (LNA), where it is further amplified but at the same time does not introduce additional noise to the system maintaining the signal-to-noise (SNR) ratio [68]. After the signal is amplified, it is then transported to the receiver through an RF-cable. These cables are transmission lines for Radio Frequency (RF) signals ensuring minimum losses throughout the transmission. Usually they are coaxial cables, composed of four co-centric layers of conductive and insulating material [69].

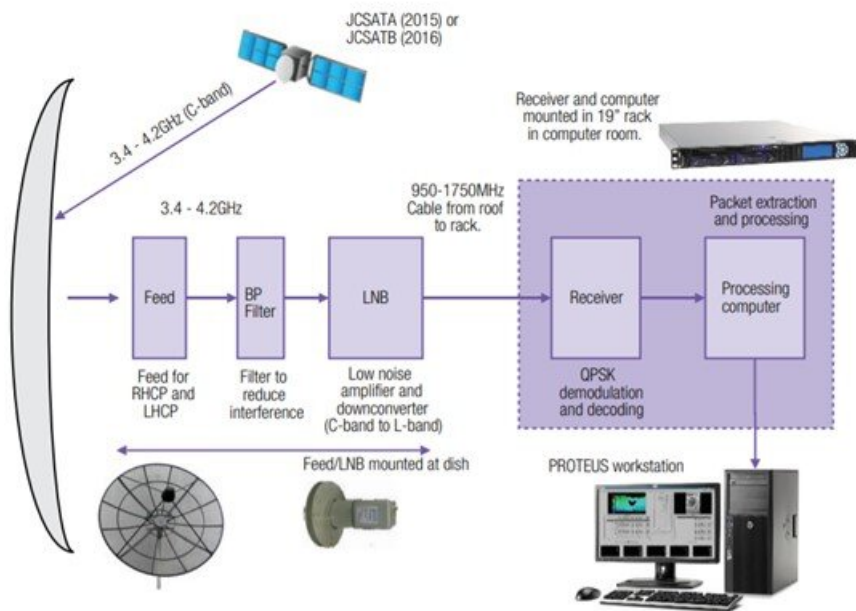


Figure 3.49: A typical, but simplified ground station setup operating in C-Band [70].

Afterwards, the signal reaches the receiver where it gets demodulated and decoded. A common digital modulation process used for satellite telecommunications is Quadrature Phase-Shift Keying (QPSK). QPSK conveys data by changing the phase of the carrier wave of the signal. The carrier wave phases encode an equal number of bits that form the symbol rate, for which the demodulator is specifically designed. It determines the phase of the received signal and tracks the symbol that it came from, recovering the original data [71]. QPSK uses four phases at a time, which gives it the ability to encode two bits per symbol, to minimize the bit error rate. Finally, the packet from the receiver containing the demodulated and decoded signal is extracted and ready to be processed in the processing computer of the ground station.

3.6.2.2 Design Development

Choosing the Ground Station location lines up with the requirements given by the *Fly Your Satellite!* requirements by ESA. The ground station must be operated by the university, as it can be seen in the Requirements so the DTU existing ground station is going to be used for this with some modifications.

Before this requirement was adopted a plethora of options was explored. First of all, the ESA and NASA ground station network was considered. Their network is far-reaching and they cover all the frequencies that can be used in satellites telecommunications. Since the choice of ground station is tightly connected with the frequency band used, in the process of choosing a frequency band the choice of ground stations changed respectively. Moreover, both networks contain Deep Space Network (DSN) ground stations, which is very crucial since a deep space mission was considered in the very beginning. The ground station network for both ESA and NASA are shown in Figure 3.50 and Figure 3.51 respectively.



Figure 3.50: ESA ground station network. [72]



Figure 3.51: Nasa ground station network. [73]

The ground station choice at the beginning of the project was effected by the type of mission, hence the orbit that is going to be used. As mentioned above, a deep space mission was suggested in the beginning, and for this the deep space network of ESA and NASA were suggested. They both consist of three ground stations each operating in S-, X- and Ka- bands, and can be shown in Figure 3.50 and Figure 3.51 respectively.

Later on it was decided that the mission is going to be a Low Earth Orbit (LEO) mission. This allows for optical telecommunications as well, but that idea quickly came to an end. For the LEO mission Ka-band as well as Ultra High Frequency (UHF) and Very High Frequency (VHF) were suggested. The VHF and UHF requirement meant the revisit of the list of ground stations that can receive and transmit in these bands since not all of them (both ESA and NASA ones) are equipped for these bands. Thankfully, NASA has three ground stations supporting VHF, ESA has one station. But VHF and UHF are also very convenient frequencies because one can build their own station exactly in their requirements. Such ground stations can be purchased from companies such as ISISPACE.

In the process of searching for ground stations that cover VHF and UHF, the concept of Ground Station as a Service (GSaaS) was introduced [74]. At the same time, the orbit was decided to be geostationary, so it was important that the ground stations are near the equator. This introduced commercial ground segments such as LeafLine, the Kongsberg Satellite Service (KSAT) and in particular the KSAT^{lite} service that contains more geographical locations and lesser costs than using their main service. Plus, their stations operate in UHF complementary so, this was great for the mission. Their ground station network is shown in Figure 3.52.



Figure 3.52: Ksat^{lite} Ground Stations Network

Finally, due to design restrictions of the cubesat that came in time with the adoption of the *Fly Your Satellite!* requirement, the antenna used in the design changed and UHF were no longer an option. This opted out for an S-band antenna instead and the location of the ground station to be at the university. So, the existing ground station at DTU is used for the mission, but with some modifications in order to suit the mission. The ground stations chosen throughout the weeks working for the project are gathered in Table 3.12 and the compartments that the ground station consists of are further analysed below.

3.6.2.3 Final Design

The block diagram of the ground station is shown in Figure 2.2. DTU has an already existing ground station. It was set up by Flemming Hansen and it has been used to accommodate DTUSat-2. It is located at the roof of building 348 with its exact coordinates being 55.7821 North, 12.5165 East. The control room is located on the third floor of the building and it is basically a room on its roof. The access to this room is by a specific key. The ground station is to be operated by one to two people. It is shown in Figure 3.53.

The components of a ground station are mentioned already in the introduction. In this

	ESA	NASA	DTU	KSAT ^{LITE}
X-S-(DSN)	New Norcia Station Australia(NNO) Cebreros Station Madrid (DSA2) Malargüe Station Argentina(DSA3)	Goldstone Deep Space Communications Complex Madrid Deep Space Communications Complex Canberra Deep Space Communication Compex (CDSCC)		
X-Band S-Band	Kourou Station French Guiana Santa Maria Station Azores		NanoCom GS2000 -buying the transceiver-	
Ka-Band	Redu Station Belgium			
UHF			ISISPACE -buying and make one from scratch	Existing Commercial Network

Table 3.12: Ground Station choices though out the whole process.



Figure 3.53: DTU ground station antennas on top of building 348. Credits: Flemming Hansen

case the antenna is a quad helix antenna of a 20.41 dB gain with a parabolic dish with a diameter of 60 cm shown in Figure 3.54. It is set on a mast on top of the roof and directly onto it is a LNA, next to the LNA are a local oscillator and a down converter. A relatively small dish is used in order to avoid interruption from weather such as strong winds that are common in Denmark. The signal downlink is in S-band at 2400 MHz, which are then down converted to 144 MHz. It operates with a right hand circular polarisation (RHCP). The signal is then transferred to the control room using a $\frac{1}{2}$ " coax cable through a cable duct below the surface of the roof.

Figure 3.55 shows the antenna controller turned on (big gray box). The gray box in the middle is the interface between the transceiver and the antenna controller, while the white box acts as the interface between the transceiver and the processing computer. The transceiver used already exists in the ground station and it is the YAESU Transceiver FT-847.

The control room is equipped with two computers that are not being used currently. The best option is to use one of the desktops that remains there all the time and it is used primarily for the control of the antenna rotor, monitoring and used for the maintenance of

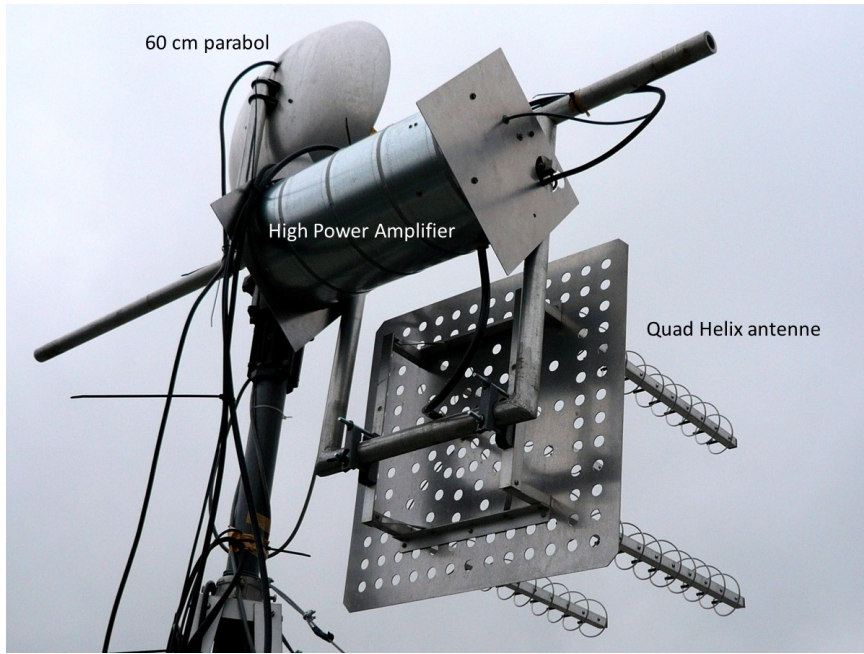


Figure 3.54: 60 cm parabolic dish antenna. Credits: Flemming Hansen



Figure 3.55: 60 cm antenna dish controller and interfaces. Credits: Flemming Hansen

the hardware, as well as the tracking of the cubesat using a software such as GPredict. This software shows the orbit as well as the ground coverage of the satellite and the antennas can be operated accordingly. It has been calculated that the satellite is going to be visible for a maximum of ten minutes from the ground station.

Finally, the processing of the signal can be done by the laptops of the people caring for the station can be used. The processing is done using the SDR software, which can be installed on the laptops using an RTL-SDR RTL2832U dongle shown in Figure 3.56. The software works for modulations between 24-1700 MHz, this is why the LNA is needed. For the processing the SDRsharp (SDR#) software is used for signal demodulation. It provides a spectrum analyser and a frequency waterfall, displaying the signal strength as well. The dongle as well as the modulation of the signal (QPSK) and parameters such as the resolution, the spectrum speed and the time markers must be specified in the software in order to proceed to the demodulation. After the demodulation is done, the signal is saved into a wav file, which then need to be decoded. This can be done using a

CHOOSE A GENUINE RTL-SDR BLOG V3

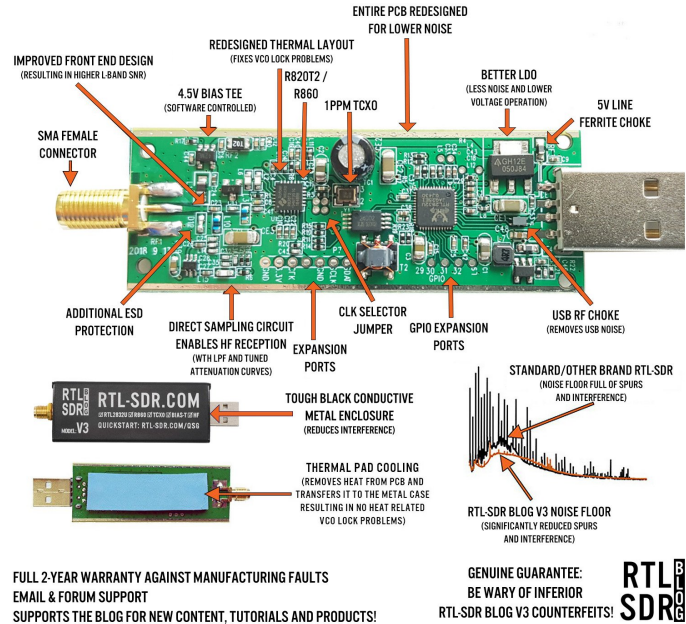


Figure 3.56: RTL-STR dongle configuration [75]

Matlab or python script.

3.6.3 On-board Antenna

3.6.3.1 Introduction

The satellite antenna is a critical component in a satellite, it plays a vital role in the success of the mission since it enables the transmission of scientific data. Like every other component, the antenna is a complex device that must strictly meet the mission requirements. In this context, among them, the most critical ones were the size, weight, power consumption and the radiation pattern.

3.6.3.2 Design Development

In the beginning, two completely different mission concepts were proposed. The first mission was aiming to stay in a low Earth orbit, while the second one was supposed to explore deep space to test the payload in its future working environment. From an antenna point of view, these two proposals are completely different. In fact, the frequency band, the radiation pattern, the pointing needed, and many other parameters were radically diverse. The only common factor shared between the two mission concepts was to build a small satellite, in particular, CubeSat, which affects the physical specification of the antenna.

This led to a first exploration of the possible small satellites antenna designs, from low-gain omni-directional antennas to high-gain ones (Figure 3.57), which were previously employed in space missions.

During the second iteration, the decision to stay in a low Earth orbit was taken, which narrowed the search down to a few options. The next step was to choose the frequency of operation. Given a fixed transmission time window, a higher frequency allows to transmit more data when compared to a lower one. However, higher frequencies are more sensitive to weather conditions and have a higher free path loss. The crucial factor in determining the band to operate in was the volume of data generated from the payload.

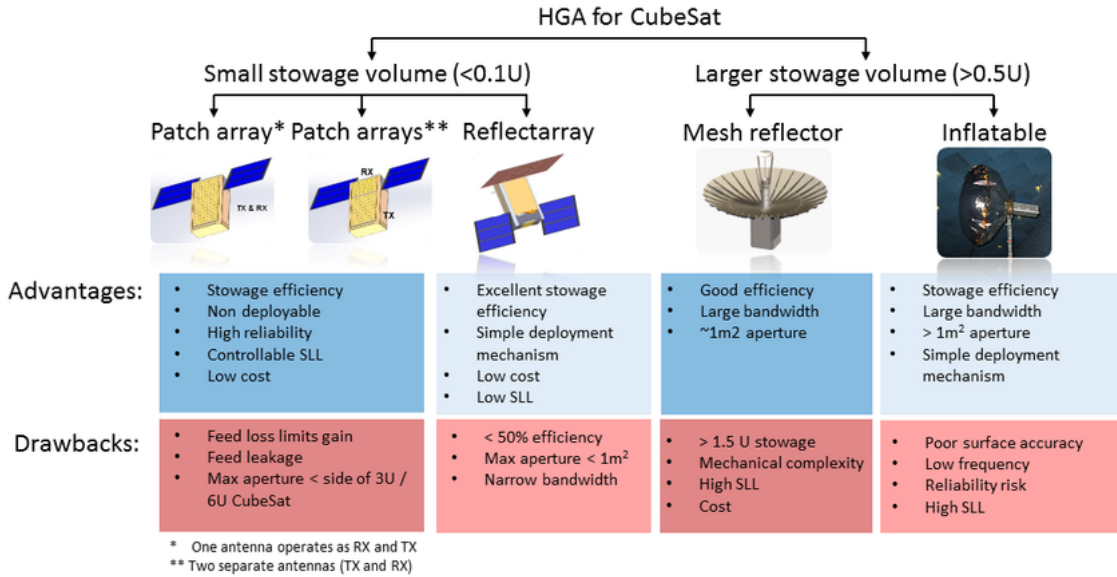


Figure 3.57: Trade-off between possible High Gain Antenna configurations for CubeSats [76]

The exact figure was unknown, however, since the X-ray optics are the only science instruments on-board and the expected output is a position in space, the amount of data to transmit was assumed to be small. With this assumption in mind, the research turned its focus to UHF antennas. The widespread usage of the Ultra High Frequency (UHF) in CubeSat missions has resulted in a wide range of antennas available on the market, with many of them having a strong mission heritage.

In particular, the ISIS - Deployable Antenna System for 6U/12U was the selected one. In addition to the already stated advantages, the reasons behind this choice were that it was suitable for a 6U CubeSat, due to having four poles, it was possible to configure it for various setups. Moreover, since it was an omni-directional antenna, the pointing accuracy was not a significant concern, and the spacecraft rotation could be focused more on pulsar pointing. The mounting configuration is illustrated in Figure 3.58.

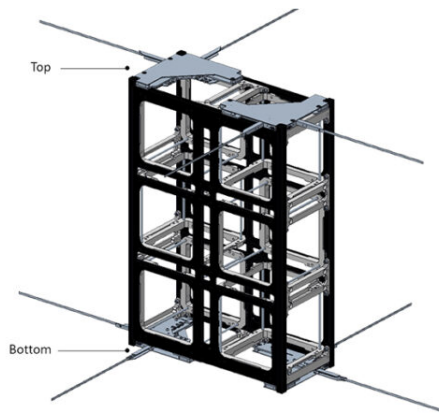


Figure 3.58: Possible mounting configurations for the ISIS 6U UHF Antenna [77]

The optics occupy one of the 2x1 sides of the CubeSat. The need to point the payload towards the pulsars consequently led to the idea of mounting the antenna on the opposite side. However, after some consideration with the Electrical and Power Subsystem, it was found that the antenna's poles were colliding with the solar array during its deployment.

As a result, a design change was needed.

To avoid this collision, the design shifted towards a patch antenna. Furthermore, to meet the requirement stated in Chapter 3.6.1 that specifies that the university shall operate the Ground Station, a modification was made to the operational frequency. In fact, DTU designed and launched a S-Band satellite in 2014 [78], indicating that the university possesses part of the necessary equipment to operate within this frequency range (Chapter 3.6.2).

3.6.3.3 Final design

After the above considerations, the final Telecommunication Subsystem design includes the GomSpace NanoCom ANT-2150 antenna (Figure 3.59a). It is a patch antenna operating in the S-Band. In particular, the frequency spacing during transmission is from 2200 to 2290 MHz, while during receiving is from 2025 to 2110 MHz. The possible mounting positions in a 6U cubesat are displayed in Figure 3.59b, while the antenna parameters are shown in Table 3.13.

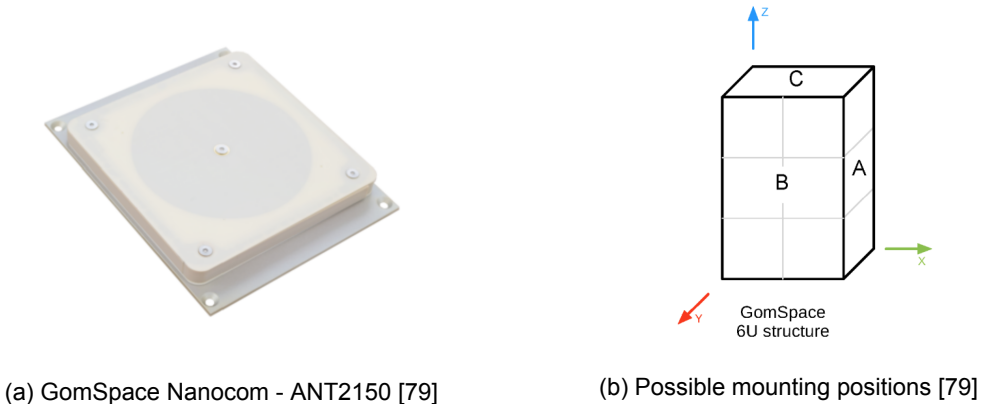


Figure 3.59: Design of the antenna and its possible mounting positions in a 6U CubeSat.

It is worth mentioning that the antenna can handle up to 4W, however, in accordance with the Electric and Power Subsystem it was decided to limit the power to 1.5 W, in order to respect the requirement 4.2.11 from *Fly Your Satellite!* program. Despite the analysis carried out in Chapter 3.6.5 indicating a favorable margin with 1.5 W, the signal to noise ratio can be enhanced by increasing the transmitted power.

NanoComm ANT2150	
Size	98 x 98 x 20.1 mm
Mass	110 g
Gain	8 dBi (Medium)
Power TX	1.5 W (Up to 4W)
Min Temperature	-40°C
Max Temperature	+85°C
Signal Modulation	QPSK
Polarization	Circular (Right Hand)

Table 3.13: GomSpace Antenna ANT2150: Parameters

As previously mentioned, the antenna is not omni-directional, and thus it must be directed towards Earth to transmit data to the ground station. However, as it can be seen from

Figure 3.60, the radiation pattern provides some flexibility and does not demand high precision accuracy.

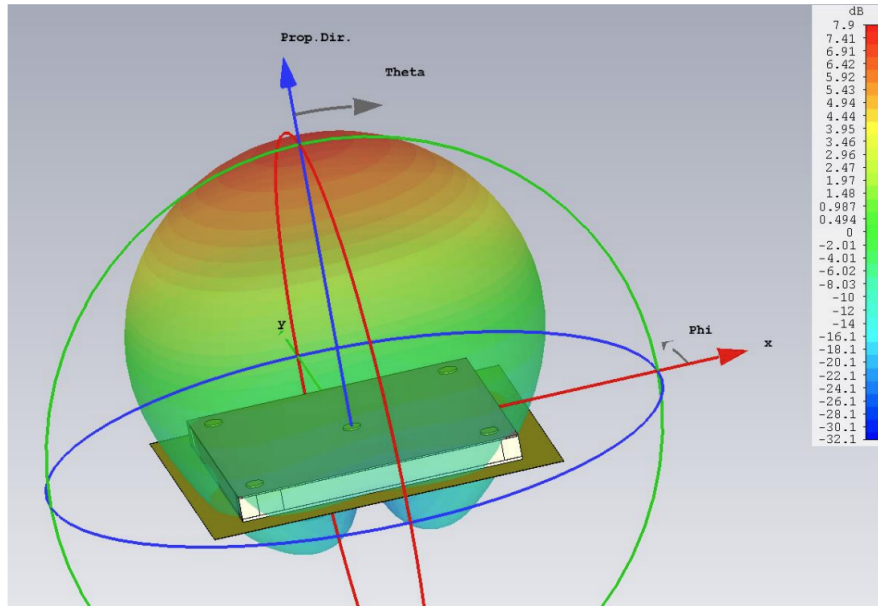


Figure 3.60: ANT2190 Radiation Pattern [79]

3.6.4 Transceiver

3.6.4.1 Introduction

The transceiver is a component that integrates both the transmitter and the receiver into a single unit and it is needed in combination with the antenna to establish a functioning communication system on-board.

3.6.4.2 Workflow

The selection process for a transceiver is closely linked to the antenna one, as the two components communicate with each other. Initially, an UHF transceiver from Endurosat (Figure 3.61a) was selected for the communication system. However, after the design change described in Chapter 3.6.3, it was decided that the GomSpace SDR2000 (Figure 3.61b) would be a more suitable option.



(a) Endurosat - UHF Transceiver[80]



(b) GomSpace - NanoCom SDR2000 [81]

Figure 3.61

3.6.4.3 Final design

As written above, the final design will include the transceiver NanoCom - SDR2000 from GomSpace, which has the following features. It operates in the same frequency range as the antenna, with a transmission range of 2200-2290 MHz and a reception range of 2025-2110 MHz and the power transmission will be limited to 1.5W.

The transceiver can be set up to support different data rates, ranging from 0.5 MBaud/s to 7 MBaud/s. The lowest symbol rate option was chosen as it is sufficient for the mission's requirements.

The modulation scheme supported is Quadrature Phase-Shift Keying (QPSK), which involves coding using the phase of the signal, in particular phases corresponding to 0°, 90°, 180° and 270° are utilized. As a consequence, 2 bits for every symbol are needed, thus, the modulation factor m is equal to 2, while the Forward Error Correction (FEC) code rate is usually set to 1/2. This is done to have more robust and reliable data.

In order to express the data rate in bits per second instead of Baud per second, the conversion formula presented in the equation 3.16 was applied.

$$DataRate = SymbolRate \cdot m \cdot FEC \quad (3.16)$$

This indicates that the transceiver is capable of transmitting data at a rate of 500kbps for a 500kBaude/s data rate.

The supported protocol is the CubeSat Space Protocol (CSP), which proposes a much lighter frame structure than the other protocols used in the major space missions. In Figure 3.62 is shown the protocol frame structure, where ASM is a synchronization marker and the R-S parity block takes 32 out of the 255 bytes available.

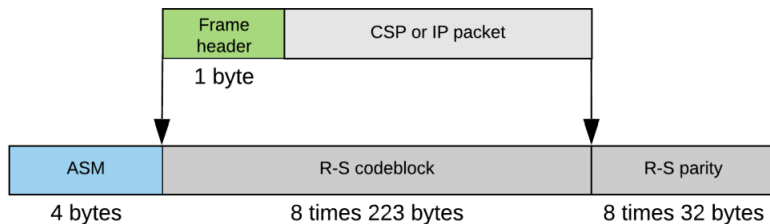


Figure 3.62: CubeSat Space Protocol [81]

3.6.5 Link Budget

Satellite communication relies on the transmission of electromagnetic signals from the ground station to the satellite and back to the receiving station. The link budget is a critical parameter that determines the quality of the satellite communication system. The link budget analysis involves the computation of the signal-to-noise ratio (SNR) at the receiving station and the estimate of the link margin, which is the difference between the received signal power and the minimum required signal power for a given level of performance. When designing a telecommunication subsystem for a satellite, it's of fundamental importance to have a good margin in the link budget, in order to take into account for losses derived from unpredictable sources such as the forecast at the ground station and any pointing losses. The link budget is mostly important for the downlink, from the satellite to the ground station, as it's easier to adjust the hardware on Earth to meet the requirements for a good transmission. This is also because the important data from the payload and

the telemetry data are stored into the satellite and needs to be transmitted on the ground limiting the losses as much as possible.

The link budget equation, includes many different components that are dependent both on the physical characteristics of the instruments and on the location and the attitude of the spacecraft. Specifically, in the link budget equation it's possible to find the transmitted power P_{TX} which is the power of the electromagnetic signal transmitted from the satellite to the ground station or vice-versa. The transmitted power is usually expressed in watts or decibels relative to one watt (dBW). The transmitted power is one of the parameters that determines the coverage and the maximum distance allowed to have transmission. As a rule of thumbs, the higher the transmitted power the higher is the coverage and the higher is the allowed distance. In terms of downlink, the transmitted power depends both on the antenna used and on the transmitter/transceiver present on the spacecraft. This parameters depends on both the antenna and the transmitter used for the transmission of the data. The antenna gain is a measure of the directivity and efficiency of the frequency beam and it's typically expressed in decibels (dB). A higher antenna gain results in a higher received power and, therefore, a higher Signal to noise Ration and link margin. For deep space missions, the antenna is usually a high gain antenna, in order to counteract the effect of the path losses. The high gain in those cases is usually provided through bigger diameter antennas following, in case of parabolic dishes, the relationship expressed in eq.3.17.

$$G = \left(\frac{\pi D}{\lambda} \right) \cdot \eta_A \quad (3.17)$$

Where λ is the wavelength of transmission, D the diameter of the antenna and η_A the aperture efficiency, which describes the capacity of the antenna to use its area for communication purposes and it usually ranges between 0.55 and 0.7. As a consequence a higher antenna gain also requires a larger and heavier antenna, which may not be practical for CubeSats: in fact, as a reference, the antenna placed on the Voyager 1 mission has a gain of 48.2 dB obtained with a 3.66 [m] diameter antenna. The EIRP (eq. 3.18) is the effective isotropic radiated power and express the power radiated by an ideal antenna in a specific direction, for this reason it's expressed in *dBW*. It takes also into account for attenuation losses L_l due to the transmission wiring.

$$EIRP = P_{TX} + G_{TX} - L_l \quad (3.18)$$

On the receiver side the important parameter that must be taken into account is the gain G_{RX} of the receiving antenna, as this determines the quantity of signal caughted and thus transmitted successfully. On the other hand, especially on the receiver side, must be taken into account the loss in the signal caused by the noise at the receiving station. The noise can be cause by all the electronic components present in the hardware of the ground station such as resistors or the Low noise amplifiers, but can be also captured from the antenna itself. The losses in the antenna feeds includes internal cabling, cable and connectors between the antenna and the LNA, losses in a possible duplex filter required to separate transmitting and receiving frequencies or bandpass filter to eliminate out-of-band signals and other resistive losses. As noise calculations always rely on power considerations, it's possible to find the noise loss at the receiver following eq.3.19 where T_e is the equivalent temperature at the receiver, k the Boltzmann's constant and ψ the bandwidth of the signal.

$$P_n = kT_e\psi \quad (3.19)$$

In order to find the equivalent temperature T_e it's first necessary to pass through the noise figure F of the receiver (equation 3.20). To do so, all the calculations are related to a universally accepted noise temperature of $T_0 = 290K$, therefore in any case the expectation

is to find $F \geq 1$.

$$F = 1 + \frac{T_e}{T_0} \quad (3.20)$$

Following eq. (3.20) is possible to find the relative temperature T_e as $T_e = T_0(F - 1)$. This process must be held for every two ports system present between the antenna and the decodification of the signal: every resistive loss L present in the path between the antenna and the receiver need to be taken into account in order to find the equivalent temperature T_e . The loss L can be assumed equal to the noise figure of the receiver, therefore applying Friis' formula for n resistive components the obtained relationship is:

$$F_{tot} = F_1 + \frac{F_2 - 1}{G_1} + \frac{F_3 - 1}{G_1 G_2} + \dots + \frac{F_n - 1}{G_1 G_2 \dots G_{n-1}} \quad (3.21)$$

thus the equivalent temperature can be found following the equation for T_e derived from eq.3.20 and it's possible to find the total receiver noise temperature as:

$$T_{RX} = T_0(L - 1) + L \cdot L_{LNA} + \frac{L}{G_{LNA}} T_3 \quad (3.22)$$

Which is the receiver noise temperature that is referred to the terminals just behind the antenna, including noise generated in the antenna itself, but does not include the noise picked up by the antenna from the sky or the surroundings. The thermal noise picked up by the antenna has different contribution such as Cosmic Microwave background, Galactic sources, attenuation in the dry atmosphere, absorption due to water vapour (22.2 GHz) and O₂ (60.4 GHz) resonances and the receiver quantum noise limit. In order to find the temperature that derives from these noisy losses, the graph in fig.3.63 is used. The total temperature T_{sys} used in the link equation takes into account of the temperature of the sky picked up by the antenna but also the temperature of the Earth for very low elevation angles, and eventually the temperature of the noise in the back end of the receiver. Transmission however is not only affected by the physical properties of the transmitter and the receiver, but also the relative position between them must be taken into account. This is called path loss L_{path} , it's measured in dB and follows eq.3.23:

$$L_{path} = 32.45 + 20 \cdot \log \frac{d}{1 \text{ km}} + 20 \cdot \log \frac{f}{1 \text{ MHz}} \quad (3.23)$$

where f is the frequency of transmission and d the distance between receiver and transmitter that can be found with geometrical relationships. From eq.3.23 it's clear that the higher is the frequency employed in the transmission, the higher will be the loss associated to the distance d . Eventually, to make the estimate more precise and in order to take into account for other losses it's possible to subtract other terms for polarisation loss L_p , de-pointing loss L_θ and rain attenuation L_r . Finally, the link budget equation is expressed in eq.3.24 and takes into account all the losses and gains for both receiver and transmitter. The result is called $EbN0$ which is the energy per bit over the noise spectral density.

$$EbN0 = EIRP - L_p - L_\theta - L_r - L_{path} + G_{RX} - 10 \log(k) - 10 \log\left(\frac{R}{1 \text{ Hz}}\right) \quad (3.24)$$

Where k is the Boltzmann's constant in $\left[\frac{J}{K}\right]$ and R the data rate. Eventually it's possible to define the Signal to Noise Ratio (SNR, eq.3.25) which is the last parameter used to estimate the goodness of a link and describes the ratio between the power received and the power spectral density of the noise:

$$SNR = EbN0 \cdot \frac{R}{B} \quad (3.25)$$

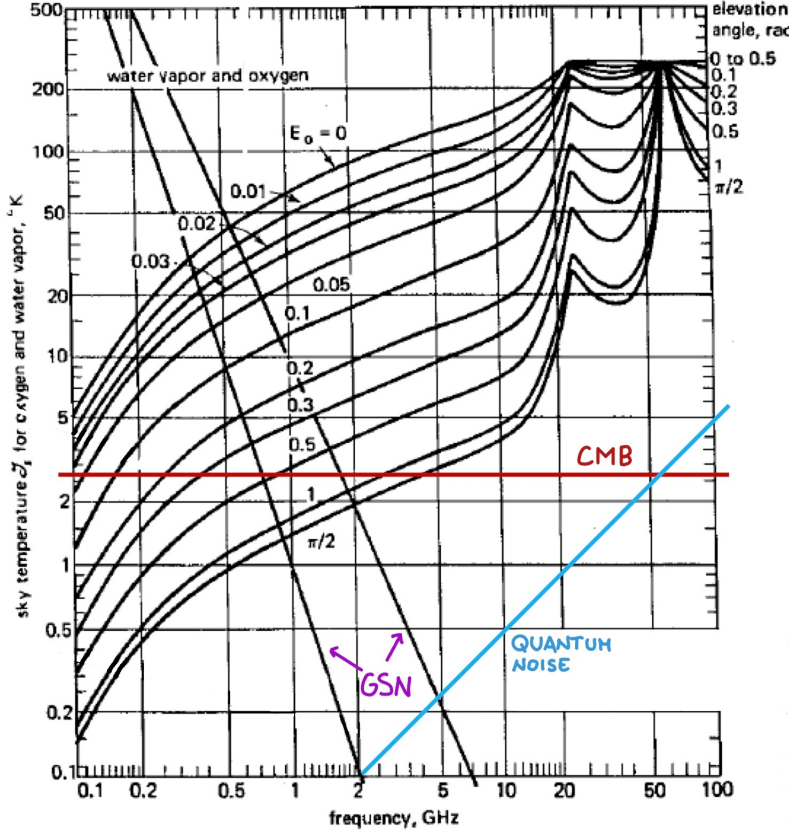


Figure 3.63: Atmospheric losses from horizon to zenith. Red line is the Cosmic microwave background, the blue line represents the receiver quantum noise and the purple one represents the galactic synchrotron radiation in the direction of the galactic plane (left) and away from it (right). [Credit: Flemming Hansen]

3.6.5.1 Link Analysis

The link budget has been estimate for the final configuration chosen for PANTSat which consists of what explained in section 3.6.3.3, specifically for the downlink the antenna has a gain of $G_{TX,max} \simeq 8.5 dB$ and a power of transmission furnished by the transceiver of $P_{TX} = 1.5 W$. Must be taken into account that the spacecraft attitude can present some errors when pointing the Ground Station, as a consequence, following fig.3.64 and assuming a maximum of 20° pointing error, the gain of the antenna can be assumed to be $G_{TX} \simeq 7 dB$. Assuming $L_l = 2 dB$ the EIRP is derived with eq. 3.18 obtaining $EIRP = 6.7609 dB$. In order to assure the transmission of data, the link budget must be evaluated in the worst case scenario, i.e. when the satellite approaches smallest elevation angle allowed by the ground station, where the path loss and the noise picked from the antenna have their maximum value. Theoretically, this case is the case when the satellite is at horizon, with 0° elevation above it. In reality, antennas in the ground station usually do not point towards the horizon, therefore for the PANTSat mission is assumed that the minimum elevation angle reachable by DTU ground station is 15° .

For the ground station, DTU uses a Kuhne Electronic low noise down-converter which presents a noise figure of $N = 0.7 dB$ and a gain of $G_{LNA} = 30 [dB]$. As a consequence the noise figure in the scalar domain can be found as $F = 10^{\frac{N}{10}} = 1.175$. The temperature of the receiving system then is found from eq.3.22 to be $T_{RX} = 50.7 K$. The antenna used at the ground station has a diameter of $D = 0.6 m$ thus the obtained gain following

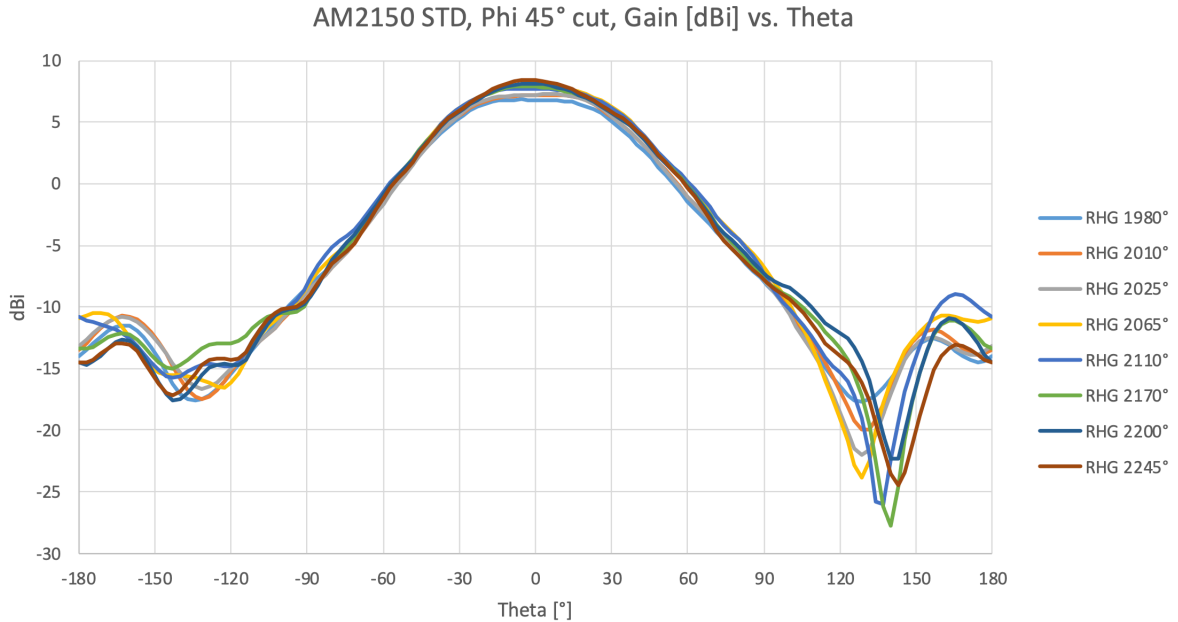


Figure 3.64: Gain attenuation as a function of the pointing accuracy [79]

eq.3.17 is $G_{RX} = 20.41 \text{ dB}$ where an aperture efficiency of $\eta = 0.55$ has been assumed. The distance between the satellite and the ground station in this case is $d \simeq 1204 \text{ km}$, thus the path loss following eq.3.23 is $L_{path} = 161.1 \text{ dB}$. From figure 3.63 it's possible to derive the noise temperature picked up from the antenna at 15° elevation: the sum of all the temperatures from the different noise sources gives $T_{ant} = 14.16 \text{ K}$. Once again assuming that the antenna has a fairly large beam, at 15° elevation it will see a third of the ground temperature (280K) and two thirds of the sky temperature, thus the temperature of the antenna can be found as:

$$T_{ant,15^\circ} = \frac{1}{3} \cdot T_{ground} + \frac{2}{3} \cdot T_{sky} = 156.8 \text{ K} \quad (3.26)$$

Therefore it's possible to apply eq.3.24 to find $EBN_0 = 15.71 \text{ dB}$. The bit rate used is given by the transceiver, therefore with 0.5 MBaud data rate PANTSat will be able to send to the ground station an entire day of data in 160 seconds of transmission assuming the worst case scenario for the quantity of data provided by the payload. The downlink therefore can happen just once per day without compromising the transmission of all the data.

Figure 3.65 shows the different modulations allowed for telecommunications, in this case the chosen modulation is the QPSK because is the modulation used by the transceiver. In order to have a good transmission the aimed Bit Error Rate (BER) should be around 10^{-4} but as the EBN_0 obtained is very high it's possible to aim at a BER of 10^{-6} , thus the required EBN_0 is 10.5 dB . The correspondent link margin is of 5.21 dB which is above the requirement for the PANTSat mission, set at 3 dB . It's also possible to pick a higher BER in order to have a bigger margin, assuming a BER of 10^{-4} and a correspondent required EBN_0 of 8.5 dB the obtained margin will result of 7.21 dB . The margin of 3 dB is met also when the error in the pointing of the Ground Station hits 30° but in this case the margin for a BER of 10^{-6} is just 0.21 dB .

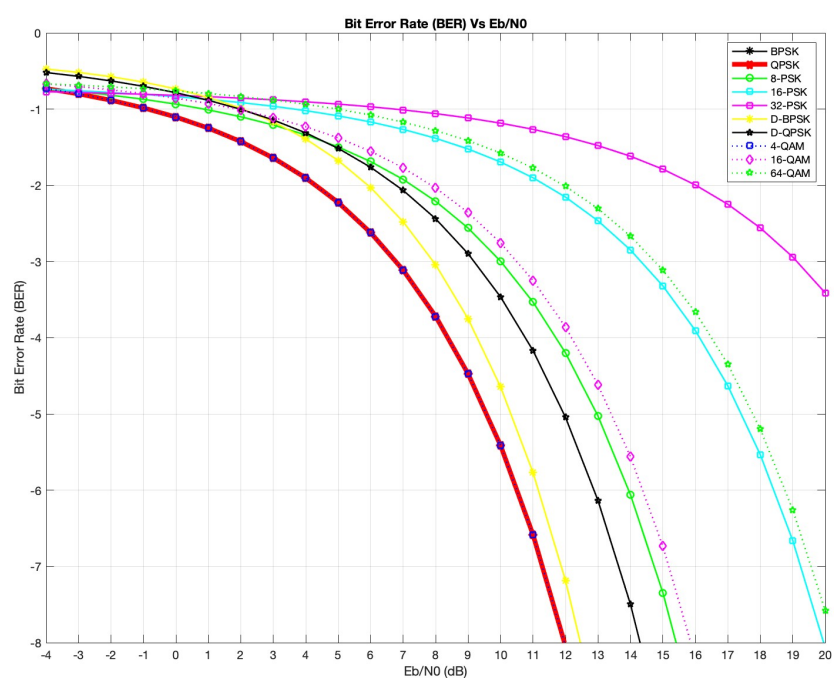


Figure 3.65: BER vs EB_N0 for different modulations

3.7 Structures and Mechanism

This section presents the structure and the optics extension mechanism. Firstly, the requirements for the frame, optical extension, and the other subsystem are described. After taking the requirements into consideration, the current design of the satellite and the extension mechanism are presented.

3.7.1 Requirements

3.7.1.1 Frame

It has been chosen that PANTSat will be launched with NanoRacks (see Section 3.4.4, therefore we will have to examine the requirements for the structure given by NanoRacks [82]. Before launch, NanoRacks will perform an inspection of the satellite to verify it meets its requirements. The two most important things are mass properties and critical mechanical dimensions. To get this information the Interface Definition Document (IDD) from NanoRacks has been read and taken into account when making the CubeSat. PANTSat will be deployed with a NRDD, which is a self-contained CubeSat deployer system for small satellites staged from the ISS. This can house one 12U CubeSat or two W6U CubeSats, where the only form factor between these types of CubeSats is the total length in the Z-dimension.



Figure 3.66: NanoRacks DoubleWide Deployer [82]

NanoRacks provide NRDD to both tab and to rail configurations. The specifications for that in short form is:

1. The CubeSat shall have four integrated rails, to allow the payload to slide on the rail interface of the NRDD as defined in Figure 3.67.
2. From the dimensions on Figure 3.67, rails must be within +/-0.1mm, and the envelopes must have a maximum of this dimension.
3. The edges of the rails shall be rounded to a radius of 0.5mm (+/-0.1mm).
4. The CubeSat shall have load points within +/- 0.25mm of the rails on the +/- Z faces.
5. The rail length shall be 366mm (+0.0 / -65.0).
6. The rails shall be continuous. That means no gaps, holes, fasteners, or any other features may be on the rails (Z-axis) in regions that contact the NRDD rails.
7. The only thing that may make contact with the NRDD is the rails.
8. Rails points shall extend beyond the +/-Z faces of the entire payload, including all external features, by no less than 2mm

9. All rails and load points shall have a hardness equal to or greater than hard-anodized aluminum
10. All rails and load points shall have a surface roughness of less than or equal to $1.6\mu\text{m}$

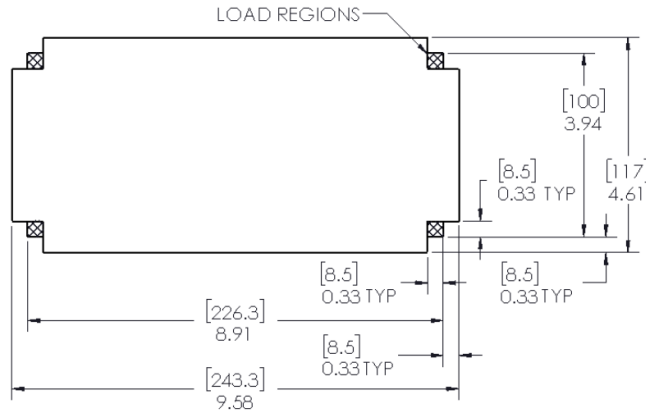


Figure 3.67: NRDD with Rails Payload Envelop and +/-Z Load Points [82]

The maximum mass for a 6U CubeSat is 12kg. (This mass is for a CubeSat assumed to not have any attitude control and design features. If a CubeSat has some of these things the ballistic number will change and will drive the mass requirements.) The mass needs to be equally distributed over the system so the center of mass (COM) is located in the following range: X-axis +/- 5cm, Y-axis +/-3cm, and Z-axis +/- 8cm.

NanoRacks have eight requirements for the deployment switches, which is the component that controls that the CubeSat does not turn on during launch. The important part of the eight requirements is: The CubeSat shall have a minimum of three switches, and they must be in the same Z-face on the CubeSat. The switches shall have a minimum actuation travel of 1mm to accommodate for design slop. The payload needs to go in a pre-launch state, if the switches are cycled in the first 30 minutes. The maximum force from the switches is 18N.

They also have two requirements for deployable systems. The first is that deployable systems, such as solar arrays or payload boom, shall have an independent mechanism for deployment and may not rely on the NRDD dispenser. The second is that the CubeSat shall be capable of being integrated forwards and backwards inside of the NRDD. There are also two requirements for the deployment of the CubeSat from NRDD. The first is that the CubeSat shall be capable of withstanding a deployment velocity of 0.5 to 1.5m/s at ejection. The second is the CubeSat shall be capable of withstanding up to 5deg/sec/axis tipoff rate.

Even when fulfilling the given physical requirements, the CubeSat must also be able to withstand the trip to space. To ensure this, a random vibration environment test is required. There are two ways NanoRacks make this test, with soft-stow flight and hard-mount configuration. An example of this is shown in Figure 3.68. Here ASD (acceleration spectral density) is used to specify random vibration [83].

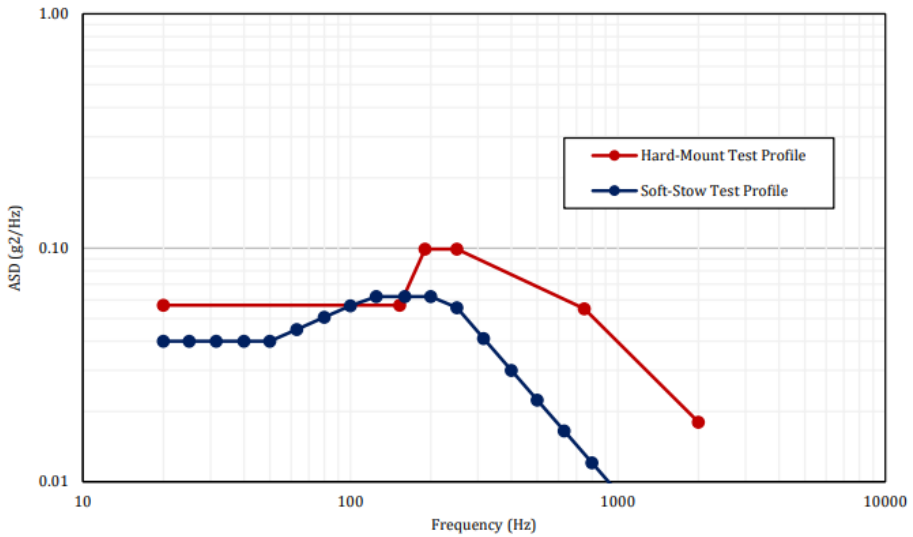


Figure 3.68: Random Vibration Test Profiles [82]

3.7.1.2 Optical extension

As stated in Section 3.1, the optics require a focal length of 430 mm, which is beyond the dimensions of a W6U cubesat which has a maximum length of 340.5 mm. In order to fulfill both requirements an extension mechanism is required for the instrument to be able to perform. The requirements for this mechanism are as follows:

- Has to fit within cube-sat whilst optics are as close as possible
- Extend up to a minimum of 422 mm in focal length
- Must overcome all sources of friction
- Must have redundancy or good heritage
- Must provide rigid pointing accuracy which when combined with AOCS pointing is below 0.03 deg

3.7.1.3 Other subsystems

To complete the mission some of the other subsystems have made requirements for the mechanical structure and the placing of the different parts.

Optic and Sensor box The optics shall be on one of the sides, so the extension can be used. From the need for two optics and a long focal length, it could only be placed one way. The belonging sensor box must be placed in the opposite end of the optic to measure the incoming data. The dimensions of the sensor box are given, but the placement of the sensors themselves could be redesigned. For more info see Section 3.1.

Attitude Control The Attitude Control System must be placed close to the COM. If the COM is not around the same place pre-launch and after deployment of optic and solar arrays, they want to be closest to the COM after deployment. The attitude control system is also equipped with a star camera. The optimal way for the camera to look is the same way as the optic. More info is available in Section 3.

Antenna To get a connection to Earth PANTSat needs an antenna. To use the antenna and the optics at the same time or without turning the whole CubeSat, the requirement for the location of the antenna is that it must not be on the same side as the measurement direction of the optics. Information about the antenna can be found in Section 3.6.3.

Solar array To mount the solar arrays a 10x10cm space on a Z-face is needed. Because the optics are extended out of one of the Z-faces the solar arrays must be placed on the other end. This also makes sense, as it will distribute the mass in both ends of the CubeSat. The solar arrays are described in more detail in Section 3.5.3.

3.7.2 Frame

3.7.2.1 Developing our own W6U structure

Early in the project, we were considering designing a W6U CubeSat structure ourselves. This process is very time consuming and difficult since we must think of how to comply with all the many requirements listed in Section 3.7.1.1 for a CubeSat. This also means there is not a lot of freedom in the design process, so there is no big advantage in making itself. If we could change the dimensions, we could fit the optic better in it and that would have been an advantage.

3.7.2.2 The GomSpace W6U structure

The main structure of the W6U will be bought from GomSpace. With this structure, we get a high degree of freedom for mounting the hardware, both on mounting rings and directly on the structure. The material is aluminium 7075-T7351 and with an outer size of 340.5 x 226.3 x 100.0mm, this gives a total mass for the structure of 716g. Each side has multiple threaded holes that give a good connection between components and structure. The structure is made from two large frames and four corner brackets to join the frames, the assembled frame can be seen in Figure 3.69. The corner brackets are assembled with two screws, one in each frame part. The rest of the holes have multiple purposes: Countersunk holes for internal mounting rings, holes for central covering plates, holes for solar panels, holes for antenna release, and mounting holes for external systems.

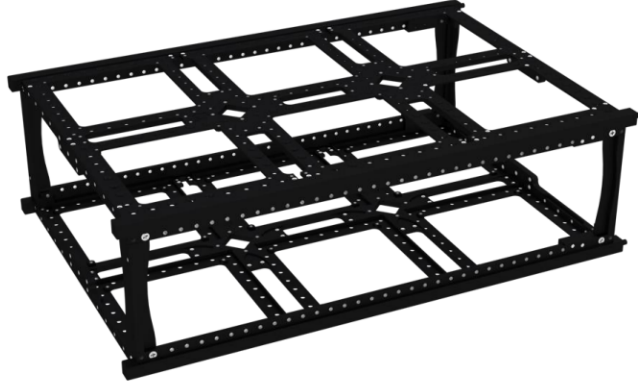


Figure 3.69: The frame made of GomSpace[84]

There are already four kill switches, which is one more than required for a 6U. These switches are also called deployment switches. They sit in one end of the structural frame and are pressed down while the cubesat is placed in its orbital deployer. The switches make sure that the satellite cannot be powered before deployment, and as soon as it is deployed it can power up. The switches can be connected in both serial and parallel setups, but regardless of the connection, the spring plunger is installed to provide a uniform separation force of 6 N. To mount all subsystems to the structure mounting rings is the most common to use. This structure gives stability to the system and makes it easy to place in different directions as can be seen on Figure 3.70. In most cases the mounting rings are placed to be pointing in the Z-direction, but in PANTSat we need them to point in the X-direction. GomSpace produces mounting rings that can be smaller or bigger than

a 1U. Because our optic is bigger than a 1U in the X-direction, smaller mounting rings will be used. Before we can use these mounting rings, we need to attach the different subsystems on a PCB/plate in the correct size of the mounting ring.

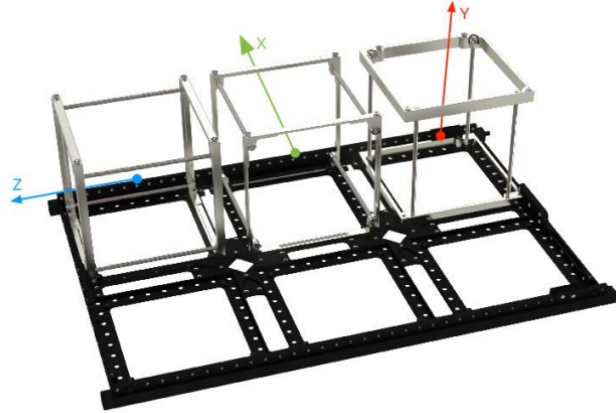


Figure 3.70: The different ways the mounting rings can be placed[84]

Another big advantage of using GomSpace's structure is that they have done environment testing, to test for both launch and space. NanoDock SDR has been exposed to several different environment tests and has been used several times and works perfectly [84].

3.7.3 Optical extension mechanism

As stated in Section 3.1, the optics require a focal length of 430 mm, which is beyond the dimensions of a W6U CubeSat that has a maximum dimension of 340.5 mm. In order to fulfill both requirements an extension mechanism is required for the instrument to be able to perform.

This part is a potential mission killer, and so extreme importance is put onto reliability of this extension, and not on extending the optics with precise linear precision.

3.7.3.1 Extension By Mechanical Mechanism

As far as extendable objects go, using springs and other purely mechanical mechanisms are the most reliable method for one time use deployment. Therefore, this became the initial basis for PANTSat's optics extension mechanism. In addition there would be no extra requirements set on EPS or the OBC, which is desirable.

As there is little room between the optics and the sensor inside the satellite itself, it's important that the extension mechanism can be incredibly compact and still be able to extend the required amount. This fits the description of a boom incredibly well, as they can extend many times their compressed size. They have been shown to work in multiple space missions, as this is a common method for deploying instruments such as magnetometers.

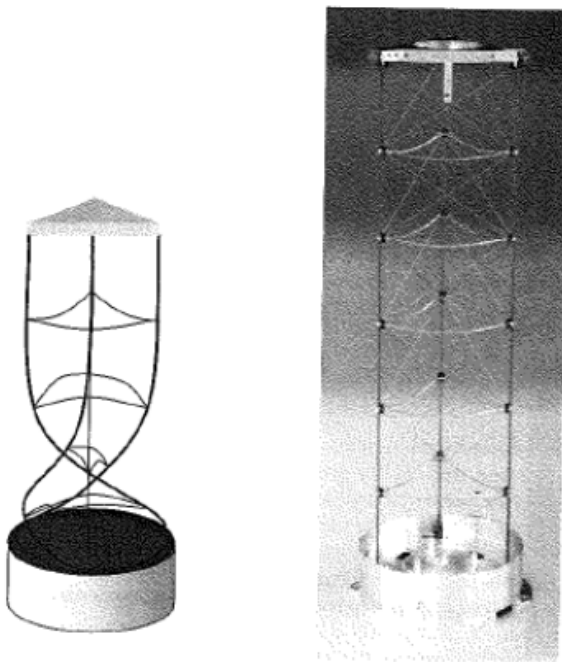


Figure 3.71: Example of extendable boom mechanism[41]

This idea was, however, discarded due to the complexity of the shape itself being difficult to produce and design. Additionally, and critically, the satellite is required to change attitude relatively quickly, which means that the boom not only has to be rigid in the extendable direction, but also perpendicular to the axis of extension. A boom, particularly with heavy optics at the end, could possibly permanently bend or start large oscillations which would take time to dampen, thereby impeding measurements.

3.7.3.2 Extension by Electric Motor

Another method to create this extension is by use of an electric motor. This is a more complex system than mechanical, however, it has some benefits in design freedom, accuracy and it enables possible secondary uses. In order to translate the electrical motor's torque into a linear movement, a gearing system will be required. For this 3 different systems have been considered:

Spur	Ball Screw	Worm Drive
Awkward dimensions	Desirable dimensions	Desirable dimensions
Little friction	Requires Lubrication, High Friction	High Friction
Flexible ratio	Flexible ratio	Complex ratio changes

Initially the spur gearing system was chosen, due to the low friction the motor would have to overcome and due to the flexibility in gear ratio changes not necessitating any major changes in design. From this came the concept seen in Figure 3.72:

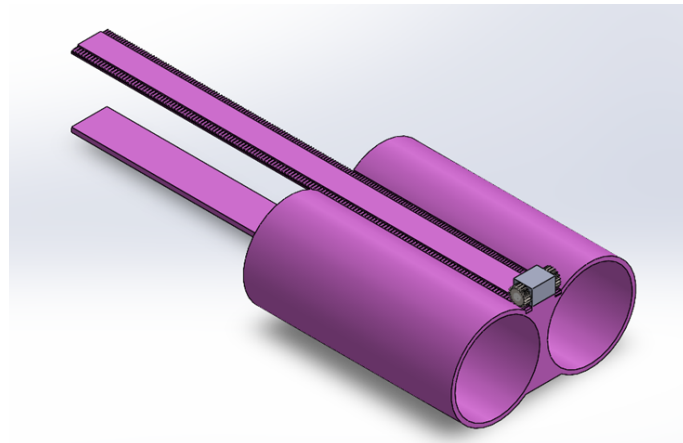


Figure 3.72: Optical extension mechanism using a spur-rack system with a dual axis 15 mm long electric motor

The motor itself does cause some issues. Due to the severe size constraints put on the satellite, the optics must be positioned together as tightly as possible which imposes requirements on the motor sizes themselves. As no suppliers of electrical motors in this size could be found, this design was again discarded in favour of the worm drive.

The Worm drive was chosen over the ball bearing due to simplicity of design and lower friction by the worm drive. Therefore the final concept motor concept became the worm drive, rack gearing system seen in Figure 3.73

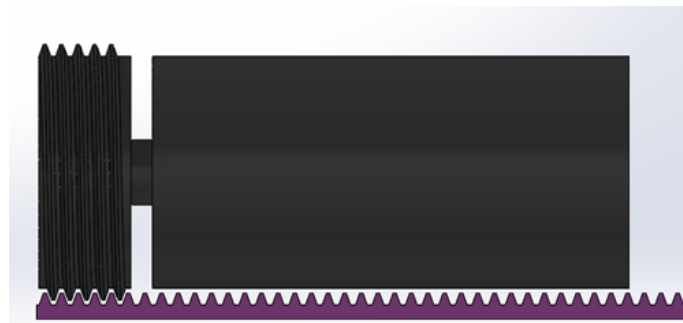


Figure 3.73: Nanotec electrical motor with worm drive, rack system

At this point, specific materials and calculations had to be made in order to determine the viability of this concept. The materials chosen between surfaces with friction must be different and have as low friction as possible. For implementing redundancy it is also required for the motor to be able to not only overcome all surface friction within the system, but also the internal friction of a second failed motor. A worm drive is difficult to build around redundancy as this type of gearing is difficult to push load from rack to worm drive. This can, however, be remedied by increasing the angle of contact between the worm-drive and rack.

3.7.3.3 Material Selection and Viability Study

The defining material in this electrical motor system will be that of the optics casing (purple), which has friction between both the worm drive and through the opening of the satellite itself. For this material the following characteristics are desired:

- Low friction coefficient with aluminium in vacuum
- High rigidity
- Producible into advanced shapes
- Different materials at friction surfaces

It is important to note that the chosen material will be different from the material chosen for the worm drive and the outer wall in order to avoid cold fusing. One material which fits all 4 of these requirements is the DuPont Vespel SP-21 plastic, which is a graphite enhanced plastic material ideal for rigid, low friction applications where no lubricants are available.[85] This will be the material chosen for the optical casing, whilst the worm drive and outer casing seen in Figure 3.74 are aluminium. Particularly the material of the worm drive may be subject to change, however, this has not been researched at this time.

Using the torque provided by the Nanotec DC motor [86] and the angle of the worm drive, the friction between the motor and the rack can be determined:

$$F_{worm} = \mu N = \mu \frac{L_{motor}}{r_{worm}} \sin \theta \quad (3.27)$$

Where F_{worm} is the friction between our rack and worm drive with the friction coefficient of μ , and an angle of θ between the rack and the worm drive gears. L_{motor} is the torque from the chosen Nanotec DC motor. The values applied for these calculations are stated in the following table.

Variable	μ	θ	L_{motor}	r_{worm}	F_μ
Value	0.15	7.8 deg	0.8 N cm	11 mm	0.01 N

This is possible for the motor to pull as the maximum force it can exert is $\frac{L_{motor}}{r_{worm}} = 0.73$ N. Redundancy, however, is a requirement leading to the system having 2 motors and in order for redundant motors to function, the motor must be able to overcome the additional friction caused by a motor failure.

In the case of 1 motor failing the added friction will be on the second rack along with the internal friction of the second DC motor which the rack is pushed up against. Assuming the internal friction is 10% of F_{motor} , the added total friction of the system becomes:

$$F_\mu = 2F_{worm} + 0.1 \frac{L_{motor}}{r_{worm}} \frac{1}{\sin \theta} = 0.57N \quad (3.28)$$

As this is below the force applied by 1 DC motor, it can be concluded that the Nanotec DC motor has enough torque to extend the optics even if one motor fails.

Important to note is that some assumptions have been made in this calculation, where primarily the internal friction of the DC motor may have a major impact on performance. Further research and/or testing is required to verify this assumption.

The pointing accuracy can be estimated by using the characteristics of the plastic material combined with the maximum amount of torque provided by the ACS in a cantilever configuration. This will provide the maximum load which the optics may experience at any time, how much displacement will be caused by this torque and from this the maximum pointing accuracy. This displacement can be calculated using equation 3.29:[41]

$$\delta = \frac{FL^3}{3Ewt^3} \quad (3.29)$$

Using the current dimensions of the optics, the torque provided from the reaction wheels along with material properties of SP-21, the following characteristics are found:

F	δ	ϕ
0.017 N	0.78 μm	$1.6 \cdot 10^{-4}$ deg

here F is the approximate force which will be applied to the end of the satellite seen from the PANTSat inertial reference frame. As the forces involved are small, and the plastic is relatively thick and very rigid this displacement is below a μm results in a pointing accuracy ϕ well below the required 0.03 deg.

Besides the bending angles, inaccuracies in the dimensions of the optic slits can contribute to pointing inaccuracies. The relationship of this inaccuracy can be determined using by the length of the supported plastics b by:

$$c \cdot \cos(\phi) = b \quad (3.30)$$

Where c is the hypotenuse of the triangle created by the length b and the inaccuracy of the manufacturing method. The dimensional accuracy of laser cut parts are $2.5 \cdot 10^{-3}$ mm, and applying this we arrive at an angle $\phi = 0.01$ deg. This is quite substantial, however this calculation does not take the curved shape into account which will reduce this angle substantially. Combined with the accuracy of the ADCS, the required 0.03 deg of accuracy is still fulfilled.

As this system passes all the previously stated requirements for the optics extension mechanism, the final design became the one shown in Figure 3.74.

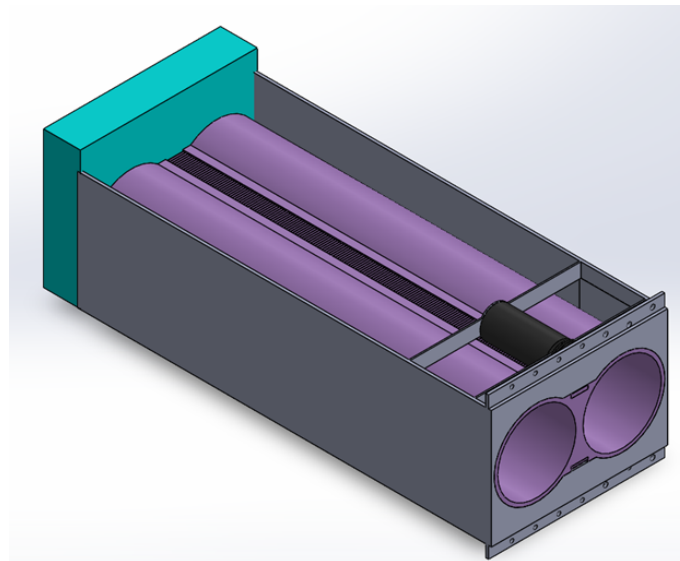


Figure 3.74: Complete Optical System

with the components seen in Table 3.14:

Part Name	Optics Casing	Outer Casing	Sensor	DC Motor	Worm Drive
Dimensions[mm]	60x120x300	100x124x300	120x90x20	22x55.7*	24.25x9.42*
Material Number	DuPont SP-21 1	Aluminum 1	Various 1	Various 2	Aluminum 2

Table 3.14: List of components with dimensions used for the optical extension
(*Diameter of cylinder first)

3.7.3.4 Possible improvements

All though a viable solution has been made, there may still be improvements to the current design or with different concepts. One such concept takes inspiration from the mechanism used by toy cars.

Certain toy cars are equipped with torsion springs, which can propel the car forwards as it is being released. This is a very interesting solution which would simplify the mechanism from an electrical and software standpoint, and could very likely provide larger pushing force than provided by the worm drive. In future work this solution should be studied and designed in detail as a potential improvement to the current design.

3.7.4 Spacecraft Configuration

Provided the mass and size properties of all the subsystems of the satellite, a virtual assembly could be made using the Solidworks software. Some of the subsystems had specific requirements regarding placement on/in the satellite, so these would have to be considered in the layout. In this report, A simple model of the spacecraft configuration will be presented along with a more detailed version.

3.7.4.1 Simple model

The simple version of the spacecraft assembly is seen in Figure 3.75. Two configurations of the spacecraft are shown. During launch and release, the satellite will be in a stowed configuration (left). After release and detumbling the solar arrays and the optical extension mechanism will be deployed (right). All subsystem components are listed and colour coded in Table 3.15

Component	Number of components	Size [mm]	Mass [g]	Requirement	Colour
6U structure	1	340.5x266x100	730		Grey
Optical system	1	120x60x278	3300	Optics extension pointing outwards	Blue
Sensor box	1	124.5x96.5x26	300	Placed in line of optics	Turquoise
Atomic clock	1	40.6x35.3x11.4	35		White
Aluminium side panels	1	Thickness: 2	810		See through
Thermal control box	2	27.7x15.4x38.1	28		Dark red
OCB	1	90x90x1.9	130		Purple
Attitude	1	100x100x75.4	1230	Star camera pointing outwards. Different side from antenna	Pink
Transceiver	2	88.9x92x23.4	270		Yellow
GNSS	1				Dark green
Antenna	1	98x98x20.1	110	Placed on outside. Different side from optics and star camera	Green
Battery pack	1	94x84x23	270		Red
EPS	1	90x96x19.8	191		Orange
Solar Panels	1	Stowed: 330x208x90, Deployed length: 930	750	On large side	Light grey

Table 3.15: Components and their sizes in the simple model

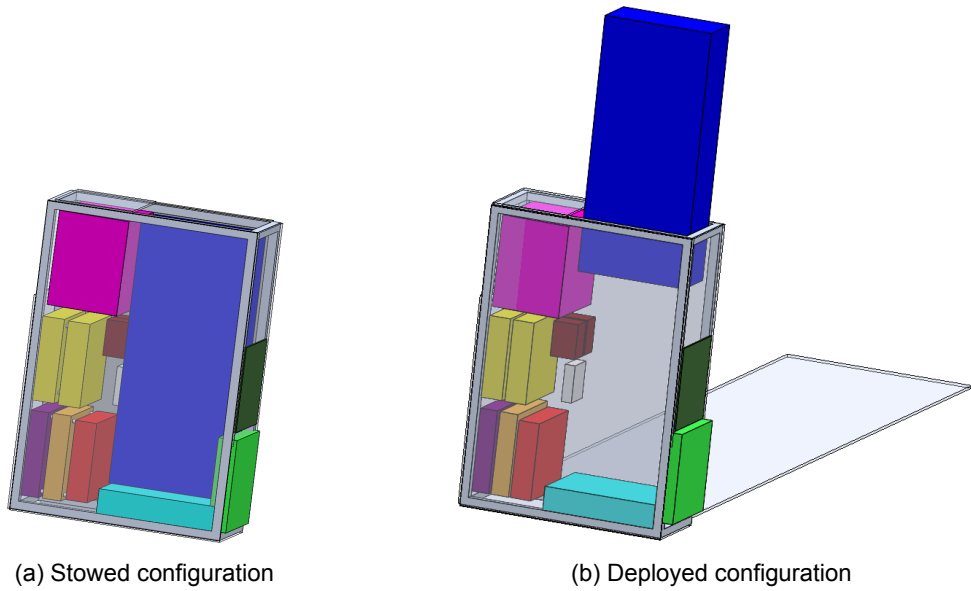


Figure 3.75: The simple Solidworks assembly seen in two configurations. A stowed configuration for launch and release of the satellite (left) and a deployed configuration after deployment of the solar panels and the optical extension mechanism (right).

There are several advantages of making a simple model first. One advantage is that subsystems and components are easy to move around when changes to the layout occur. These changes have occurred relatively often throughout the mission design due to the subsystem teams' constantly improving knowledge throughout the project. Another advantage is the simplicity in illustrations. It is easy for externals to get a good overview of the structure of the satellite. The simple model also provides a good basis for calculations of the satellite's center of mass (COM) and moment of inertia.

The COM of the satellite is calculated by Solidworks. However, the origin of the model is not in the center of the assembly in Solidworks. Therefore, corrections have been made to calculate the COM from a reference frame where the origin is in the geometric center of the assembly. After correcting this, the coordinates of the center of mass in the stowed and deployed configurations are shown in Table 3.16. The COM in the stowed configuration is seen to be within the requirements presented in Section 3.7.1.1. When the optics and solar arrays are deployed the COM changes as the mass distribution is changed. Since the COM requirements are only relevant for launch and release of the satellite the COM in this configuration is not a problem, but it is relevant for the attitude control group (see Section 3).

Direction	Stowed COM [mm]	Deployed COM [mm]
X	37.62	37.3
Y	25.57	43.92
Z	13.51	83.23

Table 3.16: COM stowed and deployed

The initial vibration simulations would also be carried out on the simple model as the complexity of the detailed model would likely require too much computing power. In order to prepare the simple model for vibration simulations, the subsystems would have to be

definitively mounted within the satellite as they would be in the detailed version and subsequently in a real world assembly as well. The goals of vibration simulations and tests are to determine the resonance frequency/frequencies of the fully assembled spacecraft and whether the spacecraft is able to withstand the loads and vibrations from launch. This is extremely important as a mechanical failure could occur in the system which in turn could have fatal consequences for the mission [87]. The current status is that preparations for vibration simulations are being done at the moment. This means that the final mountings of the subsystems are being discussed and implemented. A more in depth description of vibration tests is given in Section 4.2.1.

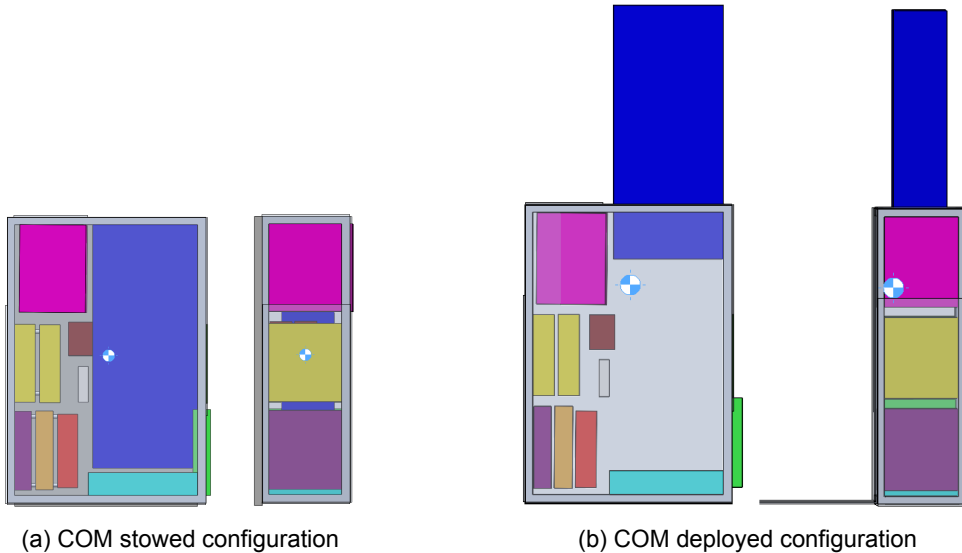


Figure 3.76: The COM of the satellite showed in the stowed (left) and deployed (right) configurations. The deployed configuration shown here does not show the entire solar array.

Deployment and movement of the solar panels will produce a moment of inertia and therefore spin the satellite unless corrected by the attitude control system. The moment of inertia of the solar array deployment and movement will need to be analysed by looking at the force at which the arrays are deployed and the velocity of the movements. This could be done from tests of the solar array deployment and movement where the accelerations on the satellite can be measured directly.

3.7.4.2 Detailed model

Once the details of the satellite subsystems got more specific, it was possible to create a more detailed assembly of the spacecraft. For the subsystems from GOM Space it was possible to obtain CAD files directly from the manufacturer. This made the detailed assembly a lot easier since GOM Space would provide large components such as the frame and solar arrays for the PANTSat mission. The detailed model also includes the in-house developed deployable mechanism for the X-ray optics. A detailed illustration of the satellite is seen in Figure 3.77

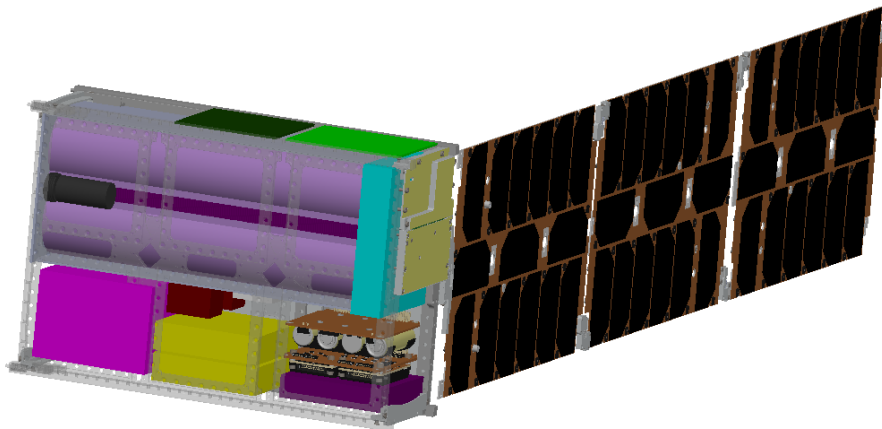


Figure 3.77: The detailed assembly of the spacecraft

3.7.4.3 Future actions and considerations

A big issue with the current iteration is that the off-the-shelf attitude control system is too large to fit within the spacecraft. In fact, all the subsystems are a little crammed inside the satellite which is quite simply due to the size of the payload which is very wide. This is also the reason why the stacks are oriented along the X-axis. In Figure 3.78 the attitude control system has been fitted in two different orientations within the spacecraft. The mechanical team have been discussing the possibilities for making the attitude control system fit within the satellite in any of these two configurations:

- Option 1: The manufacturer of the chosen attitude control system are flexible in the configuration of their subsystem. This indicates the possibility of having a custom made subsystem built for this specific mission. The downside of this option is that it would likely be a lot more expensive. Discussions should also be held with the attitude control group to ensure the changes are not made at the detriment of performance.
- Option 2: Talking with the manufacturer of the frame about the possibility of making the attitude control system a part of the frame in any of the two configurations. This could either prove to be an easy fix or it might break structural integrity of the satellite which in turn could lead to a mechanical failure.
- Option 3: In Figure 3.78b it is seen that the system is awfully close to being able to fit through the rails of the frame (approx. 2 mm). In this option, the physical size of the attitude control system and its sub-components (see Section 3.2.3) will be analysed to evaluate whether it is possible to file down the box by a few millimeters. This could be done in cooperation with the manufacturer.

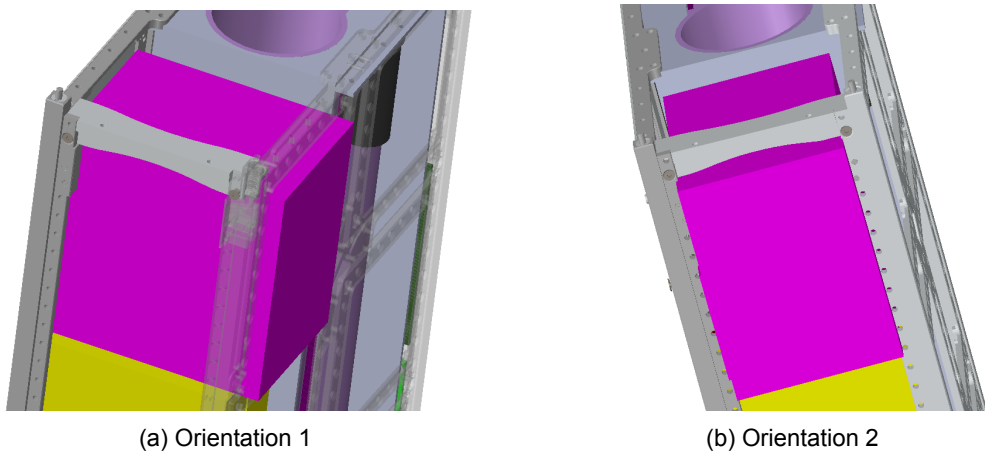


Figure 3.78: Illustration of the attitude control system being too large to fit within the satellite in two different orientations.

3.8 Thermal Control

3.8.1 Introduction

The thermal control system is responsible for maintaining operational thermal conditions for each subsystem in the satellite. The challenge is to design a system that is able to maintain these thermal conditions for each system, which each require a specific temperature range, throughout the many cycles of solar exposure and solar eclipse over the entire mission duration in a way that is cost efficient, power efficient, and minimizes weight.

3.8.1.1 Work-flow

The thermal control design process conducted here begins with identifying thermal requirements for each subsystem. Following this, first estimates of the cold-side (eclipse) minimum and hot-side (in the view of the sun) maximum temperatures are made using both steady state and transient analyses. With this information, trade studies into passive and active thermal control methods are conducted in order to select the optimal thermal method for the PANTSat mission. The steady state and transient calculations are conducted once again, with the new passive and active systems considered, in order to verify the design. Lastly, technical challenges are addressed and suggestions for the next design iteration are discussed.

3.8.2 Thermal Requirements

The thermal budget (Table 2.6) listed in Section 2 defines the primary thermal requirements of the system with margins included.

Overall, the requirements for the thermal system are as follows:

1. Maintain internal satellite temperatures between (+10,+30)°C.
2. Integrate redundancy into the thermal control design.
3. External insulation should not interfere with other subsystems or the NanoRacks launch system.

The thermal range requirement was addressed by incorporating this range in the design goal of the thermal control system. With MLI and active thermal control, the thermal control system is designed to operate between 11 and 16°C. For redundancy, there are two separate thermal control boxes and 14 thermal sensors, each connected to a patch heater. This allows the systems to run separately, and continue operations if one fails. Consideration was taken for the placement of the external multi-layer insulation (MLI) with respect to the solar panel stowage and fitting PANTSat into the NanoRacks deployment case.

3.8.3 Thermal Environment

At an orbital altitude between 413 and 420 km, atmospheric pressure for moderate solar activity is near $1.5e^{-8}$ mb. At this pressure, atmospheric drag is minimal, and any aerodynamic heating is small and can be neglected [41]. Additionally, low atmospheric pressure prevents any convective heating to effect the spacecraft. For PANTSat, the primary heating agent will be due to radiation. The radiation sources that are included in the thermal balance of the spacecraft are as follows:

- Direct solar radiation
- Solar radiation reflected off of Earth (albedo)
- Thermal radiation from Earth (planetary)
- Spacecraft radiation into space

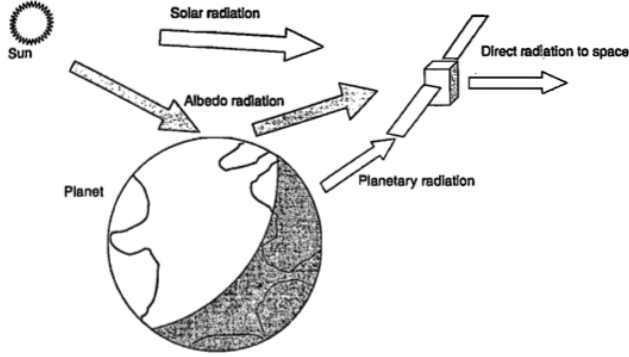


Figure 3.79: Schematic of the thermal environment for a satellite in LEO [41].

Thermal radiation from other planetary bodies are not included in the analysis as their effects are small in comparison. The thermal balance involves the combination of each of these heating terms.

Solar radiation intensity J_s at a distance d from the Sun, where the total power output from the sun is $P = 3.856 \times 10^{26} \text{ W}$, is calculated as:

$$J_s = \frac{P}{4\pi d^2} \quad (3.31)$$

At 1 AU, the Earth's average distance from the sun, this is $1371 \pm 5 \text{ W/m}^2$. At Earth's periapsis and apoapsis, these values are $J_{s,max} = 1414 \text{ W/m}^2$ and $J_{s,min} = 1322 \text{ W/m}^2$ [3]. For this mission, with an average altitude of 416.5 km, we will assume that the solar radiation intensity is the same on the satellite as it is on Earth. In actuality, the intensity of incoming solar radiation will vary throughout the year because the Earth's orbit is elliptical about the Sun. The intensity of radiation for a given day of the year (n) is calculated as in equation 3.31, where $J_{s,c} = 1376 \text{ W/m}^2$ is the current accepted solar constant.

$$J_s = J_{s,c} \left(1 + 0.033 \cdot \cos \left(360^\circ \cdot \frac{n}{365} \right) \right) \quad (3.32)$$

The planetary albedo radiation is the fraction of the solar radiation that is reflected off of the Earth.

$$J_a = J_s a F \quad (3.33)$$

For Earth, planetary albedo (a), is a function of surface type, weather, and ice/snow cover extent. Earth's albedo generally ranges from 0.31 to 0.39 [41]. For these calculations, we will take the average, 0.35. The visibility factor F is a function of altitude and beta angle. For this relationship, Earth is assumed to be a diffuse reflecting sphere. Maximum and minimum beta angles over a year's time are calculated as $\pm(i+23.45)$ degrees, where i is inclination [88]. This will be the limiting case for our beta angle. So, over the course of a year, the beta angle for the CubeSat orbit will vary from -75 to +75 degrees.

$$\beta_{uplim} = (51.6 + 23.45) = 75.05^\circ \quad (3.34)$$

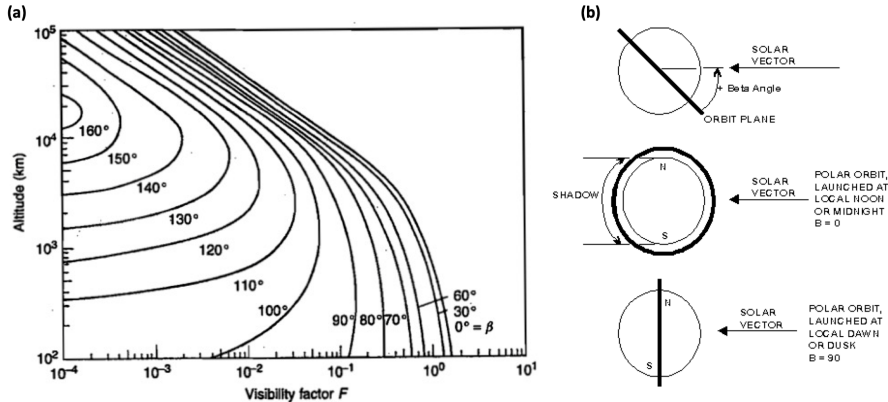


Figure 3.80: (a) Visibility factor F as a function of altitude and β angle. (b) Beta angle, β is defined as the angle between local vertical and the Sun's rays [41].

This maximum beta angle will be utilized in the steady state calculations for a 'worst-case' estimate. Then from Figure 3.80, This corresponds to a visibility factor of 0.4 for $\beta = 75$ deg at $h \sim 416.5$ km. Plugging this into equation 3.33, we get an estimate for the albedo radiation from Earth.

We assume the Earth radiates thermal heat at an intensity of 237 W/m^2 and that the dissipation is uniform across the entire Earth sphere [41]. The planetary radiation at a given altitude is calculated by:

$$J_p = 237 \frac{R_E}{r} \quad (3.35)$$

For the radius of the Earth $R_E = 6371.1$ km and orbit radius $R_E + 416.5$ km. The planetary radiation intensity then becomes $J_p = 222.425 \text{ W/m}^2$. This value will in reality fluctuate throughout the day, typically between values of 160 to 320 W/m^2 [89]. The calculated radiation intensity values are shown in Table 3.17.

	J_s	J_a	J_p
$[\text{W/m}^2]$	1371	191.9	222.5

Table 3.17: Calculated radiation intensity values from equations 3.31 - 3.35.

3.8.4 First Estimate

In order to construct the thermal design, a first analysis of the heating the satellite will encounter throughout the orbit must be done. This generally depends on the orbit of the satellite, its orientation throughout the orbit, its surface finish or external material, and time of year. Now that the primary sources of heating for a satellite in LEO have been introduced, a first estimate of the steady state thermal analysis for various surfaces and finishes is conducted. This provides the thermal design with a starting point to go off of in choosing thermal solutions. In addition, a first estimate of the transient thermal analysis is conducted to further guide the thermal design.

3.8.4.1 Steady State Analysis

For the thermal balance, the focus will be on a hot-case and a cold-case. The hot-case considers the thermal equilibrium of the satellite in full view of the sun, while the cold-case will consider the thermal equilibrium of the satellite in the Earth's eclipse. The thermal balance that we wish to solve assumes steady state heat transfer (the amount of heat

absorbed must equal the amount of heat radiated). The basic energy balance is shown by equation 3.36.

$$\frac{dE_{int}}{dt} = mc_w \frac{dT}{dt} = \dot{Q}_{in} - \dot{Q}_{out} \quad (3.36)$$

In steady state, $\frac{dE_{int}}{dt} = 0$ and $\dot{Q}_{in} = \dot{Q}_{out}$. For our spacecraft, this thermal balance reduces to:

$$\dot{Q}_{sun} + \dot{Q}_{albedo} + \dot{Q}_{planetary} + \dot{Q}_{int} = \dot{Q}_{sat2earth} + \dot{Q}_{sat2space} \quad (3.37)$$

Spacecraft are not black bodies, they emit and absorb radiation as grey bodies. As a result, they will absorb only a fraction α of the incident energy and emit a fraction ϵ of the radiation that a black body at the same temperature would. α and ϵ are known as the absorptance and the emittance, and they are dependent on the materials choice of surface and finish for the satellite.

The relation of incident, absorbed, and radiated intensity is as follows:

$$J_{absorbed} = \alpha J_{incident} \quad (3.38)$$

$$J_{radiated} = \epsilon \sigma T^4 \quad (3.39)$$

Where σ is the Stefan-Boltzmann constant $= 5.67 \times 10^{-8} W/m^2 K^4$ and T is the equilibrium temperature. For the thermal balance, we must define some projected areas.

A_{solar} = projected area facing the Sun

A_ϵ = emitting area

A_{albedo} = projected area receiving albedo radiation

$A_{planetary}$ = projected area receiving planetary radiation

$A_{surface}$ = total surface area of the spacecraft

Here, we will assume $A_{planetary} = A_{albedo}$ and $A_{surface} = A_\epsilon$, for simplicity. The projected areas are not yet defined throughout the mission. The satellite will point in many directions over the course of the mission depending on which pulsars are currently visible. For this reason, the solar and earth facing projected areas are taken as the maximum they could possibly be for the steady state calculations. This is calculated as three sides of the satellite facing the respective planetary body. It is then assumed that the spacecraft is iso-thermal, and we take the following relationships into consideration:

$$\dot{Q}_{sun} = J_s \alpha_s A_{solar}$$

$$\dot{Q}_{albedo} = J_a \alpha_s A_{albedo}$$

$$\dot{Q}_{planetary} = J_p \epsilon_s A_{planetary}$$

$$\dot{Q}_{sat} = \sigma T^4 \epsilon A_{surface}$$

\dot{Q}_{int} = internal heat dissipation from electronics

\dot{Q} = Heat dissipation or addition from active thermal control

Where \dot{Q}_{sun} is the heat received from solar radiation, \dot{Q}_{albedo} is the heat received from planetary albedo, $\dot{Q}_{planetary}$ is the planetary infrared contribution, \dot{Q}_{sat} is the heat the

satellite radiates to space and earth, and Q_{int} is internally dissipated power [41]. Based on an average efficiency of 70% [89], it is assumed that the internal dissipated heat from electronics within the spacecraft is 30% of the average power consumption, which comes out to about $Q_{int} = 2.94W$. Then, assuming all radiation intensities are constant, the thermal balance equation can be written as:

$$A_{surface}\sigma T^4\epsilon = (A_{solar}J_s A_{albedo}J_a)\alpha + A_{planetary}J_p\epsilon + Q_{int} + Q$$

$$T^4 = \frac{A_{planetary}J_p}{A_{surface}\sigma} + \frac{Q + Q_{int}}{A_{surface}\sigma\epsilon} + \frac{(A_{solar}J_s + A_{albedo}J_a)}{A_{surface}\sigma} \left(\frac{\alpha}{\epsilon}\right) \quad (3.40)$$

The steady state temperature T can then be estimated for a chosen ratio of absorptivity and emissivity - α/ϵ . This value is adjusted based on the desired temperature, and can be changed by optimally selecting the outer coating. For chosen projection areas, the equilibrium temperature can be calculated for the hot-case and cold-case for a range of different surfaces. Note that in the cold-case calculations, the only heat sources are from planetary radiation and internal heat dissipation. Table 3.18 shows the results of the steady state calculations for various surfaces. A list of surfaces and finishes can be found in Figure 3.79 [41].

α/ϵ	Material	$T_{min}[^{\circ}C]$	$T_{max}[^{\circ}C]$
3.00	Polished Aluminum	-14.17	192.81
1.12	Black paint (epoxy)	-56.06	93.69
0.84	Silver paint	-50.82	73.24
0.63	Aluminized Kapton	-54.03	53.11
0.34	Aluminized FEP	-51.49	18.68

Table 3.18: Steady State analysis applied to various surfaces and finishes.

3.8.4.2 Transient Analysis

In reality, the satellite will maintain some latent heat from the hot-side of the orbit as it enters the eclipse side. For this reason, transient calculations are needed to find the actual temperature the satellite will reach at the end of both the hot-side and the cold-side. The energy balance shown by equation 3.36, where $dT/dt \neq 0$, can be solved using the minimum and maximum temperatures from the steady state solution as a nonlinear differential equation [90].

$$\frac{mc_w}{\epsilon A\sigma} \int_{T=T_0}^T \frac{dT}{T_s^4} = \int_{t=0}^t dt \quad (3.41)$$

In which the background temperature of space is assumed to be near zero degrees K. This can then be integrating for the sun-side phase and the eclipse phase.

$$\Delta t_{heat} = c_h \left[\left(artanh \left(\frac{T_a}{T_s} \right) + arctan \left(\frac{T_a}{T_s} \right) \right) - \left(artanh \left(\frac{T_0}{T_s} \right) + arctan \left(\frac{T_0}{T_s} \right) \right) \right] \quad (3.42)$$

$$\Delta t_{cool} = c_c \left[\left(artanh \left(\frac{T_a}{T_E} \right) + arctan \left(\frac{T_a}{T_E} \right) \right) - \left(artanh \left(\frac{T_0}{T_E} \right) + arctan \left(\frac{T_0}{T_E} \right) \right) \right] \quad (3.43)$$

Where T_s is the equilibrium sun-side temperature, T_E is the equilibrium eclipse side temperature (T_{min}), T_0 is the starting temperature of the calculation, T_a is the actual temperature, and the constants c_c and c_h are calculated by:

$$c_h = \frac{\sum m_i c_{w_i}}{\epsilon A \sigma} \quad (3.44)$$

$$c_c = \frac{\sum m_i c_{w_i}}{2T_E^3} \quad (3.45)$$

Where A is the total surface area of the satellite. For these calculations, the specific heats (c_w) and masses (m) of the satellite are simplified to that of the external structure and an internal total. The overall specific heat of the internal spacecraft components $c_{w,SC}$ was taken as a similar value as used in a study of the thermal design of Compass-1 [90].

	Al	SC
m [kg]	0.73	8.90
c_w [Nm/kg - K]	980	800

Table 3.19: Mass and specific heat for the aluminum structure (Al) and the internal spacecraft components (SC).

From the orbital calculations, we have the average time of eclipse and time on the solar side for each orbit, $\Delta t_{cool} = 2083.44[s]$ and $\Delta t_{heat} = 3490.56[s]$. Plugging these values in to equations 3.42 and 3.43, the actual temperatures at the end of each phase, T_a , can be numerically solved for.

The results of the initial transient analysis over one orbit for various surfaces and finishes is shown in Table 3.20. In these calculations, the calculations begin by setting $T_0 = T_{min}$ such that the satellite has is at the end of its eclipse and entering into the sun-side, and solving equation 3.42. The solution, the actual temperature at the end of the sun-phase T_a , then becomes the starting temperature T_0 for equation 3.43.

α/ϵ	Material	$T_{a,E}$ [$^{\circ}$ C]	$T_{a,S}$ [$^{\circ}$ C]
3.00	Polished Aluminum	10.75	11.49
1.12	Black paint (epoxy)	9.63	29.43
0.84	Silver paint	-17.64	-13.69
0.63	Aluminized Kapton	-20.78	-15.20
0.34	Aluminized FEP	-36.98	-35.38

Table 3.20: Transient analysis applied to various surfaces and finishes with $c_{w,sc} = 800$ Nm/kgK.

At first glance, it would seem that the polished aluminum performs quite well at keeping the satellite within the desired temperature range. However, with the uncertainty in the specific heat of the internal components, these ranges could vary substantially. For $c_{w,sc} = 200$ Nm/KgK, the transient temperature range for polished aluminum becomes (+35.85, +39.72). For this reason, we have chosen to implement additional passive control in order to assure better assure that the most extreme temperatures from the transient analysis fall within the desired range for many different specific heats.

In order to minimize complexity, we have chosen to operate cold and implement active heating. This means that instead of choosing a thermal system that could get slightly too hot on the sun-side and slightly too cold on the cool side, we have chosen to develop a system that runs cold and requires active heating. In doing this, we simplify the system by not also requiring an active cooling system. Choosing to implement active heating rather than active cooling was also to minimize complexity, as active cooling systems often require pipes and coolant, while active heating can be as simple as a patch heater. The following section explores the components of passive thermal control and active heating that were considered and explains the process leading to the chosen thermal design.

3.8.4.3 Discretization and Time Marching Scheme

The finite element method (FEM) is a numerical method used to solve partial differential equations that arise in various engineering and scientific fields. In ANSYS, the FEM is used to solve thermal problems involving conduction, convection, and radiation heat transfer. The FEM discretizes the computational domain into small elements, and the governing equations are then solved using a set of algebraic equations derived from the elemental equations.

Discretization Scheme:

The discretization scheme used in ANSYS is the Galerkin method, which is a weighted residual method. In the Galerkin method, the residual equation is weighted by a set of test functions and integrated over the entire domain. The resulting system of equations is then solved numerically to obtain the temperature distribution. The thermal energy equation describes the transfer of thermal energy in a solid or fluid medium. In ANSYS, the thermal energy equation is discretized using the Galerkin method, which involves approximating the temperature distribution within each element using a set of nodal values and assumes the test functions are piecewise linear or quadratic over each element. The elemental equations are then derived using the principle of virtual work and integrated over the entire domain.

The discretized thermal energy equation can be written as:

$$\rho c_p \frac{\partial T}{\partial t} + \nabla \cdot \mathbf{q} = \dot{Q} \quad (3.46)$$

where ρ is the density, c_p is the specific heat, T is the temperature, \mathbf{q} is the heat flux vector, and \dot{Q} is the internal heat generation rate.

Using the Galerkin method, the temperature distribution within each element can be approximated using a set of nodal values, T_i , as:

$$T(\mathbf{x}, t) = \sum_{i=1}^N N_i(\mathbf{x}) T_i(t) \quad (3.47)$$

where $N_i(\mathbf{x})$ is the shape function for node i , and $N_i(\mathbf{x}) = 0$ for all nodes except node i .

Substituting the above equation into the thermal energy equation and integrating over each element, the elemental equation can be obtained as:

$$\int_V \rho c_p N_i \frac{\partial T}{\partial t} dV + \int_S \mathbf{q} \cdot \mathbf{n} dS = \int_V \dot{Q} N_i dV \quad (3.48)$$

where V is the volume of the element, S is the surface of the element, \mathbf{n} is the outward unit normal vector to the surface, and dS is the surface area element.

The heat flux vector, \mathbf{q} , can be divided into three components: conduction, convection, and radiation. The conduction term can be expressed as:

$$\mathbf{q}_{cond} = -k\nabla T \quad (3.49)$$

where k is the thermal conductivity.

The convection term can be expressed as:

$$\mathbf{q}_{conv} = h(T - T_{\infty}) \quad (3.50)$$

where h is the convective heat transfer coefficient, and T_{∞} is the ambient temperature.

The radiation term can be expressed as:

$$\mathbf{q}_{rad} = \sigma\epsilon(T^4 - T_{\infty}^4) \quad (3.51)$$

where σ is the Stefan-Boltzmann constant, ϵ is the emissivity, and T_{∞} is the ambient temperature.

The resulting system of algebraic equations can then be solved numerically using the backward Euler method for transient problems or a direct solver for steady-state problems.

Time Marching Scheme:

The time marching scheme used in ANSYS depends on the type of problem being solved. For transient heat transfer problems, ANSYS uses the backward Euler method, which is an implicit scheme. In the backward Euler method, the temporal derivative is approximated using a finite difference scheme, and the resulting equation is solved numerically using an iterative scheme. The backward Euler method is unconditionally stable, but it can be computationally expensive for large systems.

For steady-state heat transfer problems, ANSYS uses a direct solver to solve the system of algebraic equations. The direct solver calculates the exact solution of the equations, but it can be computationally expensive for large systems.

In summary, ANSYS uses the Galerkin method for discretization and the backward Euler method for time marching in transient heat transfer problems. For steady-state heat transfer problems, ANSYS uses a direct solver to solve the system of algebraic equations.

3.8.5 Thermal Solutions

The thermal solutions investigated here include passive thermal control such as insulation or louvers and active thermal control in terms of different kinds of heaters. The following sections show the trade-analysis conducted for each.

3.8.5.1 Passive Control

For passive solutions, Multi-Layered Insulation (MLI), Aerogel (AG) and mechanical louvers were considered. The trade analysis compared these options based on a range of comparison factors, each with a significant weight (Wt.) indicating the importance for our design. The utility value (U) is a ranking for the specific system and comparison factor ranging from 1-10, with 10 being the best. The weighted value (W) is then the utility value multiplied by the significant weight. The weighted total for each passive solution is computed as a way to compare solutions and select the most optimal.

The relative utility values (higher or lower than one another) for each solution were chosen based on comparable metrics between options such as thermal conductivity, number of

moving parts, average weight, and potential points of failure. The absolute values take this relative comparison into account, but also contain the biases of the thermal engineer, so this analysis must not be taken as absolute truth.

All three of the systems considered are TRL-9 and have history in spaceflight. MLI blankets are generally composed of layers highly reflective radiation shields made of polyimide or polyester and low thermal conductivity spaces. The reflective shields are generally coated with some metal, such as aluminum. MLI operates by reducing incident energy (radiation) with every layer [91]. Aerogel is an extremely light substance with impressive thermal insulation power. It is typically made from a silica gel that is put under supercritical fluid extraction, and the resulting material is a light, porous, and strong structure [92]. Louvers are shutters that effectively change the surface properties of the satellite at different phases of its spaceflight. While louvers have proved efficient for large spacecraft, they bring issues with integration, mass and required power input for smaller spacecraft [93].

Passive Cooling Systems	Thermal Performance		Simplicity		Monetary Cost		Mass		Risk (Heat Leak)		Weighted Total	
	Wt. = 2.5		Wt. = 2.0		Wt. = 2.0		Wt. = 1.5		Wt. = 2.0			
	U	W	U	W	U	W	U	W	U	W		
MLI	6	15	10	20	8	16	6	9	4	8	68	
AG	8	20	6	12	2	4	9	13.5	4	8	57.5	
Louvers	6	15	3	6	6	6	2	3	3	6	36	

Figure 3.81: Trade analysis of passive cooling systems.

From Figure 3.81, it can be seen that MLI outranks aerogel and mechanical louvers. This is due to the advantage of MLI in monetary cost (while expensive, aerogel is much more costly [94]) and simplicity of implementation. While aerogel beats out MLI in mass and thermal performance, aerogel contains amorphous silica, which causes respiratory issues when breathed in [95]. For this reason, the use of aerogel complicates the handling of aerogel during the construction phase. MLI on the other hand, can be ordered easily from manufacturers such as DUNMORE in the form of a small satellite kit, allowing the insulating material to easily be cut into the desired shape and applied. Mechanical louvers scored relatively low in all comparison categories. This is primarily because they do not provide insulation (they only change surface properties), meaning temperature gradients are not well controlled. Secondarily, louvers require mechanical structures for opening and closing at different periods during the mission. This increases the complexity of the design and the addition of moving parts increases the risk of failure. The use of 10 layers of MLI here alters the effective emittance and absorptance to be $\epsilon = 0.3$ and $\alpha = 0.15$, respectively.

3.8.5.2 Active Control

The active control solutions considered are all different types of electrical heaters, as these can be flexible, small, and provide a high heat output density. Two of the heaters listed here, the kapton heater by Minco and the All Flex Polyimide heater are both forms of patch heaters. These generally operate as two layers of polyimide film (kapton) with a layer of foil (usually nickel-based alloy) etching in between them. The foil etching acts as a resistance element, and when a current is applied, heating is supplied. Patch heaters are extremely flexible, lightweight and are the most common type of heater used for small spacecraft [93]. The Mica insulated heaters by Minco operate in the same way, but instead of polyimide layers, the etching is held between layers of mica.

Heater	\dot{Q} [W/cm ²]	Density [g/cm ²]	Thickness [cm]	Mounting Method	Complexity Rating	Operational T-range [C]
Kapton Patch Heater by Minco	7.8	0.04	0.23 (max – with leads)	Stretch Tape or Clamped	1	(-200, +200)
Mica Insulated Heater by Minco	17.05	> 0.04	0.62	Clamp - unaffected by cold conditions	3	(-150, +600)
All Flex Polymide	~6-9	~0.04	0.025	Adhesive	1	(+150, +200)

Figure 3.82: Trade analysis of active heating systems.

Based on Figure 3.82, we have selected the kapton patch heater by Minco for our design. The primary reason for this choice is the flexibility that comes with utilizing kapton, the lightness of the material, and the compatibility with other Minco products. In choosing the Minco patch heater rather than the All Flex option, which are similar in all categories, the Minco thermal sensors and thermal control box are directly compatible. While the mica heater provides a greater heat density (\dot{Q}), the flexibility of the heater is lost with the use of mica.

3.8.5.3 Components

The specific components for the active and passive thermal systems are outlined in Table 3.21.

Component	Product	Dimensions [cm]	Elements	Manufacturer
Heater	Kapton Thermofoil	thickness = 0.23	14	Minco
Sensors	S651PDY24A	0.76 x 0.76 x 0.2	14	Minco
TCB	CT325	2.77 x 1.54 x 3.81	2	Minco
MLI	Satkit	SA x 0.4±0.1	1	DUNMORE

Table 3.21: Thermal component list for active and passive systems. SA = Surface Area of the satellite. TCB = Thermal Control Box.

The choice of 14 kapton heaters and 14 thermal sensors is to provide redundancy and modularity to the design. This will allow just one of the kapton heaters to turn on in the case that one section of the cubesat drops below the threshold temperature. Additionally, there are two thermal control boxes, so that if one fails the backup is still operational. This amount may be excessive,

3.8.6 Final Design

The final design features a layer of patch heaters underneath 10 layers of MLI. Initially, the design featured MLI covering the entirety of the spacecraft, aside from the solar panels. The following section describes the changes in the design after receiving feedback from the PDR and the current operations of the thermal control system.

3.8.6.1 Action Items from the PDR

The primary action item from the PDR was whether the 0.5 cm of MLI would create an issue when fitting the spacecraft into the Nanoracks frame for launching.

Upon further investigation of the Nanoracks tolerances, we found that the MLI will fit along the main faces of the cubesat without issue. The structure (outlined in 3.15) fits within the NanoRacks NRDD specifications with at least 5 mm of margin on all sides [96]. However, we then came to realize that the railings of the structure need to be exposed in order to integrate with the NanoRacks deployer, as specified in the interface documentation. This

poses a new issue, as any area not covered by the MLI will be points of major heat sink for the satellite. To combat this, we considered a new configuration of the thermal control system consisting of MLI, patch heaters, tailorabile emittance coatings (TEC), and thermal breaks.

An expanded view of the updated design is shown in Figure 3.83. What this schematic shows is a layer of kapton patch heaters underneath 10 layers of MLI. The MLI however doesn't connect at the edges, as this is where the NanoRacks require a connection, and is instead painted with a TEC with surface properties similar to that obtained with MLI ($\alpha = 0.1$, $\epsilon = 0.25$) [93]. While these properties are desirable, the flow of heat from the aluminum plates underneath the MLI to these edges will be a significant heat loss. To combat this, we are suggesting the use of thermal breakers to connect the aluminum plate to the structure edges. One option for the material for these thermal breakers could be metals coated in the previously mentioned aerogel. Aerogel is an extremely efficient insulator, which is a desirable property of structural connectors in order to mitigate heat transfer from the MLI insulated aluminum panel to the edges, where heat would radiate to space much easier. While aerogel is TRL-9, this specific application of aerogel requires lab testing before implementation to develop the optimal thickness of the coating and ensure performance.

A secondary issue considered is the side of the satellite from which the solar panels are deployed. MLI cannot be placed on the outside of the satellite here, because the panels need a clear connection to the side of the satellite for when they are in their stowed position. For this reason, the MLI will be placed on the inside of the aluminum plate on this back side of the satellite, and the outside of the aluminum will be painted with TEC. We did not decide to utilize MLI totally on the inside for this mission due to the desirable emittance and absorptivity that are attained when it is used on the outside of the structure. Additionally, internal MLI would subject the aluminum structure to large heat fluxes. These heat fluxes would induce thermal expansion to the spacecraft bus, which is not ideal for the precision needed by the polycapillary x-ray optics. Taking the effective areas of each surface, the updated absorptivity and emissivity of the satellite becomes $\alpha_{\text{eff}} = 0.1314$ and $\epsilon_{\text{eff}} = 0.2814$.

3.8.6.2 Thermal Control System operations

The satellite will operate in two different modes: the warm-up mode and the standard mode. The following section will go into detail on the reasoning for these modes, when they will occur, and how much power they will require.

The updated transient calculations with the implemented MLI and TEC edging for various spacecraft specific heats is shown in Table 3.22. The calculations show that the passive system is able to maintain desired internal temperatures throughout the orbit for a wide range of spacecraft average specific heats. These results are nice, as the true specific heat of the spacecraft is uncertain. However, these values have one important requirement - they assume that the satellite temperature is initialized at 20°C. Once the satellite has been launched from the NanoRacks and has powered on, an initial warm-up period is required. During this period, the kapton heaters will require a greater amount of power to heat the satellite to the optimal 20°C.

An analysis of the transient heat loss over 10 orbits was then conducted, and is shown in Table 3.23. Based on these estimates, we found that the satellite will loose roughly 6 degrees of heat in ten orbits and that temperatures decrease at a slower rate for lower temperatures. In order to maintain a 'steady' temperature on the eclipse side and prevent temperatures from dropping below the ideal operational range, we have chosen to im-

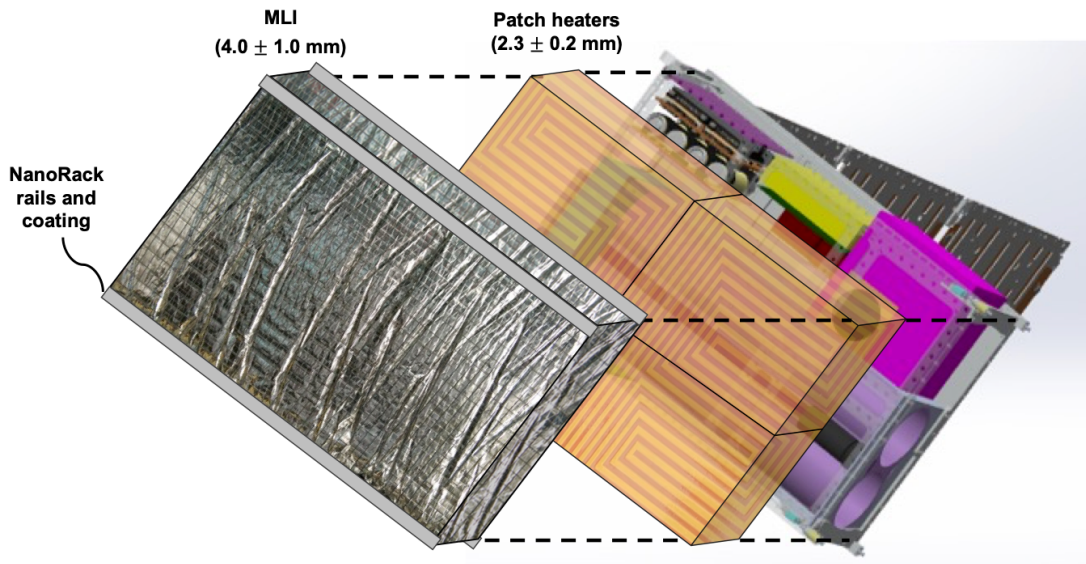


Figure 3.83: Schematic of the thermal design consisting of MLI (the outer silver layer) the kapton patch heaters (the inner orange layer) and the TEC. Images of MLI and kapton heaters from [97] and [98].

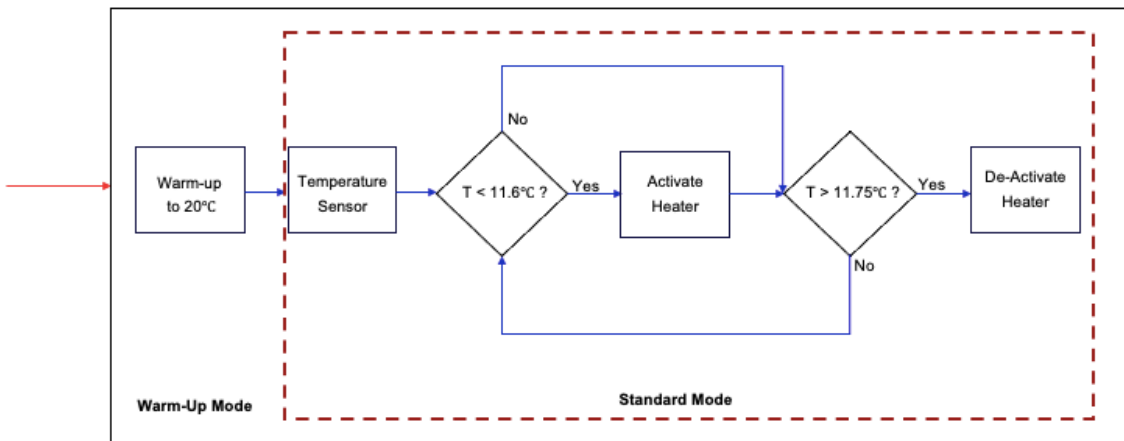


Figure 3.84: Diagram of thermal operations.

plement a temperature threshold at 11.60°C , at which the active heating will be activated until the satellite temperature reaches 11.75°C . This heating phase will happen during the standard mode, which continues for the entire mission after the warm-up period. In standard mode, the patch heaters will activate each orbit when the eclipse side temperatures reach the threshold temperature. Effectively, this should maintain a temperature range of $(+11, +17.5)^{\circ}\text{C}$. This threshold temperature was chosen due to the slower rate of temperature change between orbits for colder temperatures. Additionally, a 1.5 degree margin is left between the satellite temperature and the edge of the ideal operational temperature range.

To asses the power draw of the warm up period and the heating mode each orbit, the following equations were utilized.

$$Q = mc(T_f - T_i) \quad (3.52)$$

$$t_H = Q/P_{eff} \quad (3.53)$$

Where Q is the required heating to heat the satellite from the initial temperature T_i to the final temperature T_f , m is the mass of the satellite, and c is the effective specific heat (calculated from $c_{w,al}$ and $c_{w,sc}$). For the warm up mode, the minimum steady state temperature in the eclipse was taken as the initial temperature. The value P_{eff} is the effective power, where we have assumed a power efficiency of 70%. The power provided from the EPS system is 10W for the warm-up period and 3W for normal operations. From this, along with the heating required for both the warm-up mode and the standard mode, the amount of time that the heaters need to be activated is calculated. These results are shown in Table 3.24. Based on the voltage ratings of the thermal control box the current availability, the standard mode will operate with 3.3V and 1 A, and the warm-up mode will operate with 3.3 V and 3A.

Figure 3.85 depicts what percentage of the orbit the heaters will be activated as a percentage of the orbit for the standard mode. The numerical model developed in MATLAB, considering a simplified model of the CubeSat, has provided a good first estimate for the thermal behavior of the spacecraft. This design for the thermal system is limited and much simplified. However, to validate the design and optimize the thermal control system, a more detailed analysis is necessary. A detailed thermal model, including some material properties, can provide more accurate results for the thermal performance of the CubeSat. The ANSYS software is a powerful tool that can simulate the thermal behavior of the spacecraft with high precision, taking into account all the complex interactions between the different components and subsystems.

$c_{w,sc} [Nm/kgK]$	$T_{a,E} [^{\circ}C]$	$T_{a,S} [^{\circ}C]$
200	13.67	26.83
400	15.71	25.24
600	16.79	24.25
800	17.45	23.57
1000	17.87	23.07

Table 3.22: Transient analysis for various average spacecraft internal specific heats for one full orbit after the warm up period.

Orbit No.	$T_{a,E} [^{\circ}\text{C}]$	$T_{a,S} [^{\circ}\text{C}]$
1	17.45	23.57
2	15.65	21.52
3	14.37	20.07
4	13.46	19.03
5	12.81	18.30
6	12.34	17.77
7	12.01	17.39
8	11.76	17.12
9	11.60	16.92
10	11.47	16.78

Table 3.23: Transient analysis for $c_{w,sc} = 800 \text{ Nm/kgK}$ over 10 orbits periods after warm up.

Mode	$P_{eff} [\text{W}]$	$Q_{req} [\text{kW}]$	$t_H [\text{hr}]$
Warm-up	7	432.15	17.15
Standard	2.1	1.06	0.14

Table 3.24: Power demands of the active thermal system for the warm-up and standard modes. Power efficiency is assumed to be 70%.

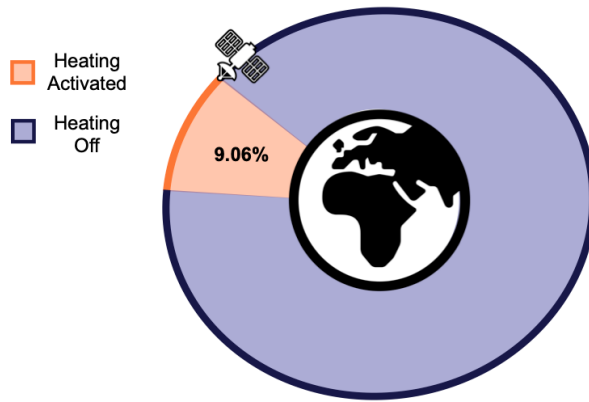


Figure 3.85: The standard heating mode as a percentage of orbit.

3.8.7 Thermal Analysis Workflow in ANSYS for CubeSat Design

The steps taken to achieve a thermal model for the CubeSat is as follows:

3.8.7.1 Loading Geometry and assigning Material Parameters

The model include all relevant components, such as solar panels, batteries, electronic components, Multi-Layer Insulation, etc. To Thermal Model for the given Mechanical Model, ANSYS Mechanical software [21] was used. The material properties were assigned to each component in the CAD model. The material properties include thermal conductivity, heat capacity, and emissivity.

This is a version # 1 model with simplified physics, thus all the inner components which alter thermal conditions (that is do not generate or absorb significant heat) are lumped together to form inner body of CubeSat, while major components like solar panels, Insulation layer, Battery, extruding optics and frame of CubeSat were assigned thermal properties of their corresponding materials which are given in the following table:

Material	Heat Capacity at Constant Pressure C_p (J/Kg K)	Thermal Conductivity κ (W/m K)	Surface Emissivity ϵ	Density ρ Kg/m ³	Surface Absorbtivity α
Silicon	678	148	0.83	2320	0.95
Aluminised Kapton (MLI)	1200	0.25	0.85	1400	0.1
Aluminum 7075-T6	960	130	0.22	2810	0.3
Carbon fiber / epoxy	1130	162.5	0.9	1700	0.7
Inner body (Complex)	800	20	0.8	2000	0.3

Table 3.25: Thermal properties of materials used

3.8.7.2 Meshing

In numerical simulations, meshing is the process of dividing a geometric domain into smaller subregions called elements or cells. These elements are used to represent the physical domain, and the solution to the governing equations is obtained at discrete points within each element. The accuracy and computational efficiency of a numerical simulation depend heavily on the quality of the mesh used. ANSYS provided automated meshing tool which creates mesh for the given geometry with some minor inputs like mesh density. In this model Coarse mesh is utilised to keep things simplified. Details of Mesh quality and Mesh rendered over geometry is shown in the figures 3.86 and 3.87 respectively.

Initial Size Seed	Assembly
Bounding Box Diagonal	1.5392 m
Average Surface Area	8.5795e-003 m ²
Minimum Edge Length	1.9e-003 m

Figure 3.86: Details of Mesh

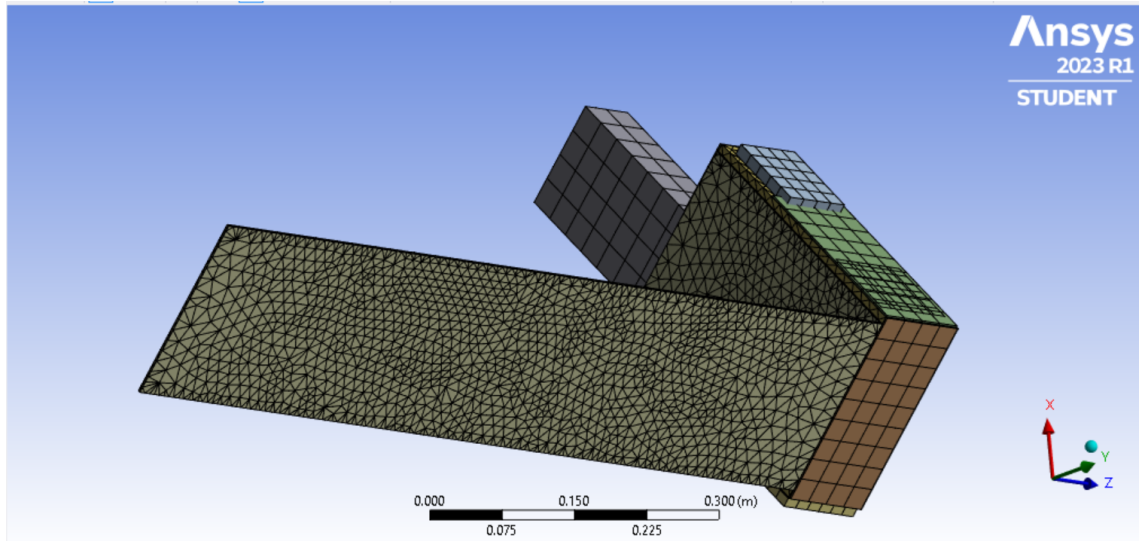


Figure 3.87: Meshed Geometry of PANTSat

3.8.7.3 Initial and Boundary Conditions

In thermal simulation, boundary and initial conditions are essential to determine the temperature distribution inside a system.

Boundary conditions specify the temperature at the boundaries of the system. In the

model, we have used one of the most common boundary conditions in thermal analysis is the Dirichlet boundary condition, which specifies the temperature directly at the boundary. Mathematically, it can be represented as follows:

$$T(x, y, z, t) = T_b(x, y, z, t) \quad (3.54)$$

where $T(x, y, z, t)$ is the temperature at a point (x, y, z) and time t , $T_b(x, y, z, t)$ is the prescribed temperature at the boundary.

Initial conditions specify the temperature distribution inside the system at the beginning of the simulation. Mathematically, it can be represented as:

$$T(x, 0) = T_0(x), x \in \Omega \quad (3.55)$$

where $T(\mathbf{x}, 0)$ is the temperature at a point \mathbf{x} inside the system at the initial time $t = 0$, and $T_0(\mathbf{x})$ is the prescribed initial temperature distribution. For Steady-state Analysis, we have kept the initial temperature of the outer surface of the cubeSat to be at $15^\circ C$.

3.8.7.4 Setting up model and Solver Configuration

ANSYS offers various solver configurations for thermal simulations, depending on the complexity of the model and the level of accuracy required. This model is made on Steady-State Thermal Solver. The following settings were chosen for time-marching and solver controls:

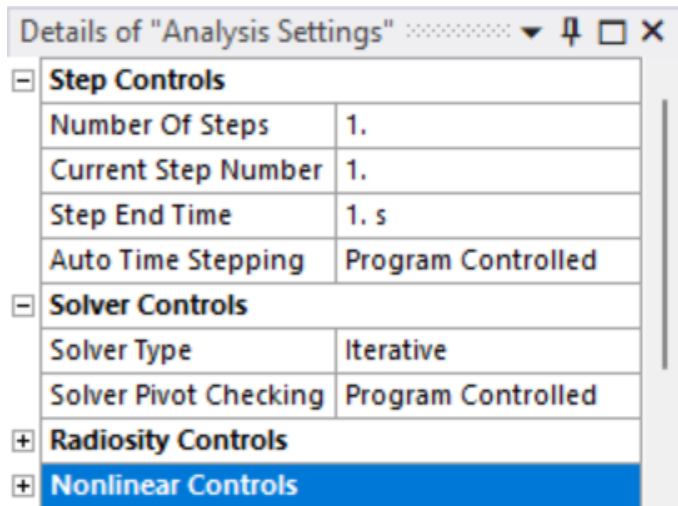


Figure 3.88: Configurations used to setup model

The model contains 3 Heat sources - Sun, Earth and the Battery (Heat liberated due to charging-discharging cycles). The radiation fluxes from Sun and Earth were modelled to be hitting 3 faces each respectively to get the worst-possible estimate of the Directional heat fluxes at the surface and body of CubeSat. The following parameters were used to model the heat sources in the model:

Parameters	Value
Solar radiation	1367 W/m^2
Earth IR flux	193 W/m^2
Internal Heat generation in CubeSat	5 W/m^2
Albedo Constant	0.35

Table 3.26: Constant Parameters used in the Model

3.8.7.5 Steady-State Simulation

Steady-State Simulation was generated for Hot case (when CubeSat is on non-eclipse part of the orbit). The result was rendered in form of Temperature as well as Directional Heat fluxes rather than just temperature because the temperature often depends only on geometry. The heat flux, and the thermal reaction, always depend on the material thermal conductivity. Therefore, it is always necessary to examine both the temperatures and heat flux to assure a correct solution.

The figures 3.89, 3.90, 3.91 and 3.92 show the result of steady-state hot case simulation of cubeSat with worst case scenerio 3-sided sun-earth Radiation.

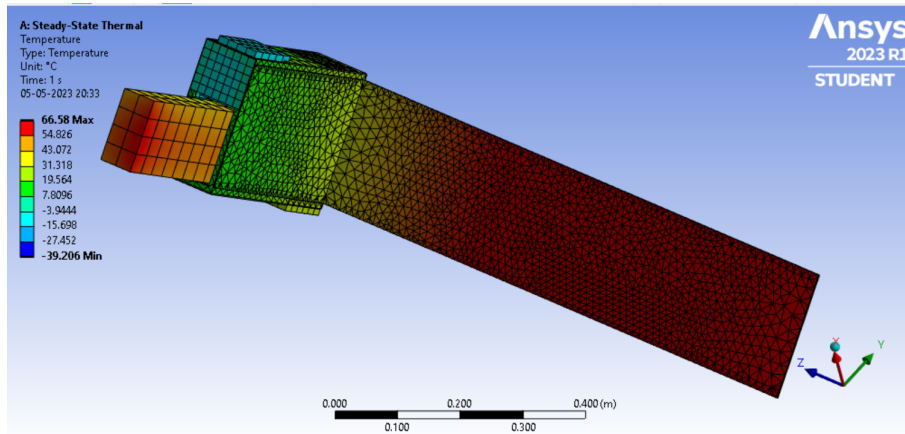


Figure 3.89: Side#1 showing Temperature distribution over the CubeSat

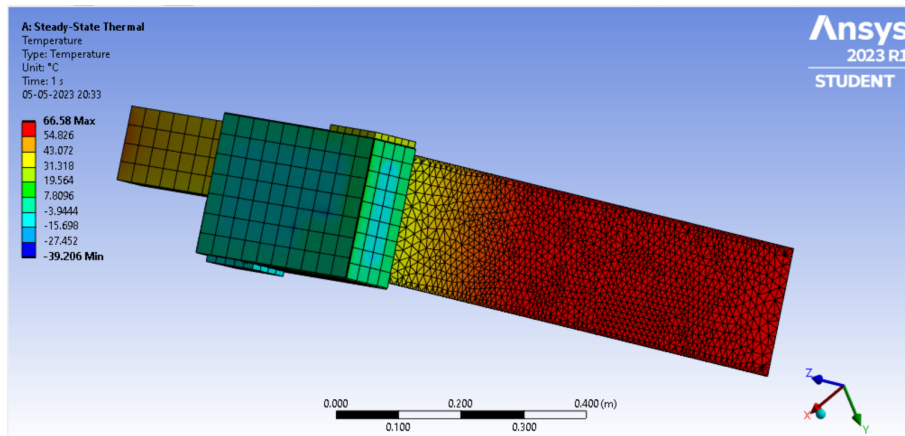


Figure 3.90: Side#2 showing Temperature distribution over the CubeSat

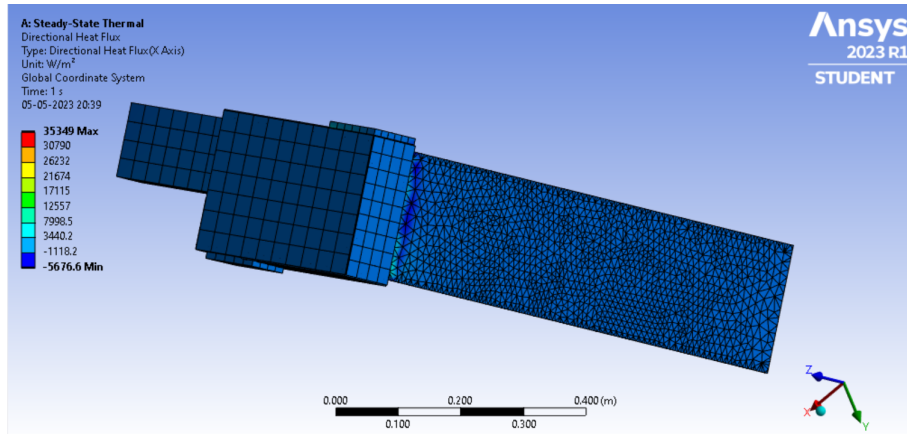


Figure 3.91: Side#1 showing Directional Heat Flux distribution over the CubeSat

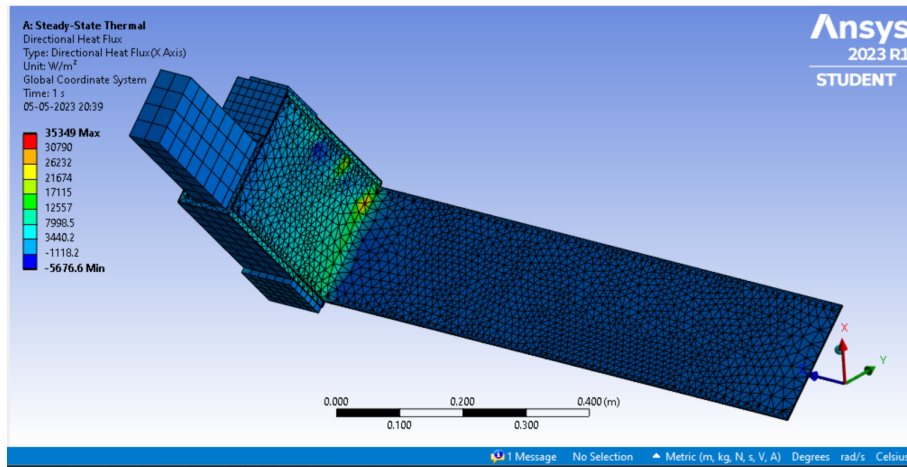


Figure 3.92: Side#2 showing Directional Heat Flux distribution over the CubeSat

Based on the results of the steady-state thermal simulation, it can be concluded that the Cubesat will experience a maximum temperature of 48.3°C during its mission on Sun-side of the orbit. The maximum Directional Heat is approximated $13.6\text{KW}/\text{m}^2$ which occurs around a contact point of MLI and solar Panel. This could be matter of concern and during next iteration these hot-spots would be rectified by redesigning. The average Heat flux of the CubeSat during Hot case was approximately $615.2\text{W}/\text{m}^2$. This information is useful in designing the spacecraft's thermal control system to ensure that it can operate within safe temperature limits.

However, it is important to note that the steady-state analysis assumes constant thermal conditions, which may not be the case during the Cubesat's mission. Thus, a transient analysis, which takes into account the changing thermal conditions during the mission, may provide more accurate and detailed results. The transient analysis can account for factors such as varying solar flux, eclipses, and the heating and cooling of different components during the mission. Therefore, further detailed analysis using transient analysis should be performed to obtain a more accurate understanding of the Cubesat's thermal behavior during its mission.

4 Assembly and Verification

This chapter shall be a description of the Assembly, Integration and Testing (AIT) process. As well as the related verification tools (GSE and facilities) and associated project planning and workflow.

4.1 Systems Engineering Management Plan (SEMP)

Different specialists have been selected and hired for this project, The PANTSat team is composed of the following teams with precise responsibilities:

- **Payload:** Define the mission fundamental requirements as well as study the working principle of the Bolt-On Pulsar X-ray receiver
- **System Engineering:** Provide support to other subsystems design, schedule, cost and requirements.
- **Telecommunication:** Communication, data link, data rate, bandwidth and ground segment.
- **Electrical Power System (EPS):** Provide power during the mission phases and power budget.
- **On Board Computer (OBC):** Design the processing unit or provide a suitable COTS solution, communication messages and internal data interfaces.
- **Attitude Control System (ACS):** Provide attitude control via active elements, orientation and pointing accuracy to perform the science mission.
- **Trajectory Analysis:** Provide a launch solution, the orbital parameters and time windows for the operation modes.
- **Mechanical Structure:** Define the internal structure (configuration and structure), the payload extension mechanism and provide the mass budget.
- **Thermal System:** Thermal considerations, heat dissipation and space environment analysis.

In Figure 4.1, a non-exhaustive diagram shows the main tasks of each sub-system and the project dependencies, i.e. how other systems' design is affected and how the information-flow is shaped. In particular, the starting point is the Payload where the most upper level requirements are decided. PANTSat was build around the optical instrument thus mainly constraining its volume and dimensions along with the critical choice of a CubeSat platform development.

The arrows in the diagram shows the dependencies. As an example, following the information regarding the amount of scientific data to process, the on-board computer team is able to forward to the communication sub-system the total data-rate (house-keeping included) to prepare the link budget. Moving further, the ground station position is then relevant for the orbital analysis team in order to determinate the communication window and back to the OBC to calculate the required memory size.

From the graph, it may seem that the system engineering team receives no input, however within the concurrent engineering paradigm, the role of it was central. As the other sub-systems progressed and reported their design choices, conflicts resolution and critical

design choices were made. Incidentally, the decision of a deployable solar array instead of a wire antenna and identifying design flows such as the placement of the star-sensor next to the patch antenna (facing the ground) are examples of such process. Finally, below the relevant sub-system, a colorful corner-rounded box represents the main responsibility regarding mission budget to be provided.

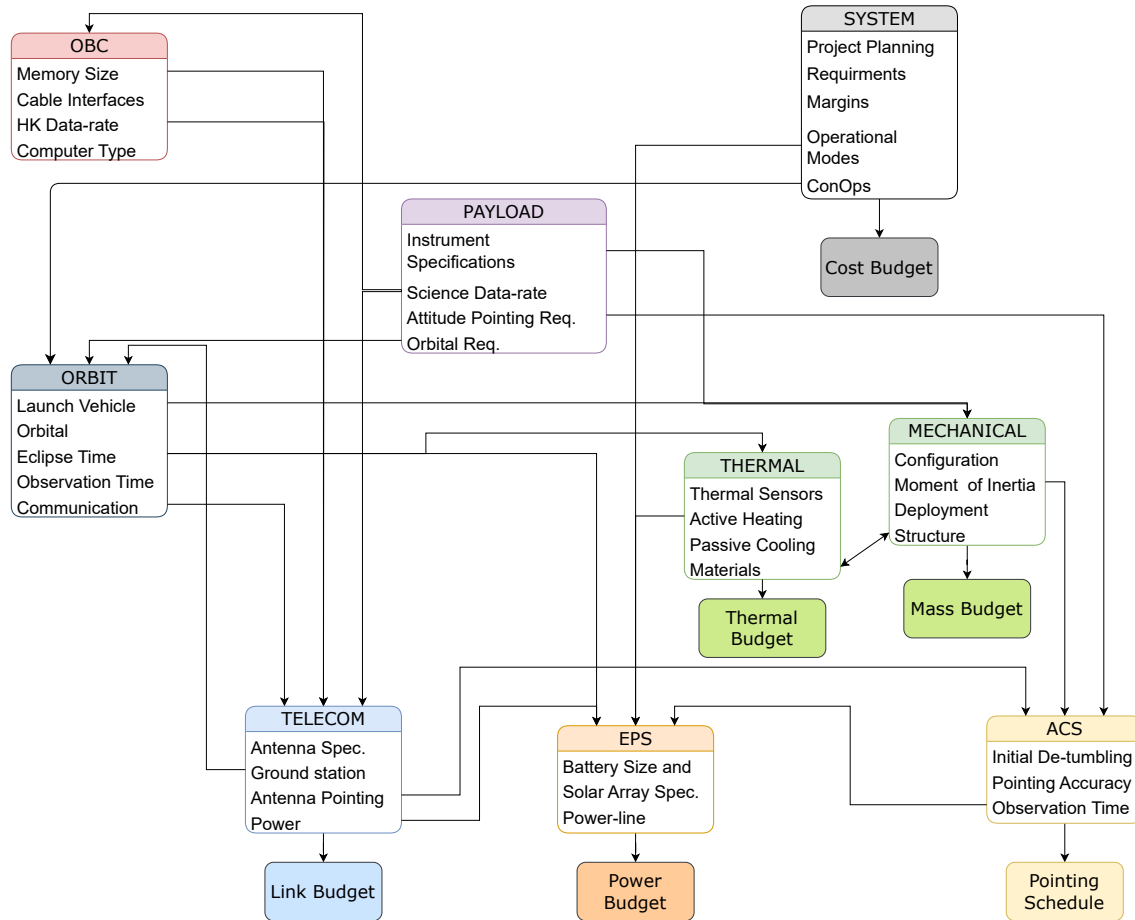


Figure 4.1: Dependencies and communication flow between all the subsystems.

4.1.1 Project Planning

The specific mission phases and the mission timeline has been explain in Paragraph 1.4. According to the NASA life cycle chart, Figure 4.2, the current mission proposal has reach the PDR maturity.

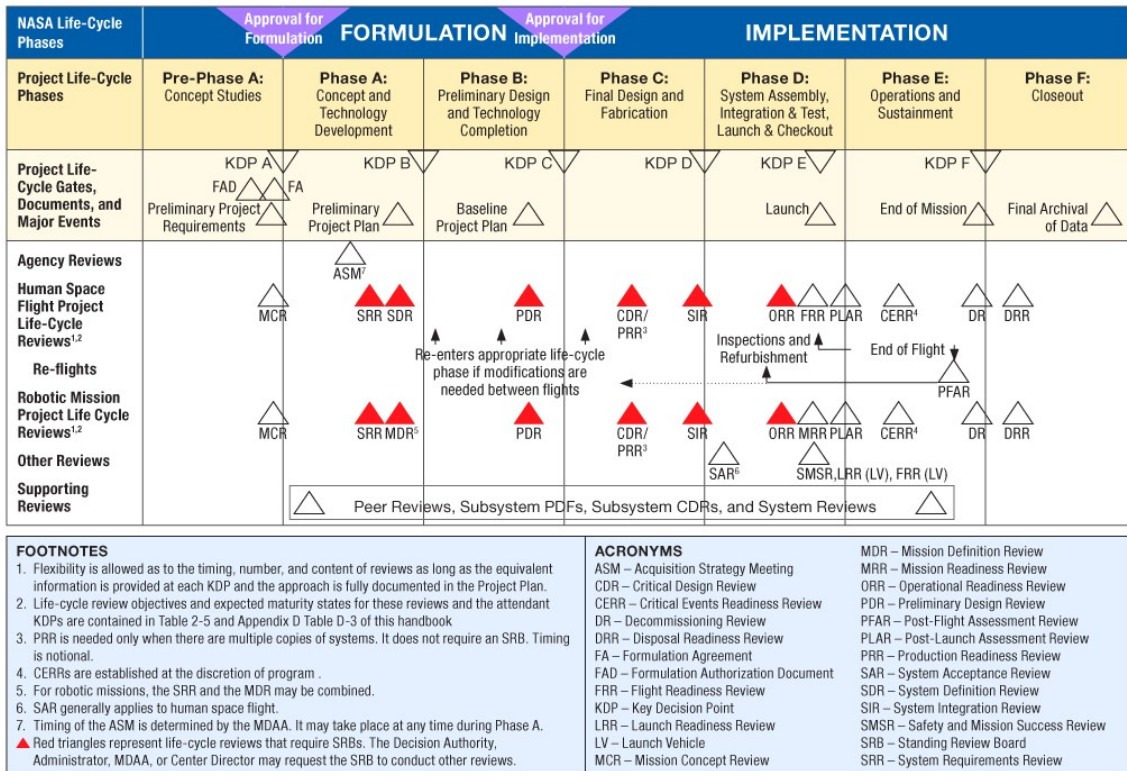


Figure 4.2: NASA Space Flight Project Life Cycle from NPR 7120.5E. Source [99].

In this section we will present the global planning of the PANTSat project from the resource management perspective, showing the duration of each tasks and indicating the key project milestones from the Pre-phase A to the end of Phase B. The best way to do so, is by inspecting the project plan reported in Figure 4.3. ProjectLibre¹ was used to prepare the planning Gantt chart.

The project started official on Wednesday 1st of March 2023 with the presentation of two different scientific instruments to be tested in space. Quickly the main team consisting of 25 students of different nationalities and background was formed (Table 0.1).

Resource Management

During the PANTSat project, the predefined communication tool was Microsoft Teams. Additionally the team had weekly meetings to physically communicate with other sub-teams, pitch-up on the latest results, constrains or cooperate. During the second week a team-building activity involving wine-tasting was held; even if participation was not total, the team started the project with enthusiasm. Unfortunately not everyone contributed equally. At system-level, the work progressed without interruption. however, inside the sub-team tasks, resources were not available to meet or were not actively participating neither in class or online until the very end. Eventually, all the students were involved in at least one aspect of the design, even if not all the requirements or objectives of a task were completely fulfilled.

¹ProjectLibre is free and open-source project management software. Website.

Pre-phase A

Wednesday 8th of March the Pre-phase A begins. The potential stakeholder for the mission are identified and a baseline for the mission is prepared. Incidentally the main team was divided into three smaller ones of equal size. Each of them investigated a different mission concepts as presented in 1.2. This phase was concluded with the Mission Concept Review milestone, whereas after a session with the main stakeholder for the X-ray Instrument (Dr. Robert Sharrow), it was decided to use a CubeSat platform for the mission.

Phase A

This phase lasted exactly three weeks, whereas each week represents a different iteration in the concurrent engineering methodology (more in Section 4.1.2). During this phase the design rapidly evolved from a 3U to a wide 6U CubeSat. Significant choices regarding the trajectory planning and the launch opportunity together with a better understanding of the payload specifications, lead to define precise mission requirements. During the Easter holidays the Mission Definition Review (Mission Definition Review (MDR)) was performed.

Phase B

Following the MDR the concurrent approach was substitute by a more conventional approach where consolidation of the design and preparation for the PDR were the main concerns. In this phase the requirements were updated and a baseline for the interfaces as well as an implementation plan were carried out. These tasks ultimately lead to the Systems Engineering Management Plan (Systems Engineering Management Plan (SEMP)) preparation and the computation of the cost, power, mass and link budgets.

Post-Phase B

After the PDR, the project plan consisted in further strengthening of the design based on the action items (Section 4.3.2) received during the latter, together with further consolidation, including margins for all the sub-systems. Finally the writing of this technical report in \LaTeX has taken place.

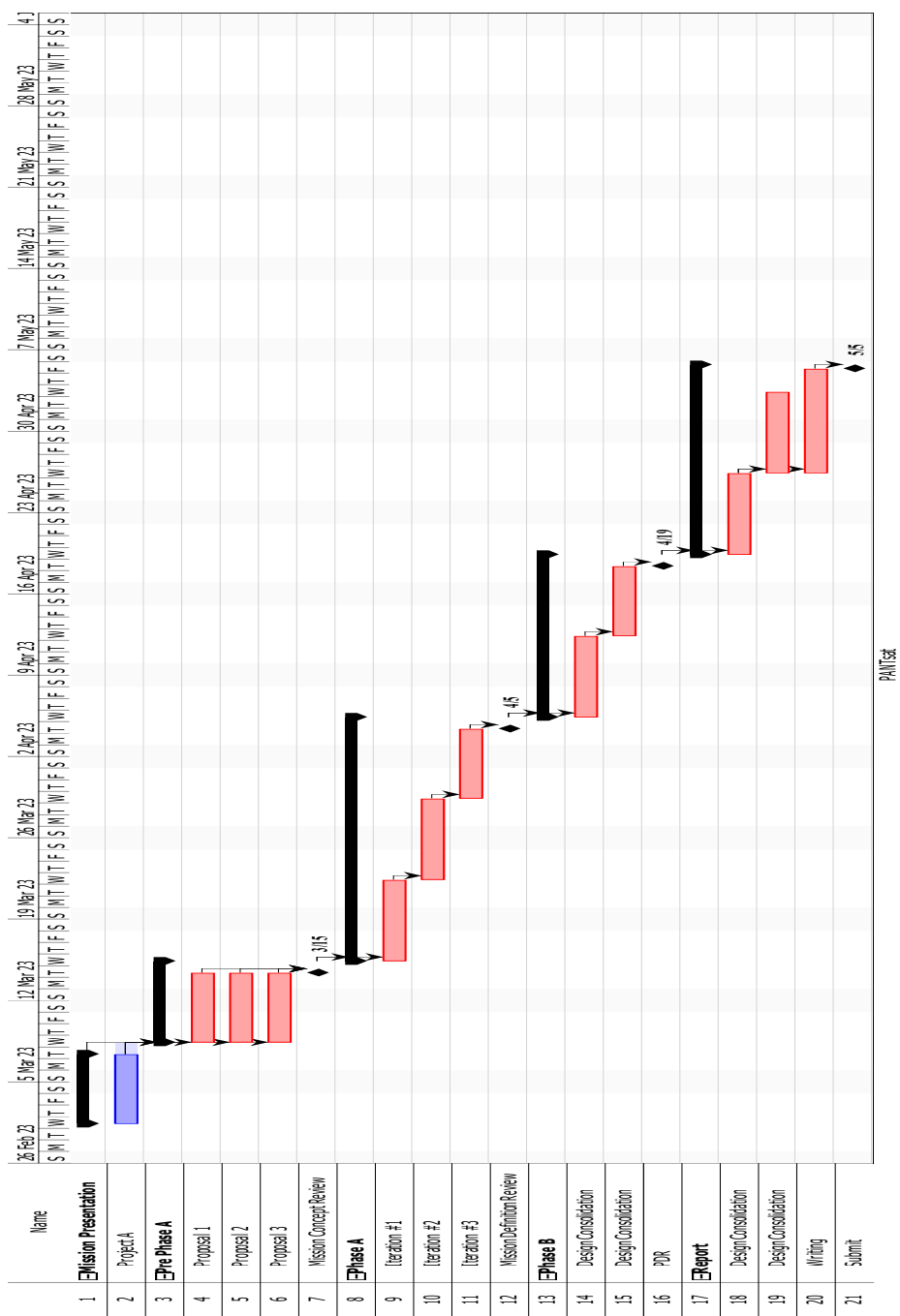


Figure 4.3: PANTsat Project Planning

4.1.2 Concurrent Engineering

Concurrent Engineering is a systematic approach to integrated product development that emphasises the response to mission requirements (stake-holder expectations). It embodies team values of cooperation, trust and sharing, in such a manner that decision making is by consensus, involving all perspectives in parallel.

Specifically, concurrent engineering is a multi-team management technique whereas a team can be composed of one or more persons, Figure 4.4.

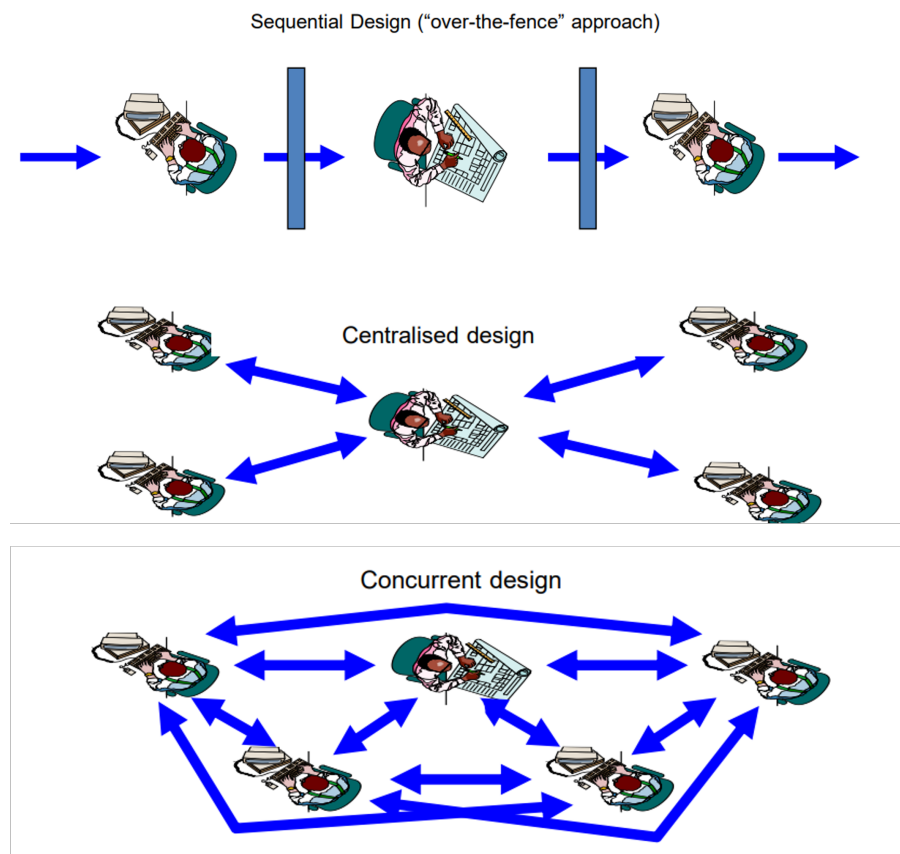


Figure 4.4: Different design approaches. Source ESA.

Usually, engineers develop a product within a sequential design, the problem of such 'over-the-fence' approach is that the teams are connected by a sequential chain which is both time consuming and not flexible, meaning that cross-talking is extremely difficult.

Parallel work is a solution to reduce the development time, thanks to management instruments such as critical chains, independent teams can work on different tasks and deliver their results to a central manager. However, this centralized approach still penalizes teams' cross-talking and only a limited amount of personas have a good overview of the development and can make design decisions.

Due to the short time available to complete this project (2 months), the concurrent approach was immediately identified as the optimal solution to lead the workflow. The workflow is highly parallelized and each team has the opportunity to make critical decision in the design while cross-talking is highly encouraged.

Each week of the project represents an iteration of the design, in the beginning each team works on assumptions until the following interaction data and results from the previous

team in sequential chain are available. Each module is sharing information with the other on a weekly basis approach.

4.1.2.1 Critical Path

Designing a spacecraft for instrument testing is a complex task. Assuming the use of a cube-sat platform, in Figure 4.3 the different design phases are reported while in Figure 4.1 the dependencies between sub-systems.

The critical chain analysis accurately estimates the total project duration while also identifying task dependencies, resource constraints and project risks. In the first place, due to inexperience in cube-sat design, we assumed equal priority and equal time estimate for all the subsystems, so equal resources (workforce) have been entrusted to them. For this reason, the Gantt chart lacks a more deep level of detail where the estimated time (of one subsystem) to complete a given task is missing. A better project planning could have helped in assessing *a priori* the critical path. During the project development, it was clear that performing mechanical simulations was the most time demanding task.

Originally, the mechanical structure sub-system was also in charge of thermal control. Eventually the two sub-system split apart to focus of different areas of development. It is suggested, for future mission design, to have a dedicate thermal sub-system from the beginning. Nonetheless, the mechanical team was still understaffed given the amount of tasks to perform. Configuration in particular should also be assigned to a specialized team, giving more freedom to the mechanical to design structure (optical extension module) or perform vibration and mechanical stress analysis.

On the other hand, some teams had an over-plus of resources. Due to the low complexity of the orbit, a selected team of students was enough for completing the drag and trajectory analysis. Resources were then re-allocated to more in-need sub-system as the attitude control for example.

4.1.2.2 S curve

As a final consideration, the 'S-curve' graph is presented, Figure 4.5. Incidentally, the final design we presented in this report, it's still not mature. After a creativity phase (Pre-phase A) where teams were working on assumptions, the productivity rate has now increased exponentially within every interaction. Eventually, the turning point where the time and effort invested is greater than the achieved design improvement has been reached and the design is now in a consolidating phase.

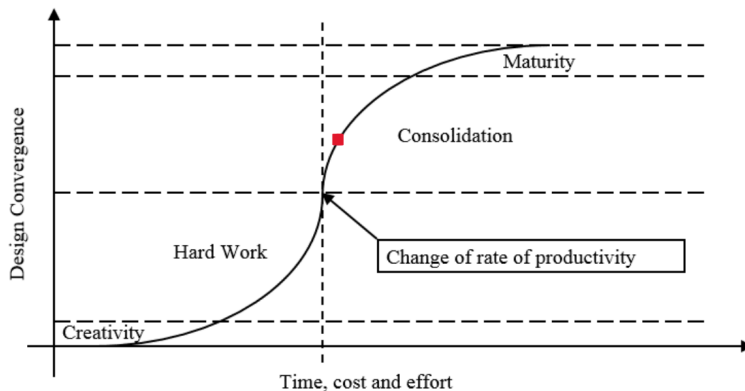


Figure 4.5: S-curve, current position in red. Source ESA.

4.2 AIT Activities and Schedule

In this section, the main activities during the assembly (Phases C and D), integration and testing process of the model(s) including major test activities which have been performed on subsystem level and on integrated system level are described. For each test activity, the test objective, duration and expected results are included.

Assembly and integration activities (AIT) will take place in DTU Space Laboratories. Each subsystem will be tested separately with the objective to meet the specific requirements. Subsystem-level tests will involve subjecting each subsystem to different scenarios and conditions to ensure that they operate effectively under different circumstances. The majority of the components will be subjected to functional, as well as vibrational tests, the latter of which will be performed at the Nanoracks facilities.

Below we present the most important facilities that can be involved for our purpose and their respective descriptions and functionalities :

1. **Smart Converter Lab:** The lab contains a variety of edge microprocessors ranging from dSPACEs to Raspberry Pis and proprietary processors from industrial vendors. It also has AFE drive converters, electrical motors and analog power amplifiers. The lab also has an industrial grid-tied battery and 10+ programmable dc electronics sources. This facility is ideal to develop and test the relevant batteries corresponding to the Electrical Power System.
2. **Radio Anechoic Chamber:** The Radio Anechoic Chamber at DTU Electrical Engineering, part of the DTU-ESA facility, widely known for producing accurate measurements, as well as for the characterization and calibration of antennas for ESA space missions. This facility can be utilized for the calibration and measurement tests on our antennas.
3. **Thermal Analysis Lab:** The Thermal Analysis Lab at DTU Energy will be used to verify estimates of the spacecraft average specific heat, test the insulation properties of Aerogel (AG) coated connection pieces between a heated aluminum plate and one that is not heated, and verify the estimated heat leak. This lab can also be utilized to estimate the degradation of the thermal system over time. Since the thermal chamber does not contain the proper conditions to simulate artificial sunlight, only the stowed configuration will be tested. The solar array will be tested separately as well, while the combination of the solar array and the stowed system will be tested at the ESA CubeSat Support Facility (CSF) in Belgium.
4. **Satellite Communications Lab:** The Fabrication department of the Satellite Communications Lab is ideal for experimental activities including assembly of various mechanical parts and can be utilized by the Mechanical and Thermal subsystem.
5. **Nanoracks facilities:** Finally, the vibration tests. ensuring that the satellite can withstand the vibrations and shocks during the launch and operation in space. The tests will take place in the Nanoracks facilities in USA.

The testing process at the relevant DTU laboratories is estimated to last about 5 months.

4.2.1 Vibration testing (All systems integrated)

This test is part of project phase D and is one of the final verification tests. The objective of the test is to ensure the spacecraft structure, payload and other subsystems can withstand the mechanical environment during launch, release and deployment while being able to function as needed afterwards. The spacecraft will be exposed to the following types of vibration tests on a shaker:

- Sine-burst test: This will test the strength of the primary structure of the satellite (frame and launch vehicle interface). The sine burst is carried out at a specific frequency with varying amplitudes.
- Random vibration test: This will test the strength of the secondary structures (electronic boards, brackets etc). The frequencies (typically 20-2000 Hz in the space industry) are introduced simultaneously by a shaker at random amplitude and phase.
- Sine-sweep test: This test will identify natural frequencies of the satellite by gradually varying the frequency within a set frequency range. If the natural frequency of the satellite matches a high power frequency of the launch vehicle, the forces imposed on the satellite are amplified which could lead to fatal consequences.

For the test, the spacecraft must be mounted as it would be during the launch.

Before this test is able to take place, all subsystems must be manufactured and assembled in the flight configuration. Vibration simulations are also done prior to any vibration testing, to get a ball park estimate of what to expect from the system and eliminate any obvious problems early in the process. If the necessary preparations are not done, the cost of a failure at this stage could prove very costly, as it would likely require changes in the overall structure/assembly of the system [9].

4.2.1.1 Integrated Loads Environment

The CubeSat will be able to withstand a force of 1200N across all load points equally in the Z direction. The number is not definitive and will be further examined in the Nanoracks facilities based on qualification testing and further analysis by Nanoracks.

4.2.2 EPS testing

A first round of test should be performed once the EPS parts are procured. An electrical test to check all parts have continuity and all the specified ports should be performed.

4.2.2.1 Interface testing

The interface between EPS parts should be tested to ensure a correct management of the subsystem is met. An artificial On-board computer connected through the FMP test connector would ensure test all different mode, situations and orders that the EPS is able to perform.

The interface between EPS parts should be tested to ensure a correct management of the subsystem is met. Contrary to using Stack and Molex connectors, many sub-systems are using different interface. Prior to testing the interface its important to have all the EPS modules configured accordingly and battery levels set with respect to the battery pack used during mission. For the ACU module one can start with selecting the type of MPPT used - fixed or tracking, then selecting the values and limits for charging voltage for the battery. Individual inputs from the solar panels should be checked for proper functioning and then telemetry parameters should be configured using the GOSH terminal. A very similar process is required for the PDU and the Dock module. Its advisable to have consistent values for battery charging voltages and current across all boards as each board features a software voltage protection and changes the mode of operation given these values. Both the ACU and the PDU feature a FPC connector for debugging whereas the DOCK features a RS424 - Molex at 50000 baud. The important thing for the DOCK is to select which battery pack is in use and set the operation limits accordingly, rest of the procedure is same as described before. For the PDU the output channels are configured and can be set to work according to the battery state. As the battery state changes as the mission state the sub-systems are also powered accordingly. The PDU also features a FPC connector and GOSH terminal to interact.

4.2.2.2 Operation testing

Communication with the On-board computer and the correct recognition of all sent orders should be carried out.

4.2.2.3 Batteries Testing

Further important components that are required to be tested are flight cells and battery packs. Aforementioned components will be subjected to an approved set of accepted screening tests to determine whether the cells can perform in the required load and environment without any leakage or malfunction. Lithium batteries will be subjected to a standard procedure issued by Nanoracks. In addition, protection circuit and safety features implemented at the cell level, will be evaluated for fault tolerance by Nanoracks, to prevent internal short circuit.

4.2.3 Thermal Testing and Simulation

The design for the thermal system is still a simplified model and requires much more detailed modeling and coupling of orbit-model along with thermal model to get a complete Thermal Model of CubeSat. Simulation of the thermal system over many orbits should validate that the thermal design works as expected. This model has not yet been implemented due to the thermal systems dependency on other teams. A complete simulation requires an estimate of all material properties within the satellite, the orientation of the satellite along its orbit, the orbit itself, and more. In the first several weeks, the orbit of the satellite was changed from a highly elliptical one to a LEO, which meant the thermal calculations needed to begin again.

For future iterations of the design, a complete thermal simulation is of focus. Additionally, thermal distortion has not been modeled or discussed much here. While the choice of MLI took the need to minimize thermal gradients into account, an estimate of the thermal distortion with the current design is of importance for future work.

After the simulation, the CubeSat assembly, will be subjected to a series of physical tests at the ESA facilities in Belgium, in order to verify that the system can withstand harsh environment conditions. Specifically the whole system will be placed in a thermal vacuum chamber to simulate extreme temperature variations and vacuum conditions encountered in the space environment. In addition, the satellite's resistance to radiation will be tested.

4.2.4 Computer Software

An important component of testing is simulating the system, some flight software (such as KubOS) comes with simulation functionalities, for other software, this has to be developed from scratch. Additional standard software testing and verification methods such as unit tests and formal verification methods would be required.

As specified in the operation-state diagram, Figure 3.29, the system should also perform automated tests itself, and know how to deal with various problems (by restarting/rebooting various systems). These in-flight testing systems should also be simulated and verified during development.

An important feature of the OBC is that it needs to be available for updates and tests during the integration phase. This is due to this phase being where the majority of the problems are being detected, and why we need to be able to handle this on-location. Otherwise this would be much more costly and time consuming.

4.3 Technical Challenges

In this section the major criticalities to the technical performance and safety of the system, the project schedule, and an assessment of the follow-up actions will be identified.

4.3.1 Risk Management

When developing a CubeSat, each subsystem presents unique risks that must be addressed and mitigated in order to ensure a successful mission. These risks can include malfunctions or failures of components, environmental hazards in space or issues with integration and communication between subsystems. We will briefly summarize the relevant risk each subsystem presents.

1. ADCS: Several points have to be addressed here. The antenna and solar array orientation conflict, the white spaces between total pointing intervals, the rotation time, the drag constraints relating to the solar panel's velocity vector and finally perform the detumbling process.
2. EPS: The two main scenarios that could jeopardize the mission are the non-deployment of the solar array or its partial functionality. In the first case, the satellite would not be able to operate in the science mode. In the case that 1 out of 3 solar panels are malfunctioning, resulting to the rapid degradation of the battery. In the case that 2 out of 3 solar panels are malfunctioning, it would result in the depletion of the battery in just 1 eclipse period.
3. Mechanical structures: The size of the attitude control system compared to that of the spacecraft is critical, in fact there may be not sufficient space for the other systems inside the satellite, taking into account that the payload is very wide.
4. Thermal control: The concern is the potential heat loss from the aluminum plates underneath the MLI to the edges. Aerogel AG could be used as an insulator to prevent this.
5. Trajectory Analysis: The drag analysis has shown that without proper attitude control, the drag area can lead the orbit to be decay after only 4 months. However in case of active control of the mission life-time can be extended up to 11.5 months enough to validate the payload navigation functionalities.
6. System Engineering / Management: From the subsystem and team management point of view, the issue of minimizing the chances of the mission's time-frame and schedule integrity and continuation being jeopardized, is an integral part of the mission. Therefore, a few critical potential scenarios have been considered, concerning mainly the timeline and manufacturing processes during phases B and C. Specifically, the lead time during the realization of various subsystems parts during Phase C has been accounted for by adding extra time on the planning of that stage, as previous missions and external advisors suggest that its duration may greatly fluctuate as a result of chip shortages, manufacturing and processing errors, shipping delays and unexpected behaviour. In addition, the prototyping process has also been added to our timeline during phase C and the duration of that phase has been adjusted with some headroom to accommodate any potential hurdles that may arise during this early, experimental phase of the CubeSat manufacturing and testing.

However, a time extension can only account for recorded and estimated delays and setbacks and it is acknowledged that other obstacles may occur. Such deviations from our schedule could lead to further delays as the mission's observation window and therefore its launch date are strictly defined. It is thus emphasized that a strict

routine ensuring the continuation of the mission timeline will be employed to deter such instances.

4.3.2 Action Items

Following the PDR, action points were issued for every PANTsat sub-system. Table 4.3.2 includes description of the them and how we fixed open issues. Freedom was given in handling them, specifically in Chapter 3 they were addressed individually in the responsible sub-system.

Action Items	Responsible team	Solution
Project and problem description	SE	Added to the introduction REF
Consider lead time of equipment	SE	Lead Time considered in Figure 1.1, new proposed launch date
Margins on requirements	SE	Added to all subsystem using ESA Margin Policy [10]
Key driving requirement	SE	Added in section 1.3 as a list
Add prototyping into schedule	SE	Added AIT schedule (Section 4.2) and Validation Model (Section 4.4)
Detail out phase A-B in schedule	SE	Added in Section 4.1.1 with Gantt Chart
Length of launch window	Orbit	Problem described and addressed in section 3.4.5 with schedule
Reduced orbit/mission lifetime due to high drag area	Orbit	Problem described and how to be addressed in section 3.4.3.2
Pointing and stability	Payload	The sum should be $< 0.03^\circ$, referring Section 3.1.8
Identify key technology items for enabling final mission	Payload	In particular polycapillary optics and extendable mast, see Section 3.1.8
Is it true that the center of S/C is most radiation, make sure to take other units into account.	Payload	See Section 3.1.8
Window of communication	AOSC	Simulated common operations and created tables/figures.
Micro vibrations	AOSC	Estimated error caused by moving parts,
Did the specs include the simulation? Next step for simulation, take inertia, actuator and disturbances into account full performance from simulated-inertia not achieved in this rapport.	AOSC	Smaller effects have been calculated,
Follow up on pointing requirements to AOCS needs pointing accuracy < 30 deg	Comm	Antenna is not omnidirectional ,
Scheme/schedule: pointing for x-ray, power or Communications	Comm	Parameters given to AOCS: solid angle, transmission time, n. of transmission per day
How long can you survive in tumbling/safe mode? What is the scheme of operation in safe mode?	EPS	Using batteries only, the S/C would be able to survive in safe mode up to 65 minutes. More details about safe mode in the power budget 2.2.2 and the final EPS design selection section 3.5.
Follow up with safe mode depletion time of battery	EPS	After 2 years of battery usage, the spacecraft would survive up to 65 minutes in safe mode.
Take into account fill time of the battery charging and maximum charge and discharge. Is 80 % the optimal for not reducing lifetime too much?	EPS	The batteries will be normally operating between 20 to 80 % to extend their lifetime. Exceptions made when safe mode is triggered.
Include moment of inertia including solar panel deployment	Mech	Provided in Tables 3.5 and 3.16
Wobble on sunpanel	Mech	
Consider redundancy	Mech	2 motors as described in 3.7.3.3
Launch shock and vibration specs/req	Mech	Vibration resonance in Figure 3.68
Does the MLI fit into the mechanical structure	Thermal	Looked into NanoRacks documentation, adjusted MLI placement

4.4 Validation Model Philosophy

When developing a CubeSat mission, selecting the appropriate model philosophy is critical to ensuring that the satellite is designed, built, and tested to the required standards. The Validation philosophy determines the types of models that will be used for the various phases of the mission to prove that the right product has been developed to satisfy the mission statement and stakeholder expectations.

The most commonly used model philosophy for CubeSat missions is the Development Model (DM) approach [99]. Under this approach, the development of the CubeSat is based on a single model that is incrementally modified throughout the design, build, and test phases of the mission. This approach is often used for missions with shorter timelines or less complex requirements, where a full suite of models may not be necessary. However, more complex missions have suggested a more sophisticated model that iterates and covers more real world scenarios and manages to better prepare a mission until launch [100]. For example, the ESA has developed a model philosophy for CubeSat missions, that serves as a hybrid model, called the Hybrid Validation Model (HVM) philosophy. This combines the benefits of different models, such as the Engineering Model (EM), the Qualification Model (QM), the Flight Model (FM), and the Protoflight Model (PFM), which are described in Table 4.1. The Hybrid Validation Model (HVM) is designed to address the limitations of traditional model philosophies, such as the DM philosophy, which are often not sufficient to validate a CubeSat's design in full flight configuration.

Model	Description	Purpose	CubeSat Scenario	Model Philosophy
Engineering Model	Functional model	Test of subsystem performance	Complex	HVM (ESA Hybrid)
Qualification model	Basis of FM design (quality)	Environmental & Stress Testing	Complex	HVM (ESA Hybrid)
Flight model	Model for launch into Space	Environmental & Stress Testing	Basic & Shorter	DM / HVM (ESA Hybrid)
ProtoFlight Model	Replica of the FM	Same test as FM (without the instrument)	Complex	HVM (ESA Hybrid)
Validation Model	Functional Integrated CubeSat with COTS	Early identification of design issues	Complex	HVM (ESA Hybrid)

Table 4.1: Models of validation and Model Philosophy application (DM & VM)

The Validation Model (VM), is an extra model included in the HVM approach, which is built with commercial off-the-shelf (COTS) components and materials that are representative of the final design and serves as an intermediate step between the EM/QM and FM/PFM, and its purpose is to validate the design before the FM is built. The VM is a fully functional and integrated CubeSat, and it is subjected to a series of environmental tests, including thermal vacuum, vibration, shock, and radiation, to verify that it can withstand the space environment. Moreover, it is a valuable tool for mitigating risks associated with CubeSat development, as it allows for early identification and resolution of design issues that may not be apparent during earlier testing phases. ESA has successfully employed this HVM philosophy in a number of CubeSat missions, including the GomX-4B mission, which was launched in 2018. The GomX-4B CubeSat was built utilizing a VM in its pipeline, and it successfully demonstrated a range of technologies, including a new intersatellite link system and a nanosatellite positioning system [101].

However, considering the scope, budget and timescale of our mission, it is far more feasible to adopt a DM philosophy for our testing of the complete assembly. However, a with Hybrid Validation Model philosophy can be applied to smaller subsystems of the satellite. Those would be the OBC unit, as well as parts of the EPS subsystem, as they can be developed at a relatively low cost and small time-frame. It is acknowledged that the lack of a wholesome, more elaborate and complex model philosophy for the complete system may increase the chances of unexpected errors occurring throughout the process of manufacturing, testing and flight. In spite of that, as this is a in-orbit science demonstration mission and of a relatively small scale, testing and validation can be applied on the CubeSat that is bound for Space flight (DM), providing the necessary grounds for achieving confidence in the product verification, with the shortest planning, and a suitable weighting of costs and risks.

4.5 Verification Philosophy

The PDR demonstrates that the preliminary design meets all system requirements with acceptable risk before proceeding with a more detailed design [99]. In particular, the verification methods include analyses, inspection, demonstration, and test.

- **Analysis (A):** Use of mathematical modeling and analytical techniques to predict the compliance of a design to its requirements based on calculated data or measured data.
- **Demonstrations (D):** Showing that the use of an end product achieves the individual specified requirement. Can involve the use of physical models or mock-ups.
- **Inspection (I):** The visual examination of a realized end product.
- **Test (T):** The use of a realized end product to obtain detailed data to verify or validate performance or to provide sufficient information to verify or validate performance through further analysis.

The chosen engineering tool for verification is the so called Verification Matrix, Table 4.2. As the design matures throughout each iteration, the requirements are updated and refined as needed. In some cases, the complete verification of a given requirement might require more than one method, if so the verification criteria or the required documentation is specified.

In the matrix each sub-system has a different call-name, specifically mechanical (M), thermal control (TC), Orbit (O), Attitude Control and OBC (A), eletrical power (E) telecommunication (T) and payload (P). Each requirement has either a specific origin (section or number of an attached document) or it is derived from a specific upper-class requirement (the predecessor is indicated). In particular, the reference documents are:

- **Document A:** ESA Fly Your Satellite Design Specification v4-0 [8]
- **Document B:** Physical Requirements Reconsideration. Appendix A
- **Document C:** NanoRacks DoubleWide Deployer (NRDD) System [9]
- **Document D:** Custom Derived Requirements
- **Document E:** System Margin Policy for ESA IOD CubeSat Projects [10]
- **Document F:** Internal into this document

Moreover, the symbol for a verified requirement is a green **V** box, conversely a red **N** is shown. Missing compliance has mainly two causes, the first, is the lack of technical

maturity or work-force for addressing that particular task, the second and most common, is the necessity of testing for verification, in this scenario verification must be carried out at a later mission phase. Therefore, the matrix contains indication for preparing a more detailed verification plan, i.e. establishing the method of verification and facility where it has to be performed and in which phase of the mission life-cycle

Requirement No.	Document	Paragraph	Statement	Verification Method		Facility or Lab	Phase	Result	Verification Success Criteria / Product
				-	Blueprints				
M-1	B	4.1.3	The CubeSat dimensions should be within the 6U form factor, i.e. the following dimensions: X-direction: 226.3 ± 0.1 mm wide Y-direction: 100.0 ± 0.1 mm wide Z-direction: 366.0 ± 0.1 mm wide			I	Datasheet	0	V
M-2	B	4.1.8	Rails shall have a minimum width of 8.2 mm			T	DTU Space	D	N
M-3	C	4.1.3	The maximum mass must be 12kg			I	Blueprints	0	V
M-5	C	4.1.3-2	The CubeSat center of mass (CM) shall be located within the following range relative to the geometric center of the payload. a. X-axis: (+/- 3cm) b. Y-axis: (+/- 3cm) c. Z-axis: (+/- 8cm)			D	Blueprints	0	V
M-4	F	2.6	The CubeSat shall be protected with 2.5mm aluminum shield from radiation			A	SolidWorks	A	N
M-6	C	4.3.5	The CubeSat shall be capable of withstanding a force 1200N across all load points equally in the Z direction.			A,T	SolidWorks / Nanoracks facilities	0	N
M-7	C	4.3.6	The CubeSat shall be capable of withstanding the random vibration environment to the Maximum Expected Flight Level (MFFL) for a duration of 60 seconds			I	SolidWorks	0	Vibration Analysis/test Report
M-33	D	P-1	The optical extension component must have redundancy or space heritage			D	Blueprints	0	Redundancy
M-9	D	P-1	The mechanism should be able to extend to a minimum focal length of 422mm			A,T	SolidWorks / DTU Space	D	Structural Analysis Report
M-10	F	3.7.1	Structure rigidity shall guarantee minimum pointing accuracy of 0.03deg			I	SolidWorks/Blueprints	N	All the components from list are in the model
M-11	D	S-1	Structure shall be able to fit all subsystems						
TC-1	A	4.7.6	Minimum of two test temperature sensors shall be installed inside the spacecraft.			D	Blueprints	0	Two are installed by design
TC-2	F	3.8.1.2	The temperature inside the S/C shall be contain between 10C and 35C			T	Thermal Analysis Lab	D	Temperature Analysis Report
O-1	A	4.9.1	The mission must last more than 6 months			A	STK	0	11.5 months free re-entry
O-2	A	4.11.4	The satellite must freely re-enter after 25y.			A	STK	0	11.5 months free re-entry
O-3	C	4.4.9	The satellite should have no propulsion.			D	Blueprints	0	No propulsion system needed
O-4	C	4.5.2.2	CubeSats over 5kg shall provide an Orbital Debris Assessment Report (ODAR) that verifies compliance with NASA-STD-8739.14.			A	ODAR	D	N
T-1	A	4.2.11	RF power output no greater than 1.5 W at the transmitter antenna's			T	Radio Anechoic Chamber	D	V
T-2	A	4.9.6	Cubesat shall use passive or active on-orbit tracking aids to facilitate post-launch satellite identification, increase the satellite trackability, and facilitate teh accurate and precise determination of its position in orbit.			I	Design Information	0	V
T-3	A	4.9.7	The ground station should preferably be controlled and operated by the university			D	Operations	D	GNSS module integrated by the OBC
T-4	A	4.12.3	Cubesats and ground stations shall comply with International Telecommunication Union (ITU) requirements			I	Datasheet	0	DTU ground antenna
T-5	F	3.6.4.3	The deployment of the antenna shall not interfere with the deployment solar array			D	Design Information	0	Compliance with S-band regulation
A-1	A	4.4.1.1	The CubeSat shall be tolerant to an initial tumbling rate of 90 deg/s per axis at deployment			A	Matlab simulation	0	Patch antenna
A-2	D	P-2	The pointing requirement is minimum 0.03deg accuracy			I	Datasheet	0	30 minutes to achieve zero spin
A-3	E	2.4	Any on-board memory (Random Access Memory RAM used for code and / or data) shall include a memory margin of at least 50%			I	Design Information	0	0.008deg accuracy
A-4	A	4.3.1	The cubesat should allow modification of the on-board software after the satellite assembly is completed and while on ground			D	Physical model	D	The margin is 96%
A-5	A	4.6.3	It shall be possible to turn the satellite on/off via an umbrellal connection			D	Physical model	D	USB port on the OBC
A-6	A	4.4.3	The magnetic field outside the Cubesat static envelope shall be limited to 0.5 Gauss above Earth magnetic field			A	Matlab simulation	0	Power on/off
A-7	A	4.3.3	The on-board software shall implement a command/loss timer that triggers a recovery routine			D	Design Information	0	Below 0.25 Gauss at worst case
E-1	A	4.2.2	The CubeSat shall have at least 2 deployment switches			I	DTU Space	D	15 Minutes each pass over ground station
E-2	A	4.2.12	The CubeSat shall be able to survive up to nine months without access after the installation in the depolyer on the ground until the deployment			T,A	DTU Space	D	Physical switches need to be installed in the circuit
E-3	C	4.2.1.1	All electrical power storage devices shall be internal to the Cubesat			I	Design Information	0	N
E-4	C	4.4.7.3	All flight cells and battery packs shall be subjected to an approved set of acceptance screening tests to ensure the cells will perform to a standard statement of work issued by NanoRacks (NR-STD-139).			I,T	Smart Converter Lab	D	Aging simulations or testing to prove survivability
E-5	E	2.2	The Power budget margin shall be at least 20%			I	Design Information	0	By design the batteries are internal and shielded from radiation
P-1	F	3.1.1	The optic module shall fit inside a 6U cubesat structure			I	Design Information	0	Battery Test Report in Compliance with NR-STD-139
P-2	F	3.1.2	X-ray detector shall have a microsecond time resolution			T	DTU Space	D	The EPS margin is 25%
P-3	F	2.6	The maximum dosage inside of the Cubesat shall be 1krad per year			A	Spurious	0	The optical module is 135mm long
									Imaging testing with ultrafast x-ray source
									Absorbed radiation is 0.75krad/year

Table 4.2: Requirements Matrix

5 Conclusion

PANTsat, Pulsar Autonomous Navigation and Timing Satellite, is a in-orbit demonstrator mission proposal. The XNAV technology was presented in the frame-work of the course *Space System Engineering* and was proposed by Dr. Robert Sharrow. The original proposal was to test an innovative instrument for better navigation in space "Spacecraft Bolt-On Pulsar X-ray Receiver Concept for Autonomous Navigation and Timing". The mission concept aims to bring XNAV one step closer to realization by designing an in-orbit demonstrator for the XNAV technology thanks to a miniature X-ray receiver.

In Pre-phase A, the original proposal was to be part of the ESA *Fly Your Satellite!* program. However, given the size of the XNAV instrument, during the development the design evolved into a 6U platform with a different launcher system and trajectory since the program CubeSat's dimensions are constrain to up 3U. Nonetheless, for the project planning, requirements and other parts of the life-cycle were reused or derived from the original concept.

The instrument package proposed in this study was shown to adequately fulfill the needs for observing X-ray pulsars and deriving a positioning solution. The overarching goal is to provide an autonomous positioning system that can help offset the increasing demands on the DSN in support of future deep-space scientific missions. The poly-capillary optics trade study maximized the performance given the dimensional constraints of a 6U CubeSat platform. The observable Pulsars were identified, and a road map of observations to provide a technology demonstration of X-ray navigation was outlined. Furthermore, the design considerations regarding different instrument mounting and configurations were described.

Using a W6U cube-sat structure from Gom-space it is possible to meet all dimensional and mass requirements given by all subsystems whilst meeting NanoRacks' launch mass and size requirements. A viable extension mechanism has also been designed, however, improvements to the current design are certain and possible torsion spring-based mechanism may prove optimal.

Designing the EPS showed to be a complicated task in the beginning. After encountering all the issues and learning how to go around them, the design became clearer, which allowed us to study multiple risk case scenarios, hardware interface compatibility between subsystems and more, which provide a wider view on the EPS functionalities. The proposed EPS has shown to be functional under the power requirements for each operational modes.

The Telecommunication Subsystem design is strictly linked to every other subsystem, as a consequence, the choice of the various components followed step by step the development of the entire mission. In conclusion, the final design of the antenna, transceiver and components of the ground station described in Chapter 3 was not only developed to meet the requirements of our subsystem, but to ensure the correct operation of the entire spacecraft.

The design of Thermal Model takes into account heritage from previous mission and uses of ANSYS Software for thermal modelling and steady state thermal simulations. With the aid of MATLAB, first estimate calculations for steady state and transient thermal analysis were conducted. Thermal controls were identified, and passive thermal control using 10 layers of MLI was chosen, along with the implementation of 14 Kapton patch heaters and 14 thermal sensors for active thermal control during the eclipse phase of the orbit.

These heater-sensor pairs are linked to two thermal boxes which control heating. These redundancies in the system make it operationally fail-safe thermal control. Although the current thermal design looks promising.

The orbit of a space mission is very important, as it defines so many critical aspects of the mission, and is usually defined very early on in a mission. Aspects such as occultation, lifetime and atmospheric drag gave us the opportunity to design a realistic orbit for our mission. The action items given to us at the PDR have been taken into account, and a well-rounded orbital model has been produced that fulfills the mission requirements. An action item that was brought up most recently has also been added and described in the report, as it turned out to be a potential mission-killer. This was the mean drag area, which turned out to affect the orbit lifetime much more than previously thought. This has affected the mission lifetime to 11.5 months, down from 18 months and a period and inclination similar to the ISS at 92 minutes and 51.6° respectively. However, the orbit still lies within the given requirements.

With the high pointing requirement for the mission success, it was important to find a high performing system for the CubeSat - beyond the standard attitude and control systems normally used. This resulted in an integrated attitude control and determination system produced by Blue Canyon Technologies, which included a CubeSat-ready star camera, to support our pointing precision needed. In-flight test of similar missions, and initial simulations show that this system is fulfilling the requirements for the technology demonstration mission. The choice of the onboard computer and software solutions were also important, as the attitude system is needed for the different modes of operation to perform as planned. An OBC system from Endurosat was chosen, and controls the dataflow between the subsystems, as well as autonomous operations. It has been successfully proven that the chosen system can effectively manage the delicate phase of the spacecraft's tumbling, allowing for it to be stabilized to a degree that allows for precise attitude control performances.

Further analysis and testing are required to determine the structural strength and effects of vibrations on PANTSat for completion of the last viability study. Much of future work may surround detailing specific attachment points for integration and stacking of all sub-systems.

As a future improvement, the ADCS needs to perform more tests for the initial phases of the mission, such as de-tumbling and deploying stage, although it was already discussed and demonstrated that is achievable within the current configuration.

Regarding thermal control, a detailed thermal transient simulation using ANSYS or Solid-works is desired in order to validate the proposed solution and investigate effects of thermal expansion with respect to time.

Previously, only NASA has been working to demonstrate X-ray navigation in space [102]. On NASA's website, the development of the instrument called Station Explorer for X-ray Timing and Navigation Technology (SEXTANT) is described [103]. The SEXTANT Project Manager Jason Mitchell said "*This demonstration is a breakthrough for future deep space exploration*".

We, the PANTSat team, strongly believe in those words.

In this technical report we proved the feasibility and advantages of an in-orbit CubeSat demonstrator mission. Within the frame-work of the course, our aim is to support Dr. Robert Sharow and contribute to cutting edge technologies for the deep-space exploration.

Bibliography

- [1] J. Collins P. Graven. "XNAV for Deep Space Navigation". In: *American Astronautical Society, 31st ANNUAL AAS GUIDANCE AND CONTROL CONFERENCE, AAS 08-054* (2008).
- [2] EoPortal. *ISS Utilization: NICER/SEXTANT (Neutron-star Interior Composition ExploreR / Station Explorer for X-ray Timing and Navigation Technology)*. Accessed on 01-05-2023. 2016. URL: <https://www.eoportal.org/satellite-missions/iss-nicer-sextant#iss-utilization-nicersextant-neutron-star-interior-composition-explorer--station-explorer-for-x-ray-timing-and-navigation-technology>.
- [3] Suneel Sheikh et al. "Deep space navigation augmentation using variable celestial X-ray sources". In: *Proceedings of the Institute of Navigation, National Technical Meeting* 1 (Jan. 2009), pp. 34–48.
- [4] S. J. Schonfeld et al. "Expanding the deep space network to support the heliophysics system observatory". In: *Frontiers in Astronomy and Space Sciences* 9 (2023). ISSN: 2296-987X. DOI: 10.3389/fspas.2022.1051527. URL: <https://www.frontiersin.org/articles/10.3389/fspas.2022.1051527>.
- [5] Remi Labelle and Chau Buu. "Uplink and Downlink Electronics Upgrades for the NASA Deep Space Network Aperture Enhancement (DAE) Project". In: May 2014. ISBN: 978-1-62410-221-9. DOI: 10.2514/6.2014-1711.
- [6] NASA. *NASA's Mission Operations and Communications Services*. Oct. 2014. URL: https://deepspace.jpl.nasa.gov/files/6%5C_NASA%5C_MOCS%5C_2014%5C_10%5C_01%5C_14.pdf.
- [7] Donald S. Remer, Josef S. Sherif, and Harry R. Buchanan. "Modeling the deep space network costs for future space missions by using major cost drivers". In: *International Journal of Production Economics* 28.2 (1992), pp. 193–202. ISSN: 0925-5273. DOI: [https://doi.org/10.1016/0925-5273\(92\)90031-2](https://doi.org/10.1016/0925-5273(92)90031-2). URL: <https://www.sciencedirect.com/science/article/pii/0925527392900312>.
- [8] *Fly Your Satellite! Design Specification Version 4.0*. Unclassified Document but accessible only on request. Oct. 2021. URL: https://www.esa.int/Education/CubeSats_-_Fly_Your_Satellite>List_of_documents.
- [9] Robert Adams. *NanoRacks DoubleWide Deployer (NRDD) System Interface Definition Document (IDD)*. Unclassified Document but accessible only on request. 20 2017. URL: <https://nanoracks.com/products/iss-launch/>.
- [10] Roger Walker. *System Margin Policy for ESA IOD CubeSat Projects*. Accessed on 02/05/2023. Feb. 2016. URL: https://www.ntnu.no/wiki/download/attachments/112275035/IOD_CubeSat_Margin_Policy_iss1_rev_0.pdf?version=1&modificationDate=1504517546000&api=v2.
- [11] Stark J. Fortescue P. Swinerd G. *Spacecraft Systems Engineering*. Tech. rep. 2011.
- [12] *Blue Canyon Technologies*. last visited: 04/05/2023. URL: <https://www.bluecanyontech.com/>.
- [13] Hilmi Sundu and Nimeti Doner. *Detailed Thermal Design and Control of an Observation Satellite in Low Earth Orbit*. 2020. URL: https://www.researchgate.net/publication/353660180_Detailed_Thermal_Design_and_Control_of_an_Observation_Satellite_in_Low_Earth_Orbit.

- [14] NASA. *AMES Cost Model*. 2015. URL: https://www.nasa.gov/sites/default/files/files/56%5C_AMES%5C_Cost%5C_Model%5C_Aug%5C_25%5C_2015%5C_Presentation%5C_V5%5C_submit%5C_tagged.pdf.
- [15] NASA. *Cost Estimating Handbook*. URL: <https://www.nasa.gov/content/cost-estimating-handbook#AppendixK>.
- [16] Project Air Force RAND. *Guidelines and Metrics for Assessing Space System Cost Estimates*. URL: https://www.rand.org/content/dam/rand/pubs/technical%5C_reports/2008/RAND%5C_TR418.pdf.
- [17] UK Space Agency. *Apply for funding: space-related R&D, innovation and education*. 2014. URL: <https://www.gov.uk/guidance/apply-for-funding-academic-community-and-educational>.
- [18] Federal Grants. *CubeSat-based Science Missions*. 2023. URL: <https://www.federalgrants.com/CubeSat-based-Science-Missions-for-Geospace-and-Atmospheric-Research-33658.html>.
- [19] National Space Grant Foundation. *NASA SPACE GRANT COLLABORATION*. 2023. URL: <https://spacegrant.org/2023/03/12/nasa-space-grant-collaboration-w-stmd-and-gcd-makes-strides-in-team-challenge/>.
- [20] National Science Foundation. *CubeSat-based Science Missions*. 2018. URL: <https://www.nsf.gov/pubs/2018/nsf18553/nsf18553.htm>.
- [21] ANSYS, Inc. *ANSYS Workbench*. Accessed on May 5, 2023. URL: <https://www.ansys.com/products/platform/ansys-workbench>.
- [22] European Cooperation for Space Standardization. “ECSS-E-ST-10-12C Methods for the calculation of radiation received and its effects, and a policy for design margins”. Version 1.0. In: (2018).
- [23] Doug Sinclair and Jonathan Dyer. “SSC13-IV-3 Radiation Effects and COTS Parts in SmallSats”. In: Apr. 2021.
- [24] Y.M. Seo et al. “Cumulative ionizing effect from solar-terrestrial charged particles and cosmic rays for CubeSats as simulated with GEANT4”. In: *Current Applied Physics* 12.6 (2012), pp. 1541–1547. ISSN: 1567-1739. DOI: <https://doi.org/10.1016/j.cap.2012.04.033>. URL: <https://www.sciencedirect.com/science/article/pii/S1567173912001721>.
- [25] European Space Agency. *Space Environment Information System*. 2022. URL: <https://www.spenvis.oma.be/>.
- [26] N. Reinecke, O. Pedersen, and R. Harboe-Sorensen. “Heavy ion and proton SEL characterization on selected EEE component types used in ISS equipment”. In: *Proceedings of the 7th European Conference on Radiation and Its Effects on Components and Systems, 2003. RADECS 2003*. 2003, pp. 157–162.
- [27] Finn E. Christensen and Brian D. Ramsey. “X-Ray Optics for Astrophysics: A Historical Review”. In: *Handbook of X-ray and Gamma-ray Astrophysics*, (2022). DOI: https://doi.org/10.1007/978-981-16-4544-0_1-1.
- [28] Carolyn A. MacDonald. “Focusing Polycapillary Optics and Their Applications”. In: *Hindawi Publishing Corporation X-Ray Optics and Instrumentation* (2010). DOI: [doi:10.1155/2010/867049](https://doi.org/10.1155/2010/867049).
- [29] Abigail C. AllWood et al. “Planetary Instrument for X-Ray Lithochemistry”. In: *Space Sci Rev* 216:134 (2020). DOI: <https://doi.org/10.1007/s11214-020-00767-7>.
- [30] NASA Jet Propulsion Laboratory Robert Sharow et al. *r20125 principal investigator robert sharow 343 final marked*. Course material.
- [31] Robert Sharow. *Pulsar Nav Overview 2023 03*. Course material. Mar. 2023.

- [32] XOS Ning Gao. *Polycapillary X-ray Optic Fundamentals, Applications and Sub-Systems*. Assessed 03-05-2023. URL: <https://www.srainstruments.com/wp-content/uploads/2020/07/Polycapillary-X-ray-Optic-Fundamentals-Presentation.pdf>.
- [33] Microsemi SA.45s Space Chip Scale Atomic Clock (CSAC). URL: <https://www.microsemi.com/product-directory/embedded-clocks-frequency-references/5207-space-csac#overview>.
- [34] NASA. *NICER Mission Guide*. last visited: 04/05/2023. URL: https://heasarc.gsfc.nasa.gov/docs/nicer/mission_guide/.
- [35] NASA. *FITS-file format*. last visited: 05/05/2023. URL: https://heasarc.gsfc.nasa.gov/docs/heasarc/caldb/docs/ogip/fits_formats/docs/rates/ogip_93_003/ogip_93_003.pdf.
- [36] Ray et al. 2017. *Characterization of Pulsar Sources for X-ray Navigation*. last visited: 05/05/2023. URL: <https://arxiv.org/pdf/1711.08507.pdf>.
- [37] NASA. *nupipeline*. last visited: 05/05/2023. URL: <https://heasarc.gsfc.nasa.gov/lheasoft/ftools/caldb/help/nupipeline.html>.
- [38] Andrea Santangelo Cosimo Bambi. *Handbook of X-ray and Gamma-ray Astrophysics*.
- [39] Suneel Sheikh. *The Use of Variable Celestial X-ray Sources for Spacecraft Navigation*. last visited: 05/05/2023. URL: https://www.researchgate.net/publication/234427761_The_Use_of_Variable_Celestial_X-ray_Sources_for_Spacecraft_Navigation.
- [40] Roberta Zanin. *The Crab pulsar at VHE*. last visited: 05/05/2023. URL: <https://arxiv.org/abs/1701.07364>.
- [41] Peter Fortescue et al. *Spacecraft Systems Engineering*. Wiley, 2003.
- [42] Christopher M. Pong. *On-Orbit Performance & Operation of the Attitude & Pointing Control Subsystems on ASTERIA*. 2018. URL: <https://dataVERSE.jpl.nasa.gov/file.xhtml?fileId=60434&version=1.0>.
- [43] Ansys Government Initiatives. Accessed on 30-04-2023. URL: <https://www.agi.com/>.
- [44] Chris Peat. *Maan*. last visited: 05/05/2023. URL: <https://www.heavens-above.com/moon.aspx?lat=0&lng=0&loc=M&alt=0&tz=CET>.
- [45] Jens T. Satre. *Sun & Moon Position Calculator*. last visited: 05/05/2023. URL: <https://www.satellite-calculations.com/Satellite/suncalc.htm>.
- [46] *Orbit of the Moon*. last visited: 05/05/2023. URL: https://en.wikipedia.org/wiki/Orbit_of_the_Moon.
- [47] Alan Buis. *Milankovitch (Orbital) Cycles and Their Role in Earth's Climate*. last visited: 05/05/2023. URL: <https://climate.nasa.gov/news/2948/milankovitch-orbital-cycles-and-their-role-in-earths-climate/#:~:text=Earth's%5C%20axis%5C%20is%5C%20currently%5C%20tilted,that%5C%20spans%5C%20about%5C%2041%5C%2C000%5C%20years..>
- [48] *Earth's Orbit*. last visited: 05/05/2023. URL: https://en.wikipedia.org/wiki/Earth%5C%27s_orbit.
- [49] Edwin Christuraj. *CubeSat Detumbling Simulator*. 2021.
- [50] Endurosat. *Endurosat OBC*. 2023. URL: <https://one.endurosat.com/>.
- [51] ENDURUSAT. accessed: 03/05/2023. URL: <https://www.endurosat.com/cubesat-store/cubesat-obc/onboard-computer-gnss/>.
- [52] E. Macias-Zugasti. "Development Of The Payload System And OBC Microcontroller Coding For A Cubic Satellite". In: (2020).
- [53] Wayne Yu. "Application of X-ray Pulsar Navigation: A Characterization of the Earth Orbit Trade Space". PhD thesis. Jan. 2015. DOI: 10.13016/M2NF01.

- [54] Wayne Yu. *Application of X-ray Pulsar Navigation: A Characterization of the Earth Orbit Trade Space*. Aug. 2016.
- [55] Eric Kulu. *Nanosats Database*. Accessed on 30-04-2023. URL: www.nanosats.eu.
- [56] *ISS Trajectory Data*. Accessed on 25-04-2023. URL: https://spotthestation.nasa.gov/trajecory_data.cfm.
- [57] *GOMspace NanoPower TSP*. last visited: 05/05/2023. URL: <https://gomspace.com/shop/subsystems/power/nanopower-tsp.aspx>.
- [58] *GOMspace NanoPower BP4*. last visited: 05/05/2023. URL: <https://gomspace.com/shop/subsystems/power/nanopower-bp4.aspx>.
- [59] *GOMspace NanoPower Motherboard*. last visited: 05/05/2023. URL: <https://gomspace.com/UserFiles/Subsystems/datasheet/gs-ds-nanopower-p60-dock-29.pdf>.
- [60] *GOMspace 6U Standard*. last visited: 05/05/2023. URL: <https://gomspace.com/6u-standard.aspx>.
- [61] *GOMspace 6U Professional Platform*. last visited: 05/05/2023. URL: <https://www.satcatalog.com/component/6u-professional-platform/>.
- [62] *Supernova Beta prototype cubesat by Pumpkin Inc*. last visited: 05/05/2023. URL: <https://spaceflight101.com/spacecraft/wp-content/uploads/sites/18/2015/10/SNbeta.jpg>.
- [63] *GOMspace 6U PREMIUM PLATFORM*. last visited: 05/05/2023. URL: <https://gomspace.com/6u-premium.aspx>.
- [64] *GOMspace NanoPower Battery 3000mAh*. last visited: 05/05/2023. URL: [https://gomspace.com/UserFiles/Subsystems/datasheet/gs-ds-nanopower_battery_3000mAh_\(DS_-_1022248_-_1_-_20\)_-_1-\(3\).PDF](https://gomspace.com/UserFiles/Subsystems/datasheet/gs-ds-nanopower_battery_3000mAh_(DS_-_1022248_-_1_-_20)_-_1-(3).PDF).
- [65] *GOMspace NanoPower ACU*. last visited: 05/05/2023. URL: <https://gomspace.com/UserFiles/Subsystems/datasheet/gs-ds-nanopower-p60-acu200-23.pdf>.
- [66] *GOMspace NanoPower PDU*. last visited: 05/05/2023. URL: <https://gomspace.com/UserFiles/Subsystems/datasheet/gs-ds-nanopower-p60-pdu200-26.pdf>.
- [67] *Band Pass Filters*. URL: <https://www.allaboutcircuits.com/textbook/alternating-current/chpt-8/band-pass-filters/>.
- [68] *Low Noise Amplifier LNA ICs*. URL: <https://www.infineon.com/cms/en/product/rf/low-noise-amplifier-lna-ics/>.
- [69] Eamon McCarthy Earls. *coaxial cable*. URL: <https://www.techtarget.com/searchnetworking/definition/coaxial-cable-illustrated>.
- [70] *Satellite Ground Stations – Everything you wanted to know*. 2020. URL: <https://www.essearch.com/satellite-ground-stations/>.
- [71] *Phase-Shift Keying*. URL: https://en.wikipedia.org/wiki/Phase-shift_keying.
- [72] *Image of ESA Ground Stations*. URL: https://www.esa.int/Enabling_Support/Operations/ESA_Ground_Stations/Estrack_ground_stations.
- [73] *NSN Global Ground Station Locations*. URL: https://www.nasa.gov/smallsat-institute/sst-soa/ground-data-systems-and-mission-operations#_Toc121310352.
- [74] *State-of-the-Art Small Spacecraft Technology*. 2022. Chap. 11.
- [75] *RTL-SDR.COM*. URL: <https://www rtl-sdr.com/buy-rtl-sdr-dvb-t-dongles/>.
- [76] *Advanced CubeSat Antennas for Deep Space and Earth Science Missions: A review*. URL: https://pureadmin.qub.ac.uk/ws/files/174234474/IEEE_Magazine.pdf.
- [77] *UHF Antenna: 4 Poles design mounting positions*. URL: <https://www.cubesatshop.com/product/isis-deployable-antenna-system-for-6u-12u-cubesats/>.
- [78] *DTUSat - 2 (Danish Technical University Satellite-2)*. URL: <https://www.eoportal.org/satellite-missions/dtusat-2#references>.
- [79] *GomSpace - NanoCom ANT2000*. URL: <https://gomspace.com/shop/subsystems/communication-systems/nanocom-ant2000.aspx>.

- [80] *Endurosat - UHF Transceiver*. URL: <https://www.endurosat.com/cubesat-store/cubesat-communication-modules/uhf-transceiver-ii/>.
- [81] *GomSpace - NanoCom SDR2000*. URL: <https://gomspace.com/shop/subsystems/communication-systems/nanocom-ant2000.aspx>.
- [82] et. al Conor Brown. *NanoRacks DoubleWide Deployer (NRDD) System Interface Definition Document (IDD)*. URL: <https://nanoracks.com/wp-content/uploads/Nanoracks-DoubleWide-Deployer-NRCSD-IDD.pdf>.
- [83] URL: https://en.wikipedia.org/wiki/Random%5C_vibration.
- [84] GOMSpace. *NanoStructure 6U*. URL: <https://gomspace.com/UserFiles/Subsystems/datasheet/gs-ds-nanostructure-6u-11.pdf>.
- [85] Curbell Plastics. *DuPont™ Vespel® SP-21*. 2023. URL: https://www.curbellplastics.com/materials/plastics/dupont-vespel-sp-21/?fbclid=IwAR1q6Vbp53xVpPPORTBBJKCe0%5C_zRaLg66MIFXcEL-IhKxKnWTToPAVWRzz8.
- [86] Nanotec. *DB22M01 – Brushless DC motor*. 2023. URL: <https://en.nanotec.com/products/624-db22m01>.
- [87] URL: https://en.wikipedia.org/wiki/Mechanical%5C_resonance.
- [88] K and K: Thermal Analysis Consulting Services. *Earth's Thermal Environment extracted from Thermal Environments JPL D-8160*. 2021. URL: <http://www.tak2000.com/data/planets/earth.htm>.
- [89] J. Claricoats and S. Dakka. *Design of Power, Propulsion, and Thermal Sub-Systems for a 3U CubeSat Measuring Earth's Radiation Imbalance*. 2018. URL: <http://www.tak2000.com/data/planets/earth.htm>.
- [90] Sylwia Czernik. *Design of the Thermal Control System for Compass-1*. 2004. URL: [https://www.raumfahrt.fh-aachen.de/compass-1/download/Design%5C%5C%5C\\$20of%5C%5C%%5C\\$20the%5C%5C%%5C\\$20Thermal%5C%5C%%5C\\$20Control%5C%5C%%5C\\$20System%5C%5C%%5C\\$20for%5C%5C%%5C\\$20Compass-1.pdf](https://www.raumfahrt.fh-aachen.de/compass-1/download/Design%5C%5C%5C$20of%5C%5C%%5C$20the%5C%5C%%5C$20Thermal%5C%5C%%5C$20Control%5C%5C%%5C$20System%5C%5C%%5C$20for%5C%5C%%5C$20Compass-1.pdf).
- [91] Dunmore Aerospace. *Multilayer Insulation Films*. 2023. URL: <https://www.dunmore.com/products/multi-layer-films.html>.
- [92] NASA. *Aerogels: Thinner, Lighter, Stronger*. 2011. URL: <https://www.nasa.gov/topics/technology/features/aerogels.html>.
- [93] NASA. *State-of-the-Art of Small Spacecraft Technology: Thermal Control*. 2022. URL: <https://www.nasa.gov/smallsat-institute/sst-soa/thermal-control#%5CToc120613733>.
- [94] Nitin Shukla, Ali Fallahi, and Jan Kosny. "Aerogel thermal insulation - Technology review and cost study for building enclosure applications". In: *ASHRAE Transactions* 120 (Jan. 2014), pp. 294–307.
- [95] Shannon Global Energy Solutions. *A LOOK AT AEROGEL AS INSULATION*. 2022. URL: <https://shannonglobalsenergy.com/a-look-at-aerogel-as-insulation/>.
- [96] NanoRacks. *NanoRacks DoubleWide Deployer (NRDD) System Interface Definition Document (IDD)*. 2017. URL: <https://nanoracks.com/wp-content/uploads/Nanoracks-DoubleWide-Deployer-NRCSD-IDD.pdf>.
- [97] Avion Alloys. *The Importance of Multi-layered Insulation*. 2017. URL: <https://avionalloys.com/importance-of-multi-layered-insulation/>.
- [98] Ali Express. *Square Kapton Film Flexible Heater*. 2022. URL: <https://www.aliexpress.com/item/4000529498913.html>.
- [99] Steven R Hirshorn, Linda D Voss, and Linda K Bromley. *Nasa systems engineering handbook*. Tech. rep. 2017.
- [100] *Space engineering Testing*. ECSS-E-10-03A. Rev. 3. EUROPEAN COOPERATION FOR SPACE STANDARDIZATION. Feb. 2002.

- [101] Pérez Laura León, Koch Per, and Walker Roger. "GOMX-4 – the twin European mission for IOD purposes". In: *Proceedings of the 32nd Annual AIAA/USU Conference on Small Satellites, Logan UT, USA* 1 (Aug. 2018), pp. 4–9. URL: <https://digitalcommons.usu.edu/cgi/viewcontent.cgi?article=4108&context=smallsat>.
- [102] NASA. *NASA Team First to Demonstrate X-ray Navigation in Space*. 2018. URL: <https://www.nasa.gov/feature/goddard/2018/nasa-team-first-to-demonstrate-x-ray-navigation-in-space>.
- [103] https://www.nasa.gov/directorates/spacetech/game_changing_development/projects/archived/station-explorer-for-x-ray-timing-and-navigation.

A Appendix A: Thermal Properties Tables

Table 11.3 Equilibrium temperatures for a simple spacecraft in LEO

Surface finish	White paint $\alpha = 0.15$ $\varepsilon = 0.9$	Black paint $\alpha = 0.9$ $\varepsilon = 0.9$	Electroplated gold $\alpha = 0.25$ $\varepsilon = 0.04$
No eclipse	-61 °C	+20 °C	+176 °C
Maximum eclipse	-70 °C	-2 °C	+138 °C

Table 11.4 α and ε values for several surfaces and finishes [5,6,7]

Surface	Absorptance (α)	Emittance (ε)	α/ε
Polished beryllium	0.44	0.01	44.00
Goldized kapton (gold outside)	0.25	0.02	12.5
Gold	0.25	0.04	6.25
Aluminium tape	0.21	0.04	5.25
Polished aluminium	0.24	0.08	3.00
Aluminized kapton (aluminium outside)	0.14	0.05	2.80
Polished titanium	0.60	0.60	1.00
Black paint (epoxy)	0.95	0.85	1.12
Black paint (polyurethane)	0.95	0.90	1.06
—electrically conducting	0.95	0.80–0.85	1.12–1.19
Silver paint (electrically conducting)	0.37	0.44	0.84
White paint (silicone)	0.26	0.83	0.31
—after 1000 hours UV radiation	0.29	0.83	0.35
White paint (silicate)	0.12	0.90	0.13
—after 1000 hours UV radiation	0.14	0.90	0.16
Solar cells, GaAs (typical values)	0.88	0.80	1.10
Solar cells, Silicon (typical values)	0.75	0.82	0.91
Aluminized kapton (kapton outside)	0.40	0.63	0.63
Aluminized FEP	0.16	0.47	0.34
Silver coated FEP (SSM) (OSR)	0.08 0.07	0.78 0.74	0.10 0.09

Note: SSM, Second Surface Mirror.

OSR, Optical Solar Reflector.

Figure A.1: Various surfaces and finishes and their respective emissivity and absorptivity [41].

B Appendix B: Requirements

PHYSICAL REQUIREMENTS RECONSIDERED FOR W6U

4.1. Physical requirements

Dimensions

4.1.1. The CubeSat shall use the coordinate system as defined in Figure 1. The origin of the CubeSat coordinate system is located at the geometric centre of the CubeSat [CDS 3.2.1].

Note: The +Z axis corresponds to the ejection direction.

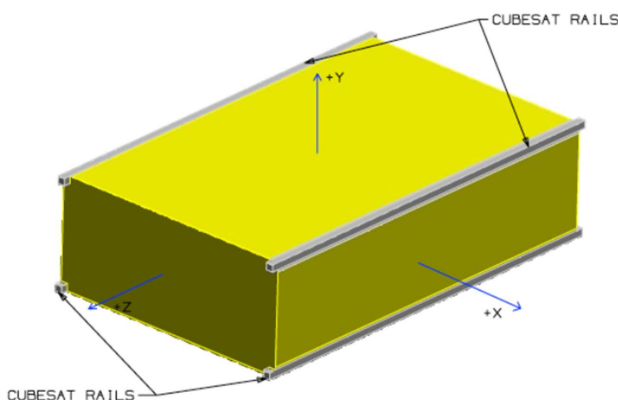


Figure 1 CubeSat Configuration (source: 6U CubeSat Design Specification)

4.1.2. The -Z face of the CubeSat will be inserted first into the deployer [CDS 3.2.2].

4.1.3. The CubeSat dimensions should be within the following dimensions:

X-direction: 226.3 ± 0.1 mm wide

Y-direction: 100.0 ± 0.1 mm wide

Z-direction: 366.0 ± 0.1 mm wide

as per Figure 2.

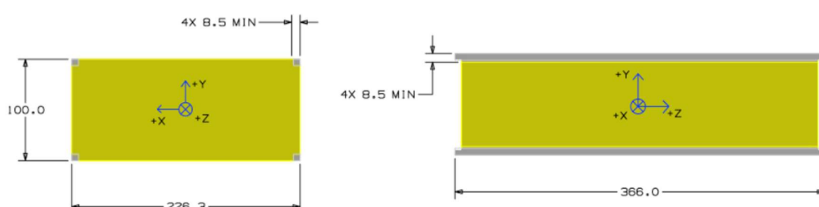


Figure 2 Physical Dimensions in X, Y and Z [mm] (Source: 6U CubeSat Design Specification)

4.1.4. No components on the yellow shaded faces shall exceed 10 mm normal to the surface [CDS 3.2.3].

4.1.4.1. The structural analysis shall demonstrate that the components located on the side faces of the CubeSat, under elastic deformations created by the dynamic loads, do not exceed the geometrical envelope defined in requirement 4.1.4.

4.1.5. Deployables shall be constrained solely by the CubeSat itself. The CubeSat Deployer rails and walls shall not be used to constrain deployables [CDS 3.2.4].

Rails

4.1.8. Rails shall have a minimum width of 8.5 mm [CDS 3.2.5].

4.1.9. Rails shall have a surface roughness of less than 1.6 μm [CDS 3.2.6].

4.1.10. The edges of the rails shall be rounded to a radius of at least 1 mm [CDS 3.2.7] or chamfered to at least 1 mm \times 45°, as per Figure 6.

4.1.11. The rail ends in +/- Z faces shall be coplanar within +/- 0.1 mm.

4.1.12. At least 75% of the rail shall be in contact with the deployer rails. 25% of the rails may be recessed and no part of the rails will exceed the specification [CDS 3.2.8].

Mass Properties

4.1.14. The mass of the CubeSat shall not exceed 12.00 kg [CDS 3.2.9].

4.1.15. The CubeSat centre of gravity shall be located:

within 4.5cm from its geometric center in the X-direction

within 2.0cm from its geometric center in the Y-direction

within 7.0cm from its geometric center in the Z-direction

